MATHEMATICAL MODELLING OF HEAT TRANSFER AND WATER VAPOUR TRANSPORT IN APPLE COOLSTORES

A thesis presented in partial fulfilment of the requirements for the Degree of Doctor of Philosophy in Biotechnology and Bioprocess Engineering at Massey University.

Nevin David Amos
B.Hort.Sci. (Hons) (Massey)

1995

ABSTRACT

A study of heat transfer and water vapour transport in a large industrial apple coolstore was undertaken. A set of measurements was made including product cooling rates in both pre-cooling units and the bulk-storage area, evaporator and fan performance, floor and building shell temperatures, door opening frequency and air temperature, relative humidity (RH) and velocity variation with both position and time.

Measurements within pallet pre-coolers showed large variations in product cooling rate between apple cartons but this could not be attributed to any positional factor studied. The spread of data was probably due to widely differing airflows through and around each apple carton. A staggered pallet pre-cooler configuration had a 30% faster cooling rate on average than an in-line pallet arrangement. Measurements of cooling rates within single cartons showed large variation of cooling rate with position within a carton, probably resulting from non-uniform airflow within the carton.

Existing heat conduction-based models were unable to predict the level of variability of cooling rate within cartons. A multi-zoned conduction and convection model was developed which predicts apple temperature and weight loss, air temperature, enthalpy and humidity, and packaging temperature with position within the carton. Testing of the model against measured data showed good fit for air and apple temperatures, but insufficient data were available for comprehensive testing of the humidity and weight loss sub-models. Difficulties in developing methodology to accurately define the patterns of airflow within cartons were not adequately overcome, so measurements to determine airflow patterns would be required before predictions could be made for alternative packaging systems.

Within the coolstore measured there was significant positional variation in air temperature and humidity associated with local heat sources (such as pre-coolers, doors, uninsulated floor, and warm fruit batches), and the degree of air circulation as quantified by local air velocities. In addition, temperature and humidity showed a diurnal fluctuation associated with the operation of the coolstore. These results suggested the need for a multi-zone dynamic model to enable predictions of both the time and the positional variation to be made.

Such a model was developed which included component models for zone air, external surfaces, floors, heat generators, inert materials such as internal structural components, evaporators, fans, doors and product. Novel features of the model compared to existing models are that it estimates airflow between zones using fixed user defined pathways, rather than complex hydrodynamic models; it considers water vapour transport in detail as well as heat transfer; condensation on surfaces and water absorption by packaging are modelled; and the product sub-model both allows movement of product batches during the simulation and accounts for differences in cooling rate within a batch.

Single-zone, 5-zone, 8-zone and 34-zone versions of the model were tested. The 1-zone model predicted mean thermal conditions for the coolstore adequately. The 5-zone model which differentiated the pre-coolers and the bulk-storage area predicted measured data well for the pre-coolers, but more time-variability was predicted for the bulk-storage area than occurred in the measured data. Separate door zones and vertical subdivision of the bulk-storage area were allowed in the 8-zone model. The pre-cooler prediction was largely unchanged and predicted vertical temperature differences were consistent with measured data, but the predicted mean temperature in the bulk-storage area was offset from the measurements. Little accuracy improvement was achieved by further subdivision (up to 34 zones), probably because of imprecision in defining and predicting interzone airflow rates.

Irrespective of the number of zones, adequate air humidity predictions could only be achieved when water absorption by packaging was modelled as well as product weight loss, door infiltration and deposition of moisture on evaporators.

For the industrial coolstore studied use of 5 or 8 air zones appeared to be the best trade off between accuracy and complexity. The model allows study of the effect of design and operational features on coolstore air temperature, humidity, product temperature and weight loss with better accuracy than previous models.

ACKNOWLEDGEMENTS

The author would like to thank the following persons for advice and assistance during the course of this project:

Professor Donald Cleland, Department of Process and Environmental Technology, Massey University, Chief Supervisor.

Professor Andrew Cleland, Department of Food Technology, Massey University, Supervisor.

Professor Nigel Banks, Department of Plant Science, Massey University, Supervisor.

Assistance from the following during the experimental phase of the project helped make data collection possible:

Mr Hilton Talyor, Site Engineer, New Zealand Apple & Pear Marketing Board (NZAPMB) Whakatu depot.

Mr David Marden, Formerly, Forman NZAPMB Whakatu depot.

Mr Kevin Decon, Formerly, Assistant Regional Manager, NZAPMB, Hastings.

The author would like to acknowledge the NZAPMB and Steelfort Engineering Ltd for funding this project, and the NZAPMB for making available the industrial coolstore used in this work. In particular the author would like to acknowledge the support of:

Mr Mike Odey, Formerly, Engineering Manager, NZAPMB, Wellington.

TABLE OF CONTENTS

LIST OF FIGURES

LIST OF TABLES

CHAPTER 1: INTRODUCTION

The New Zealand Apple and Pear Marketing Board (NZAPMB), through its international marketing arm called ENZA (International), has, by statute, sole rights to sell New Zealand pipfruit crops on export markets. The total crop which is mainly apples has steadily increased from about 200,000 tonnes in 1983 to about 400,000 tonnes in 1992. Consistently about 50% has been exported as fresh fruit, 40% sold as processed products (particularly juice products), and 10% sold domestically as fresh fruit. Fruit for the export market is supplied to the NZAPMB direct from growers or co-operative packhouses. Cooling, coolstorage, transport to markets, and marketing the fruit is then the responsibility of the NZAPMB. The NZAPMB currently owns 80 conventional coolstores with a total capacity of 134,000 tonnes and 45 controlled atmosphere stores with 8,300 tonnes capacity.

Highest possible fruit quality is essential as the market niche for New Zealand apples is in the premium quality sector of the Northern Hemisphere counter seasonality market. The NZAPMB has actively sought to improve all aspects of its operation to improve quality. Quality is highest at harvest, thereafter apples continue to respire and lose moisture. These two processes are the main physiological contributors to deterioration and ultimate loss of quality. Their rates are significantly reduced at lower temperatures, hence refrigeration is the prime means of preservation. In addition to temperature control auxiliary treatments such as controlled atmosphere (CA) and modified atmosphere packaging (MAP) are used for a small proportion of fruit. Good temperature control, and MAP or CA storage make longer storage times possible, but longer storage times allow more time for weight loss. Weight loss occurs due to both respiratory carbon loss and evaporative water loss (transpiration). As well as dehydration causing visible shrivel and loss of crispness, weight loss also represents a direct loss of revenue when selling on a weight basis. Although lower temperatures reduce weight loss, control of air relative humidity (RH) can give substantial benefits and has become increasingly important in overall fruit quality management.

The increase in apple crop volumes over the past decade coupled with longer storage times and tighter temperature and RH specifications, dictated by market requirements, has meant that a substantial coolstore building and modification program has been undertaken by the

NZAPMB. In trying to provide improved apple cooling and storage facilities, NZAPMB engineers have had to compromise between expenditure and benefits, as any coolstore construction has to be performed within strict capital constraints due to the seasonal nature of their use (3-6 months operation each year). Design and operational factors considered to improve temperature and RH management include the provision of fruit pre-cooling systems; appropriate levels of insulation for the walls and floor; product handling systems including type of door, and door operation and protection devices; design of evaporators, fans and associated control systems; airflow patterns; and product stacking patterns. Recently the two main objectives have been to provide pre-cooling of all early season fruit before bulk stacking into the coolstore, whilst maintaining temperature control of stored fruit, and to increase RH in the coolstores to greater than 90%. The first has been achieved using pre-coolers operating within coolstores also used to store fruit. Increasing the evaporator surface area has been the main design change used to achieve the second objective. Whilst this policy has had demonstrated benefits, in that fruit pre-cooling has been possible with resulting fruit quality improvements, and higher RH has been achieved in newer stores, it is unclear whether the new designs are cost-effective. Also there is some evidence of problems with the RH being too high, including loss of packaging strength and split skins of some fruit.

The basis of many effective design and management processes is the use of predictive models. Historically any program to improve quality maintenance in the apple coolchain has been restricted by the paucity of techniques to allow quantitative assessment of alternative coolstore designs and operation. Appropriate mathematical models would allow quantitative prediction of important variables, alternative designs and management systems to be studied, and what-if scenarios to be tested, reducing the need to perform experiments or use a trial and error approach which can prove to be expensive and time consuming. Most of the currently available models in the horticultural product storage area have concentrated on heat transfer aspects and largely ignored the mass transfer, and have not considered the time-variability of the coolstorage system or variation in environmental conditions throughout the coolstore.

The overall aim of this work was to develop mathematical models of heat transfer and water vapour transport (mass transfer) in a large horticultural coolstore that overcome some of the limitations of existing models. The models would take into account all of the important heat and water vapour transport pathways, their interactions, and the operational characteristics of the system. The models should then allow simulation of coolstore operation and aid in both the design and operation of the stores to achieve optimum apple quality in a cost effective manner.

CHAPTER 2: LITERATURE REVIEW

All apple coolstores in New Zealand use air as the heat transfer medium between the product and the refrigeration system; thus only air-based coolstore systems are considered in this review.

Whilst a complete model of the apple coolstorage system would consider both the refrigerated application (coolstore) and the associated refrigeration system, this work considers only the modelling of the coolstore in detail. Although the refrigeration system can be influential on the behaviour of the coolstore, if excess refrigeration capacity is available and/or good evaporator control can be achieved then there is less need to model the full refrigeration system (Cleland 1990). This is generally the case for apple coolstores in New Zealand, so the evaporator which is the component that links the refrigeration system and the coolstore, is the only refrigeration component that needs to be considered in detail. Modelling of refrigeration systems have been extensively considered elsewhere (James *et al.,* 1986; Cleland, 1990; Lovatt, 1992).

The coolstore system for horticultural products is complex with a number of interrelated component heat transfer and water vapour transport pathways, as shown in Figure 2.1. The relevant literature on modelling of heat transfer and water vapour transport in coolstores can be divided into four main areas. The first is literature on general principles of mathematical modelling; the second is models of overall coolstore systems; the third is application component models of the overall system such as product, door, surface, and coolstore air models; and the fourth is refrigeration system component models. For horticultural coolstores, the product temperature and water status are the most important factors affecting quality, hence the way the product and the air interacts is particularly important. Because of this importance, this review has split the application component model literature into one section considering product component models and another considering non-product component models.

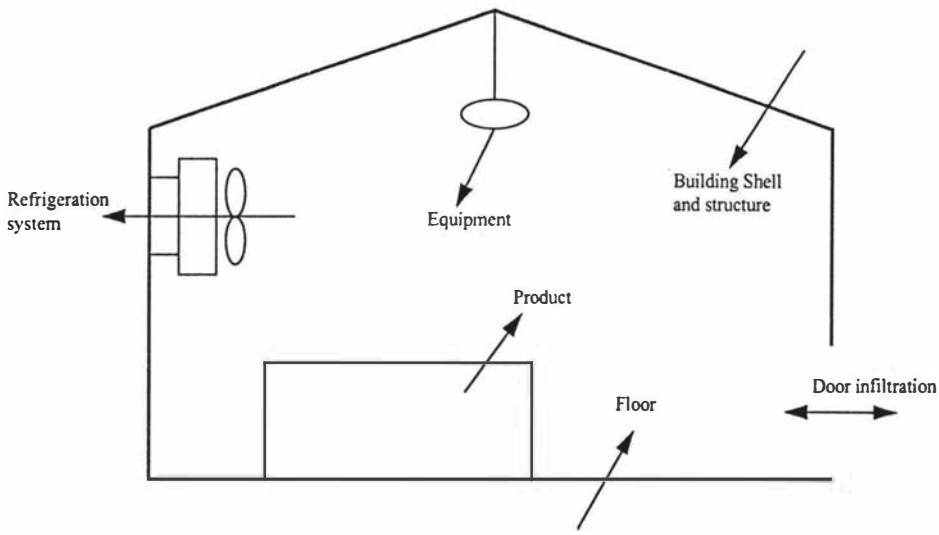

Figure 2.1 Coolstore heat transfer and water vapour transport pathways

2.1 MODELLING PRINCIPLES

Mathematical models of coolstore systems can be classified according to their method of formulation, and their method of time and space discretisation.

2.1.1 Formulation Approach

Two types of information can be available when a model is to be developed (Touber, 1984):

1. Knowledge of the structure of the system to be modelled; and
2. Experimental data constituting observations of system inputs and outputs.

The first leads to models variously described as deductive, white box, structure level or mechanistic, whilst the second has been labelled inductive, behaviour level, black box or empirical modelling (Touber, 1984; Cleland, 1990). Mechanistic models are models derived analytically by making use of appropriate fundamental physical laws and principles such as

the first and second laws of thermodynamics, Newtons law of cooling, and principles of the conservation of mass, energy and momentum. Empirical modelling relies on fitting output data as an arbitrary function of input data. In practice there is a continuous spectrum of modelling approaches from mechanistic to empirical. The main advantage of mechanistic models are that they can be used to predict performance of alternative systems, whereas empirical models are generally only applicable to the system and the ranges of conditions for which they were developed. This work has concentrated on mechanistic models due to their more universal application.

2.1.2 Model Complexity

The appropriate level of model complexity for dynamic simulation of refrigeration systems is a compromise between model implementation cost and model accuracy, and also depends on the area of application of the model (Cleland and Cleland, 1989; Cleland, 1990).

Cleland (1990) states that the key question in testing models is one of appropriateness, not whether all known physical effects are included. A model that includes all known physical effects might be prohibitively complicated, or the measurements required to quantify values of all necessary parameters for using it could be too expensive. Hence such a model may not be as appropriate as a simpler model that incorporates only the most important effects, yet provides a description of the process that is sufficiently accurate for the application under consideration. Likewise Touber (1984) states that in almost every modelling situation there is more than one mathematical model able to represent the real world situation. All of these models will not be equally appropriate for the goals of the modelling exercise, and usually one can be selected as an "optimal" model.

The complexity of the models used is largely affected by the approach used for time and space discretisation.

2.1.2.1 Time Discretisation

Models can be classified as being steady-state or dynamic (unsteady-state or continuous). Steady-state modelling has commonly been used for design of refrigerated facilities.

Evaporators, compressors and condensers are sized to meet the design heat load typically estimated on a 24 hour basis for a given set of worst case weather and operating conditions (Dossat, 1981; Cleland, 1990). Unsteady-state models are able to assess time-variability of heat load and conditions within a facility which are critical for control system design, to assess the effects of discrete events such as door openings, and to define the true operating characteristics of the plant (Cleland, 1990; Lovatt, 1992). Steady-state models are usually less complex than full dynamic models, require less detailed data and less computational time. Hybrid models that use a number of consecutive steady-state analyses allow time-variable behaviour to be approximated without excessive computational effort (Pham *et al.*, 1993).

2.1.2.2 Space Discretisation

There are several approaches which can be used for modelling positional variability of conditions, including lumped parameter, fully distributed and plug-flow models (Wang and Touber 1990). Fully distributed models consider the full position-variability using partial differential equations. Lumped parameter models reduce complexity and computational time by assuming that there is no change in conditions within one or more zones (lumps). For each zone an ordinary differential equation is adequate for each condition. Plug-flow models assume that a well defined flow pathway exists for the component of interest. Generally position-variability is modelled by splitting the domain into a series of zones along the flow pathway with flow through the system in a sequential fashion.

2.2 OVERALL MODELS OF REFRIGERATED FACILITIES

2.2.1 Steady State Models

The most common models of refrigeration facilities are simple steady-state heat transfer models which have traditionally been used by design engineers to size and select equipment. These models generally use average heat loads over 24 hour periods and are usually performed on a worst case scenario (Dossat, 1981; ASHRAE, 1990). With these methods

there is little opportunity to assess likely space- and time-variability within the facility, and to judge the effect of design and operational variables, and control systems on the variability. There is also little ability to systematically design for relative humidity (RH). Generally the only consideration given to RH design is to set target temperature differences between the refrigerant and coolstore air (Dossat, 1981). These methods also largely separate the air flow design from the thermal design leading to potential problems of spatial variability within the facility.

Meffert and Van Beek (1983, 1988) presented a model for predicting air circulation and temperature distribution within refrigerated containers. Air flow was modelled using an electrical resistance analogy and temperatures were assumed to vary solely as a function of the air flow pattern. Air flow through the product was ignored as was the thermal and physical properties of the product which meant that simulation of product heating or cooling was not possible. The air distribution predicted from the model fitted the experimental data of Irving and Sharp (1976) reasonably well. No testing of the predicted temperature distribution against measured data was presented.

Baird *et al.* (1988) developed a steady state engineering and economic model of forced air cooling. The model included subroutines for product heat transfer, air flow through bulk stacked or palletised product, refrigeration system and economic analysis. The model was used to assess the effect of design variables including product size, depth of product, carton vent face area, air velocity, air temperature, initial product temperature, ambient air temperature, evaporator and condenser size, and operating time per year on cooling efficiency and cost. No testing of the model was presented.

Pala and Devres (1988) developed a steady-state model for power consumption and weight loss in a coldstore. The model was run as a series of successive steady-states over a 32 week period for an apple store. No testing against experimental data was reported. Devres and Bishop (1992) also used a modified version of this model for predicting power consumption and weight loss in potato stores. The model was tested against 2 seasons experimental data and had reasonable agreement.

2.2.2 Dynamic Models

James *et al.* (1986), Cleland (1990), Wang (1991) and Lovatt (1992) have all recently reviewed dynamic models of refrigerated facilities. Dynamic modelling of refrigeration systems has increased over the past decade but there are still few comprehensive models of refrigeration applications. Most have concentrated on the refrigeration system not the application and none are for horticultural coolstores, although many of the principles are generally applicable. Most models reviewed were application specific and were not applicable to other systems.

Van der Ree *et al.* (1974) used a finite element program denoted BERTEM for simulating the transients of air temperature in a refrigerated container. Extensive input data and computational time was required to run the model. Predictions from a container filled with products showed that the rate of air circulation and the stacking pattern of product significantly affected the temperature distribution within the container. No testing of the model against experimental measurements was reported.

Marshall and James (1975) developed a model to simulate a vegetable freezing plant. The air space was treated as eight perfectly mixed zones, with an ordinary differential equation (ODE) representing the enthalpy of air in each zone. The refrigeration plant was also modelled in detail. The full model consisted of 46 differential equations and 105 algebraic equations and was system specific. Predictions from the model fitted experimental data well.

Cleland *et al.* (1982) developed a model of the hold of a small fishing vessel and the associated compressor, condenser and evaporator. The air in the hold was modelled as a single perfectly mixed zone and ODE's were used for product temperature, temperature of structures, freezing front position within fish in the hold, and ice thickness on the evaporator. The condenser and evaporator were modelled with lumped thermal capacity models and the compressor was treated algebraically. The model showed reasonable agreement with measured data, although some lack of fit was found during loading times and close to start-ups.

Cleland (1983) outlined a generally applicable simulation model for industrial refrigeration plants. The model described was used to simulate a New Zealand meat works which contained a variety of applications from air conditioned spaces to low temperature freezers. The air in each application was assumed to be perfectly mixed and was modelled by ODE's for air temperature and humidity. The model contained product freezing and chilling models as well as thermal models of the refrigeration plant. The validation of this model was described by Cleland (1985a) in which data from a New Zealand meat works with a refrigeration capacity of 2.5 MW was used. Model predictions of the air, freezing and chilling temperature time profiles were good. The model was worst for short times following step changes in plant operation. This model now forms part of the commercial RADS (Refrigeration Analysis, Design and Simulation) package as described by Cleland (1985b) and Cornelius (1991).

Gloeckner and Findeisen (1984) described a software package (LF74) developed for simulating the dynamic behaviour of fruit and vegetable coolstores. No information about the details of the model or any testing against experimental data was given.

Szczechowiak and Rainczak (1987) developed a dynamic simulation model of a cooling chamber, for food chilling and storage, and an evaporator. The refrigeration plant was not modelled. The chamber was modelled by assuming one dimensional airflow (plug-flow) across the chamber and using partial differential equations for both air and the product in the chamber. The model was validated against measured data and good agreement was achieved.

Wang and Touber (1988) developed three refrigerated room models. The first utilised the Navier-Stokes equation for predicting the air flow within the room but was found to be very complex due to the complicated boundary conditions found in refrigerated applications. The second used the method of Wang and Touber (1987) for predicting energy and mass flows within the room based on temperature measurements. However this method has limited application because of the difficulty of measuring temperature simultaneously throughout large refrigerated rooms and because there must be temperature variation within a room

whether there is air flow or not. The third approach used a resistance network approach to simplify the Navier-Stokes equation. This approach was used to model temperature and humidity distribution within a room. Model predictions agreed well with measured data for a small coolstore loaded with 24 wooden boxes containing electrical heating mats.

Van Gerwen and Oort (1989, 1990), Van Gerwen *et al.* (1991), Wang and Touber (1990) and Wang (1991) all developed models of refrigerated applications by decoupling the momentum equation from the heat and mass transport equations. They used fluid dynamics models to predict air velocity patterns and then assumed that these remained constant with time. Temperature and humidity patterns within the rooms were then predicted based on the calculated air velocities. Good agreement between measured and predicted data was reported from all of these models for small coolstores containing bins or pallets in fixed positions. Very long (100 hours) computational time for calculating the air velocities were reported by Wang and Touber (1990).

Gloeckner *et al.* (1990) described a general simulation model for refrigeration systems denoted STASAN-PC. The software contains subroutines for the refrigeration system and components of the refrigerated application. It appears to be general in nature allowing simulation of a wide range of applications in a similar manner to the RADS package (Cleland, 1985b). However, few details were given on the mathematical approaches used in the models or of any testing of the model against measured data.

Dominguez *et al.* (1991) developed a dynamic model of a beef cooling tunnel using an electrical analogy. Heat capacity, temperature, heat flows and thermal conductivities were made equivalent to capacitance, potential differences, intensities and the inverse of electrical resistance respectively. An electrical circuit was built up to represent the cooling tunnel. Simulation of a cooling cycle was achieved by dividing the total cooling time into a series of finite time intervals and analysing the circuit for each interval. The model was used to assess the effect of different thermal capacities and air flow rates on the cooling rate of the beef. No testing against measured data was undertaken.

2.3 PRODUCT COMPONENT MODELS

If product cooling occurs within the coolstore then the product is a major source of time- and space-variability of conditions. Important considerations in modelling the product include: product heat transfer (temperature versus time and heat load versus time relationships), weight loss, and respiration.

2.3.1 Product Heat Transfer

There are two general situations involving product heat transfer in a horticultural coolstore. Firstly when the product enters the coolstore at a temperature significantly greater then the air and is cooled. Secondly, the heat transfer between the air and the product once the product is close to storage temperature (due to respiration, condensation or evaporation and/or fluctuations in air temperature). The physical description is the same in both these situations but the types of model used can differ substantially.

Cleland (1990) and Gaffney *et al.* (1985b) both present comprehensive reviews of the large number of studies on product heat transfer in refrigerated facilities. This literature can be divided into two general sections, heat transfer from single product items, and heat transfer from multiple product items either packaged together and/or bulk stacked.

2.3.1.1 Heat Transfer for Single Product Items

Heat transfer from single product items is the simplest case. The relevant physical model is one of conductive heat transfer within the object, as most horticultural products are solid in nature, with convective and/or radiative and evaporative heat transfer at the surface. Two generic types of models can be identified, those that have been developed to predict the temperature-time relationship of the product, and those to determine the product heat load on the refrigeration system.

Temperature-Time Models: Nearly all models are based on conduction within the product with convection only at the surface. Radiation and evaporation at the surface are either ignored, or treated as pseudo-convection. Often heat generation within the product is assumed to be negligible (Gaffney *et al.*, 1985b). The most important locations within the product are the thermal centre, and the mass average. The first is important as it is slowest to change in temperature, whilst the second represents the equilibrated temperature and is closely related to heat load (Cleland, 1990). Product heat transfer models can be further classified as being analytical, approximate analytical, empirical or numerical.

a) Analytical Models: Analytical solutions exist for heat transfer in simple regular shaped objects (sphere, infinite cylinder, infinite slab, infinite rectangular rod, rectangular brick and finite cylinder) if the following assumptions apply (Newman, 1936; Carslaw and Jaegar, 1959):

1. internal heat transfer is by conduction only;
2. surface heat transfer is by convection only;
3. the object is homogenous in composition;
4. the initial temperature of the object is uniform;
5. the temperature of the surroundings is constant with time;
6. the surface heat transfer coefficient is constant with time and uniform over the surface of the object; and
7. the thermal properties of the object are constant with time and temperature.

The general form of these solutions is a rapidly converging series that predicts the change in temperature as a function of time, and position within the object. Heisler (1947), Henderson and Perry (1955) and Pflug *et al.* (1965) all presented charts for determining mass average and centre temperatures for regular shaped objects cooling under constant conditions, based on these solutions.

b) Approximate Analytical Models: In most cooling processes, particularly those characterised by conduction with convection, the temperature profiles follow a simple pattern. After an initial "lag", the temperature at any position decreases in an exponential fashion, often referred to as the "regular regime" or "constant half-life" period. For simple

shapes this corresponds to only one term being significant in the analytical solutions. More generally this pattern is identified by a straight line on a semilog plot of fractional unaccomplished temperature change versus time (Figure 2.2). The slope is inversely proportional to the half-life time. The intercept (lag factor) is related to the length of the lag phase. This trend is the basis of most approximate analytical and empirical methods.

Ball (1923), Baehr (1953), Ball and Olson (1957), Rutov (1958), Pflug and Blaisdell (1963) and Kopelman and Pflug (1968) all presented approximate analytical solutions based on equations using first term approximations to the infinite series solutions for heat transfer in a range of simple shapes. Equations for determining the intercept and slope were presented. These methods are still subject to the restrictions imposed on the analytical solutions and they are only valid after the initial lag phase has been completed.

Smith *et al.* (1967) defined a geometry index, G, as a shape factor. G is the ratio of the slopes of the semi-log plots, at infinite Biot number, for the real shape and a sphere of the same characteristic thickness. Irregular shapes were related to the nearest equivalent ellipsoidal model shape that had orthogonal cross-sections of the same area as the actual shape. Clary *et al.* (1971) used this method to develop charts describing transient temperatures at the mass average and centre locations of different shaped ellipsoids and developed nomograms to account for the effect of Biot number on G.

The geometry index and Biot number of the irregular shape were related to an equivalent Biot number for an infinite slab, infinite cylinder or sphere. Testing of this method against plastic objects was carried out for a small range of conditions. Prediction method uncertainty was small compared with uncertainty in the experiments and thermal property data.

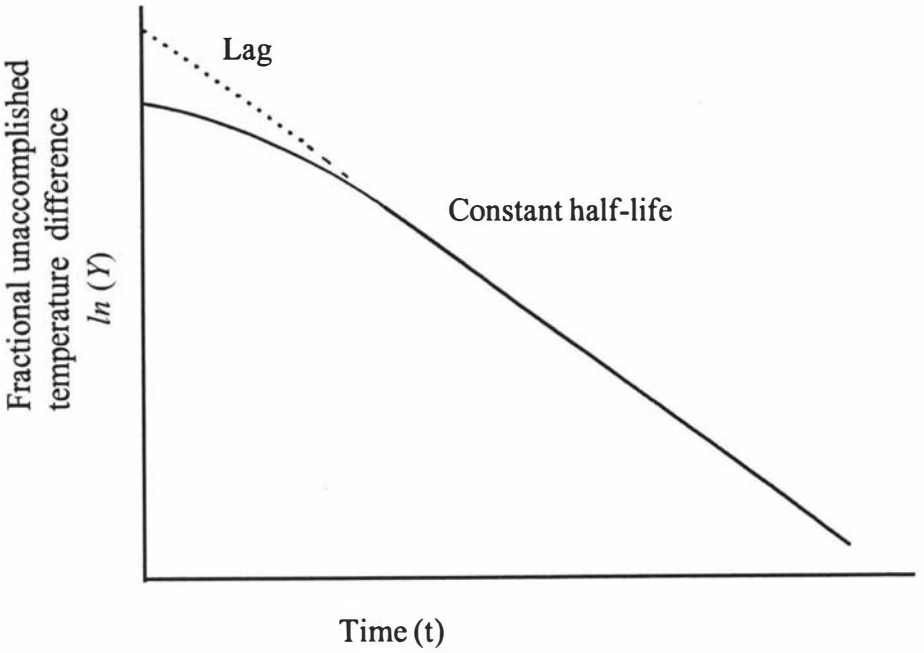

Figure 2.2 Fractional unaccomplished temperature change versus time semi-log plot

Cleland and Earle (1982) developed a shape factor denoted equivalent heat transfer dimensionality (E). E was 1.0 for an infinite slab, 2.0 for an infinite cylinder and 3.0 for spheres. An alignment chart was provided for predicting final centre fractional unaccomplished temperature change based on E, the Biot number and the number of elapsed half life times. The model was tested against known analytical solutions and found to predict within 12% with 95% confidence for a wide variety of shapes. Chuntranuluck *et al.* (1989) sought to develop a method using E as a shape factor which would apply to all shapes, would predict both thermal centre and mass average temperatures, and would involve simple algebraic equations. Some possible forms of equations relating E to shape and Biot number were presented. Lin *et al.* (1993) extended the work of Chuntranuluck *et al.* (1989) and presented equations for calculating thermal centre and mass average temperatures for a range of shapes. The method was tested against analytical solutions for regular shapes and was found to predict temperatures sufficiently accurately for practical applications.

Fikiin and Fikiina (1971) curve-fitted a relationship between Biot number, Fourier number, and fractional unaccomplished temperature change during the chilling of different shapes.

The shape factor used was constant irrespective of Biot number and would be expected to lose accuracy at high values of the Biot number (Cleland, 1990). Over 256 experimental tests by Fikiin (1983) found that this method was accurate within ±9%.

Hayakawa (1971) developed a technique for determining the temperature of commodities subjected to time-variable external conditions. It required the slope during the linear portion of cooling or heating and intercept values to be calculated for the product in question when exposed to a constant external temperature. Equations and tables were presented to determine the transient product temperature when exposed to varying conditions by sequentially calculating the change in product temperature over time as the external temperature changes. The technique was compared with experimental data obtained for oranges, carrots and canned food and found to predict the temperature time profiles accurately.

The concept of enthalpy potential at the surface of food products was coupled to the analytical solution for one-dimensional conduction within the product by Srinivasa Murthy *et al.* (1974, 1976), Abdul Majeed *et al.* (1980), and Badari Narayana and Krishna Murthy (1981) to describe the combined effects of heat and mass transfer at the surface of moist food products. It was assumed that the Lewis relationship can be applied and that the water activity of the product was 1.0, conditions not normally found during air cooling of fruits and vegetables (Gaffney *et al.*, 1985b). Charts were presented for application of the method based on the Fourier and Biot numbers, and dimensionless temperature based on wet bulb temperature and product initial temperature. The method was tested against data for cooling of gels and appeared to underpredict cooling rates particularly at the product centre.

One approach to adapting prediction methods for homogeneous objects to heterogeneous objects has been to use effective thermal properties (density, thermal conductivity, specific heat capacity) and effective surface heat transfer coefficients. Schwartzberg (1976), Schwartzberg (1977), Miles *et al.* (1983), Choi and Okos (1986), Pham and Willix (1989), and Pham (1990) present methods for determining the effective thermal conductivity, density and heat capacity of foods from compositional data. Levy (1981) and Miles *et al.*

(1983) also present methods of calculating effective thermal properties for products which contain air voids. For packaged products a common approach is to add the resistance of outer packaging layers to the convective heat transfer resistance using a series model to calculate the effective heat transfer coefficient (Cleland and Cleland, 1992). Systematic testing of the use of such methods for cooling of heterogenous products has not been reported.

c) Empirical Models: Due to problems in developing generally applicable prediction methodologies, especially for a wide range of shapes and for situations with mechanisms other than conduction and convection, a common approach has been to experimentally determine the half-cooling time and lag factor. Table 2.1 gives examples of researchers who have used such an experimental approach. The major disadvantage of this method is that the experimental values only apply for the product, of the size, shape and composition used in the experiments, and for the particular heat transfer condition used and are restricted to conditions that are constant with time.

Earle and Fleming (1967) and Wade (1984) used a similar empirical technique to each other for predicting cooling rates of complex shapes. They defined equivalent diameters of one of the three basic shapes so that chilling time for the real shape and the analogous shape were the same. Earle and Fleming (1967) used a cylinder as the analogous shape for lamb carcasses, and Wade (1984) treated individual fruit pieces as spheres and pallets of cartons as infinite slabs.

Devres (1989) developed an analytical equation, for the case of negligible internal heat transfer resistance, to calculate product temperature of apples during cooling and storage. The equation incorporated the effects of respiration heat generation and weight loss as empirical functions of temperature. No testing of the model against measured data was reported.

Table 2.1

Researchers Who Have Experimentally Determined Product Cooling Rates.

Source	Application
Pflug & Nicholas (1960)	Heating rates of cucumber spears in different jars and syrups
Nicholas & Pflug (1961)	Heating rates of whole pickles.
Wadsworth & Spadaro (1969)	Heating rates of sweetpotato roots during immersion heating.
Parsons *et al.* (1972)	Cooling rates of pears and plums in different carton stacking arrangements on a pallet.
Haas & Felsenstein (1985)	Cooling rates of avocados packed in cardboard boxes with different vent configurations.
Arifin & Chau (1988)	Cooling rates of strawberries in cartons with different vent designs.
McDonald (1990)	Cooling of apples and pears within pre-coolers and within bulk storage for a range of packaging and stacking configurations
ASHRAE (1990)	Hydrocooling rates for a range of produce.
Watkins (1990)	Forced-air cooling rates for a range of products.
Anon. (1991)	Precooling rates of kiwifruit in different packages and positions within a forced-air precooler.
McDonald *et al.* (1993)	Precooling rates of kiwifruit in different coolstores.

d) Numerical Methods: Numerical methods such as finite difference, finite element, or control volume techniques allow the full partial differential equation for heat conduction to be solved without the restrictions listed under analytical solutions. De Baerdemaeker *et al.* (1977) outlined the use of the finite element method for modelling heat transfer in foods. Cleland (1990) reviewed finite difference schemes. Patankar (1980) described control volume methodology. Table 2.2 summarises the features of numerical models that have been used to predict heat transfer for single items of horticultural products.

Table 2.2

Numerical Single Product Item Heat Transfer Models

Source	Solution Type[1]	Effects Considered[2]				Validation Performed
		Resp.	Evap.	a_w	Rad.	
Ansari *et al.*, 1984	FD	×	√	×	×	√
Baird and Gaffney, 1976	FD	×	×	×	×	?
Bonacina and Comini, 1971	FD	×	×	×	×	√
Chau *et al.*, 1984	FD	√	√	√	√	×
Chau and Gaffney, 1990	FD	√	√	√	√	√
Haghighi and Segerlind, 1988	FE	×	√	×	×	√
Hayakawa, 1978	FD	√	√	×	×	×
Hayakawa and Succar, 1982	FE	√	√	×	×	√
Holdredge and Wyse, 1982	FD	√	√	×	×	√
Abdul Majeed *et al.*, 1980	FD	×	√	×	×	√
Misra and Young, 1979	FE	×	×	×	×	√
Patel and Sastry, 1988b	FE	√	×	×	√	√
Upadhyaya and Rumsey, 1989	FE	×	√	×	×	√
Wadsworth and Spadro, 1969 & 1970	FD	×	×	×	×	√

1 FD = finite difference, FE = finite element

2 effects considered in addition to conduction within the object and convective heat transfer at the surface:

- Resp = product respiration heat generation
- Evap = evaporative cooling
- a_w = water activity ≠ 1.0
- Rad. = radiation from product surface
- √ = effect included in model
- × = effect not included in model
- ? = not stated.

In general, finite difference models are easier to formulate and have lower implementation costs for regular shapes where evenly spaced grids can be used whilst for irregular shapes finite element and control volumes are the most practical alternatives (Cleland, 1990).

Numerical integration of differential forms of a number of the approximate analytical models have been used in situations where external conditions are time-variable (Cleland *et al.*, 1982; Cleland, 1983, 1985a; Devres, 1988; Lovatt, 1992). Although they are less generally applicable than the full numerical methods they have the advantage that data requirements and computational cost are lower. These are discussed further in the following sections on heat load models and bulk stored product models.

Heat Load Models: Any of the temperature-time models discussed in the previous section can also be used to predict the product heat load versus time if they estimate mass average temperature. Several other models have been developed specifically for determining product heat load.

Marshall and James (1975) modelled product heat load in a vegetable freezer with a single ordinary differential equation by assuming a negligible temperature gradient within the product and used an effective heat capacity (which included latent heat effects) which varied depending on the refrigerated space zone in which the product rested at any time. Testing showed that the model did not accurately predict the product freezing process, but the heat load was accurate enough for the purpose of investigating capacity control. Reynoso and De Michelis (1988) used a similar approach for a model of a cryogenic freezer. Cleland (1985a) noted that these approaches are only exact for Biot number equal to zero and become less accurate as the Biot number increases, as the assumption of no temperature gradient within the product becomes less valid.

Pala and Devres (1988), Devres (1989) and Devres and Bishop (1992) all modelled product heat load on a daily basis using an analytical equation based on predetermined half-cooling time. No comparison with measured data was presented.

Cleland (1983, 1985a) modelled heat load and product temperature during cooling using a single ordinary differential equation based on the empirical half-life method of Cleland and Earle (1982). No comparison with measured data was presented, although air temperature predictions in applications using this approach were in good agreement with measured data. Wade (1984) used a similar approach but a simpler shape factor.

Lovatt *et al.* (1993a) used essentially the same model for cooling as Cleland (1985a) when developing an ordinary differential equation model for determining heat loads during chilling, freezing and subcooling. The model predicted within 10% of measured data for freezing of a meat carton and compared favourably with the predictions from a finite difference model (Lovatt *et al.*, 1993b).

2.3.1.2 Heat Transfer for Bulk Stacked Product

In coolstorage products are commonly bulk-stacked. In this case, forced and natural convection or air through the bulk stack and the effect of packaging are significant and a simple conduction model may not be applicable.

Approaches used to model bulk stacked products have included determining effective thermal properties of the product and packaging, using empirical models based on measurements for the system, and plug flow or porous bed models. No food refrigeration system models using physically based descriptions for mechanisms such as natural convection were found, possibly due to the complexity of such approaches. A number of researchers have measured cooling rates of bulk-stacked products (Table 2.1).

Jamieson *et al.* (1993) considered cooling of cartoned cheese blocks bulk stacked onto pallets in coolstores. The boundary of the pallet as an object was taken to be the outermost cheese surface. It was assumed that packaging and air gaps outside this boundary affected the heat transfer coefficient whilst packaging, air voids and cheese inside this boundary affected the thermal properties. The series heat transfer resistance model (Miles *et al.*, 1983) based on mass and volume fractions was used to estimate effective thermal properties

for each pallet. The effective heat transfer coefficient was based on the combined resistance due to convection and conduction through packaging and immobilised air gaps. Predictions from the models showed good agreement with measured data. The cheese stacks were reasonably tightly stacked with minimal opportunity for ventilation.

Plug flow or porous bed models have been developed by a number of researchers for modelling storage of a range of agricultural commodities. These are listed in Table 2.3. These models zone product in the direction of air flow rate within the product stack. Enthalpy and humidity balances are performed for each zone as the air passes through the stack.

Table 2.3

Porous Bed Product Heat Transfer Models

Source	Product Model[1]	Effects Considered[2]		Validation Performed
		Respiration	Mass Transfer	
Bakker-Arkema & Bicket (1966)	LP	×	×	×
Bakker-Arkema *et al.* (1967)	LP	×	√	√
Yavuzkurt *et al.* (1976)	LP	√	√	√
Baird & Gaffney (1976)	FD	×	×	×
Holdredge & Wyse (1982)	LP	√	√	√
Ofoli & Burgess (1986)	LP	√	√	√
Romero & Chau (1987)	FD	√	√	√
Gan & Woods (1989)	FD	√	√	×
Bazan *et al.* (1989)	FD	√	×	√

1 = Type of model used for calculating product temperature:
LP = lumped parameter (Biot number equal to zero)
FD = finite difference (temperature gradient within product).
2 = Effects considered other than convective heat transfer at the surface.
√ = effect considered
× = effect not considered

Cleland *et al.* (1982) and Cleland (1983, 1985a) used an ODE based on the $Bi = 0$ assumption to represent change in stored product temperature. It was assumed that only a fraction of the product mass could change in temperature. The fraction was taken as the smaller of, 20% of the product mass, or that within 0.05 m of the exposed product surface. No validation of this model was presented although the predictions of air temperature for

the overall coolstore were in agreement with measured air temperatures. Pala and Devres (1988) used a similar approach but allowed the total product mass to change in temperature based on a predetermined half cooling time. This model was not tested against measured data.

Wang (1991) modelled bulk products as a porous solid by splitting bulk stacked products into a number of "lumps" with negligible internal heat transfer resistance and modelling heat and mass transfer between the "lumps" using the finite difference method. Good agreement between predicted and measured data was obtained.

2.3.2 Product Respiration

For situations where significant temperature change must be achieved and there is a high rate of heat transfer, heats of respiration are generally small compared with sensible heat effects and can be ignored (Gaffney *et al.*, 1985a). However respiration may be important for products with high respiration rates, or in conditions giving very slow rates of cooling, or at storage conditions (Gaffney *et al.*, 1985a). Respiration of most horticultural commodities is temperature dependent; hence it is most easily modelled using numerical methods (Cleland, 1990). Simple analytical solutions exist if respiration is constant or a simple function of temperature (Carslaw and Jaeger, 1959). Empirical equations for respiration rates as functions of temperature have been developed by Gaffney *et al.* (1985b), Hayakawa and Succar (1982), Hunter (1985), and Wang (1991) for a range of fruits and vegetables. These equations are largely product specific. Hayakawa and Succar (1982) and Hunter (1985) both included a time factor to account for the change in respiration rate with time due to physiological changes in the product.

2.3.3 Product Mass Transfer (Evaporation)

Evaporative cooling at the surface of horticultural products can have a significant effect on the rate of heat transfer. Factors affecting weight loss from foods in refrigerated storage are reviewed by Sastry *et al.* (1985) and Gaffney *et al.* (1985b). Sastry *et al.* (1978) reviewed the literature pertaining to transpiration rates of fruit and vegetables.

The main factors affecting the rate of water evaporation from fruits and vegetables are: the exposed surface area of the product, the water vapour pressure difference (sometimes referred to as vapour pressure deficit) between the product and the surrounding air, and the total resistance to water movement from the product to the air. The water vapour pressure difference depends on the temperature of the product and air, the water activity of the product, and the relative humidity of the air (Gaffney *et al.*, 1985b).

Lentz & Rooke (1964), Gentry (1970), Fockens & Meffert (1972) and Talbot (1973) assumed that the product surface temperature was the same as the surrounding air temperature, thereby neglecting the effects of evaporative cooling and respiratory heat generation on product temperature. Water activity was assumed to be 1.0. This method provided reasonably accurate predictions of moisture losses for storage of apples under conditions with moderate water vapour pressure differences. Under conditions of low and high water vapour pressure differences, predictions deviated considerably from experimental data (Sastry & Buffington, 1983).

Gaffney *et al.* (1985b), Fockens & Meffert (1972), Romero *et al.* (1986) and Chau *et al.* (1988b) calculated the overall mass transfer resistance as a function of both the product skin resistance and the resistance of the air boundary layer. The skin resistance (inverse of the commonly used term transpiration coefficient) was dependent on the structure and properties of the product skin and the air film resistance was dependent on the size of the product and the properties and flow rate of the surrounding air. The air film resistance was shown to be significant for products with low skin resistance, such as for mushrooms, but not for products with high skin resistance, such as apples (Gaffney *et al.* 1985b, Neves *et al.* 1983). Lentz and Rooke (1964) and Van Beek and Ficek (1979) observed that the skin resistance varied with vapour pressure difference between the product and the air. Patel and Sastry (1988b) found no evidence to support this finding and Chau *et al.* (1988b) and Romero *et al.* (1986) observed that the skin resistance was independent of the airflow rate, relative humidity and the degree of weight loss for most of the products they tested. Fockens & Meffert (1972), Villa (1973) and Wang (1991) all developed models which

assume that the shapes of the skin cells change due to a change in turgidity as a response to different water vapour pressure differences. Chau *et al.* (1988a) attributed the observed non-linearity in transpiration rate with vapour pressure difference to evaporative cooling and respiration heat. Van Beek (1983) found that the mass transfer resistance of fruits in storage was not constant and that there is a yearly difference attributed to changes in growing conditions.

Romero *et al.* (1986) presented transpiration coefficients of apples, blueberries, waxed and unwaxed limes, strawberries, tomatoes and brussel sprouts. Chau *et al.* (1988b) measured 17 fruits and vegetables (including apples) over time until 5% weight loss had been achieved.

2.4 NON-PRODUCT COMPONENT MODELS

Non-product components that need to be modelled in an overall coolstore heat and water vapour transfer model include: the coolstore air; walls and other surfaces which form the boundary of the refrigerated space; equipment and people working within the coolstore; doors; refrigeration evaporators; packaging; and any structural material within the store with thermal mass which can buffer the coolstore air. The accuracy of the overall model will be dependent on the accuracy and appropriate interlinking of these component models.

2.4.1 Air Space Models

Several modelling approaches for the air space can be identified including:

2.4.1.1 Single Zone Models

These models assume that the air within the coolstore is perfectly mixed. One ordinary differential equation (ODE) is used for each of air temperature (or enthalpy with temperature derived analytically) and humidity. Any interaction with other component

models is assumed to instantaneously affect the whole air volume of the room. Examples include Cleland *et al.* (1982) and Cleland (1983, 1985a) who used this approach with ODE's for temperature and humidity for applications in the meat industry. A weakness was that the model allowed relative humidity to exceed 100%. Lovatt (1992) used a similar model but allowed moisture to condense out of the air if the humidity exceeded saturation. Pala and Devres (1988) and Devres and Bishop (1992) appear to have used a similar approach, although the equations used for air temperature and humidity were not stated.

2.4.1.2 Multi-Zoned Models

These models split the coolstore air up into a series of zones which are then each treated as perfectly mixed. Air transfer between zones is modelled either as plug-flow with a well defined air flow path from the fan discharge to intake, or in some other fashion.

Marshall and James (1975) modelled a vegetable freezer using 8 air zones linked together in a plug-flow fashion. Pham and Oliver (1983) suggested the use of a two zone interconnected model, in order to more accurately predict door exchange rates into a coolstore, with one zone adjacent to doors and the other to model the rest of the bulk store. Setting each zone to half the total coolstore volume and having a flow between the zones of 1.1 times the calculated volume flowrate through the door gave good fit with measured data for a high rise store. Liao and Feddes (1992) developed a 12 zone model for predicting dust concentration in ventilated airspaces. A flowrate matrix was used to calculate flow between zones based on the total flow rate into the facility. The model was tested against measurements of talcum powder concentration in a test chamber at two different air flowrates and against predictions from a single zone lumped-parameter model (Liao and Feddes, 1990). Good agreement between measured and predicted concentration was achieved for both air flowrates for the 12 zone model. The single zone model had reasonable agreement with measured data for the low air flowrate but underpredicted by 30-40% for the high air flowrate. Data were presented for only one of the 12 measured zones. It was unclear whether the underprediction was due to the mean value across the facility being lower than the value for the zone presented, or whether the single zone model underpredicted for all zones.

2.4.1.3 Distributed Models

These models use full hydrodynamic prediction of air movement based on the Navier-Stokes equations for fluid flow using a complete finite difference, control volume, or finite element discretization of the air space.

Van der Ree *et al.* (1974) modelled a refrigerated container with well defined product stacking patterns by linking the fluid flow predictions to heat and mass transfer models. Extensive input data and computational time were required. No testing of the model was reported. Meffert and Van Beek (1983, 1988) and Wang and Touber (1988) used a resistance network approach to reduce model complexity in predicting air flow patterns within containers and small coolstores with well defined and constant stacking arrangements. Good agreement with measured air flow was achieved. Other workers have decoupled the air flow predictions from heat and mass transfer to reduce complexity. In this manner, for any room configuration only one fluid flow prediction is required. Wang and Touber (1990), Wang (1991), Van Gerwen & Oort (1989, 1990) and Van Gerwen *et al.* (1991) found this approach gave good agreement with measured temperature and velocity data for containers and small coolstores with fixed product stacking arrangements. Computational effort was still high compared with zoned models.

2.4.2 Building Shell

The simplest approach to modelling heat transfer through surfaces is to use quasi steady state models based on the temperature difference across the surface and the resistance to heat flow of the material, assuming the wall has negligible thermal capacity. This approach has been used by Cleland *et al.* (1982), Szczechowiak & Rainczak (1987), Reynoso & de Michelis (1988), Pala and Devres (1988) and Devres and Bishop (1992). Cleland (1983, 1985a) and Lovatt (1992) used a similar approach but separately included the thermal capacity of the surface by treating it as a structure. In this manner the heat load through the wall interacted directly with the air in the application which was then buffered independently by the thermal capacity in the structures. Wang (1991) modelled the heat flow through and

the temperature of surfaces using a full finite difference approximation to the conduction. No independent testing of any of these approaches has been reported.

Knowledge of temperatures on the outside of surfaces is required to use any of the models listed above. Solar radiation effects on exposed surfaces may also be important. The standard design technique uses worst case summer conditions (Dossat, 1981; ASHRAE, 1990). Cleland (1985a) used a constant ambient temperature throughout the simulation period. Pala and Devres (1988) and Devres and Bishop (1992) used the average of three measured air temperature readings over each day for air temperature and used a constant soil temperature. Solar radiation was also modelled using a degree day approach and using sol-air temperature increments for exposed walls (ASHRAE, 1990). The "Room" module of the RADS package fitted a sine wave to user input daily maximum and minimum temperatures but does not model the effect of radiation (Cornelius, 1991). Kimball and Bellamy (1986) reviewed models for calculating diurnal temperature and relative humidity from daily weather data, and presented new models which fitted New Zealand weather data well.

2.4.3 Doors

Infiltration of warm air can be a major factor in the design, operation and performance of coolstores. It can constitute more than half the total heat load, it is usually the main source of water vapour causing frost to form on the evaporator coils, and it causes temperature and humidity fluctuations that can badly affect product quality (Pham & Oliver, 1983).

2.4.3.1 Air Flowrate Through Doors

Tamm (1965) derived an equation for predicting the air exchange rate through an open door based on air density difference across the door and the door height. Moreno (1987) developed a simplified version of Tamm's equation based solely on air temperature difference, thereby avoiding the necessity of calculating air densities. No testing of the equation was reported. Pala and Devres (1988) also used an equation based solely on air

temperature difference. It appears simpler to use than Tamm's equation, but it included an empirical constant and no testing against measured door exchange data was presented.

Pham & Oliver (1983) used tracer gas methods to measure the actual flow through an open cool room door and compared the results to Tamm's predictions. Measured values were lower than those predicted, and the lower half of the measured profile with respect to height was flatter than the theoretical, suggesting that floor frictional effects were significant. Correction factors for Tamm's equation were suggested for various door types and protective devices. The modified Tamm's equation had good agreement with measured data for short duration door openings, but overpredicted for long door openings. This was attributed to imperfect mixing of air in the room. For long door openings the air immediately adjacent to the door warms causing lower density driving force and lower interchange rates. Fritzsche & Lilienblum (1968) also found that turbulence and mixing of ingoing and outgoing streams reduced the difference of density at any height and hence the rate of airflow. Pham and Oliver (1983) suggested the use of a two zone interconnected model to overcome this effect. Balbach & Schmitz (1991) and Gosney & Olama (1975) both found that the full effect of air exchange does not occur immediately as the door is opened, with anywhere from 15 seconds to a minute before the air streams reached a steady-state.

The overall system models of Cleland (1983, 1985a) and Lovatt (1992) used a modified Tamm's equation in accordance with the results of Pham & Oliver (1983b). Wang (1991) used Tamm's equation modified by a discharge coefficient as determined experimentally by Gosney & Olama (1975).

2.4.3.2 Door Open Time

Cleland *et al.* (1982) closely matched measured timing and duration of hold hatch openings for a small fishing boat by preset times, but only had three per day. Cleland (1983, 1985a) modelled a user input door open fraction using random numbers to decide door position at each time step in the numerical integration. The fractional door open time could be varied

for different periods during the day. Wang (1991) did not state how door position was determined. Lovatt (1992) used a similar approach to Cleland (1983, 1985a) but assumed that the door openings occur at irregular intervals. The times between door openings were modelled by an exponential distribution and it was assumed that the length of the door closing times followed a normal distribution. Pala and Devres (1988) and Devres and Bishop (1992) both calculated door open time based on the number of pallets entering and leaving the store per day and a user input value for the time of opening per pallet. None of these approaches were identified as significantly causing lack of fit of the predicted data, but no independent testing of door heat loadings was reported.

2.4.4 Equipment and People Load

Any equipment or people working within a store add to its heat load. The main types of equipment which have to be considered include lights, fan motors, and forklifts. The instantaneous heat load is commonly taken as the power input to the equipment and is usually assumed to be constant with temperature (Cleland, 1990). Other than fans, the equipment heat load is usually a minor component of total heat load, but it can be a localised source of heat, which may influence local air and product temperatures and relative humidity.

People introduce both heat and moisture into the store air due to respiration, convection and possibly radiation. A constant load per person is used in the RADS package (Cornelius, 1991).

2.4.5 Packaging and Structures

It is often assumed that packaging has negligible thermal capacity, because the heat extracted due to temperature change in the packaging is negligible compared to the heat extracted from the product. On the other hand packaging adds further thermal resistance to product items and needs to be considered when the surface heat transfer coefficient is calculated (Cleland, 1990). Pala and Devres (1988) and Devres and Bishop (1992) both

modelled packaging heat load by assuming that the packaging reached the temperature of the room air within 24 hours of entry. Cleland (1983, 1985a) and Cornelius (1991) did not model packaging directly but allowed them to be added to the structure's thermal mass.

Packaging can act as a source or sink for water vapour within the store. Wink (1961) and Liebenspacher and Weisser (1989) both present methods for determining moisture content of cellulosic packaging materials in response to air relative humidity. No coolstore model was found that considered packaging moisture content.

Any structural material of significant thermal mass will act to buffer the coolstore air. Models of structures could include lumped parameter models where the mass average temperature of the structure is modelled, or finite difference and finite element techniques where the temperature change with position within the structural material is modelled. The RADS package uses a lumped parameter model (Cornelius, 1991). No complete coolstore models were found where finite difference or finite element models of structures were used.

2.5 AIR COOLING COIL MODELS

The air cooling coil (evaporator) represents the boundary between the application and the refrigeration system. If the objective of the overall model is to analyse heat and mass transfer in the coolstore air, then the air cooling coil is the only part of the refrigeration system that needs to be modelled. Evaporators used in horticultural coolstores are almost exclusively of the finned tube type. Evaporator models have been reviewed recently by Cleland (1990), Wang (1991) and Lovatt (1992). The simplest approach to modelling the evaporator is to consider only the overall heat transfer performance. An alternative is to breakdown the heat transfer into the air-side and refrigerant-side components. With this approach models with a wide range of levels of complexity are possible.

2.5.1 Refrigerant-Side Models

For modelling the refrigerant side of the evaporator the following approaches have been used:

a) Black box models. Stoecker (1966) and Najork (1975) represented the evaporator by a series of transfer functions with constants determined through experiments.

b) One zone models where the refrigerant side of the evaporator is modelled as a single zone (Chi & Didion, 1982; Marshall & James, 1975; Hargreaves & James, 1979; Cleland, 1983; Cleland, 1985a).

c) Two zone models where the evaporator is split into two zones; the two-phase (evaporation) and single-phase (superheat) flow regions are treated separately (Wedekind & Stoecker, 1966; Dhar & Soedel, 1979; de Bruijn *et al.*, 1979; Yasuda *et al.*, 1983; van der Meer, 1987; Bonte & Veldhoven, 1983; Broersen & van der Jagt, 1980).

d) Distributed models where the evaporator is modelled as a number of sections (MacArthur, 1984; Wang, 1991).

If excess refrigeration capacity is available and good evaporator temperature and refrigerant flowrate control are achieved then the refrigerant-side temperature is controlled to meet the application heat load whilst holding the air temperature setpoint. There is then no need for detailed refrigerant side modelling (Cleland, 1990).

2.5.2 Air-Side Models

The air-side heat transfer has two components: sensible heat transfer due to change in the air temperature as it passes through the coil; and latent heat transfer due to condensation or frosting of moisture on the coil surface which leads to change in air humidity. For many

horticultural coolstores the air temperature is close to 0°C, so the coil surface is below 0°C and frosting occurs. As frost forms, it decreases air flow because the free area available for flow decreases, and it also insulates the coil surface from the air. A number of studies have been carried out on evaporator performance under frosting conditions and on frost properties (Gatchilov *et al.*, 1979; Sekulic, 1983; O'Neal and Tree, 1985; Kondepudi and O'Neal, 1987; Smith, 1989; O'Hagan *et al.*, 1993a, 1993b).

The air-side of the evaporator can be modelled using either steady-state or unsteady-state methods. A common approach is to model only sensible heat transfer in a steady-state manner, based on a heat transfer coefficient between the air and the refrigerant, the effective surface area of the coil and the temperature difference between the air and the refrigerant (Cleland and Cleland., 1992). The heat transfer coefficient is chosen to take account of the combined effect of different forms of refrigerant flow rate control and air flow rate. This model is used extensively by refrigeration engineers for selecting and sizing evaporator coils. It generally leads to conservative designs, and does not quantify the rate of water vapour removal which is necessary to determine air relative humidity. Also the change in coil performance due to frosting is often ignored. Marshall and James (1975), Cleland (1983) and Szczechowiak and Rainczak (1987) used this approach as part of their application models. Cleland *et al.* (1982) modelled heat transfer only, but included the build up of a frost layer on the coil surface and its insulating effect.

The simplest approach to take account of the latent heat transfer component is to adjust the rate of sensible heat transfer by a sensible heat ratio (the ratio of sensible to total heat removal from the air). Cleland (1985a), Cornelius (1991) and Lovatt (1992) used this approach. Early versions of the RADS software (Cleland, 1985a) estimated the sensible heat ratio based on a straight line approach of air-on condition to saturated air at the refrigerant temperature, but did not consider the change in coil performance with frosting. In recent versions of RADS (Cornelius, 1991) the sensible heat ratio is based on the approach to an estimate of the coil surface temperature rather than the refrigerant temperature. The surface temperature to air temperature difference was estimated as a simple fraction of the refrigerant to air temperature difference. Such models are essentially

steady-state as the evaporator performance is assumed to be independent of the amount of frost.

Wang (1991) developed a finite difference model for both air and refrigerant side heat and mass transfer. The model allowed dehumidification of air as it passed across the evaporator coil but did not model frost growth and its effect on evaporator performance.

The only comprehensive model of evaporators that includes the effect of frost growth on evaporator performance is given by Kondepudi and O'Neal (1991, 1993a, 1993b). It was not part of an overall application model.

Defrosts are frequently required to prevent excessive performance loss of coils. Cleland (1985a) modelled defrosts by setting the evaporator heat removal rate to zero for the appropriate defrost period. This was considered appropriate in cases where defrost heat is removed in the condensate and could be ignored (Cornelius, 1991). Other models included heat input to the application during defrost (Pala and Devres 1988; Devres and Bishop, 1992).

None of the evaporator models used in overall coolstore models have been independently tested against measured data, but good fit of air temperature in the applications has been shown. No testing of air relative humidity predictions in application models was found.

CHAPTER 3: PRELIMINARY CONSIDERATIONS

3.1 SUMMARY OF LITERATURE

Of the existing models in the refrigeration area discussed in Chapter 2 the vast majority have concentrated on modelling of refrigeration system components, with only a few researchers focusing on the refrigerated application. Of those who have modelled the refrigerated application, most have considered only heat transfer in detail, have not considered positional variation of air and product conditions within the application, and have not attempted to model water vapour transport in any detail. A number of these models were also situation-specific and could not be used as general models without major modifications. Several models have been developed which include full air flow predictions, but these have proved to be both data- and computationally-intensive and have been used only for small facilities where product stacking patterns and operational characteristics have been fixed with time, and less detailed models of the other components contributing to the heat load were used.

Most of the existing work on product heat transfer has concentrated on predicting product temperature-time profiles during cooling for single product items. There has been limited validation of product heat transfer models for cooling of bulk-stacked product where the effect of packaging and ventilation through the product could be significant.

3.2 RESEARCH OBJECTIVES

Taking into account these factors and the requirements of the NZAPMB the specific objectives of this work were to:

(1) measure the rates (and variation of rates) of apple cooling within pre-coolers and in bulk storage within apple coolstores for various stacking configurations, thus achieving a data base of industrial information;

(2) measure rates of apple cooling within cartons in environmental test facilities at Massey University to provide higher quality data for model testing;

(3) use data from (1) and (2) to assess the use of existing product cooling models for bulk apple cooling and, if necessary, develop improved models so that accurate predictions can be made for any likely apple cooling situations;

(4) measure the variation in air and product conditions with time and position within an industrial apple coolstore, to establish typical conditions and the extent to which positional variability is significant;

(5) use the data from (1) and (4) to assess existing coolstore component models for heat transfer and water vapour transport, and where necessary develop new ones to improve accuracy;

(6) implement the new, improved, or existing component models as appropriate into a computer model of heat transfer and water vapour transport in coolstores;

(7) validate the overall model by comparing predictions with measured data from an industrial apple coolstore.

Although the overall coolstore model will be developed in the context of apple coolstores, because the component models should preferably be mechanistic in nature, it is expected that the overall model will be generally applicable requiring only appropriate input data for application to other products.

CHAPTER 4: MEASUREMENTS OF APPLE COOLING RATE

Measurements of apple cooling rates were undertaken in both forced air pre-coolers and bulk-stacked pallets within an industrial coolstore, and within test facilities at Massey University. The former provided a database on cooling within industrial coolstores, whilst the latter provided higher quality data for model formulation and testing to aid in the development of an appropriate model for apple cooling.

4.1 INDUSTRIAL PRE-COOLING TRIALS

Practical constraints meant that large numbers of coolstores could not be studied. Most of the industrial data were measured in a single coolstore. That chosen was located in the NZAPMB's Whakatu depot in Hawkes Bay. Figure 4.1 shows plan and cross-sectional views. The store was built in 1988 and has floor dimensions of 60 m by 60 m with a peaked roof between 8 m and 11 m high. Walls and roof had a sheet steel exterior (supported by a steel portal frame) onto which 50 mm polyurethane foam insulation had been sprayed on the walls and 65 mm on the ceiling. The floor was 150 mm thick concrete without insulation. Two manually operated main doors (3.7 m high by 2.8 m wide) opened from an outside area and were unprotected. Two personnel doors were seldom used.

The coolstore had four sets of pump-circulated ammonia air cooling coils located behind a false wall at one end. Associated with each coil set was a two speed fan drawing air from the coolstore. Fans 1 and 4 discharged into the immediate vicinity of the coils, through two 300 mm high by 22.5 m wide horizontal slots. Fans 2 and 3 discharged into a 3.3 m high by 4.2 m wide tapered central duct. There were a number of discharge points along the length of the duct. The fans were operated on high speed (37.5 m^3/s) during pre-cooling, and low speed (22.5 m^3/s) otherwise. Sequential water defrosting of each coil was performed daily. Air temperature was controlled by evaporator pressure regulating valves on each coil. If pre-cooling was being performed air-off temperature was the controlled variable, otherwise air-on temperature was controlled.

The coolstore had the capacity to store 3760 tonnes of apples at 0.0 ±0.5°C and was operated for about six months each year starting mid-February. All fruit was handled as pallets of fifty 20 kg cartons (18.5 kg of fruit, 1.5 kg of cardboard packaging). The cartons were of the telescopic box and lid type, constructed from corrugated cardboard, and had one 80 mm by 40 mm handhole/vent in each end (Figure 4.2). Apples were supported on between 4 and 6 cardboard trays within the cartons, depending on apple size. The cartons were hand stacked on the pallets as shown in Figure 4.3. Carton orientation was alternated between layers to provide greater pallet stability. Pallets were stacked three high in bulk storage.

Early in the season apples were cooled in pre-coolers. Pre-coolers were created by placing 2 rows of pallets, 2 high, on either side of the fan intakes (Figure 4.4). An in-line configuration of pallets in the pre-cooling stack was traditionally used, with pallets positioned within each pre-cooler by forklifts. A curtain was used to create a central plenum so that return air from the bulk storage areas was drawn through the pallets before passing through the coils. Each pre-cooler cooled 96 pallets of fruit from about 18°C to about 5°C, depending on the length of the pre-cooling cycle which ranged from 8 to 24 hours. Usually during each working day, pallets in the previous days pre-cooler stacks were moved into bulk storage positions between about 6.00 am and 9.00 am, and new stacks of pallets were then assembled. Stack assembly time depended on the flow of fruit into the storage facility from growers orchards and ranged from about 2 hours to about 10 hours. Pre-coolers were started as soon as the stacks were completed.

A series of measurements of apple cooling rates during pre-cooling with both the traditional in-line and an alternative staggered pallet configuration (Figure 4.4) were made during the 1990 and 1991 seasons. The objective in 1990 was to identify the effect of carton position within in-line configurations on cooling rate. The work performed in 1991 aimed to further assess positional variation and to compare cooling rates for the staggered and in-line pallet configurations.

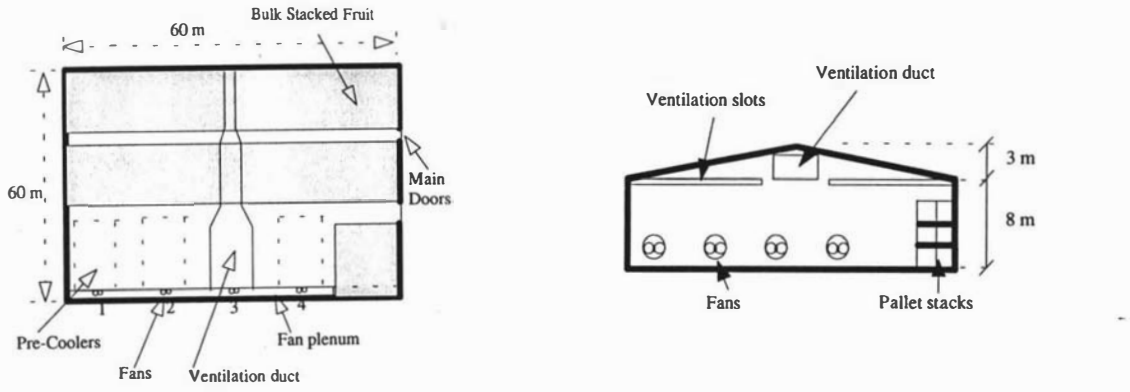

Figure 4.1: Plan and cross-sectional views of the apple coolstore used for most of the industrial scale measurements (not to scale).

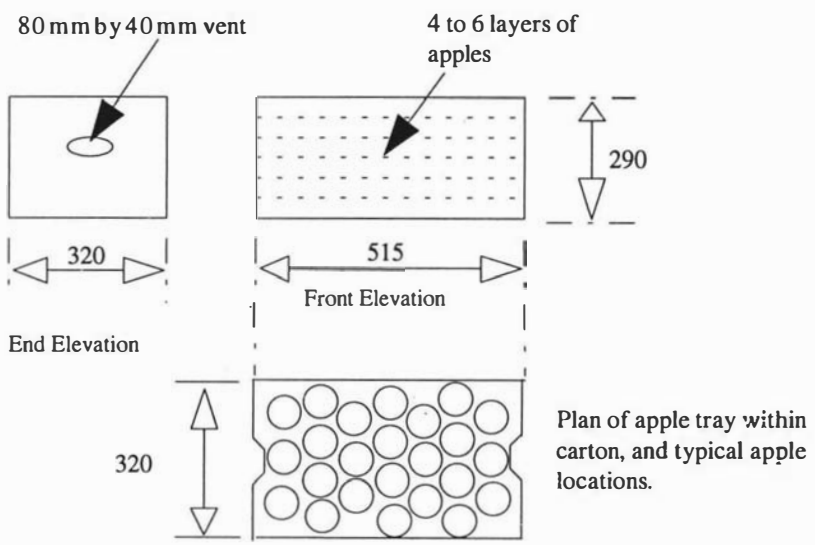

Figure 4.2: Plan and elevation views of a New Zealand export apple carton and fibreboard tray for apple support within the carton (not to scale).

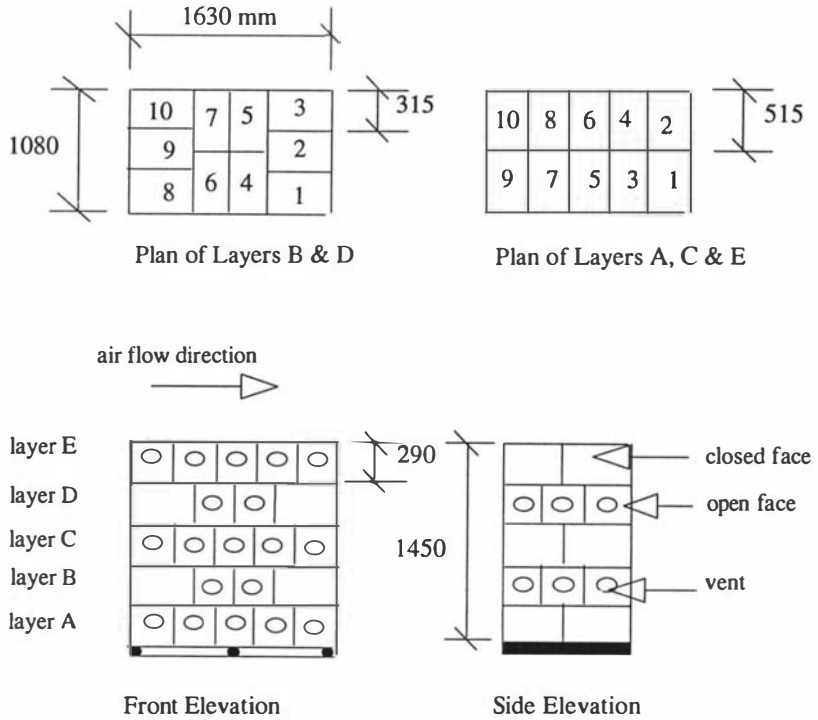

Figure 4.3: Apple carton arrangement on a typical export pallet, showing numbering system used for carton positions in experiments and approximate dimensions in mm (not to scale).

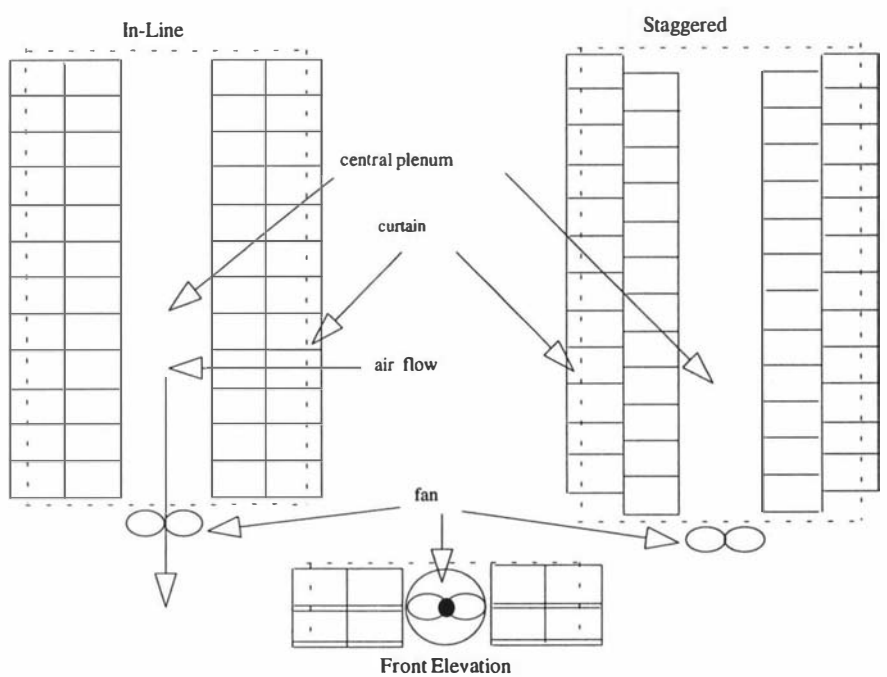

Figure 4.4: Plan view and front elevation of in-line and staggered pallet stacking arrangements used in industrial apple pre-coolers.

4.1.1 Methodology

Measurements of air and fruit temperatures, air velocities, air relative humidities (RH) and apple weight loss were made during the pre-cooling trials. Equipment used to measure these parameters included (with expected accuracy in brackets):

(1) Temperature: Type 'T' thermocouples (± 0.5°C), PT100 resistance probes (± 0.25°C), and thermistors (± 0.2°C) all calibrated with ice points. Thermocouples were used mainly for measuring product temperatures and air temperatures in cartons, thermistors and PT100's mainly for air temperatures.

(2) RH: Vaisala HMP113Y and Grant VH-L capacitance sensors calibrated with saturated salt solutions (± 3% RH), Michell Series 3000 dew point meter factory calibrated (± 0.3°C dew point).

(3) Air Velocity: Dantec 54N50 hot wire anemometer, calibrated in a boundary layer wind tunnel (0 to 5.0 m/s ± 0.02 m/s), Air Instruments Resources Ltd microanemometer with pitot tube, for pressure and velocity (0-70 m/s ±0.07 m/s).

(4) Weight: Metler PJ3600 balance (± 0.1g).

Dataloggers used to record temperature and RH throughout trials included:

(1) Campbell Scientific 21X 16 channel micrologger with two 32 channel multiplexers giving 78 single ended channels (thermocouple measurements).
(2) Two 16 channel Grant Squirrel dataloggers, (the first fitted with 16 thermistor channels and 2 RH channels, the second fitted with 16 thermocouple channels)
(3) Twenty single channel Delphi dataloggers fitted with PT100 temperature sensors.

During initial trials apple centre, apple surface and air temperature surrounding each apple were measured. Surface temperature was measured by inserting thermocouples immediately below the skin of each fruit. Results showed that cooling proceeded sufficiently slowly that there was little difference between centre and surface temperatures (i.e. low Biot number conditions), so in later trials only apple centre temperatures were recorded. Air temperature entering and leaving the pre-cooling stack was also measured for each trial. Apple weight loss was measured to within 0.1 g by weighing apples before and after each trial. Relative humidity was measured during some of the trials both for air entering and leaving the stacks and within cartons of apples. For some trials air velocity profiles were measured vertically down the outside and inside of the stacks, both between cartons on pallets and between pallets. Each of the trial runs was carried out over 10 to 24 hours depending on the operation of the pre-coolers within the coolstore at the particular time.

4.1.2 Experimental Design

4.1.2.1 1990 Trials

The following carton positional factors were investigated in the 1990 trial (coding level used in brackets {}):

(A) row of the pallet stack (inside {-1} or outside {+1});

(B) pallet position within the stack (bottom {-1} or top {+1});

(C) carton position within the pallet (plenum {-1} or bulk store side {+1});

(D) carton orientation on the pallet (closed face {-1} or open {+1}, Figure 4.3);

(E) pallet position along the length of the pre-cooler (fan end {-1}, middle {0} or curtain end {+1}).

A half-factorial design (Draper and Smith, 1981) for the four 2 level factors was used for each of the 3 levels of factor (E), giving a total of 24 combinations (Table 4.1). The half-factorial experiment was chosen so that the main factor and two factor interactions were aliased with higher order interactions.

The design was close to being orthogonal, with the cross-correlations of all main factor interactions and most two factor interactions, except those between factors AD and BC, AC and BD, and AB and CD, equal to 0. These non-zero two factor cross-correlations were not significant at the 95% level.

Limitations imposed by datalogging equipment meant that measurements were made on four separate pre-cooling stacks. Combinations recorded for each stack were selected randomly and were:

Stack A: 1, 2, 4, 6, 8, 11;

Stack B: 5, 14, 17, 19, 22, 23;

Stack C: 3, 9, 12, 15, 20, 21;

Stack D: 7, 10, 13, 16, 18, 24.

Measurements were made on apples in a standard position for each carton to minimise variation in cooling rates related to fruit position within the carton. The apple position chosen was adjacent to the exposed vent.

4.1.2.2 1991 Trials

The experiments in 1991 aimed to further assess positional variation within the pre-cooling stacks (location within cartons as well as carton position within stacks), and to compare staggered and in-line pallet configurations (Figure 4.4).

The positional factors investigated were (coding level used in brackets {}):

(A) row of the pallet stack (inside {-1} or outside {+1});

(B) pallet position within the stack (bottom {-1} or top {+1});

(C) carton position within the pallet (plenum side {-1}, middle {0} or bulk store side {+1});

(D) tray layer within the carton (5 layers in cartons, bottom layer {-2}, middle layer {0}, top layer {+2});

(E) pallet position along the length of the pre-cooler (fan end, {-1}, middle, {0}, and curtain end, {+1}).

Table 4.1

Measurement Positions and Results (half-cooling time, $t_{1/2}$, and percentage weight loss during pre-cooling) for 1990 Industrial Coolstore Apple Pre-Cooling Trials

Trial Number	Positional Factor Codes					$t_{1/2}$ (hours)	Weight Loss (%)
	A	B	C	D	E		
1	1	1	1	1	1	7.6	*
2	1	1	1	-1	-1	4.5	*
3	1	1	-1	1	-1	8.5	0.118
4	1	1	-1	-1	1	6.1	*
5	1	-1	1	1	-1	8.1	0.132
6	1	-1	1	-1	1	6.8	*
7	1	-1	-1	1	1	7.4	0.163
8	1	-1	-1	-1	-1	2.2	*
9	-1	1	1	1	-1	5.3	0.106
10	-1	1	1	-1	1	5	0.095
11	-1	1	-1	1	1	2.1	*
12	-1	1	-1	-1	-1	16.2	0.182
13	-1	-1	1	1	1	4.3	0.102
14	-1	-1	1	-1	-1	4.3	0.084
15	-1	-1	-1	1	-1	15	0.135
16	-1	-1	-1	-1	1	32	0.111
17	1	1	1	1	0	3.9	0.074
18	1	1	-1	-1	0	2.9	0.118
19	1	-1	1	-1	0	1.3	0.075
20	1	-1	-1	1	0	16.5	*
21	-1	1	1	-1	0	9.9	*
22	-1	1	-1	1	0	15.8	0.096
23	-1	-1	1	1	0	8.3	0.107
24	-1	-1	-1	-1	0	10.1	0.131

* = Missing value

Datalogging and logistical constraints prevented a standard experimental design being used. Apple positions within a tray were selected at random but identical apple, carton and pallet positions within both the staggered and in-line configurations were used to allow a paired comparison. Forty such paired measurements were made over 4 days. Details of each combination are given in Table 4.2. Trials 1 to 13 were made on day one, 14 to 22 on day two, 23 to 31 on day three, and 32 to 40 on day four. Analysis of the positional combinations selected showed no significant cross-correlation between any of the above factors and their linear or quadratic combinations at the 95% level.

4.1.2 Results

Figure 4.5 shows typical measured data for an apple centre temperature and air entering the stack. Figure 4.6 shows typical measured temperature and RH through a pre-cooling stack. Apple temperature data was normalised by calculating the fractional unaccomplished temperature change at time t (Y):

$$Y = \frac{T_{ap,t} - T_{ap,\infty}}{T_{ap,init} - T_{ap,\infty}} \tag{4.1}$$

where: $T_{ap,t}$ = apple temperature (°C) at time t .

$T_{ap,init}$ = initial apple temperature (°C).

$T_{ap,\infty}$ = expected apple temperature (°C) at equilibrium.

Cooling rates were expressed as half-cooling times calculated from the slope of the ln(Y) versus t plot (Pflug and Blaisdell, 1963):

$$t_{1/2} = \frac{-0.693}{\frac{d\ \ln(Y)}{dt}} \tag{4.2}$$

where: $t_{1/2}$ = half cooling time (hours).

t = time (s).

Table 4.2

Measurement Positions and Results (half-cooling time, $t_{1/2}$, and percentage weight loss during pre-cooling) for 1991 Industrial Store Apple Pre-Cooling Trials.

Trial Number	Factor Code					$t_{1/2}$ (hours)	$t_{1/2}$ (hours)	% Weight Loss	% Weight Loss
	A	B	C	D	E	(Staggered)	(In-Line)	(Staggered)	(In-Line)
1	-1	1	-1	-2	0	2.5	4.5	0.167	0.094
2	1	1	0	-1	-1	2.6	8.7	0.113	0.214
3	-1	-1	0	0	-1	6.8	6.6	0.177	0.184
4	1	1	1	1	0	2.6	5.1	0.136	0.116
5	-1	1	-1	2	0	7.6	6.5	0.054	0.106
6	-1	-1	0	-1	1	4.9	11.2	*	0.145
7	1	-1	-1	0	0	1.7	2.6	0.088	0.135
8	1	-1	1	2	-1	2.6	2.4	*	*
9	1	1	-1	-1	1	3.6	4.9	*	0.088
10	1	-1	1	2	0	2.8	3.9	0.125	0.136
11	-1	-1	0	0	0	7.1	3.9	0.388	0.042
12	1	1	-1	-2	1	2.5	5	*	0.209
13	-1	-1	0	1	-1	7.8	13.7	0.17	0.252
14	-1	1	-1	-1	-1	3.2	4.9	0.213	0.227
15	1	1	0	2	-1	7.2	11.6	0.138	0.211
16	1	-1	0	0	0	8.7	13.1	*	0.317
17	1	-1	1	-2	1	10.6	9.3	0.08	0.154
18	-1	-1	-1	1	1	8.5	17.7	0.244	0.085
19	-1	1	-1	2	0	5.2	8.6	0.121	0.152
20	-1	-1	0	0	0	13.7	10	0.121	0.144
21	-1	-1	0	-2	1	7.6	8.7	0.069	0.057
22	-1	1	-1	1	0	4.1	7.7	0.107	0.033
23	-1	-1	0	-2	-1	5.6	13.9	0.068	0.085
24	1	-1	0	-1	1	6.9	6.7	0.068	0.35
25	1	-1	1	1	-1	5.1	5.1	0.129	0.023
26	1	1	1	0	0	2.8	5.2	0.035	0.012
27	-1	1	0	2	-1	5.5	9.6	0.023	0.089
28	1	-1	0	0	0	2.7	7.4	0.107	0.072
29	1	-1	1	-2	0	2.3	3.9	0.118	0.132
30	1	-1	1	2	0	2.9	4.4	0.137	0.118
31	1	-1	0	0	0	3.7	5.1	0.131	0.101
32	-1	-1	0	-1	1	2.8	8.9	0.117	0.168
33	1	1	0	0	-1	8.2	4.1	0.138	0.103
34	1	-1	0	-2	0	5	6.3	0.108	0.074
35	1	1	-1	1	0	2.0	8.6	0.103	0.15
36	1	1	1	-2	0	3.5	5.0	0.11	0.091
37	1	-1	-1	1	1	4.4	3.2	0.122	0.085
38	-1	1	-1	0	0	5.5	15.3	0.128	0.158
39	-1	-1	1	2	-1	2.8	4.2	0.098	0.046
40	-1	1	0	0	0	15.2	4.4	0.173	0.066

* = missing value.

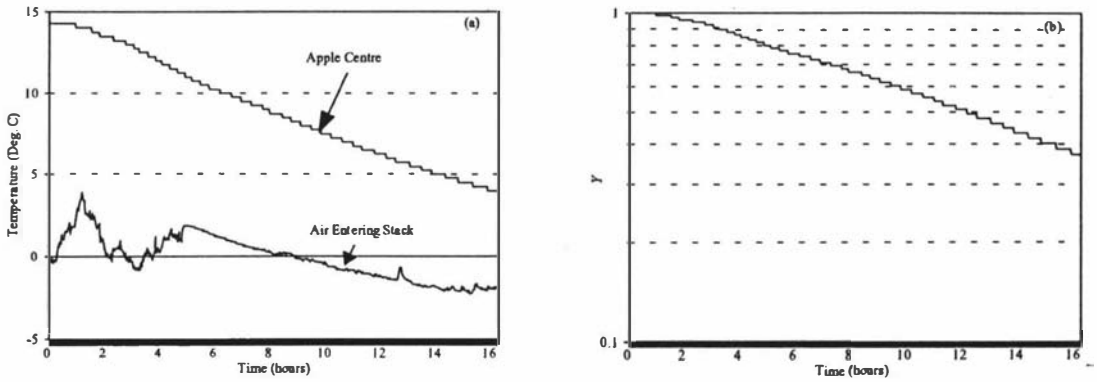

Figure 4.5: Typical measured data in the industrial pre-coolers for (a) apple centre and air temperatures and (b) fractional unaccomplished temperature change (Y) for apple centre.

Mean air temperature entering the pre-cooling stack from the rest of the coolstore was used as an estimate of the expected equilibrium apple temperature. There was slight curvature of the ln(Y) versus time relationship in some of the data. This was probably due to both air temperature rising though the stacks and bulk coolstore air temperature varying with time as activities within the rest of the store changed. The temperature rise of air as it passed through the stack was as high as 8°C at the start of pre-cooling, declining to about 2°C to 3° C at the end of most measurement periods. Coolstore air temperature generally varied by less then 2°C from its mean value and usually declined by about 1°C on average over the measurement period, (due to the air-off temperature control system operating in the coolstore during pre-cooling). The slope of the ln(Y) versus time plot used in Eqn. 4.2 was calculated for Y values between 0.8 and 0.2 (or the lowest Y value measured if 0.2 was not reached). The results for all the 1990 and 1991 pre-cooling trials are presented in Tables 4.1 and 4.2, respectively.

Step-wise linear regression analysis (Draper and Smith, 1981) was carried out on the data to assess the significance of positional factors. Terms used included linear combinations for two level factors and quadratic combinations for three level factors. None of the positional factors studied were found to have significant effects on cooling

rate or weight loss. Half cooling times for each stacking configuration were found to closely fit log-normal distributions. Figures 4.7 and 4.8 give frequency histograms of the natural logarithm of the half-cooling times for the in-line and staggered stacking configurations, respectively.

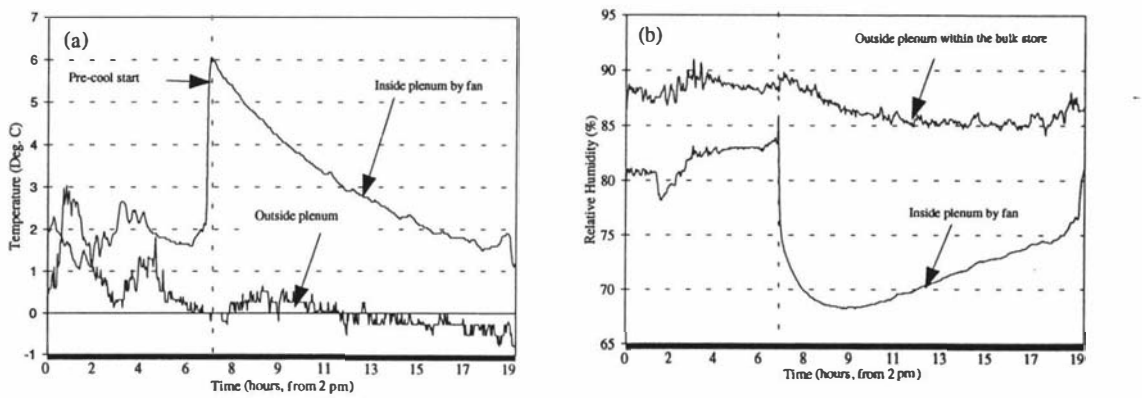

Figure 4.6: Typical measured data for (a) air temperature and (b) relative humidity, both outside the pre-cooling stack within the bulk coolstore and within the pre-cooling plenum during an industrial pre-cooling cycle.

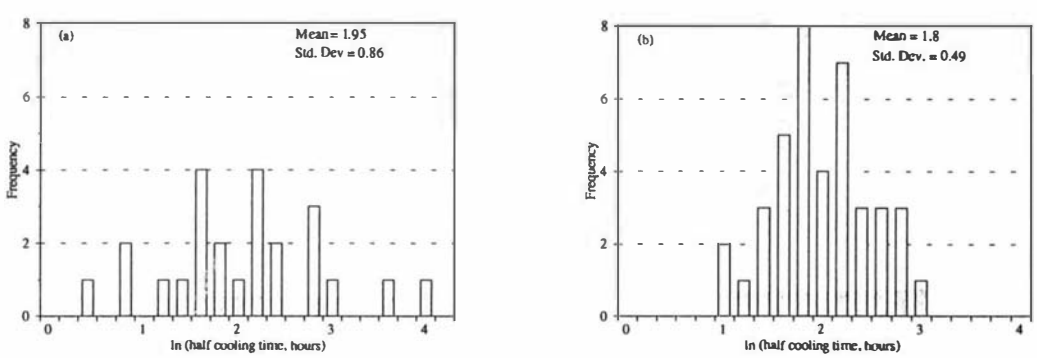

Figure 4.7: Distribution of half cooling times for the in-line stacking configuration, (a) 1990 data, (b) 1991 data.

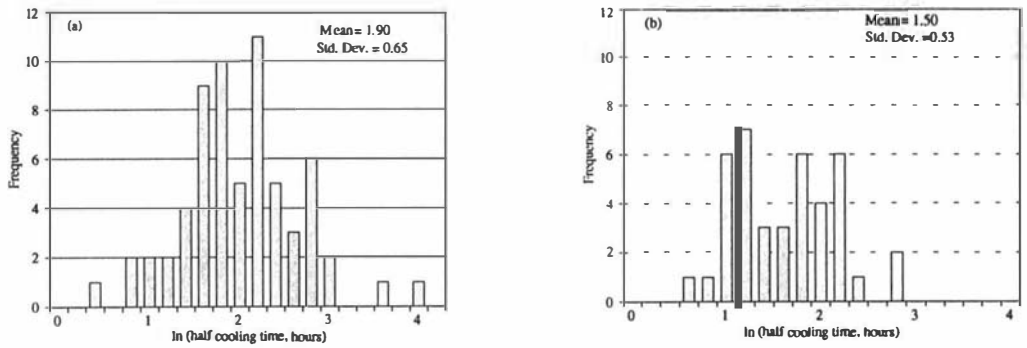

Figure 4.8: Distribution of half cooling times for different pallet stacking configurations, (a) in-line (combined 1990 and 1991 data), (b) staggered.

The mean half-cooling times and the 95% confidence intervals are given in Table 4.3. Half-cooling time was 2 hours (30%) less on average for the staggered configuration than for the in-line configuration (this difference is significant at the 99% level, using a paired t-test). Mean weight loss values are also given in Table 4.3.

Table 4.3

Cooling Rates and Weight Loss During Industrial Apple Pre-Cooling Trials

(logarithmic distribution assumed for cooling rates)

Stacking Configuration	Mean $t_{1/2}$ (hours)	95 % Confidence Interval		Average Weight Loss (%)
		Minimum $t_{1/2}$ (hours)	Maximum $t_{1/2}$ (hours)	
In-Line 1990	7.0	1.3	39	0.114
In-Line 1991	6.5	2.5	17.1	0.128
In-Line Combined	6.7	1.8	24.5	0.119
Staggered 1991	4.5	1.6	12.9	0.126

4.1.3 Discussion

There are three possible routes for air flow through pre-cooling stacks of packaged produce on pallets: through the product container, between containers on a pallet and between pallets. Optimum pre-cooler design would result in a high proportion of the air flowing through the containers, as this would lead to the fastest cooling rate. Ventilation between containers on a pallet is the next best alternative and air flow between pallets is the least desirable if cooling rate is to be maximised.

Vent area, shape and position of the container influence container ventilation (Parsons *et al.*, 1972; Arifin & Chau, 1988; Haas & Felsenstein, 1985; Watkins, 1990). The apple carton used had single vents of only 3% of the carton face area. Not all cartons had this vent exposed to the direction of air flow and within pallets alignment of vents did not always occur. In addition, gaps between cartons on the pallet were large (averaging 8% of the pallet cross-sectional area). This latter gap size was highly variable from pallet to pallet due to the imprecise placement of cartons on pallets. Gaps between pallets were relatively large (10% of stack cross-sectional area on average). The inter-pallet gaps were also highly variable in size due to both the uneven nature of the carton placement on pallets and the placement of pallets into the stacks by forklifts. Figures 4.9 and 4.10 illustrate the variability encountered in the pre-cooling stacks. The net effect was that air flow through the apple cartons was both low in magnitude and highly variable with most of the air passing around cartons or around pallets.

Figure 4.9: An example of reasonably well-placed pallets within an industrial apple pre-cooling stack.

Figure 4.10: An example of poorly placed pallets within an industrial apple pre-cooling stack.

Figure 4.11 shows the variation in measured air velocities between cartons on pallets and between pallets within a stack, using the natural log of air velocity to normalise the data. The large variation in air ventilation through the pre-cooling stack is considered to be the main reason for the large variation in measured apple cooling rates (Table 4.3). Variation in cooling rate related to this random variation in ventilation was almost certainly responsible for the inability to establish the effects of the positional factors studied.

The faster mean cooling rate for the staggered compared with the in-line configuration was attributed to reduced air bypass around the pallets and therefore greater ventilation through and around the cartons on each pallet. Staggering the stacks eliminated the direct alignment of gaps to the central plenum between pallets evident with the in-line arrangement. Variation of carton placement on pallets and pallet placement within the stacks was similar for both configurations. Thus although carton ventilation would be improved by the staggered arrangement it would still be highly variable.

General principles to optimise forced air pre-cooling of bulk stacked packaged products are to design packaging to allow: a high percentage of vents, good alignment of vents, and tight and precise assembly of containers onto pallets. If high levels of container ventilation are not possible then containers should be spaced on pallets to allow air flow between them. Close positioning of pallets to minimise gaps between them is also important (Amos *et al.*, 1993).

Weight loss results showed no significant difference between the two stacking configurations and were not correlated with half cooling times. However, this may have been due to practical constraints imposed when measuring the weight loss. Precooling stacks took up to ten hours to construct. Pallets with logged cartons may have been sitting within the precooling stack anywhere from 5 minutes to ten hours. It was only possible to weigh apples before the pre-cooling stacks were constructed and again at the completion of pre-cooling once the stacks were disassembled. This meant it was not possible to isolate the weight loss during pre-cooling from the weight loss during stack set-up.

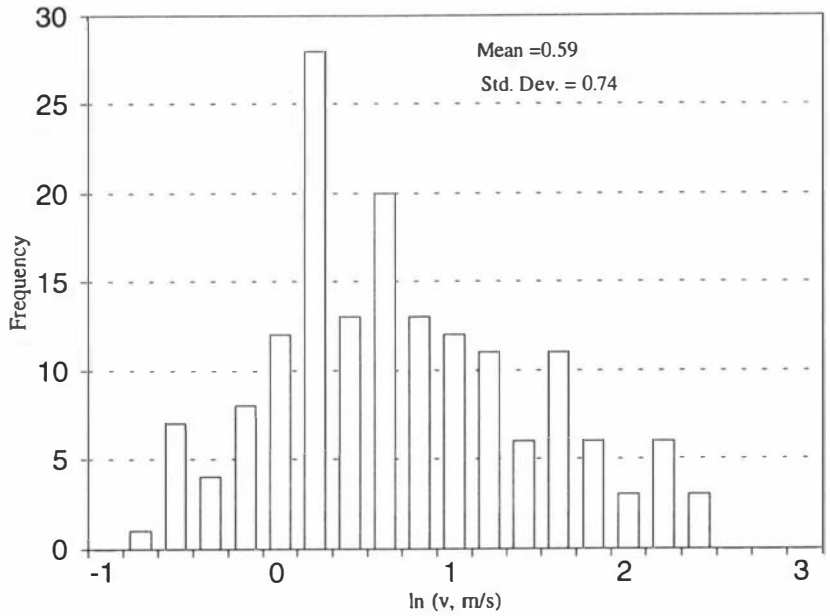

Figure 4.11: Distribution of measured air velocities through the staggered apple pre-cooling stack.

For this reason, it would be desirable in future work to have control cartons in which the weight loss during stack set-up could be measured, thereby allowing pre-cooling weight loss to be estimated.

4.2 MEASUREMENTS OF APPLE COOLING RATES IN BULK STORAGE

Measurements of the rate of apple cooling within the bulk store were also made. Operational constraints and datalogging limitations prevented a formal experimental design and limited the number of measurements possible to three trials. For each of these, apple and air temperatures were measured in a range of carton positions within a single pallet placed in the bulk store.

4.2.1 Trial One

Two apple centre temperatures in each of six cartons were measured during this trial. The apple positions were the same in each carton. One was adjacent to the exposed air vent and the other was adjacent to the air vent at the inside of the pallet. The carton positions on the pallet were C1, C2, C5, C6, C9, and C10 (Figure 4.3). In addition, air

temperatures were measured around the exposed faces and inside faces for each of the cartons. The pallet was placed in the bulk store (position 1, Figure 4.12) and left for 7 days. Temperatures were logged at 10 minute intervals. The pallet was not surrounded by other pallets within the store, and the coolstore was half full of fruit.

Each of the six cartons tested showed similar rates of cooling, indicating similar ventilation rates into each carton. Figure 4.13 shows the results for the carton in position C1. Half cooling times, calculated using the mean air temperature close to the pallet as the equilibrium temperature, ranged from 12 to 18 hours.

4.2.2 Trial Two

Temperatures at the centre of each of 3 apples were measured in each of three cartons during this trial. Apple positions chosen were adjacent to the outside and inside vents and at the centre of the carton on the same layer as the vents. Carton positions used were C1, C5, and C9. Air temperatures around the outside and at the centre of the pallet were also measured. The pallet was placed at position 2 (Figure 4.12) and was kept isolated from other pallets for seven days, although the coolstore was nearly full of fruit during this trial.

The three cartons showed similar apple cooling trends. Figure 4.14 presents the data for the carton at position C1 on the pallet. Half cooling times, calculated using the mean air temperature close to the pallet as the equilibrium temperature ranged from 12 to 36 hours.

4.2.3 Trial Three

Two apple centre temperatures were measured in each of three cartons during this trial. Apple positions were adjacent to each of the vents. Carton positions used were C1, C5, and C9. Air temperatures around the outside and at the centre of the pallet were also measured. The pallet was placed at position 3 (Figure 4.12) where it was surrounded by other pallets containing warm fruit and left for five days.

The three cartons showed similar trends. Figure 4.15 presents the data for the carton at position C5 on the pallet. Half cooling times, calculated using the mean air temperature close to the pallet as the equilibrium temperature ranged, from 12 to 30 hours.

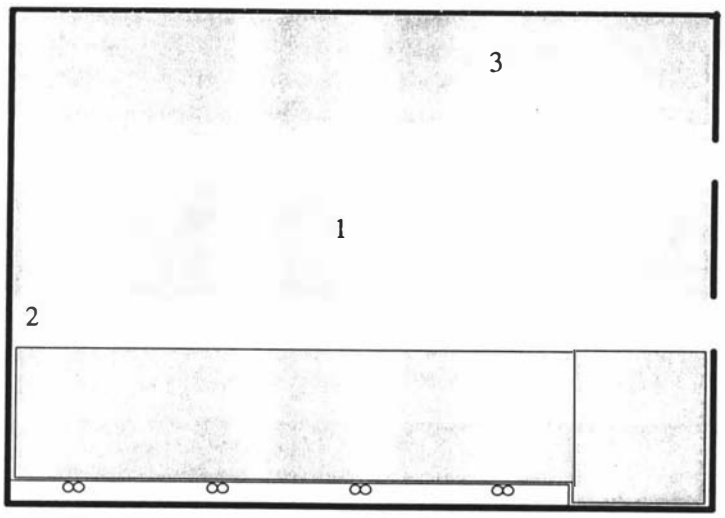

Figure 4.12: Pallet positions within the industrial coolstore used for measurements of apple cooling rates in bulk storage.

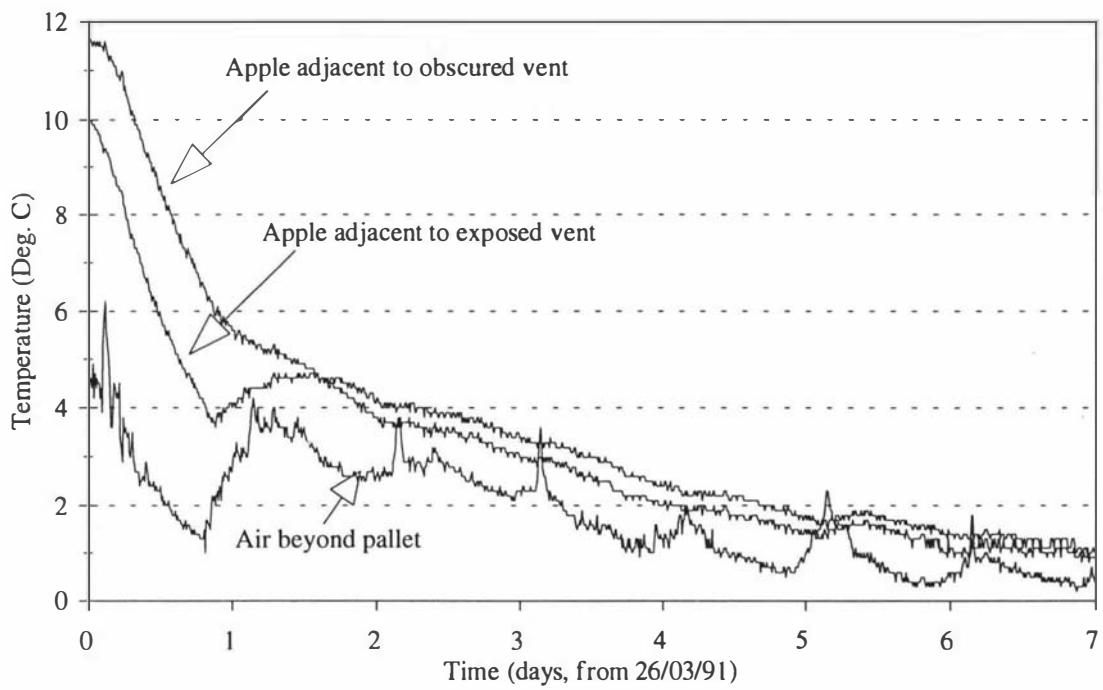

Figure 4.13: Measured air and apple temperatures for a carton at position C1 on a pallet cooled within the industrial coolstore, when the coolstore was half full (pallet isolated from other pallets, trial one).

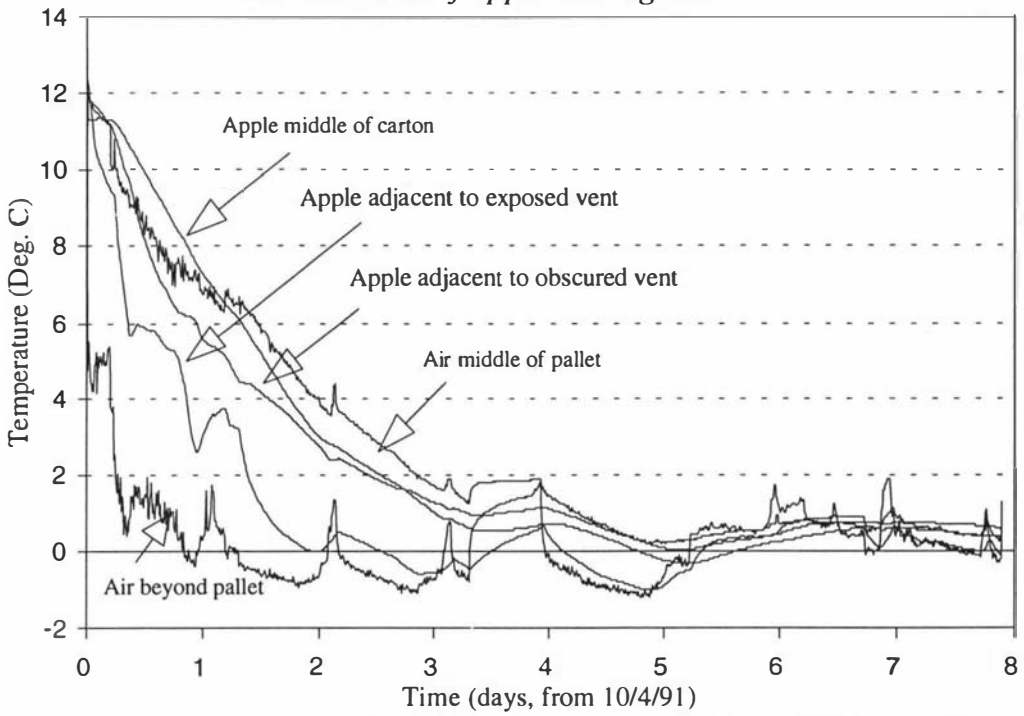

Figure 4.14: Measured air and apple temperatures for a carton at position C1 on a pallet cooled within the industrial coolstore, when the coolstore was nearly full (pallet isolated from other pallets, trial two).

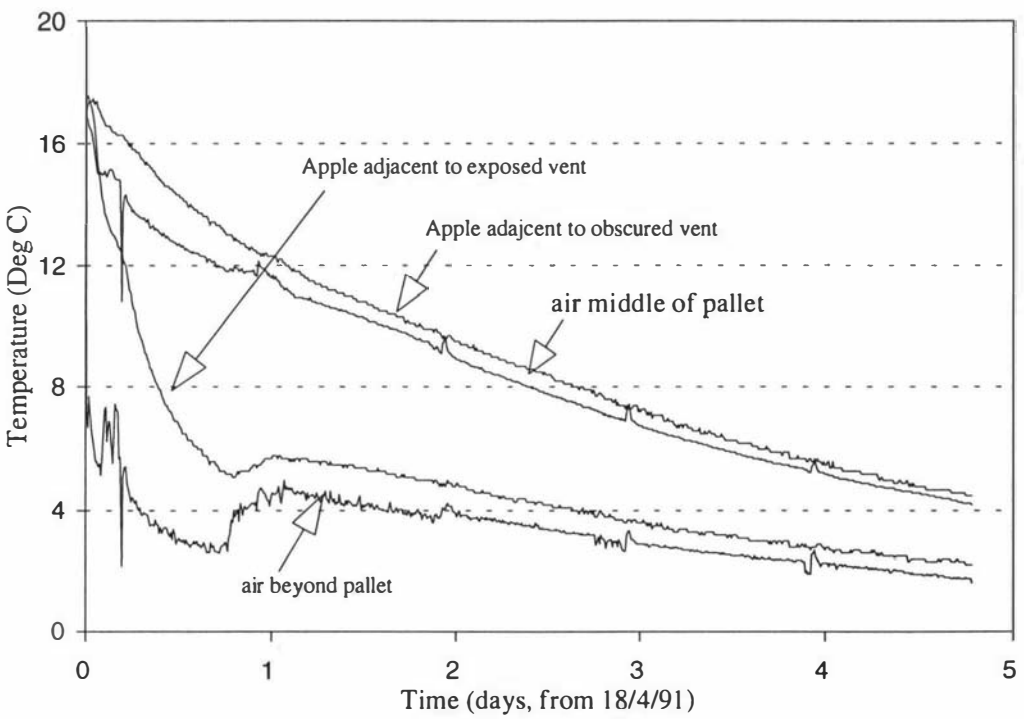

Figure 4.15: Measured air and apple temperatures for a carton at position C1 on a pallet cooled within the industrial coolstore, when the coolstore was nearly full (pallet surrounded by other pallets, trial three).

4.2.4 Discussion

Each of the three bulk stacked cooling trials gave similar results. The measured cooling rates were slower than the mean rates of cooling measured in the pre-cooling trials. Cooling rates in pallets fully exposed in the coolstore only half full of fruit showed a smaller range of half-cooling times (12 to 18 hours) compared to pallets surrounded by other pallets (12 to 30 hours) or exposed within the coolstore when it was nearly full of fruit (12 to 36 hours). These differences are probably due to reduced ventilation potential in the latter two trials. The variation in ventilation is most likely to be a result of different pallet assembly and pallet location within the coolstore. Cartons within each pallet showed small variations in cooling rate, indicating that the ventilation potential for each carton was similar for each trial.

4.3 CARTON COOLING TRIALS

Cooling rates measured in the pre-cooling trials within the industrial coolstore were highly variable and no positional factor studied was found to be significant. Thus limited information with respect to differences in cooling rate with position within cartons was obtained. The results did suggest that cartons are the most important product unit that needs to be considered to study apple cooling in a mechanistic way. It was considered likely that positional variations within cartons accounted for some of the observed variation in cooling rate. Therefore a more detailed investigation of heat transfer in cartons was undertaken.

A series of experiments were carried out in which the rate of apple cooling within export cartons was measured under controlled conditions. These experiments aimed to provide data which could be used in the development and testing of a mechanistic apple cooling model. The trials were performed in environmental test facilities at Massey University (Figure 4.16), in which controlled temperature (± 0.2°C) and uniform air velocity (0.5 to 5.0 m/s) could be achieved. All of the trials used cartons of "count" (number of fruit within the carton) 198 Royal Gala apples supplied by the NZAPMB. The fruit was divided into six layers within the carton, each supported on a cardboard tray (known as Friday trays).

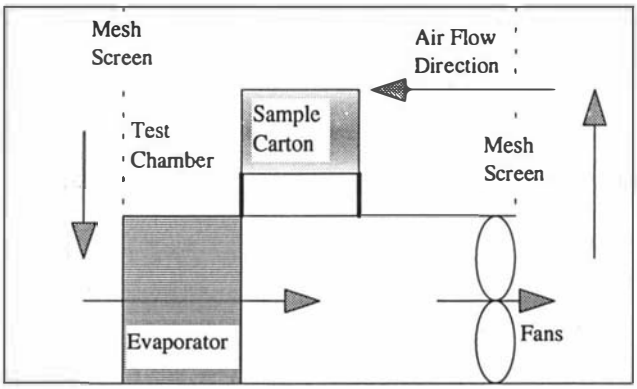

Figure 4.16: Schematic diagram of the controlled environmental test facility used for measurements of apple cooling rates within cartons (not to scale).

Within a carton a number of mechanisms of heat and mass transfer can occur including forced convection due to ventilation of air into the cartons through vents, natural convection of air within the carton if large temperature differences are present, evaporative cooling from the apple surfaces into the surrounding air, conduction within apples, conduction through exterior cartonboard, conduction from apples to Friday trays, convection from apple surfaces to the surrounding air and convection from air within each layer to the adjacent Friday trays.

Three sets of experiments were undertaken. The first of these eliminated ventilation so there was only natural convection within the carton and conduction through the exterior cardboard. The second set allowed forced convection through the carton vents but suppressed conduction through the exterior cardboard. The third set allowed all possible heat transfer pathways.

4.3.1 Cooling Without Ventilation

4.3.1.1 Methodology

The apple cartons were conditioned at 25°C in a controlled temperature room for 48 hours. Temperatures were recorded at a number of positions in all six layers of the

cartons. Figure 4.17 shows the measurement positions used. Not all of these positions were measured for every layer for each trial. In early trials both apple and air temperatures were logged for each position. However, apple temperatures were observed to be almost identical to air temperatures. Therefore in latter trials, mostly air temperatures were measured. Once the carton had been assembled, cardboard sections were taped into the vents, and the top and bottom slot of the cartons, to give a uniform cartonboard layer over the whole carton. All other openings into the carton were also taped to ensure that no ventilation of air into the carton could occur.

The carton was then placed inside a sealed polystyrene foam box with 100 mm thick walls, and left inside the controlled temperature room for a further 12 hours. The data logging equipment was also sealed inside an insulated box and left in the controlled temperature room. The time from removal of the carton from the 25°C room to when it was placed in the test facility was typically 10-20 minutes.

Measurements of temperature were made using 46 type 'T' thermocouples logged by the Campbell Scientific 21X datalogger, and 16 thermistors logged using a Grant Squirrel datalogger (as described in Section 4.1.1). It was found that the thermocouple reference panel of the Campbell Scientific 21X datalogger had some thermal lag, and did not respond quickly to the rapid change in ambient temperatures during transport from the 25°C room, causing incorrect temperature readings early in trials. Leaving the datalogging equipment in its insulated box eliminated this problem.

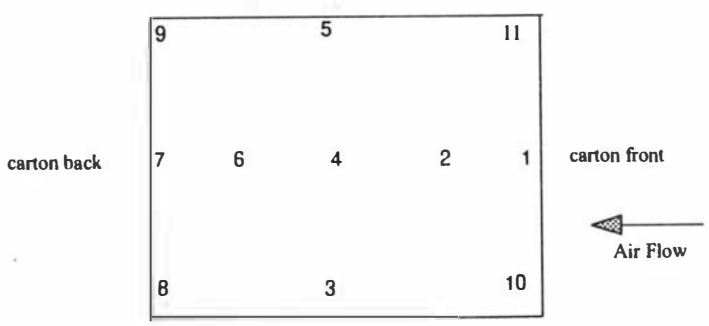

Figure 4.17: Measurement positions used for carton trials (all side thermocouples were located between 1 and 3 mm from the cardboard surface, and were held in place by taping the leads to the cardboard surface, centre thermocouples were evenly spaced down the centre of the carton).

The test facility (Figure 4.16) was run with a set point of 0°C and the cartons were placed within the facility once the air temperature had stabilised within the chamber. The cartons were placed upon a frame which elevated the carton within the chamber to enable air flow across all faces of the carton. The cartons were orientated so that the vents were aligned with the direction of air flow. The incident velocity was 1.7 m/s.

The cartons were left in the facility for approximately 24 hours, with the dataloggers recording data every 2 minutes. Four replicate trials were carried out using different cartons and apples for each one. The initial temperature lag of about 30 minutes on Figures 4.18 to 4.28 represents carton set-up before placement in the cooling tunnel.

4.3.1.2 Results and Discussion

The results for trial one are presented in Figures 4.18, 4.19, 4.20 and 4.21. Symmetric temperature distributions within the carton were observed:

i) Air temperatures generally showed symmetry down the length of the carton (positions 1,4 & 7); positions 1 and 7 cooled consistently faster than position 4, as would be expected given that positions 1 and 7 were in exterior zones and hence would have been cooling by conduction through the cartonboard, whereas position 4 was an interior zone and would have cooled predominantly by convection and conduction through the top and bottom Friday trays once a temperature difference had been established. Positions 1 and 7 cooled at a similar rate for all layers, except 3 and 6. These differences were considered to be due to be variation in thermocouple position within the carton rather than a real difference in cooling rate. The only likely causes of a real difference in cooling rate would be a difference in heat transfer coefficient (htc) through the cartonboard, or natural convection effects. A difference in the htc was unlikely given that the air velocity across both the front and back faces of the carton were similar. Also a real difference in the htc would be expected to cause a difference in cooling rate between positions 1 and 7 for all 6 layers. This was not observed. Similarly, non-symmetrical natural convection effects are unlikely as they too would probably have caused differences on all six layers, not just two as observed.

ii) There was symmetry across the carton (positions 10, 1, 11; 3, 4, 5; and 7, 8, 9). In all cases the centre position cooled at a significantly slower rate than the two positions nearer the outside of the carton.

iii) There was symmetry down the side faces of the carton (positions 10, 3, 8; and 11, 5, 9). Corner zones 10,11,8 and 9 showed similar rates of cooling, and cooled faster than positions 3 and 5 which are in the centre of the carton.

iv) Figure 4.20 shows that cooling is close to symmetrical vertically through the carton. As expected the top and bottom layers (1 & 6) cool faster than layers 2 and 5 which were in turn faster than the two centre-most layers (3 & 4).

These trends were evident in all four trials as shown by Figure 4.18. Repeatabilty between replicates was much better than in the industrial data.

Figure 4.21 shows data for the relative rates of cooling for both air and apple centre for several selected positions. These data are typical of trends found in this series of trials, and show that the apple cooling rates are very similar to the rate of carton air cooling. Because the cooling of the cartons as a whole in this series of trials was restricted to conduction through the cartonboard and natural convection and radiation within the carton, the resistance to heat transfer from the air within the carton to the bulk air surrounding the carton is high compared to the heat transfer resistance from the apples to the air within the carton. Hence the predominant use of air temperatures in some of the trials was justified.

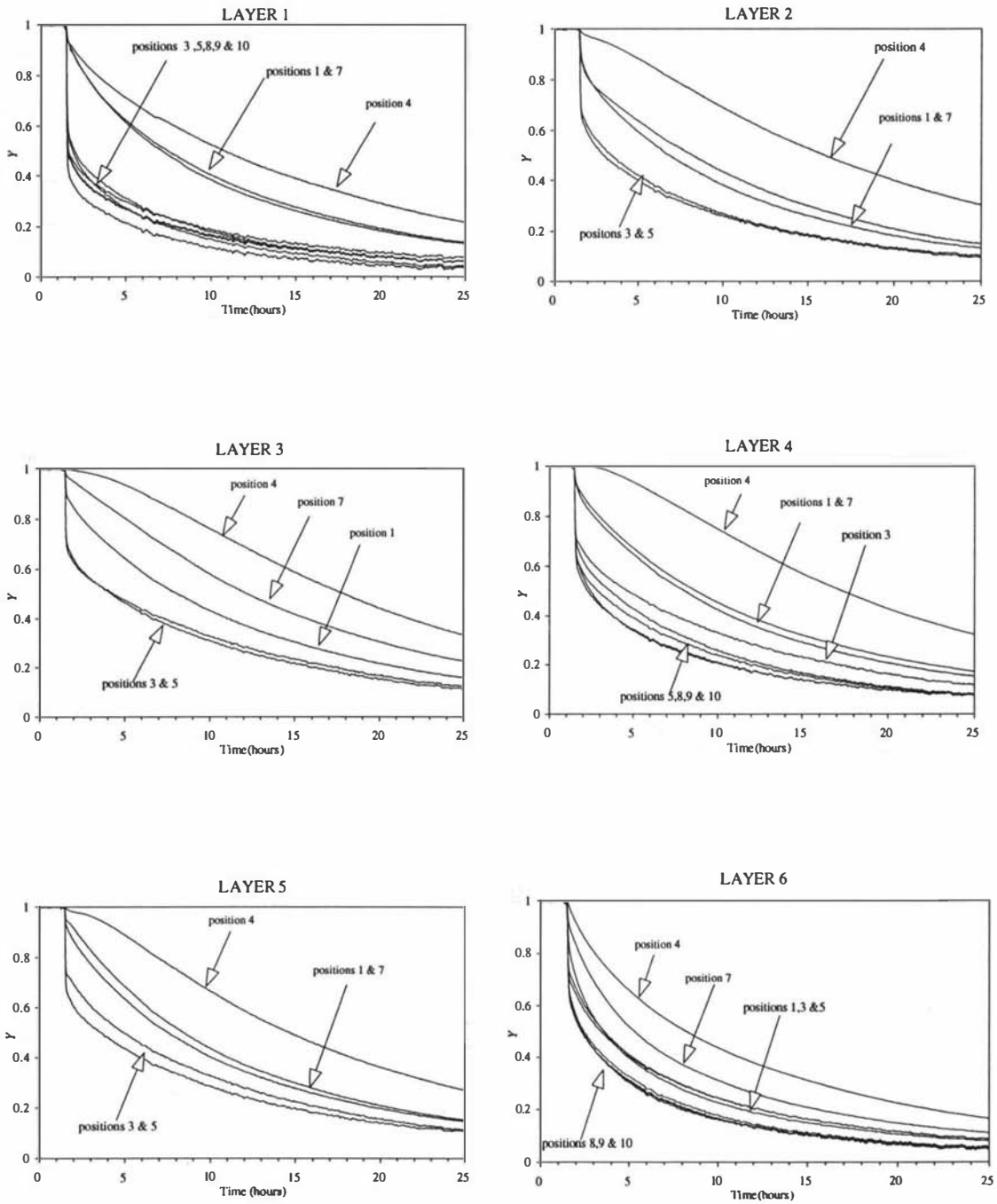

Figure 4.18: Measured fractional unaccomplished air temperatures for each layer of the apple carton during the first cooling without ventilation trial.

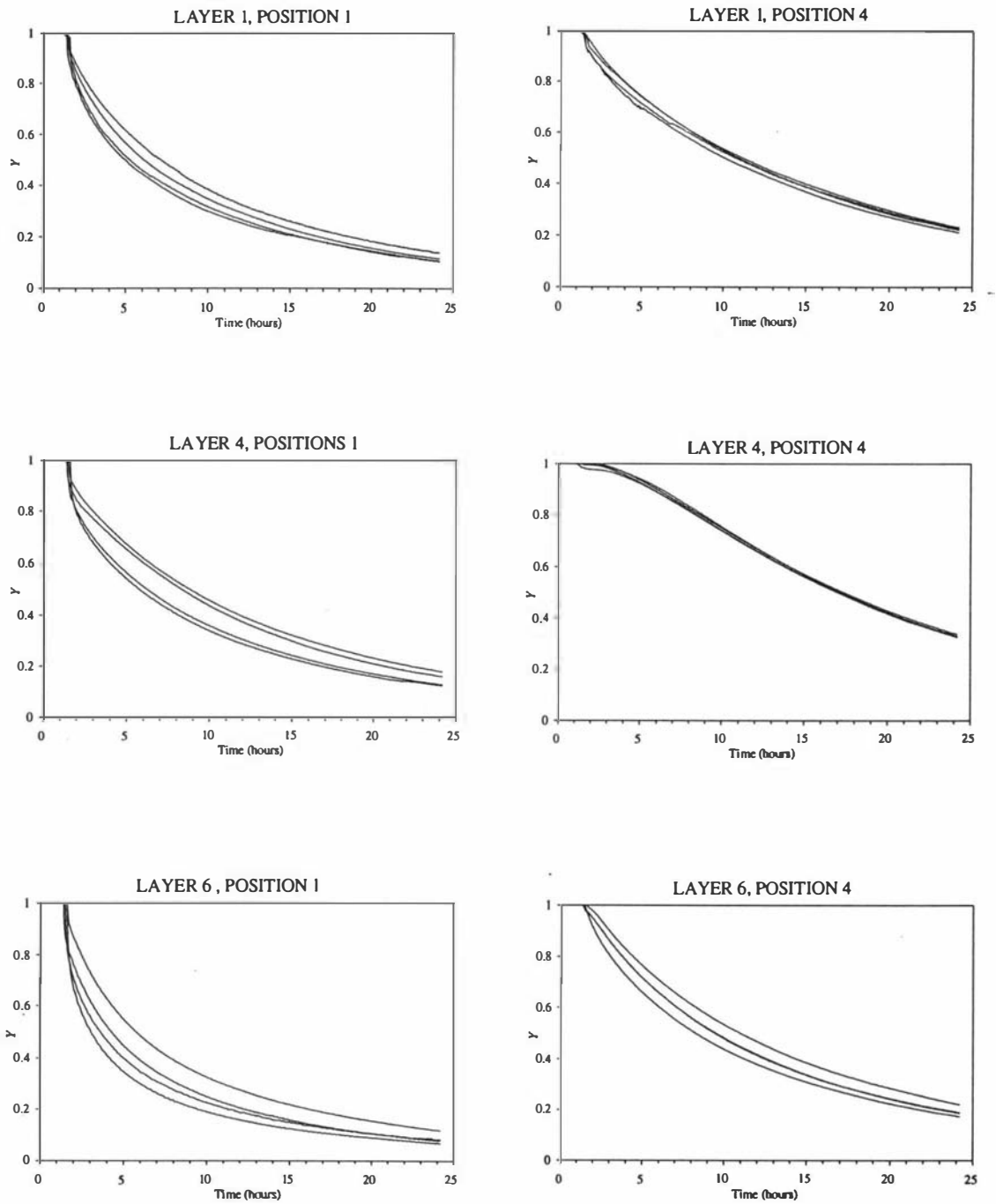

Figure 4.19: Measured fractional unaccomplished air temperature for positions 1 and 4 on layers 1, 4 and 6 of the cartons, for the four replicate cooling without ventilation trials.

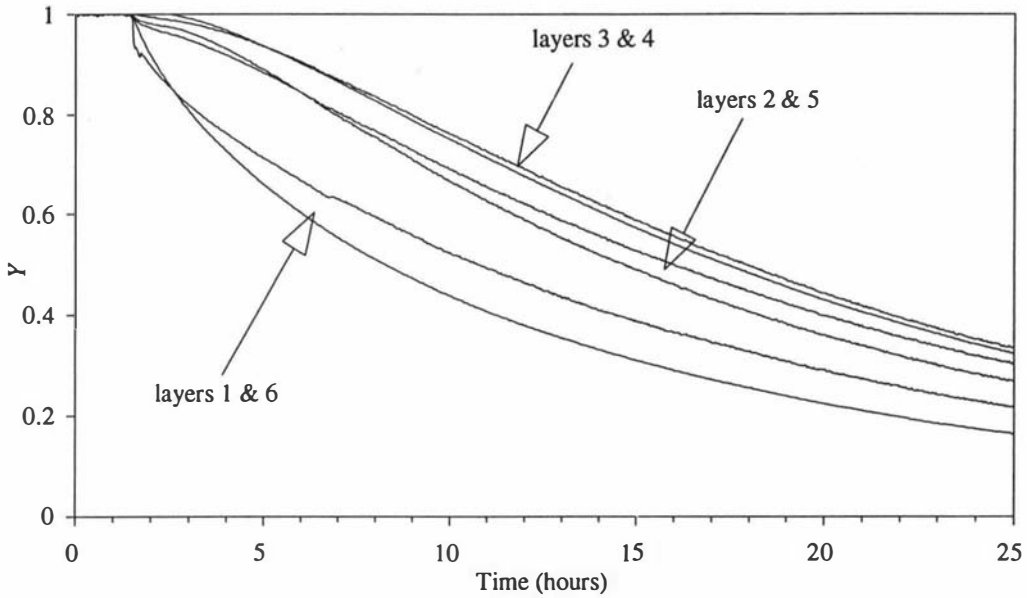

Figure 4.20: Measured fractional unaccomplished air temperatures at position 4 on each layer of the apple carton during the first cooling without ventilation trial.

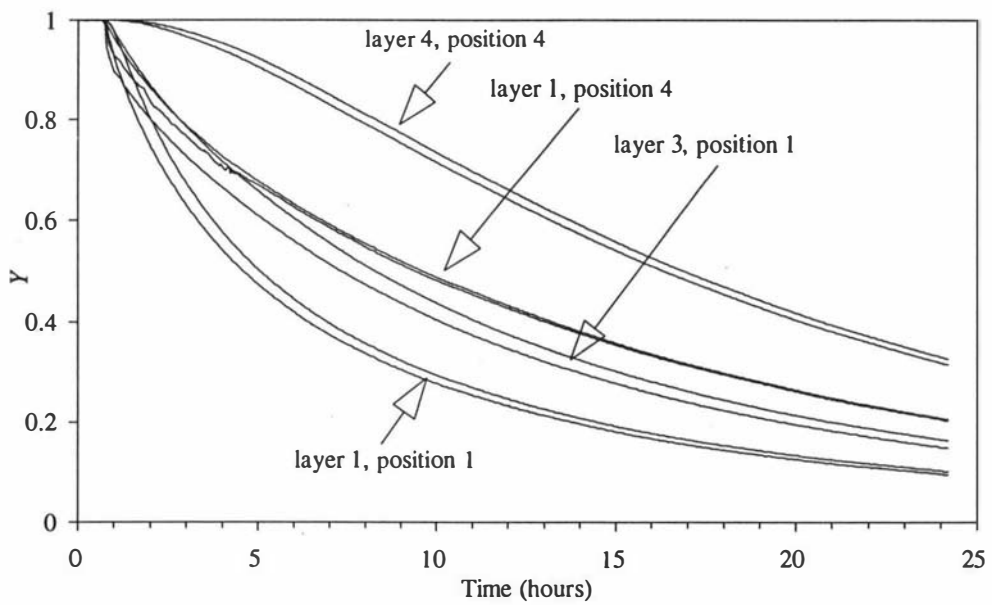

Figure 4.21: Measured fractional unaccomplished apple and air temperatures for selected positions within the apple carton during the second cooling without ventilation trial.

4.3.2 Cooling With Suppressed Surface Heat Transfer

4.3.2.1 Methodology

Two experiments were performed to establish the distribution of air throughout the carton as a function of incident air velocities onto the carton. In the first, a carton was placed in front of a fan with the vents aligned with the airflow direction. A Dantec Model 54N50 hot wire anemometer (accuracy ± 0.02 m/s) was placed in each of 9 positions on each layer of the carton (in turn), as well as in the vents. Air velocity was measured at each position by taking the mean reading over a 2 minute period. The incident air velocity was 3.2 m/s. In the second experiment, readings were taken at positions 1 and 4 on each layer for a range of incident velocities onto the carton from 1 m/s to 3.2 m/s.

To measure apple cooling rates the same methodology as outlined in Section 4.3.1.1 was followed. However in this case the vents were left open and the rest of the carton was enclosed in a 100 mm polystyrene box throughout the trial to eliminate most of the heat transfer through outside surfaces. The box was placed in the test facility with the vents aligned with the direction of the airflow for approximately 24 hours. The incident airflow across the chamber was 1.7 m/s which was close to the mean velocity measured in the industrial pre-coolers of 1.8 m/s (Figure 4.11). The air velocity measured within the exposed vent for this velocity was 1.12 m/s. Four replicate trials were performed. In the first trial cardboard temperatures were measured in addition to fruit and air temperatures. Specific locations for these extra data were in the centre of the exterior surface at: position 1, layer 6; and position 3 for layers 3, 4 and 5.

4.3.2.2 Results and Discussion

Table 4.4 shows the measured air velocities within the carton. A large proportion of the air entering the carton flows through the layers close to the vents. Layer 3 is immediately adjacent to the vents. Approximate symmetry across the carton at each measurement location is shown. Figure 4.22 shows measured air velocities as a function

of incident velocity. There was an approximate linear relationship between incident air velocity onto the carton and the velocity recorded at each position. This indicates that the airflow paths within the carton remain essentially unchanged when the incident air velocity is altered.

Table 4.4

Measured Air Velocities (m/s) For Selected Positions Within An Apple Carton With An Incident Velocity Onto The Carton Of 3.2 m/s

Layer	Position									Layer Average
	Carton Front			Carton Centre			Carton Back			
	10	1	11	3	4	5	8	7	9	
1	0.22	0.09	0.08	0.10	0.08	0.02	0.07	0.10	0.08	0.09
2	0.18	0.61	0.15	0.08	0.37	0.08	0.18	0.41	0.27	0.26
3	0.40	3.10	0.60	0.17	0.20	0.33	0.21	0.84	0.30	0.68
4	0.22	0.27	0.18	0.05	0.21	0.15	0.20	0.34	0.21	0.21
5	0.54	0.14	0.05	0.03	0.14	0.23	0.05	0.07	0.05	0.14
6	0.18	0.19	0.10	0.05	0.25	0.05	0.05	0.13	0.17	0.13
Position Average	0.29	0.73	0.19	0.08	0.21	0.15	0.12	0.32	0.18	0.25

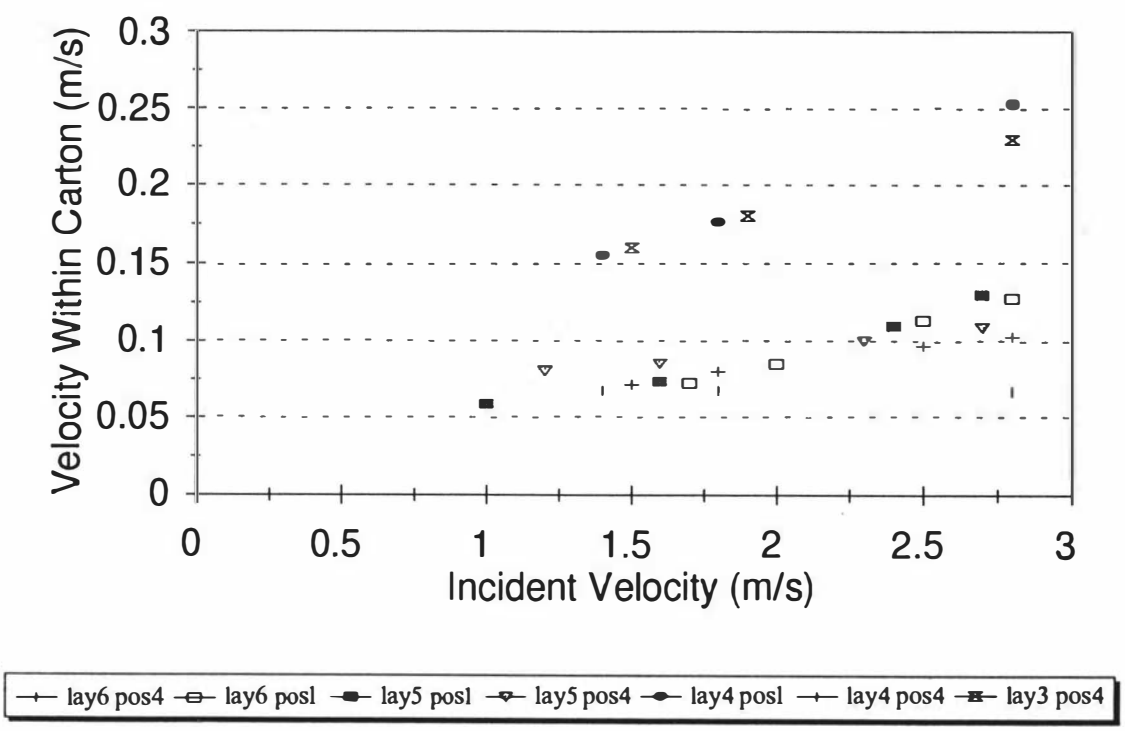

Figure 4.22: Measured air velocities (m/s) at selected positions within an apple carton as a function of incident air velocities onto the carton.

Figure 4.23 presents the data for the first carton cooling trial with suppressed surface heat transfer. As expected, rate of cooling reduced down the length of the carton (positions 1 cooled fastest, position 4 next fastest and position 7 slowest).

For all the layers except 3 (adjacent to the vents), position 10 cooled faster than position 1, and position 3 cooled faster than position 4. This suggests that more air was moving down the exterior regions of the carton, giving higher airflow rates along the outer parts of each layer. This may be explained by the Friday trays not fitting right to the edge of the carton and greater cross-sectional area available for flow, due to lower apple numbers along the edge of the carton (Figure 4.2).

Figure 4.24 shows the results for positions 1, 4, 3 and 7 for each of the four replicates. The data shows small variations between the four trials but the spread of data was larger than for the trials without ventilation. This was expected because of the greater importance of internal airflow rates in this series of trials, amplifying any effect of small differences in carton assembly.

Figure 4.25 shows measured apple, air and cardboard cooling rates for a number of positions for the first trial. There was more difference in the air and apple cooling rates at a number of positions than was evident in the trials without ventilation. This was expected because the larger air velocities present in this series of trials would lead to larger Biot number conditions. Interior zones (position 4) showed less difference between apple and air cooling rates compared to exterior zones, perhaps indicating lower air velocities in the centre zones of the carton. As was expected, due to the carton insulation, the measured cardboard temperatures were effectively indistinguishable from the air temperatures for layers 3 and 4. There was some discrepancy between air and cardboard temperatures for layer 6 and to a lesser extent layer 5. The thermocouples and thermistor wires entered the insulated box at layer 6 and although the resulting penetration was taped over it was inevitable that some non-ideality of measurement conditions occurred in this region.

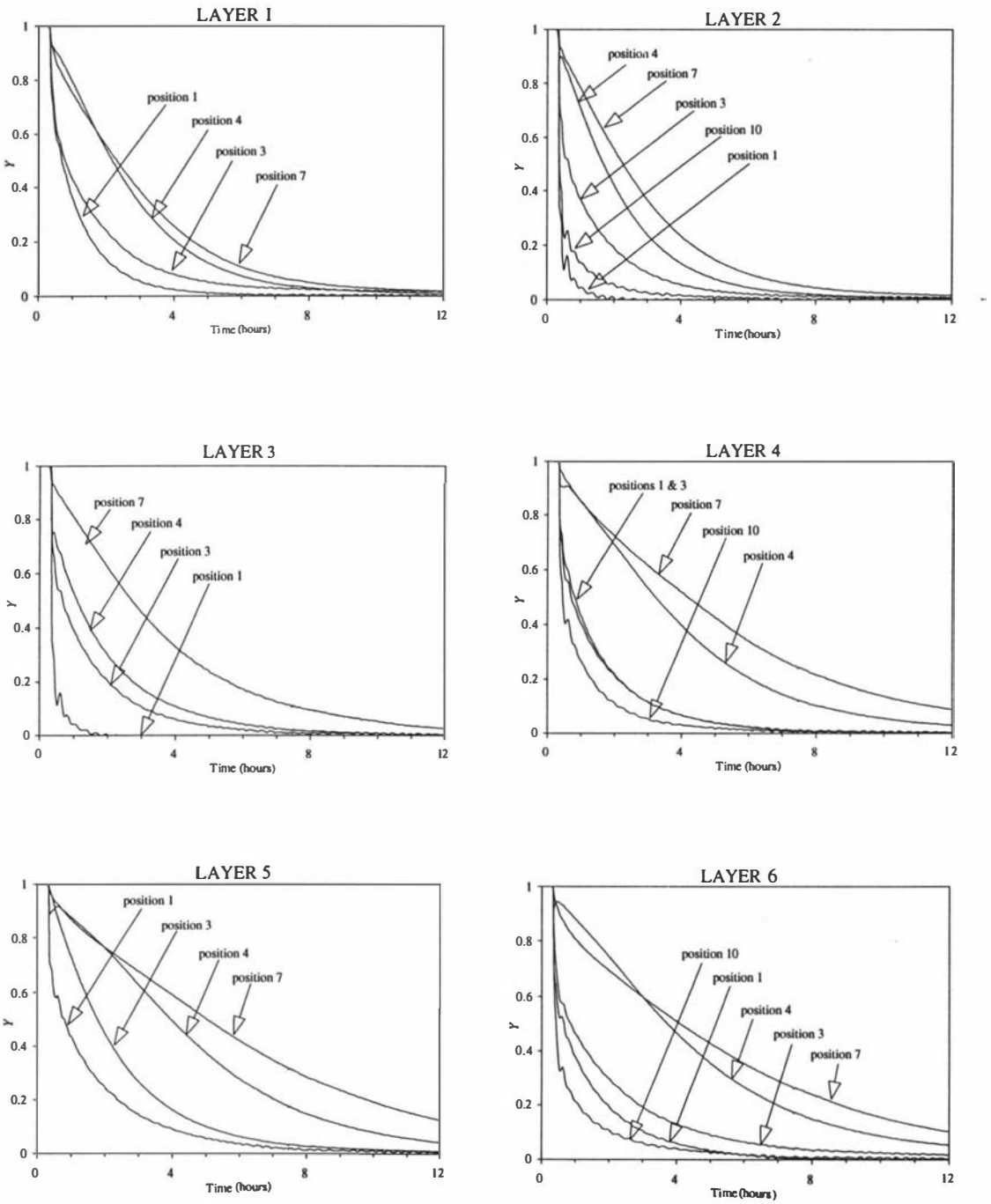

Figure 4.23: Measured fractional unaccomplished air temperatures for each layer of the apple carton during the first cooling with suppressed surface heat transfer trial.

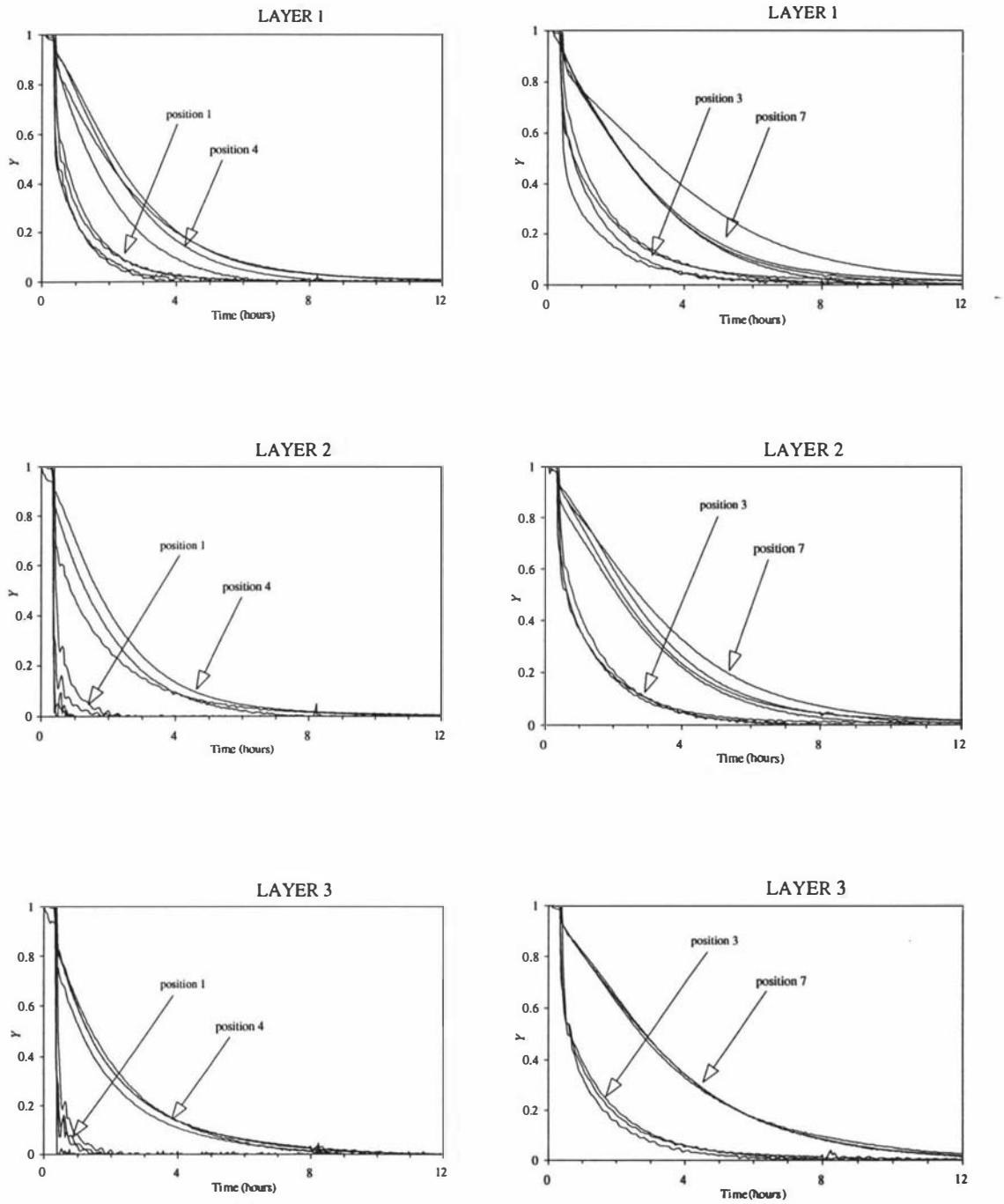

Figure 4.24a: Measured fractional unaccomplished air temperatures for layers 1, 2, & 3 during the four replicate apple cooling with suppressed surface heat transfer trials.

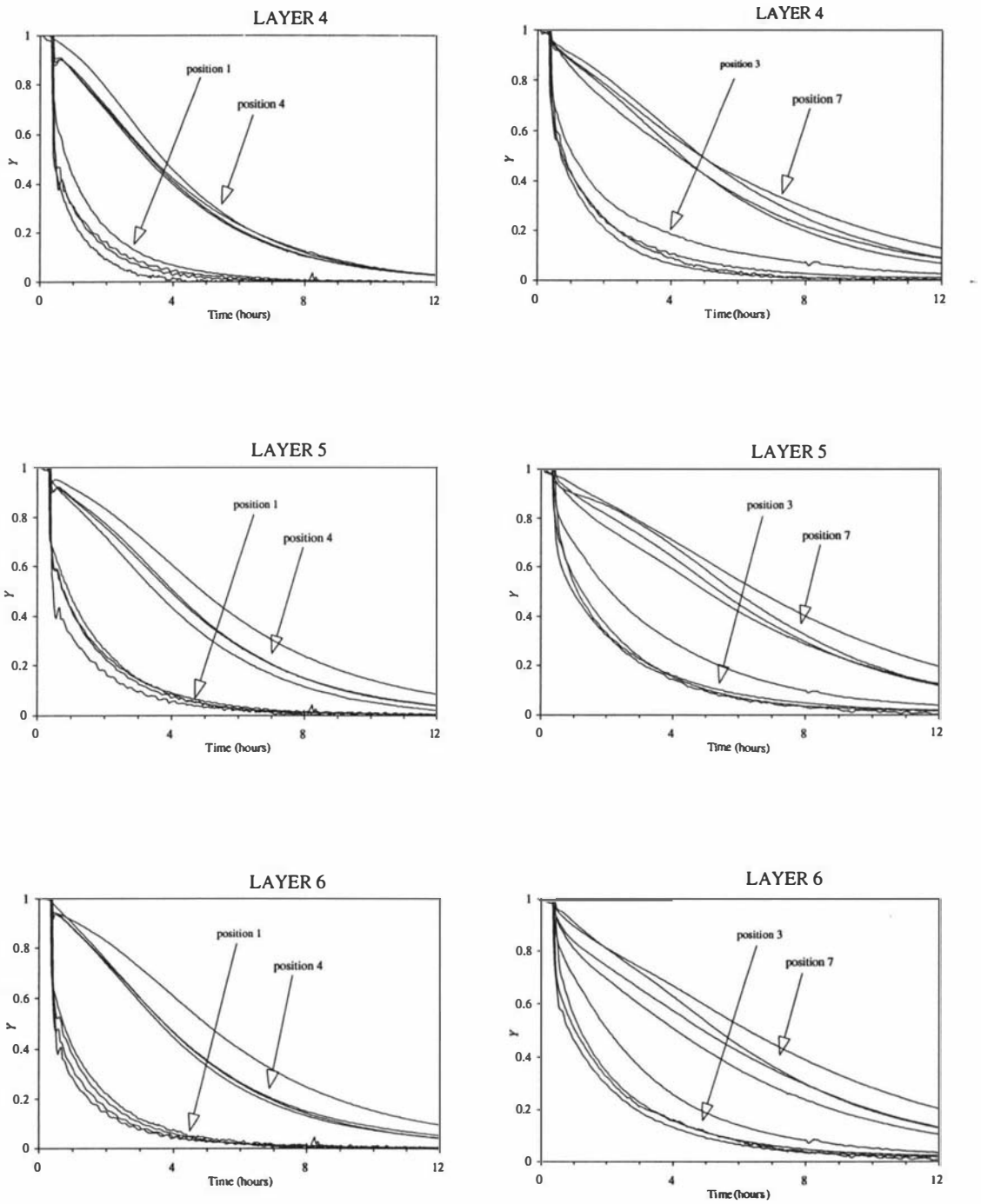

Figure 4.24b: Measured fractional unaccomplished air temperatures for layers 4, 5, & 6 during the four replicate apple cooling with suppressed surface heat transfer trials.

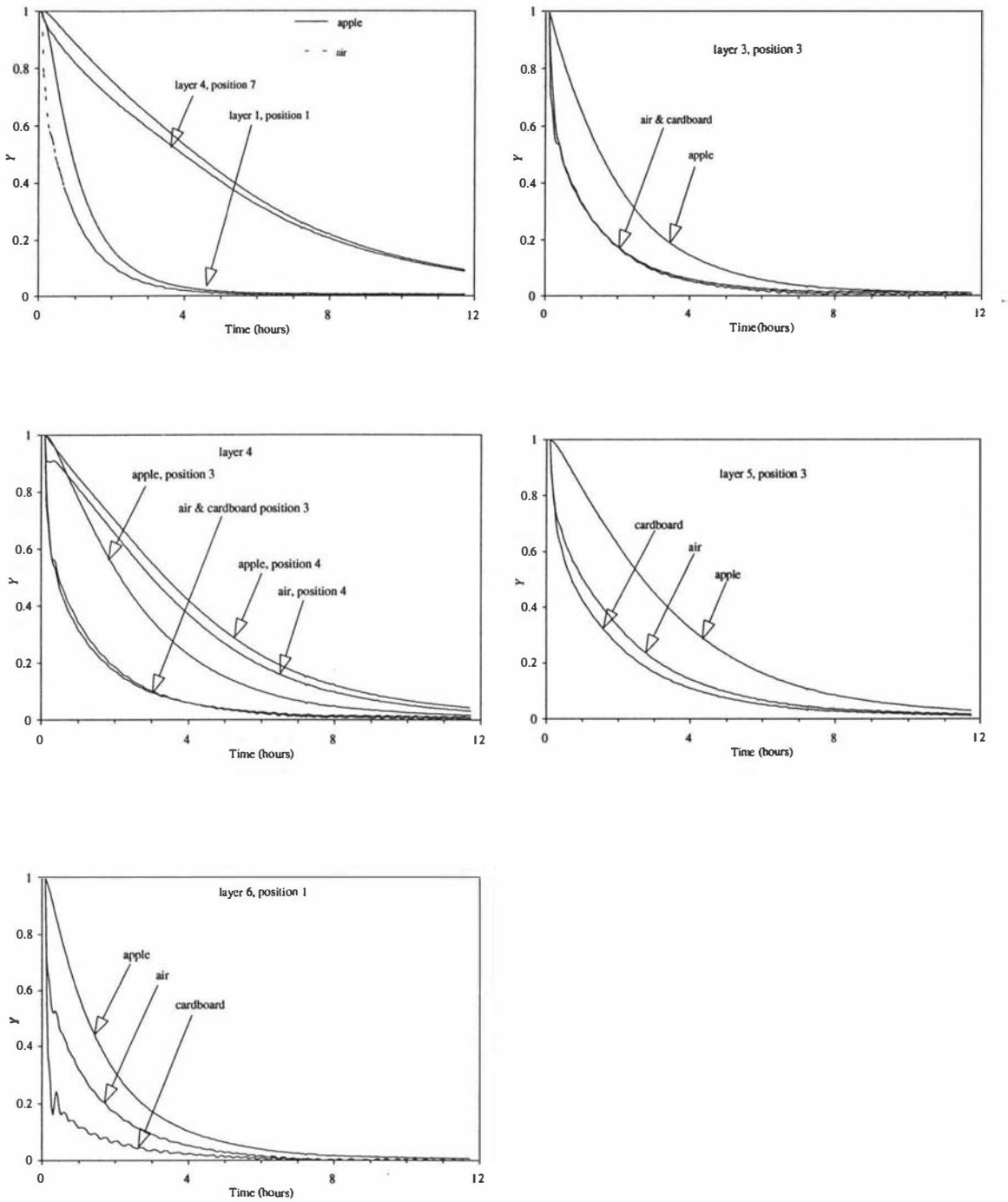

Figure 4.25: Measured fractional unaccomplished air, apple and cardboard temperatures for selected positions within the apple carton during the first cooling with suppressed surface heat transfer trial.

4.3.3 Unmodified Carton Trials

4.3.3.1 Methodology

Cartons were assembled and conditioned as outlined in Section 4.3.1.1, except that the vents were left open and all faces were uninsulated when the cartons were placed in the test facility. The vents were aligned with the airflow direction. Incident air velocity across the chamber was 1.4 m/s. Three replicate trials were undertaken.

4.3.3.2 Results and Discussion

Figures 4.26, 4.27, and 4.28 show the results for this series of experiments. The results show both very similar trends and similar rates of cooling to the trials without surface heat transfer. The major difference was that the rates of cooling for position 4 are more similar to those for position 7 than for the trials without surface heat transfer, probably due to position 7 cooling faster in this series of experiments due to increased heat transfer from conduction through the exterior cardboard.

4.3.4 Carton Heat Transfer Mechanisms

Figure 4.29 compares typical rates of cooling during the three sets of experiments at selected positions within the carton. Table 4.5 gives the measured half cooling times at a number of positions. Cooling without ventilation was significantly slower than cooling with ventilation. Because the incident air velocity was higher in experiment two than in experiment three it was not possible to directly compare the relative effect of ventilation only versus ventilation plus conduction through exterior cardboard. However the results suggest that the dominant heat transfer mechanism was ventilation (forced convection). In these trials ventilation was unimpeded. Industrial practice means that ventilation of many cartons in an industrial pallet is impeded by the stacking arrangement. This would cause natural convection to play a larger role in cooling. Thus any mechanistic model needs to consider both forced and natural convection if it is to be realistic.

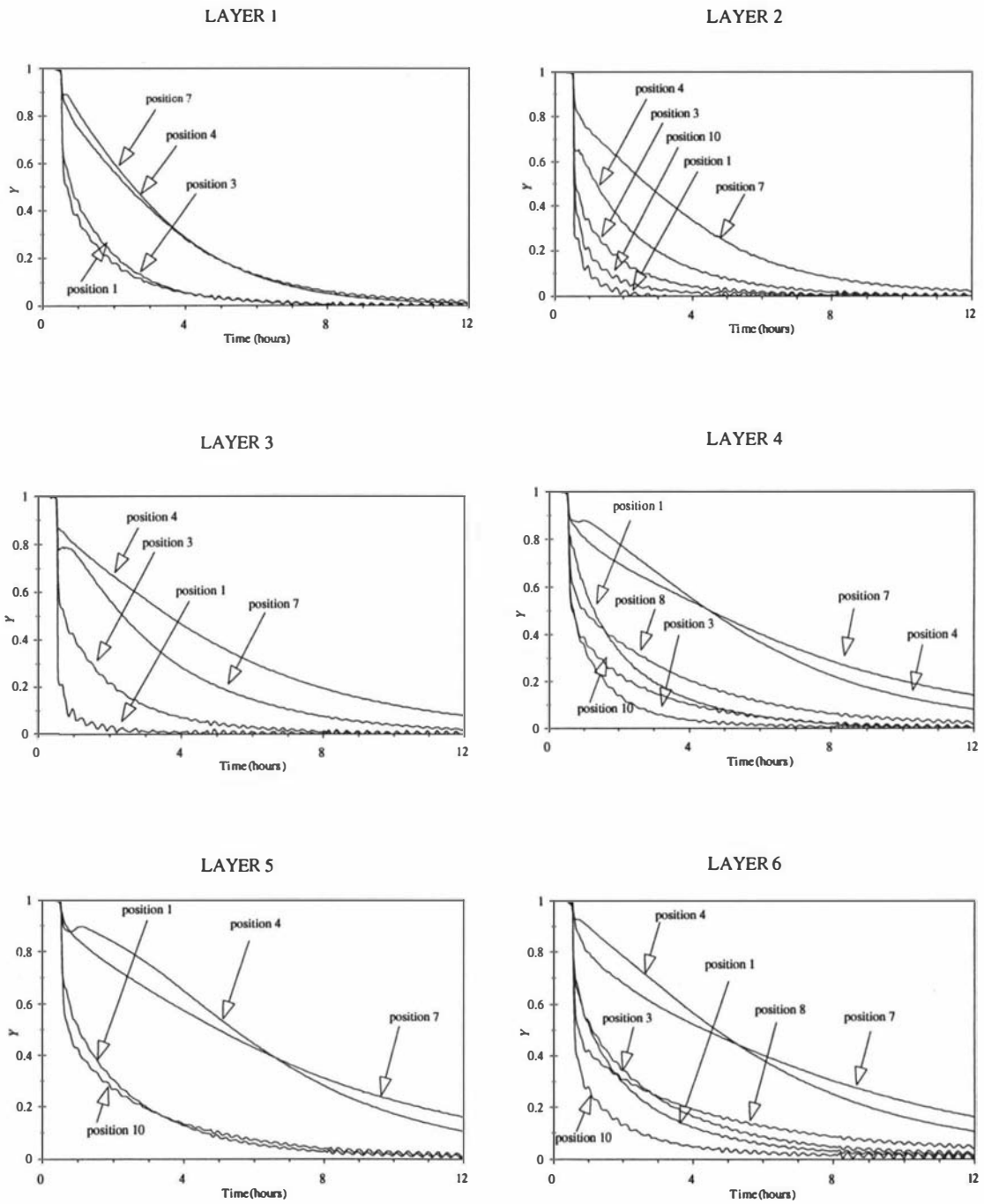

Figure 4.26: Measured fractional unaccomplished air temperatures for each layer of the apple carton during the first unmodified carton cooling trial.

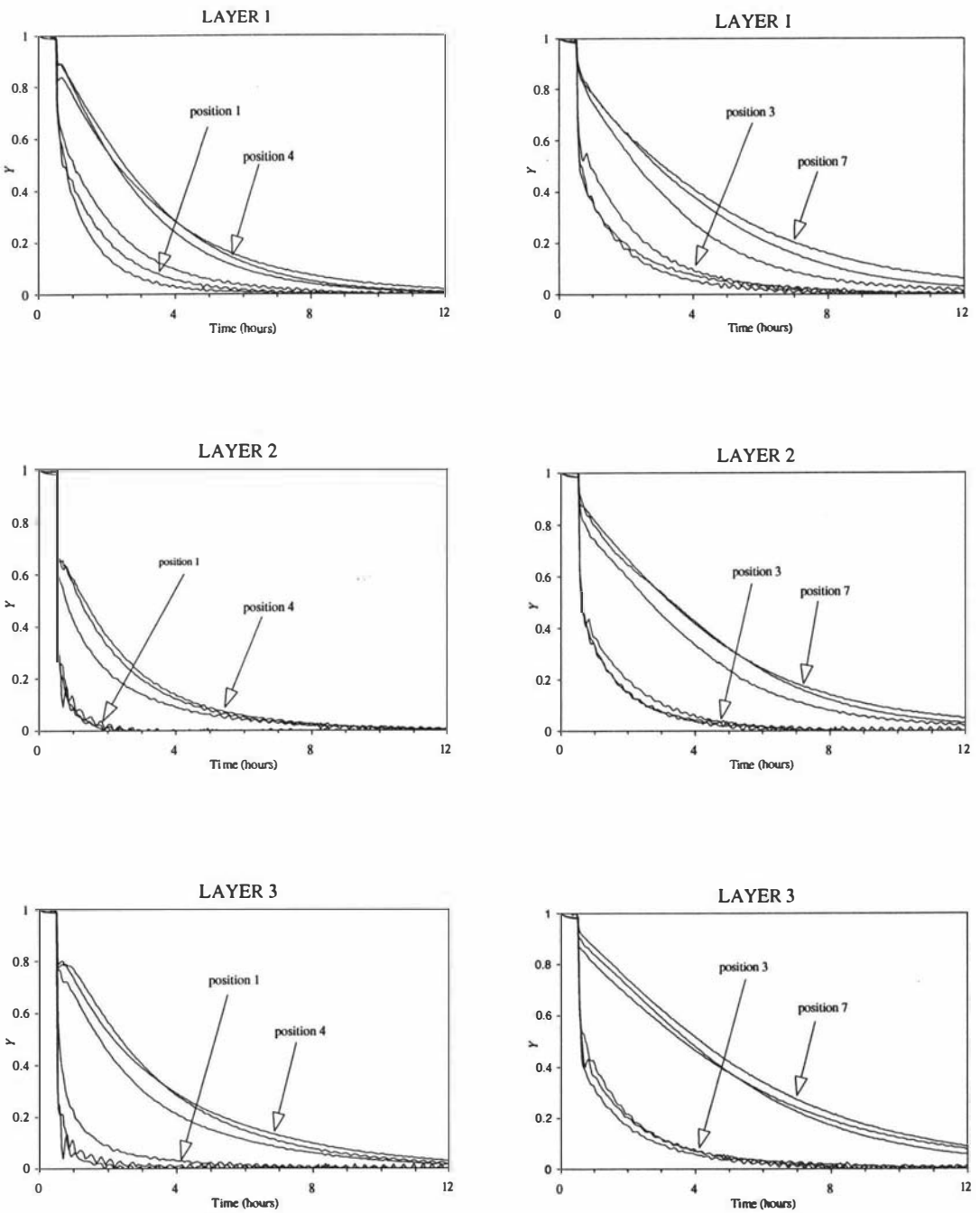

Figure 4.27a: Measured fractional unaccomplished air temperatures for layers 1, 2, & 3 during the three replicate unmodified apple carton cooling trials.

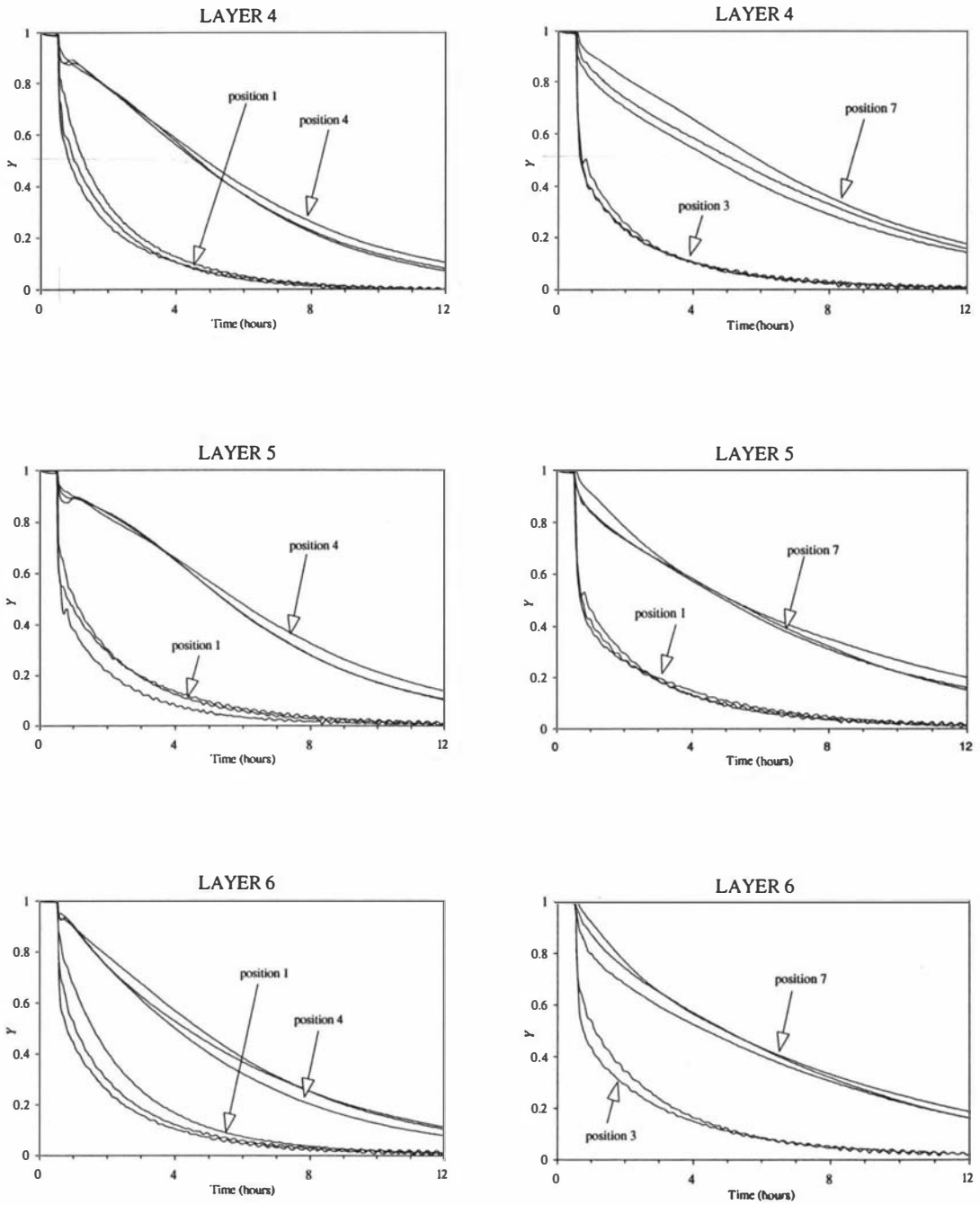

Figure 4.27b: Measured fractional unaccomplished air temperatures for layers 4 ,5, & 6 during the three replicate unmodified apple carton cooling trials.

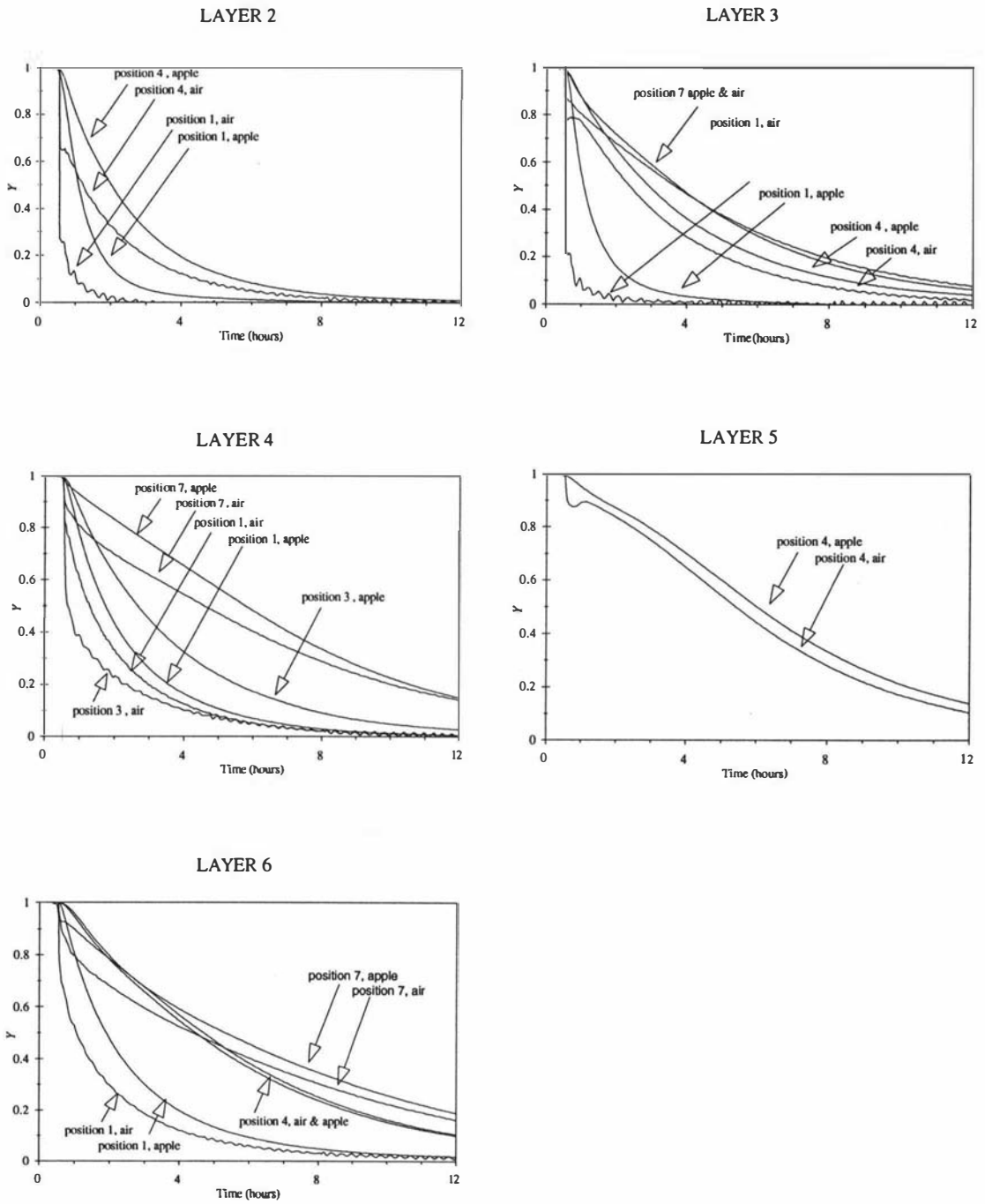

Figure 4.28: Measured fractional unaccomplished air and apple temperatures for selected positions within the apple carton during the first unmodified carton cooling trial.

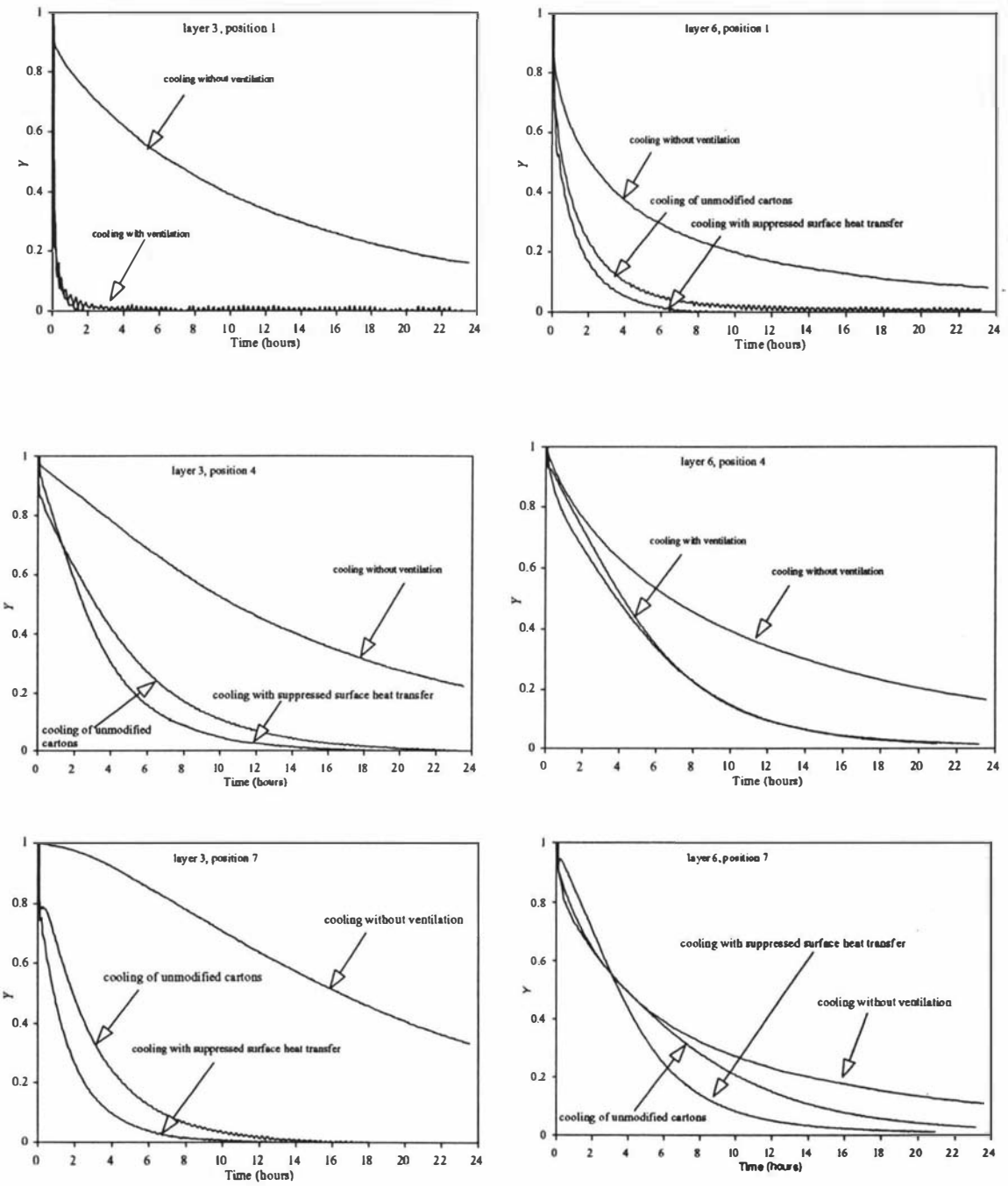

Figure 4.29: Typical measured fractional unaccomplished air temperatures for selected positions within the apple cartons for each of the cooling trials: without ventilation, with suppressed surface heat transfer, and the unmodified carton.

Table 4.5

Measured Apple $t_{1/2}$ Values For Each Of The Three Sets Of Apple Carton Experiments For Selected Positions Within The Carton.

Position Within Carton		$t_{1/2}$ (hours)		
Layer	Position	Cooling without ventilation	Cooling with suppressed surface heat transfer	Unmodified Carton
1	1	6.5*	0.7	0.7
	4	11.5	1.4*	1.9*
	7	7.7*	1.8*	2.6*
2	1	8.0*	0.3	0.5
	4	12.5	1.2*	1.4
	7	8.7*	1.7*	2.3*
4	1	8.4*	0.9	1.3
	4	12.5	2.8*	3.2*
	7	9.9*	3.6*	4.1*

* Significant non-linearity of $\ln(Y)$ versus time plot observed. For these cases $t_{1/2}$ was calculated from the slope of the $\ln(Y)$ versus time plot, for Y values between 0.8 and 0.2 (or the lowest Y value measured if 0.2 not reached.

4.4 CONCLUSIONS

The pre-cooling trials within the industrial coolstore showed that cooling rates in staggered stacks were 30% faster on average than for in-line stacks, but for both stacking arrangements large variation in cooling rates were observed. None of the carton or pallet positional factors studied were found to be significant. The variation in cooling rate was largely attributed to different carton ventilation rates arising from limited vent size into the cartons, imprecision in both pallet positioning within the stacks and carton placement onto the pallets. General principles to optimise forced air pre-cooling of bulk stacked packaged products are to design packaging to allow: a high percentage of vents, good alignment of vents, and tight and precise assembly of

containers onto pallets. If high levels of container ventilation are not possible then containers should be spaced on pallets to allow air flow through pallets. Close positioning of pallets to minimise air bypass through gaps between them is also important.

Measurements of cooling rates within the bulk store showed that differences in cooling rate with position within cartons existed, but there were not large variations in cooling rate between cartons on a pallet with similar ventilation potential. This suggested that the carton is the appropriate unit to model mechanistically. The rates of cooling measured in the bulk coolstore were significantly slower than those measured in the industrial pre-cooling trials.

Cooling trials for individual cartons showed that there was significant variation in cooling rate within an individual carton arising from the relative ease of air movement along possible airflow pathways within the carton. The ventilation rate primarily controlled cooling rate, but in cases where vent holes were not exposed to air flow, or incident velocities were low natural convection might also be important.

CHAPTER 5: APPLE CARTON COOLING MODEL DEVELOPMENT

5.1 INTRODUCTION

Development of an overall coolstore simulation model requires an appropriate sub-model for prediction of product temperature, weight loss and heat load in response to changing coolstore air conditions. The majority of studies performed on heat and mass transfer from horticultural products have been for single, unpackaged commodities. Whilst models for heat and/or mass transfer exist for these situations, little work on mechanistic modelling of bulk stacked and/or packaged commodities has been published (Chapter 2, Section 2.3.1.2). Chapter 5 presents the development of a product model for cooling of apples packed into cartons and assembled onto pallets both in pre-coolers and bulk stacked in coolstores.

The model should be able to predict apple temperature and weight loss with both position and time within the cartons and should be able to simulate different carton positions and orientations on a pallet, and different incident air conditions onto the pallet (velocity, temperature, and relative humidity, RH).

A number of heat and mass transfer pathways exist within an apple carton undergoing cooling including: convection from apples to air within the carton, radiation from apples to other surfaces, evaporation of water vapour from apples to the air within the carton, conduction between apples and friday trays, conduction within apples, convection from air within the carton to outside cardboard and friday tray surfaces, convection from outside surface of the cardboard to the air surrounding the carton, conduction through cardboard surfaces, adsorption of water vapour by cardboard, forced convection of air through the carton, and natural convection of air within the carton. The most important of these pathways will need to be considered in order to accurately model carton cooling.

Three main possibilities exist for modelling heat and mass transfer in a single carton. The simplest approach would be to measure half-cooling time for a representative range

of positions within the carton. This approach is situation-specific and not mechanistic, thus limiting the predictive ability of the model. It also requires a large number of measurements which can be expensive to perform. The most commonly used mechanistic approach for product cooling is to use a conduction model. This approach assumes all other mechanisms can be modelled in terms of conduction within a solid object and convection between the surface of the object and the surrounding cooling medium (Cleland, 1990). This approach is commonly used for single product items. If it is applied, there is a need to define effective thermal properties and convective heat transfer coefficients to take account of the other mechanisms. If other mechanisms within the carton cannot be approximated by the conduction model then the third approach would be a mechanistic model which includes appropriate models for each significant mechanism within the carton.

The first approach was rejected because of its limited applicability to alternative systems and because the measured data for the system studied showed that cooling rates were highly variable. It was decided to use the last and most complicated approach only if the simpler conduction approach proved unsatisfactory.

5.2 CONDUCTION MODEL

Although commonly used for products that are reasonably homogenous in nature, this approach has seldom been used for packaged products with significant air voids.

Jamieson *et al.* (1993) used such a model to predict cooling of pallets of cartonised cheese blocks. The pallets essentially contained alternate layers of cheese and cardboard and the series heat transfer resistance model (Miles *et al.*, 1983) based on mass and volume fractions was used to estimate effective thermal properties for each pallet. An effective convective heat transfer coefficient was estimated by adding heat transfer resistances due to the air, surface packaging, and surface air gaps in series. Predictions from the models showed satisfactory agreement with measured data.

In an apple carton, the heat transfer pathways are less well defined and neither the simple series or parallel models stated by Miles *et al.* (1983) were considered mechanistically valid. The effective medium theory approach (Pham, 1990) makes no distinction with respect to heat transfer pathways and so was selected to determine effective properties using mass and volume fractions based on measured carton components (Table 5.1). Where specific thermal property data for components were not available typical literature values were used.

The effective heat transfer coefficient at the surface of the carton was estimated using the methodology described by Jamieson *et al.* (1993) to be 2.5 W/m^2 K. Simulation of the chilling of a carton using these calculated values was carried out using a proven accurate 3 dimensional finite difference program for the conduction model (Cornelius, 1991). Figure 5.1 shows predicted and measured data for several positions within the carton for carton cooling trials (a) without ventilation, (b) with suppressed surface heat transfer, and (c) unmodified cartons (Chapter 4). The predictions were close to the measured data for the trials without ventilation. However in trials where ventilation was possible, the model predictions are inaccurate.

Table 5.1

Apple Carton Component Volume Fractions, Mass Fractions and Thermophysical Data Used In Calculating Effective Thermal Properties

Component	Volume Fraction	Mass Fraction	c (kJ/kg K)	λ (W/m K)
Apples	0.491	0.973	3.65	0.42[1]
Friday trays	0.045	0.026	2.0	0.08
Air	0.464	0.001	1.5	0.022
Overall Carton	1.0 (0.0448 m^2)	1.0 (19.01 kg)	3.60	0.25

[1] From Mellor (1978)

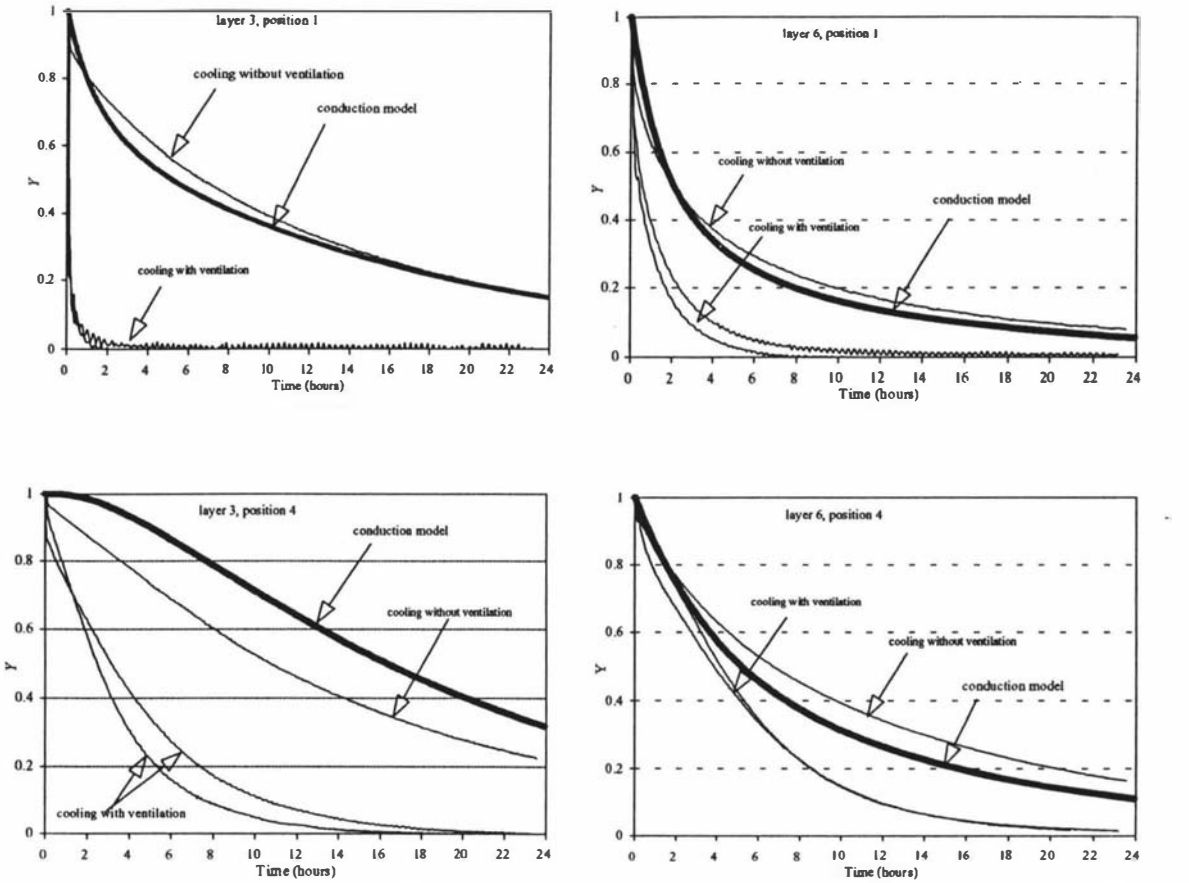

Figure 5.1: Comparison of the conduction/convection model with measured data from apple carton cooling trials.

In practice, most apple cartons within the industrial facility are likely to have some ventilation through the exposed hand holes. For this reason, and also because mass transfer predictions within the carton are not possible, the conduction approach was rejected and a more sophisticated mechanistic model of an apple carton including consideration of ventilation was developed.

5.3 CARTON MODEL FORMULATION

5.3.1 Space Discretisation

Three types of space discretisation used by researchers in refrigeration system modelling for refrigerated applications might be applied for modelling a single carton. These are: single-zoned lumped parameter, multiple-zoned lumped parameter, and fully distributed models (Cleland and Cleland, 1989).

Lumped parameter models treat the components within each zone of the system as being "perfectly mixed". A single zone lumped parameter model would represent the entire apple carton by a uniform temperature, so positional variation within the carton would not be able to be modelled. Therefore this approach was rejected.

Fully distributed models have been used for modelling small scale coolstores and containers (Van der Ree *et al.*, 1974; Meffert and Van Beek, 1983 & 1988; Wang and Touber, 1988 & 1990; Wang, 1991; Van Gerwen and Oort, 1989 & 1990; Van Gerwen *et al.*, 1991). They involve solving simultaneous partial differential equations for fluid hydrodynamics as well as heat and mass transfer between the air and solid objects. Detailed analysis of positional variation within the system is possible. However such models have proved to be very computationally intensive, and defining necessary input data can be very difficult. For these reasons this type of model was not considered appropriate.

Multiple zoned lumped parameter models split the system up into a series of discrete zones and treat conditions within each zone as being uniform. The zones are then linked together in some fashion to allow for heat and/or mass transfer between them. This approach allows positional variation to be modelled and is less computationally intensive than fully distributed models. It has been used for modelling a vegetable freezer (Marshall and James, 1975) and for modelling dust concentrations within ventilated spaces (Liao and Feddes, 1992). It was decided to use this approach for modelling the apple carton as it offered a promising compromise between accuracy and computational complexity.

The carton was modelled as a series of interconnected rectangular zones (J zones along, I zones across, K zones deep). Each zone had six boundaries where heat and mass transfer can occur with other zones via ventilation or heat transfer with cardboard surfaces via convection/conduction (Figure 5.2). To simplify space discretisation the number of vertical zones was chosen to match the numbers of fruit layers within the carton (K=6). Each layer was further split into five zones both across (I=5) and down the length (J=5) of the carton, (Figure 5.3) leading to 150 zones in total. The number

of subdivisions in each direction was chosen as a compromise between accuracy and computational cost for the model. Symmetry considerations to reduce the number of zones were not applied because some non-symmetrical applications were anticipated.

The appropriate mechanisms to be considered for each boundary of a zone are dependent on the position of the zone within the carton. Given the above discretisation, the most important are ventilation with adjacent zones or interaction with cardboard between layers or the outside of the carton. In theory there can be ventilation with up to 6 adjacent zones and interaction with up to 6 associated cardboard surfaces on each zone boundary. In practice, if I and J are greater than 1 then there can only be ventilation with a maximum of 4 associated zones and interaction with up to 4 cardboard surfaces. Figure 5.3 and Table 5.2 list the zone boundaries through which ventilation or interaction with cardboard surfaces were assumed to exist for each zone in the current carton design. In current practice vertical ventilation between zones can only occur for zones at the sides or ends of the carton, but different packaging designs could allow airflow between layers in other positions, so the model formulation has been kept as general as possible.

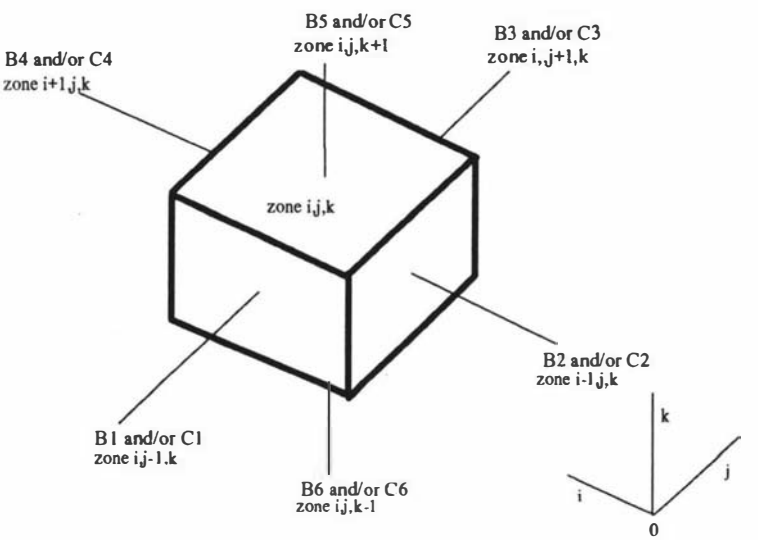

Figure 5.2: Possible ventilation or cardboard surface boundaries for a generalised zone within an apple carton.

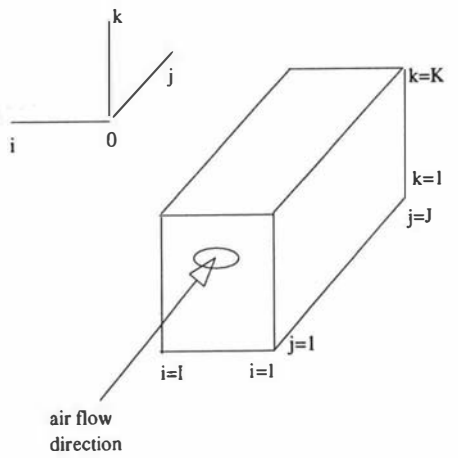

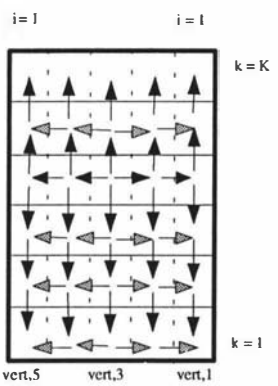

Section through carton front end

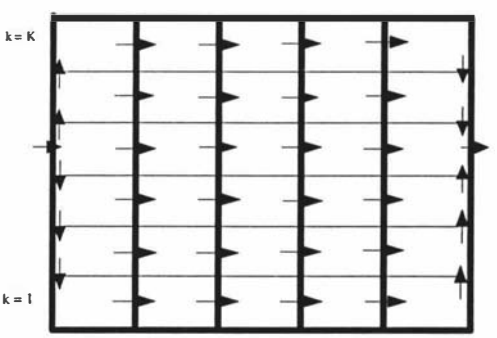

Section Through Carton Centre

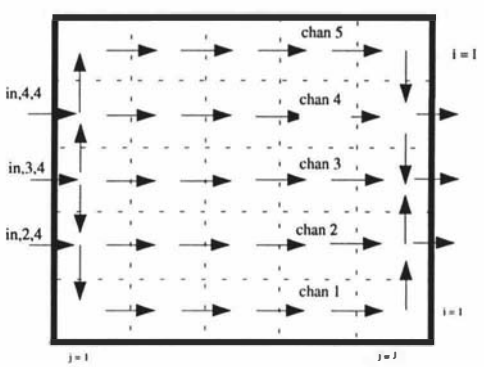

Plan for k = 4

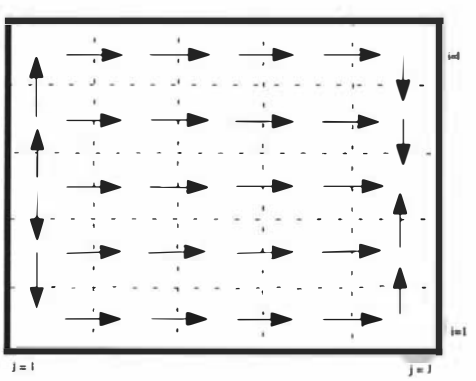

Plan for k = 1,2,3,5 and 6

Figure 5.3: Zone positions and forced convective air paths within an apple carton.

Table 5.2

Possible Boundary Mechanisms For Zones Within A Carton

Zone Position	Ventilation Boundaries[1]	Cardboard Surfaces[2]
i=1, 1<j<J, 1<k<K	B1,B3,B4	C2,C5,C6
i=I, 1<j<J, 1<k<K	B1,B2,B3	C4,C5,C6
i=1, j=1, 1<k<K	B3,B4,B5,B6	C1,C2,C5,C6
i=I, j=1, 1<k<K	B2,B3,B5,B6	C1,C4,C5,C6
i=1, j=J, 1<k<K	B1,B4,B5,B6	C2,C3,C5,C6
i=I, j=J, 1<k<K	B1,B2,B5,B6	C3,C4,C5,C6
1<i<I, j=1, 1<k<K	B2,B3,B4,B5,B6	C1,C5,C6
1<i<I, j=J, 1<k<K	B1,B2,B4,B5,B6	C3,C5,C6
1<i<I, 1<j<J, 1<k<K	B1,B2,B3,B4	C5,C6
i=1, 1<j<J, k=1	B1,B3,B4	C2,C5,C6
i=I, 1<j<J, k=1	B1,B2,B3	C4,C5,C6
i=1, j=1, k=1	B3,B4,B5	C1,C2,C5,C6
i=I, j=1, k=1	B2,B3,B5	C1,C4,C5,C6
i=1, j=J, k=1	B1,B4,B5	C2,C3,C5,C6
i=I, j=J, k=1	B1,B2,B5	C3,C4,C5,C6
1<i<I, j=1, k=1	B2,B3,B4,B5	C1,C5,C6
1<i<I, j=J, k=1	B1,B2,B4,B5	C3,C5,C6
1<i<I, 1<j<J, k=1	B1,B2,B3,B4	C5,C6
i=1, 1<j<J, k=K	B1,B3,B4	C2,C5,C6
i=I, 1<j<J, k=K	B1,B2,B3	C4,C5,C6
i=1, j=1, k=K	B3,B4,B6	C1,C2,C5,C6
i=I, j=1, k=K	B2,B3,B6	C1,C4,C5,C6
i=1, j=J, k=K	B1,B4,B6	C2,C3,C5,C6
i=I, j=J, k=K	B1,B2,B6	C3,C4,C5,C6
1<i<I, j=1, k=K	B2,B3,B4,B6	C1,C5,C6
1<i<I, j=J, k=K	B1,B2,B3,B6	C3,C5,C6
1<i<I, 1<j<J, k=K	B1,B2,B3,B4	C5,C6

[1] = Boundaries as shown on Figure 5.2

[2] = Surrounding cardboard surfaces associated with each zone (C1 to C6, Figure 5.2).

For each zone air enthalpy, air humidity, air temperature, apple temperature, apple mass, and associated cardboard temperatures were modelled.

5.3.2 Zone Air Formulation

An underlying assumption was that each zone was perfectly mixed, i.e. air temperature and air humidity and enthalpy are considered constant throughout the zone. Air energy and humidity (water vapour) balances were performed on each zone.

5.3.2.1 Zone Air Energy Balance

The enthalpy of the zone air gives a measure of the total amount of energy present in the zone air relative to a known datum. The datum value used was 0°C for the dry air component and the triple point of water (0.01°C) for the water vapour component. The air enthalpy is the sum of the enthalpy of the dry air and the enthalpy of the associated water vapour. A commonly used equation for calculating enthalpy is (Stoecker and Jones, 1982):

$$hh \approx c_a T_a + H (h_{fg} + c_v T_a) \tag{5.1}$$

where:

hh	=	air enthalpy (J/kg)
H	=	air humidity (kg/kg)
c_a	=	specific heat capacity of the dry air at constant pressure (J/kg K)
h_{fg}	=	latent heat of vaporisation of water vapour at 0.01°C (J/kg)
c_v	=	specific heat capacity of water vapour (J/kg K)
T_a	=	dry bulb temperature of the air (°C)

Eqn. 5.1 is only an approximation as c_a varies slightly with temperature, and the water vapour in the air-vapour mixture is likely to be superheated whereas the equation assumes that it is saturated. Stoecker and Jones (1982) show that the enthalpy of superheated water vapour is approximately equal to the enthalpy of saturated vapour at the same temperature and the change in c_a is small over the temperature range of

interest, so Eqn. 5.1 was considered sufficiently accurate.

The energy balance within a typical zone is:

$$\left[\begin{array}{l}\textit{Rate of accumulation of}\\ \textit{energy in zone air}\end{array}\right] = \left[\begin{array}{l}\textit{Rate of energy gain}\\ \textit{from apples by convection}\\ \textit{and evaporation}\end{array}\right] + \left[\begin{array}{l}\textit{Rate of energy gain from}\\ \textit{associated cardboard surfaces}\\ \textit{by convection to zone air}\end{array}\right] + \left[\begin{array}{l}\textit{Rate of energy gain}\\ \textit{by ventilation from}\\ \textit{associated zones}\end{array}\right]$$

This can be expressed mathematically as:

$$\frac{d(M_{i,j,k}hh_{i,j,k})}{dt} = \phi_{ap\rightarrow a} + \phi_{evap} + \sum_{n=1}^{6} \phi_{cd,n\rightarrow a} + \sum_{l=1}^{6} \phi_{v,l} \qquad (5.2)$$

where:

$M_{i,j,k}$	=	mass of dry air within zone (i,j,k) (kg).
$hh_{i,j,k}$	=	enthalpy of air in zone (i,j,k) (J/kg).
$\phi_{ap\rightarrow a}$	=	convection from apple surfaces to zone air (W).
ϕ_{evap}	=	energy flow by evaporation from apple surfaces (W).
$\phi_{cd,n\rightarrow a}$	=	convection from n^{th} surrounding cardboard surface to air (W).
$\phi_{v,l}$	=	ventilation from the l^{th} surrounding zone (W).
i,j,k	=	zone co-ordinates as shown on Figure 5.3.
l	=	l^{th} surrounding zone.
n	=	n^{th} cardboard surface associated with zone (i,j,k).
t	=	time (s).

The individual heat transfer components of Eqn 5.2 were modelled using:

$$\phi_{ap\rightarrow a} = \left[\frac{V_{ap}\ \beta_i^2\ \lambda_{ap}}{R^2} \left(T_{ma,i,j,k} - T_{i,j,k} \right) \right] \frac{A_{ap\rightarrow a}}{A_{ap}} \tag{5.3}$$

$$\phi_{evap} = \frac{dW_{ap,i,j,k}}{dt} \left(h_{fg} + c_v\ T_{ma,i,j,k} \right) \tag{5.4}$$

$$\phi_{cd,n\rightarrow a} = h_{cd,n\rightarrow a}\ A_n \left(T_n - T_{i,j,k} \right) \tag{5.5}$$

$$\phi_{v,l} = \left(m_{l,in} - m_{l,out} \right) \left(hh_l - hh_{i,j,k} \right) \tag{5.6}$$

where:

R = apple radius (m).

A_{ap} = total apple surface area (m^2).

$A_{ap\rightarrow a}$ = apple surface area exposed to air (m^2).

V_{ap} = apple volume (m^3).

λ_{ap} = apple thermal conductivity (W/m K).

$h_{ap\rightarrow a}$ = apple to air convective heat transfer coefficient (W/m^2 K).

$W_{ap,i,j,k}$ = cumulative water loss from apples in zone (i,j,k) (kg).

$T_{ma,i,j,k}$ = mass average apple temperature in zone (i,j,k) (°C).

$T_{i,j,k}$ = temperature of the air in zone (i,j,k) (°C).

T_n = temperature of the n^{th} cardboard surface associated with zone (i,j,k) (°C).

$h_{cd,n\rightarrow a}$ = convective heat transfer coefficient from zone (i,j,k) air to the n^{th} cardboard surface (W/m^2 K).

A_n = exposed area of the n^{th} cardboard surface associated with zone (i,j,k) (m^2).

$m_{l,in}$ = mass flow rate of dry air from the l^{th} zone associated with zone (i,j,k) (kg/s).

$m_{l,out}$ = mass flow rate of dry air from zone (i,j,k) to the l^{th} associated zone (kg/s).

hh_l = enthalpy of the l^{th} surrounding zone (J/kg).

β_i is the first root of:

$$\beta \cot \beta + (Bi - 1) = 0 \tag{5.7}$$

where:

$$Bi = \frac{h_{ap \rightarrow a} R}{\lambda_{ap}} \tag{5.8}$$

and

Bi = Biot number.

Eqn. 5.3 is a modified version of the ordinary differential equation (ODE) model described by Lovatt *et al.* (1993a) as will be discussed in Section 5.3.3.1. This was chosen as a compromise between simplicity and accuracy.

The Friday trays between layers and the carton itself mean that zone air interacts with cardboard surfaces above and below the zone. The temperature of the cardboard below zone (i,j,k) was designated by $T_{hor,i,j,k}$, so the cardboard surface above zone (i,j,k) would be represented by $T_{hor,i,j,k+1}$. With reference to Figure 5.3, zones across the front or back faces of the carton (j = 1 or j = J) can interact with the front or back cardboard surfaces of the carton. Zones down the right and left sides of the carton (i = 1, or i = I) can interact with the right or left cardboard surfaces. These four cardboard surfaces were modelled using $T_{front,i,j,k}$, $T_{back,i,j,k}$, $T_{right,i,j,k}$, and $T_{left,i,j,k}$ respectively.

Reference to Tables 5.2 and 5.3 is required to determine which boundaries and cardboard surfaces are associated with each zone and to determine the appropriate values of T_n and hh_l for use in Eqn's. 5.5 and 5.6.

5.3.2.2 Zone Air Humidity Balance

A humidity balance within a typical zone is:

$$\left[\begin{array}{l}\textit{Rate of water vapour}\\ \textit{accumulation in}\\ \textit{zone air}\end{array}\right] = \left[\begin{array}{l}\textit{Rate of water vapour input due to}\\ \textit{water loss from apple surfaces}\end{array}\right] + \left[\begin{array}{l}\textit{Rate of water vapour gain}\\ \textit{due to ventilation with}\\ \textit{associated zones}\end{array}\right] + \left[\begin{array}{l}\textit{Rate of water vapour gain}\\ \textit{due to diffusion through}\\ \textit{cardboard surfaces}\end{array}\right]$$

This was modelled using Eqn. 5.9:

$$\frac{d(M_{i,j,k}H_{i,j,k})}{dt} = \frac{dW_{ap,i,j,k}}{dt} + \sum_{l=1}^{6} M_{v,l} + \sum_{n=1}^{6} M_{a\rightarrow cd,n} \qquad (5.9)$$

where:

$H_{i,j,k}$ = humidity of air in zone (i,j,k) (kg/kg).

$M_{v,l}$ = water vapour gain by ventilation from the l^{th} zone associated with zone (i,j,k) (kg/s).

$M_{a\rightarrow cd,n}$ = diffusion of water vapour through the n^{th} cardboard surface associated with zone (i,j,k) (kg/s).

The individual mass transfer components of Eqn 5.9 are:

$$M_{v,l} = (m_{l,in} - m_{l,out}) (H_l - H_{i,j,k}) \qquad (5.10)$$

$$M_{a\rightarrow cd,n} = A_n \, Pe \, (p_n - p_{i,j,k}) \qquad (5.11)$$

where:

$m_{l,in}$ = air flow from the l^{th} zone associated with zone (i,j,k) (kg/s).

$m_{l,out}$ = air flow from zone (i,j,k) to the l^{th} associated zone (kg/s).

H_l = humidity of the l^{th} associated zone (kg/kg).

Pe = permeance of cardboard to water vapour (s/m).

p_n = partial pressure of water vapour "outside" the n^{th} cardboard associated with zone (i,j,k) (Pa).

$p_{i,j,k}$ = partial pressure of water vapour within zone (i,j,k) (Pa).

Appropriate zone humidity values for associated zones and partial pressure of water vapour values outside cardboard surfaces are given in Table 5.3. The rate of water vapour gain from apples into the zone (i,j,k) air is defined in Section 5.3.3.

$p_{i,j,k}$ can be calculated using standard psychrometric relationships (Cleland and Cleland, 1992):

$$p_{i,j,k} = \frac{29H_{i,j,k}\, p_t}{18 + 29H_{i,j,k}} \tag{5.12}$$

where:

p_t = total air pressure (Pa).

Table 5.3

Enthalpy (hh), Air Temperature (T_l), Humidity (H_l), Cardboard Temperature (T_n) and Partial Pressure of Water Vapour (p_n) Values Associated with Generalised Zone (i,j,k), For Use In Eqn's 5.5, 5.6, 5.10 and 5.11

l & n	Boundary Face[1]	hh_l	T_n	p_n[2]	T_l	H_l
1	B1 or C1	$hh_{i,j-1,k}$	$T_{front,i,j,k}$	p_{ab}	$T_{i,j-1,k}$	$H_{i,j-1,k}$
2	B2 or C2	$hh_{i-1,j,k}$	$T_{right,i,j,k}$	p_{ab}	$T_{i-1,j,k}$	$H_{i-1,j,k}$
3	B3 or C3	$hh_{i,j+1,k}$	$T_{back,i,j,k}$	p_{ab}	$T_{i,j+1,k}$	$H_{i,j+1,k}$
4	B4 or C4	$hh_{i+1,j,k}$	$T_{left,i,j,k}$	p_{ab}	$T_{i+1,j,k}$	$H_{i+1,j,k}$
5	B5 or C5	$hh_{i,j,k+1}$	$T_{hor,i,j,k+1}$	$p_{i,j,k-1}$	$T_{i,j,k+1}$	$H_{i,j,k+1}$
6	B6 or C6	$hh_{i,j,k-1}$	$T_{hor,i,j,k}$	$p_{i,j,k+1}$	$T_{i,j,k-1}$	$H_{i,j,k-1}$

[1] For any particular zone, Table 5.2 indicates which boundaries exist.

[2] p_{ab} = Partial pressure of water vapour in the bulk air surrounding the carton (Pa).

Water absorption from the zone air into cardboard packaging was ignored.

5.3.2.3 Zone Air Property Evaluation

The total energy and humidity balances (Eqn's 5.2 & 5.9) on the zone air are coupled differential equations. The chain rule can be used to simplify the left hand sides:

$$\frac{d(M_{i,j,k}\ hh_{i,j,k})}{dt} = M_{i,j,k}\frac{dhh_{i,j,k}}{dt} + hh_{i,j,k}\frac{dM_{i,j,k}}{dt} \qquad (5.13)$$

$$\frac{d(M_{i,j,k}\ H_{i,j,k})}{dt} = M_{i,j,k}\frac{dH_{i,j,k}}{dt} + H_{i,j,k}\frac{dM_{i,j,k}}{dt} \qquad (5.14)$$

Eqn's 5.13 and 5.14 treat the mass of air within each zone as a dependent variable. The mass of dry air can be determined from the carton volume and air density:

$$M_{i,j,k} = V_{i,j,k}\ \rho_{i,j,k} \qquad (5.15)$$

where:

$V_{i,j,k}$ = volume of zone (i,j,k) (m^3).

$\rho_{i,j,k}$ = air density in zone (i,j,k) (kg/m^3).

Using the chain rule, Eqn 5.15 can be differentiated to determine the rate of change of zone air mass:

$$\frac{dM_{i,j,k}}{dt} = V_{i,j,k}\frac{d\rho_{i,j,k}}{dt} + \rho_{i,j,k}\frac{dV_{i,j,k}}{dt} \qquad (5.16)$$

Assuming that the volume of each zone remains constant Eqn 5.16 simplifies to:

$$\frac{dM_{i,j,k}}{dt} = V_{i,j,k}\frac{d\rho_{i,j,k}}{dt} \qquad (5.17)$$

Air density can be found using standard psychrometric equations (Cleland and Cleland, 1992):

$$\rho_{i,j,k} = \frac{273.15}{22.4\ (T_{i,j,k} + 273.15)} \cdot \frac{1}{\frac{1}{29} + \frac{H_{i,j,k}}{18}} \tag{5.18}$$

Differentiating Eqn 5.18 gives:

$$\frac{d\rho_{i,j,k}}{dt} = \left[\frac{-273.15}{22.4\ (T_{i,j,k} + 273.15)^2} \cdot \frac{1}{\frac{1}{29} + \frac{H_{i,j,k}}{18}} \right] \frac{dT_{j,k}}{dt} - \left[\frac{273.15}{22.4\ (T_{i,j,k} + 273.15)} \cdot \frac{1}{18 \left(\frac{1}{29} + \frac{H_{i,j,k}}{18} \right)^2} \right] \frac{dH_{i,j,k}}{dt} \tag{5.19}$$

where:

$T_{i,j,k}$ = air temperature in zone (i,j,k) (°C).

Air temperature change can be determined from the air enthalpy and humidity using the differential form of Eqn. 5.1 as follows:

$$\frac{dT_{i,j,k}}{dt} \approx \frac{\frac{dhh_{i,j,k}}{dt} - (h_{fg} - c_v T_{i,j,k}) \frac{dH_{i,j,k}}{dt}}{c_a + c_v H_{i,j,k}} \tag{5.20}$$

Treating the mass of air within each zone as a dependent variable in this manner is mechanistically correct. However it requires the equations for enthalpy, humidity, mass, density and temperature to be solved simultaneously. This would add considerable complexity to the model, particularly as the carton is divided into a number of zones. For these reasons it was decided to assume that both the mass and density of dry air in each zone remains constant. Over a typical temperature range of 0°C to 20°C the variation in air density is at worst 5%, so the assumption was considered adequate. The

left hand sides of Eqn's 5.2 and 5.9 now simplify to:

$$\frac{d(M_{i,j,k}\ hh_{i,j,k})}{dt} = M_{i,j,k}\frac{dhh_{i,j,k}}{dt} \tag{5.21}$$

$$\frac{d(M_{i,j,k}\ H_{i,j,k})}{dt} = M_{i,j,k}\frac{dH_{i,j,k}}{dt} \tag{5.22}$$

With this assumption the temperature of the zone air can be determined algebraically from the zone enthalpy and humidity:

$$T_{i,j,k} \approx \frac{hh_{i,j,k} - H_{i,j,k}\ h_{fg}}{c_a + H_{i,j,k}\ c_v} \tag{5.23}$$

Eqn's. 5.13 to 5.20 are no longer required, and the model of zone air consists of Eqn's 5.2 to 5.12, and 5.23.

5.3.3 Apple Temperature And Water Loss

5.3.3.1 Apple Temperature

Three possibilities existed for estimating apple temperatures dynamically: a full partial differential equation (PDE) description of conduction within the apple subject to convection, radiation and evaporative weight loss at the surface (approximated using finite difference or finite element methods); ordinary differential equation (ODE) models; or analytical solutions for conduction. All three approaches have been used by researchers in the past for predicting temperature-time profiles of various products. Analytical solutions were not appropriate as they do not allow time-variable boundary conditions that will occur for an apple within the carton during cooling to be modelled. The initial approach selected was to use a finite difference scheme to solve the full PDE for conduction. However this proved to be too computationally intensive due to the number of zones in the model. Therefore the ODE solution described by Lovatt *et al.* (1993a) was used as a compromise between simplicity and accuracy. It was modified

to take account of the fact that not all of the apple surfacc area will be exposed to zone air and experiencing convectivc heat transfer. It is the basis of Eqn. 5.3.

Figure 5.4 shows the heat transfer pathways between an apple and the zone air that were modelled. The equation for determining apple temperature is a coupled equation:

$$\frac{d(M_{ap,i,j,k}c_{ap}T_{ma,i,j,k})}{dt} = M_{ap,i,j,k}c_{ap}\frac{dT_{ma,i,j,k}}{dt} + T_{ma,i,j,k}c_{ap}\frac{dM_{ap,i,j,k}}{dt} \quad (5.24)$$

$$= Q_{i,j,k} - \phi_{ap\rightarrow hor,i,j,k} - \phi_{ap\rightarrow hor,i,j,k+1} - \phi_{ap\rightarrow a} - \phi_{evap} \quad (5.25)$$

where:

c_{ap} = apple specific heat capacity (J/kg K).

$\phi_{ap\rightarrow hor,i,j,k}$ = heat transfer from apple to bottom friday tray (W).

$\phi_{ap\rightarrow hor,i,j,k+1}$ = heat transfer from apple to top friday tray (W).

$Q_{i,j,k}$ = heat generation rate due to apple respiration (W).

$M_{ap,i,j,k}$ = mass of apples in zone (i,j,k) (kg).

Treating the mass of apple as a dependent variable (Eqn. 5.24) is the physically correct way to model change in apple temperature. However the total change in apple mass during a typical cooling period is in the order of 0.1%, so to simplify the model, the equation used for calculating apple temperature assumed that the apple mass remained constant:

$$M_{ap,i,j,k}c_{ap}\frac{dT_{ma,i,j,k}}{dt} = Q_{i,j,k} - \phi_{ap\rightarrow hor,i,j,k} - \phi_{ap\rightarrow hor,i,j,k+1} - \phi_{ap\rightarrow a} - \phi_{evap} \quad (5.26)$$

The individual heat transfer components of Eqn. 5.26 are:

$$\phi_{ap\rightarrow hor,i,j,k+1} = h_{ap\rightarrow hor,i,j,k+1}\, A_{ap\rightarrow hor,i,j,k+1}\, (\, T_{hor,i,j,k+1} - T_{ma,i,j,k}\,) \quad (5.27)$$

$$\phi_{ap\rightarrow hor,i,j,k} = h_{ap\rightarrow hor,i,j,k}\, A_{ap\rightarrow hor,i,j,k}\, (\, T_{hor,i,j,k} - T_{ma,i,j,k}\,) \quad (5.28)$$

where:

$h_{ap\rightarrow hor,i,j,k}$ = heat transfer coefficient from apple to bottom Friday tray (W/m^2K).

$A_{ap \rightarrow hor,i,j,k}$ = contact area between apple and bottom Friday tray (m^2).

$T_{hor,i,j,k}$ = temperature of Friday tray below apple (°C).

$h_{ap \rightarrow hor,i,j,k+1}$ = heat transfer coefficient from apple to top Friday tray ($W/m^2 K$).

$A_{ap \rightarrow hor,i,j,k+1}$ = contact area between apple and top Friday tray (m^2).

$T_{hor,i,j,k+1}$ = temperature of Friday tray above apple (°C).

$\phi_{ap \rightarrow a}$ and ϕ_{evap} are calculated using Eqn's. 5.3 and 5.4 respectively.

An empirical correlation given by Gaffney *et al.* (1985a) was used to estimate $Q_{i,j,k}$ as a function of temperature:

$$Q_{i,j,k} = (4.59 \times 10^{-6} [T_{ma,i,j,k} + 17.8]^{2.66}) M_{ap,i,j,k} \quad (5.29)$$

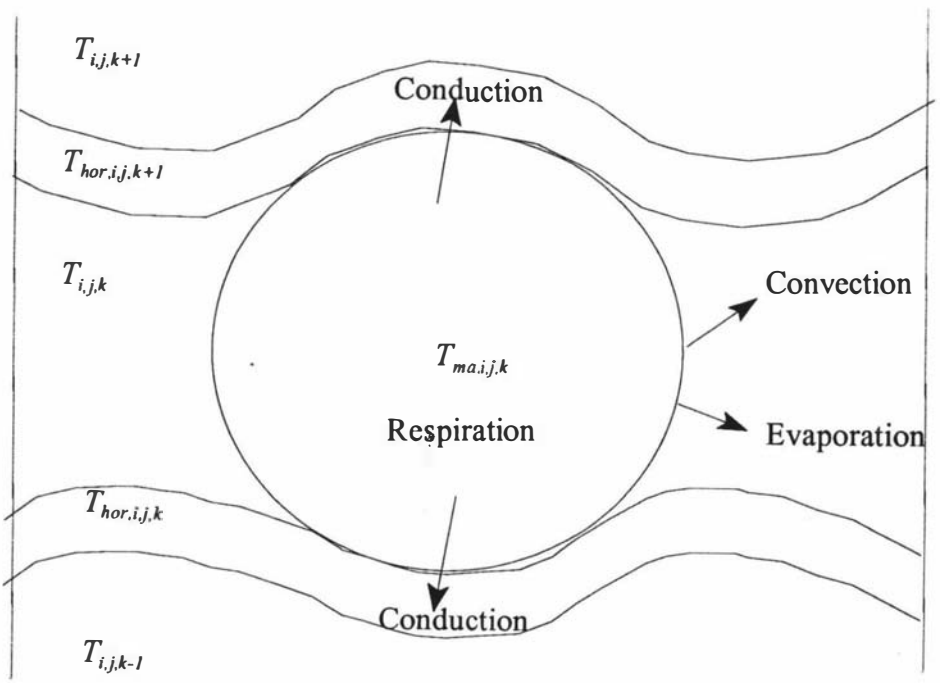

Figure 5.4: Heat transfer pathways modelled from apples.

5.3.3.2 Apple Water Loss

Water loss from apples was calculated using:

$$\frac{dW_{ap,i,j,k}}{dt} = k_{ap} A_{ap} (p_{ap,i,j,k} - p_{i,j,k}) \quad (5.30)$$

where:

$W_{ap,i,j,k}$ = cumulative water loss from apples in zone (i,j,k) (kg).

k_{ap} = mass transfer coefficient from apple to air (s/m).

$p_{ap,i,j,k}$ = partial pressure of water vapour at the apple surface (Pa).

The partial pressure of water vapour at the surface of the apples was expressed as a function of the water vapour pressure at the apple surface temperature and the water activity at the apple surface:

$$p_{ap,i,j,k} = p_{s,ap,i,j,k} a_w \quad (5.31)$$

An Antoine equation approximation for vapour pressure is (Cleland and Cleland, 1992):

$$p_{s,ap,i,j,k} = e^{\left[23.4795 - \frac{3990.56}{T_{aps,i,j,k} + 233.833}\right]} \quad (5.32)$$

where:

$p_{s,ap,i,j,k}$ = water vapour pressure at apple surface temperature in zone (i,j,k) (Pa).

a_w = water activity at apple surface.

$T_{aps,i,j,k}$ = apple surface temperature in zone (i,j,k) (°C).

Although measured data showed little difference between surface and centre temperatures for the apples, it was decided to use surface temperature rather than mass average temperature in apple weight loss calculations. Analytical solutions for calculating mass average and surface temperatures are available for a perfect sphere under constant external conditions (Carslaw and Jaeger, 1959). The approach taken to estimate the surface temperature (Eqn's 5.33 and 5.34) was to use a ratio of the

analytical solutions assuming that only one term in the series was significant:

$$T_{aps,i,j,k} = T_{ma,i,j,k} - (T_{ma_{i,j,k}} - T_{i,j,k}) \left(1 - \frac{Y_{aps,i,j,k}}{Y_{ma,i,j,k}} \right) \tag{5.33}$$

$$\frac{Y_{aps,i,j,k}}{Y_{ma,i,j,k}} = \frac{\left[\beta_i^2 + (Bi - 1)^2\right] \sin^2(\beta_i)}{3\ Bi} \tag{5.34}$$

where:

$Y_{ma,i,j,k}$ = fractional unaccomplished mass average temperature change for the apples in zone (i,j,k).

$Y_{aps,i,j,k}$ = fractional unaccomplished surface temperature change for the apples in zone (i,j,k).

5.3.4 Cardboard Temperatures

Temperature of exterior cardboard surfaces and Friday trays within the carton were modelled. Table 5.2 lists the possible cardboard boundaries/surfaces with which each zone may interact (C1 to C6). Table 5.3 lists the cardboard temperatures modelled which correspond to each of these surfaces.

The six possible cardboard surfaces associated with any zone can be further divided into surfaces where apple to cardboard contact occurs (C5 & C6), and surfaces where only air to cardboard interaction is possible (C1 to C4). The mathematical formulation for each of the two surface types is discussed in turn.

5.3.4.1 Cardboard Surfaces With Apple Contact (C5 and C6)

Figure 5.5 shows the heat transfer pathways modelled for cardboard surfaces with apple contact.

For $1 < k \leq K$:

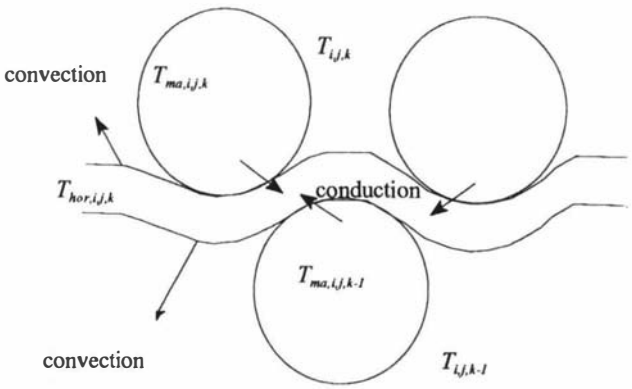

For k =1:

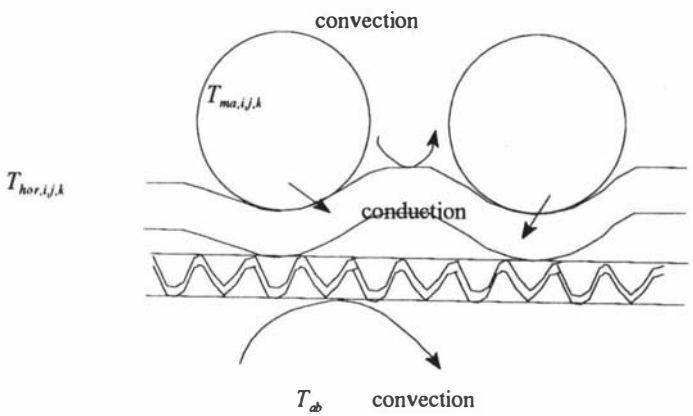

For k = K+1

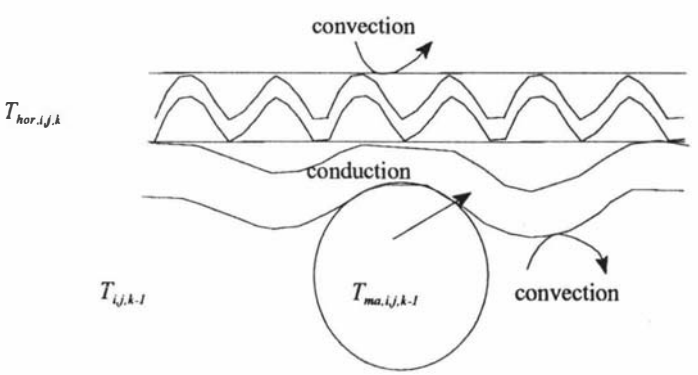

Figure 5.5: Heat transfer pathways modelled from cardboard surfaces with apple contact.

With reference to these pathways the rate of change of cardboard temperature can be expressed mathematically by Eqn's 5.35, 5.36 and 5.37:

for 1 < k < K

$$M_{hor,i,j,k}\, c_{hor,i,j,k}\, \frac{dT_{hor,i,j,k}}{dt} = \phi_{a,i,j,k\rightarrow hor,i,j,k} + \phi_{a,i,j,k-1\rightarrow hor,i,j,k} + \phi_{ap,i,j,k\rightarrow hor,i,j,k} + \phi_{ap,i,j,k-1\rightarrow hor,i,j,k} \quad (5.35)$$

for k = 1 (bottom cardboard layer of carton)

$$M_{hor,i,j,k}\, c_{hor,i,j,k}\, \frac{dT_{hor,i,j,k}}{dt} = \phi_{a,i,j,k\rightarrow hor,i,j,k} + \phi_{ap,i,j,k\rightarrow hor,i,j,k} + \phi_{hor,i,j,k\rightarrow ab} \quad (5.36)$$

for k = K+1 (top cardboard layer of carton)

$$M_{hor,i,j,k}\, c_{hor,i,j,k}\, \frac{dT_{hor,i,j,k}}{dt} = \phi_{a,i,j,k-1\rightarrow hor,i,j,k} + \phi_{ap,i,j,k-1\rightarrow hor,i,j,k} + \phi_{hor,i,j,k\rightarrow ab} \quad (5.37)$$

where:

$T_{hor,i,j,k}$ = temperature of cardboard below apples in zone (i,j,k) (°C).

$M_{hor,i,j,k}$ = mass of the cardboard below apples in zone (i,j,k) (kg).

$c_{hor,i,j,k}$ = specific heat capacity of the cardboard (J/kg K).

$\phi_{a,i,j,k\rightarrow hor,i,j,k}$ = convective heat transfer between zone (i,j,k) air and the cardboard surface (W).

$\phi_{a,i,j,k-1\rightarrow hor,i,j,k}$ = convective heat transfer between zone (i,j,k-1) air and the cardboard surface (W).

$\phi_{ap,i,j,k\rightarrow hor,i,j,k}$ = conductive heat transfer between apples in zone (i,j,k) and the cardboard surface (W).

$\phi_{ap,i,j,k-1\rightarrow hor,i,j,k}$ = conductive heat transfer between apples in zone (i,j,k-1) and the cardboard surface (W).

$\phi_{hor,i,j,k\rightarrow ab}$ = convective heat transfer between the cardboard and the bulk air surrounding the carton (W).

The water content of the cardboard and the potential for absorption of water from the air inside the carton was ignored.

The individual heat transfer components of Eqn's. 5.35, 5.36 and 5.37 are:

$$\phi_{a,i,j,k\rightarrow hor,i,j,k} = h_{a,i,j,k\rightarrow hor,i,j,k} A_{a,i,j,k\rightarrow hor,i,j,k} (T_{i,j,k} - T_{hor,i,j,k}) \quad (5.38)$$

$$\phi_{a,i,j,k-1\rightarrow hor,i,j,k} = h_{a,i,j,k-1\rightarrow hor,i,j,k} A_{a,i,j,k-1\rightarrow hor,i,j,k} (T_{i,j,k-1} - T_{hor,i,j,k}) \quad (5.39)$$

$$\phi_{ap,i,j,k\rightarrow hor,i,j,k} = h_{ap,i,j,k\rightarrow hor,i,j,k} A_{ap,i,j,k\rightarrow hor,i,j,k} (T_{ma,i,j,k} - T_{hor,i,j,k}) \quad (5.40)$$

$$\phi_{ap,i,j,k-1\rightarrow hor,i,j,k} = h_{ap,i,j,k-1\rightarrow hor,i,j,k} A_{ap,i,j,k-1\rightarrow hor,i,j,k} (T_{ma,i,j,k-1} - T_{hor,i,j,k}) \quad (5.41)$$

$$\phi_{hor,i,j,k\rightarrow ab} = h_{hor,i,j,k\rightarrow ab} A_{hor,i,j,k\rightarrow ab} (T_{ab} - T_{hor,i,j,k}) \quad (5.42)$$

where:

$h_{a,i,j,k\rightarrow hor,i,j,k}$ = convective heat transfer coefficient from the air in zone (i,j,k) to the cardboard surface (W/m^2 K).

$h_{a,i,j,k-1\rightarrow hor,i,j,k}$ = convective heat transfer coefficient from the air in zone (i,j,k-1) to the cardboard surface (W/m^2 K).

$h_{ap,i,j,k\rightarrow hor,i,j,k}$ = contact heat transfer coefficient between apples in zone (i,j,k) and the cardboard surface (W/m^2 K).

$h_{ap,i,j,k-1\rightarrow hor,i,j,k}$ = contact heat transfer coefficient between apples in zone (i,j,k-1) and the cardboard surface (W/m^2 K).

$h_{hor,i,j,k\rightarrow ab}$ = heat transfer coefficient between the cardboard surface and the bulk air surrounding the carton (W/m^2 K).

$A_{a,i,j,k\rightarrow hor,i,j,k}$ = cardboard area exposed to air in zone (i,j,k) (m^2).

$A_{a,i,j,k-1\rightarrow hor,i,j,k}$ = cardboard area exposed to air in zone (i,j,k-1) (m^2).

$A_{ap,i,j,k\rightarrow hor,i,j,k}$ = apple to cardboard contact area in zone (i,j,k) (m^2).

$A_{ap,i,j,k-1\rightarrow hor,i,j,k}$ = apple to cardboard contact area in zone (i,j,k-1) (m^2).

$A_{hor,i,j,k\rightarrow ab}$ = cardboard area exposed to bulk air (m^2).

T_{ab} = temperature of air surrounding the carton (°C).

5.3.4.2 Cardboard Surfaces Without Apple Contact (C1, C2, C3 and C4)

All exterior side faces of the carton were modelled assuming that no apple contact occurred. Front cardboard surfaces were modelled using:

$$M_{front,i,j,k}\, c_{front,i,j,k}\, \frac{dT_{front,i,j,k}}{dt} = h_{a,i,j,k \to front,i,j,k} A_{front,i,j,k} (T_{i,j,k} - T_{front,i,j,k}) + h_{front,i,j,k \to a,b} A_{front,i,j,k} (T_{ab} - T_{front,i,j,k}) \quad (5.43)$$

where:

$M_{front,i,j,k}$ = mass of the cardboard surface on the front of the carton with respect to zone (i,j,k) (kg).

$c_{front,i,j,k}$ = specific heat capacity of the cardboard surface on the front of the carton with respect to zone (i,j,k) (J/kg K).

$h_{a,i,j,k \to front,i,j,k}$ = convective heat transfer coefficient from zone (i,j,k) air to the front cardboard surface (W/m^2 K).

$A_{front,i,j,k}$ = exposed surface area between both zone (i,j,k) air and the bulk air surrounding the carton and the front cardboard surface (m^2).

$h_{front,i,j,k \to a,b}$ = convective heat transfer coefficient between the front cardboard surface and the bulk air surrounding the carton (W/m^2 K).

The right side, back and left side cardboard faces were also modelled using equivalents of Eqn. 5.43, by substituting *right, back,* or *left* for *front* respectively. Reference to Tables 5.2 and 5.3 is required to determine which cardboard surfaces are appropriate for each zone within the carton.

5.3.5 Natural and Forced Convection Air Movement

Movement of air between zones (ventilation) can be by natural convection, forced convection, or both.

5.3.5.1 Natural Convection Mechanism

The model used for the natural convection component assumed that equal mass of air interchanges between zones (Figure 5.6).

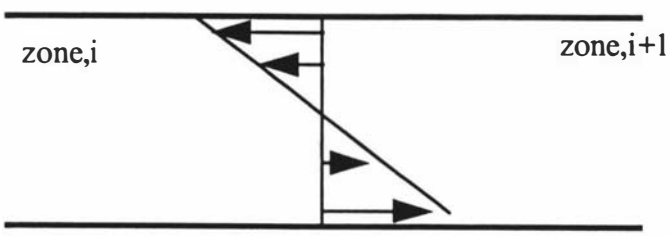

Figure 5.6 Natural convection velocity profile used at zone interfaces in the model.

This approach was chosen to reduce model complexity by ensuring that a constant mass of air is present within the zones. An alternative would be to model total pressure in each zone based on air temperature and to calculate flow based on pressure difference. This would be a mechanistically more rigorous approach to take. However it would entail modelling air mass within each zone as a dependent variable and calculating pressure algebraically. This would involve solving a series of simultaneous equations which would add considerable complexity and computational time to the model. Such an approach was not considered practical.

It is difficult to decide the most appropriate model for determining the extent of natural ventilation in a situation such as that within an apple carton. The literature is void of similar work, with most of the cited work being for convection from horizontal or vertical surfaces (Metais and Eckert, 1964), from single or groups of cylinders (Metais and Eckert, 1964), for spheres enclosed within larger spheres (Amota and Tien, 1972), between horizontal or vertical enclosures (Buchberg *et al.*, 1976; Newell and Schmidt, 1970; Flack and Witt, 1979; Warrington and Powe, 1985), or through porous beds of spherical shaped objects (Beukema and Bruin, 1983; Romero and Chau, 1987).

The apples between each Friday tray carton can be considered as analogous to heated spheres within a horizontal enclosure. Apples in each zone will be at different temperatures as cooling proceeds, and a temperature difference between the two horizontal surfaces would also be expected. Convective currents would be set up due to both the temperature difference between the two horizontal layers and the temperature difference between apples within a layer. Empirical correlations are given in the literature for convection between horizontal layers and for convective heat transfer from spheres. Convection is greatest when the lower layer is hotter than the upper layer as in this situation the higher density air is above the lower density air and hence convection is enhanced. When the lower surface is colder than the upper surface, as would be the case in the lower half of an apple carton, convection is inhibited between the layers. However convection currents would still arise due to the apple to apple temperature difference, between apples in adjacent zones.

The approach taken was to model the natural convection for internal zones as being driven solely by apple to apple temperature difference, and hence to ignore the effect of any convection arising between the horizontal layers (trays). Vertical natural convection between zones was considered for zones around the outside of the carton where the tray is not a complete barrier. The extent of natural convection was calculated using the following empirical relationship given by Holman (1990) which calculates the effective or apparent thermal conductivity between two vertical surfaces (apples):

$$\frac{\lambda_e}{\lambda_a} = 0.197 \left(Gr\ Pr \right)^{\frac{1}{4}} \left(\frac{\delta}{d_{ap}} \right)^{-\frac{1}{9}} \tag{5.44}$$

$$Gr = \frac{g\ \beta \left(T_{z1} - T_{z2} \right) \delta^3}{\nu^2} \tag{5.45}$$

$$Pr = \frac{\nu}{\alpha} \tag{5.46}$$

$$\beta = \frac{1}{T_{av}} \tag{5.47}$$

where:

λ_e = effective thermal conductivity of air including the effect of natural convection (W/m K).

λ_a = air thermal conductivity (W/m K).

Gr = Grashof number.

Pr = Prandtl number.

β = volume coefficient of expansion of air (K^{-1}).

T_{av} = average air temperature (K).

T_{z1} = temperature of apples in 1st zone (°C).

T_{z2} = temperature of apples in 2nd zone (°C).

d_{ap} = distance between vertical surfaces (apples) (m).

δ = distance between friday trays (m).

ν = kinematic viscosity of air (m^2/s).

α = thermal diffusivity of air (m^2/s).

The mass flow rate between zones was calculated by assuming that the net sensible heat flow due to ventilation could be determined from the use of effective thermal conductivity in a heat conduction model. That is:

$$\frac{\lambda_e A_l (T_{i,j,k} - T_l)}{\delta} = m_{l,nat} c_a (T_{i,j,k} - T_l) \quad (5.48)$$

thus

$$m_{l,nat} = \frac{\lambda_e A_l}{\delta c_a} \quad (5.49)$$

where:

A_l = cross-sectional area of the l^{th} zone boundary (m^2).

T_l = temperature of the l^{th} zone (°C).

$m_{l,nat}$ = natural ventilation across the l^{th} boundary (kg/s).

Appropriate zone values for T_l are given in Table 5.3.

5.3.5.2 Forced Convection Mechanism

The procedure used for modelling forced convection within the carton was to set air flow vectors within the carton (Figure 5.3). The magnitude of air flows was estimated from the total mass flow rate of air into the carton, by using proportioning coefficients based on the measured velocities within the carton (Table 4.4). Symmetry across the carton was assumed.

Total air flow into the carton was determined as follows:

$$m_{tot} = A_{vent} v_{vent} \rho_a \quad (5.50)$$

where:

m_{tot} = total air flow into and out of the carton through the vents (kg/s).

A_{vent} = area of vents (m^2).

v_{vent} = air velocity through vent (m/s).

ρ_a = air density (kg/m^3).

For zones down the length of the carton, except the end zones, (j=2 to j=J-1) all forced convection air flows except that in the j^{th} (length wise) direction were set to zero. The air flow in the j^{th} direction was calculated for j=2 to j=J using:

$$m^{j}_{for,i,k} = m_{tot}\ rv_{lay,k}\ rv_{chan,i} \tag{5.51}$$

where:

$m^{j}_{for,i,k}$ = flow rate of dry air from zone (i,j-1,k) to zone (i,j,k) (kg/s).

$rv_{lay,k}$ = proportion of total air flow into the carton (m_{tot}) which flows into the k^{th} layer.

$rv_{chan,i}$ = proportion of the total flow down the k^{th} layer which flows in the i^{th} channel across the carton.

For zones at each end of the carton the situation is more complex, as flow is possible both vertically between layers and horizontally across and down the carton. For j = 1 (nearest the inlet) and j = J+1 (nearest the outlet):

$$m^{j}_{for,i,k} = m_{tot}\ rv_{in,i,k} \tag{5.52}$$

where:

$rv_{in,i,k}$ = proportion of total flow into the carton which enters the i,1,k^{th} or leaves the i,J,k^{th} zone.

In the case of the apple carton modelled, forced convection only enters and leaves the 3 zones immediately adjacent to the vents. These are: i = 2 to 4, j = 1, k = 4 for entry; i = 2 to 4, j = J, k = 4 for exit. All other $rv_{in,i,k}$ values are zero.

Vertical flow rates at the inlet end were calculated with reference to layer k = 4, where the air enters the carton. For layers below the vent ($k \leq 4$), the vertical flow vector was:

$$m^{k}_{for,i,j} = -\ m_{tot}\ rv_{vert,i} \sum_{k=1}^{k=k} rv_{lay,k} \tag{5.53}$$

where:

$rv_{vert,i}$ = proportion of the total air flow which moves up the i^{th} vertical

channel across the carton.

$m^{k}_{for,i,j}$ = flow rate from the k-1th to the kth layer in the ith channel across the carton (kg/s).

For layers above the vent (k > 4):

$$m^{k}_{for,i,j} = m_{tot}\, rv_{vert,i} \sum_{k=k}^{k=K} rv_{lay,k} \tag{5.54}$$

For the exit vent end (j = J) the above two equations are used but the flows are reversed (opposite sign).

The sideways flows, $m^{i}_{for,j,k}$, for the zones at the entry and exit zones are calculated to ensure a mass balance on each zone. The calculations must be performed in order from the outside of the carton to the centre, i.e. i = 1 to i = I/2, and from i = I to i = I/2. For i ≥ I/2:

$$\begin{aligned} m^{i}_{for,j,k} &= m^{j}_{for,i,k} - m^{j+1}_{for,i,k} + m^{k}_{for,i,j} \\ &\quad - m^{k+1}_{for,i,j} + m^{i+1}_{for,j,k} \end{aligned} \tag{5.55}$$

where:

$m^{i}_{for,j,k}$ = flow rate from zone (i-1,j,k) to zone (i,j,k) (kg/s).

For i < I/2:

$$\begin{aligned} m^{i}_{for,j,k} &= m^{j}_{for,i,k} - m^{j+1}_{for,i,k} + m^{k}_{for,i,j} \\ &\quad - m^{k+1}_{for,i,j} + m^{i-1}_{for,j,k} \end{aligned} \tag{5.56}$$

For i = 1: $m^{i-1}_{for,j,k} = 0$

and for i = I $m^{i+1}_{for,j,k} = 0$.

5.3.5.3 Combined Natural and Forced Convection Flows

In any heat transfer process both natural and forced convection flow may occur. If the forced convection effects are large the influence of natural convection may be negligible and, similarly, when natural convection forces are very strong, the forced convection effects may be negligible.

Yuge (1960) found that the Nusselt number for heated spheres in a cross-wind is determined almost solely by the Grashof number when the Reynolds number is less than about 16 but approaches the value for forced convection as the Reynolds number increases. Monteith and Unsworth (1990) state that the ratio of Grashof number (Gr) to Reynolds number (Re) squared, Gr/Re^2, can be used as a criterion for determining the balance between forced and natural convection as the ratio is proportional to the ratio of buoyancy to inertial forces. When Gr is much larger than Re^2, buoyancy forces are much larger than inertial forces and heat transfer is governed by free convection. When Gr is much less than Re^2, buoyancy forces are negligible and forced convection is the dominant mode of heat transfer. When Gr is the same order of magnitude as Re^2 then neither natural or forced convection can be ignored. Analysis of typical velocities within a carton under pre-cooling conditions using these criteria showed that combined natural and forced convection is the most likely mode of heat transfer.

The convective heat transfer coefficient for mixed free and forced convection was based on a weighted average of the predictions for purely free or purely forced convection under the prevailing conditions (Monteith & Unsworth, 1990):

$$h_{combined} = \left(h_{natural}^{m} + h_{forced}^{m}\right)^{\frac{1}{m}} \tag{5.57}$$

where:

$h_{combined}$ = combined heat transfer coefficient (W/m^2 K).

$h_{natural}$ = natural convection heat transfer coefficient (W/m^2 K).

h_{forced} = forced convection heat transfer coefficient (W/m^2 K).

m = weighting factor.

Monteith & Unsworth (1990) state that the best correlation with measured data was obtained with $m = 3$.

In order to incorporate both natural and forced convection of air an analogous approach for combining mass flow rates into and out of each zone to that used to calculate heat transfer coefficients was assumed. Using this analogy, the mass flow rate into a generalised zone across any one face is an empirical function of both forced and natural ventilation:

$$m_{l,in} = \left(m_{l,for}^3 + m_{l,nat}^3\right)^{\frac{1}{3}} \tag{5.58}$$

where:

$m_{l,in}$ = air flow from the l^{th} zone associated with zone (i,j,k) to zone (i,j,k) (kg/s).

$m_{l,for}$ = forced convective air flow across the boundary between the zone and the l^{th} associated zone (kg/s).

$m_{l,nat}$ = natural convective air flow across the boundary between the zone and the l^{th} associated zone (kg/s).

To ensure that a mass balance was maintained for each zone, some back-mixing must occur out of the same boundary into the l^{th} associated zone:

$$m_{l,out} = m_{l,in} - m_{l,for} \tag{5.59}$$

where:

$m_{l,out}$ = air flow from zone (i,j,k) to the l^{th} associated zone through the l^{th} boundary (kg/s).

5.3.6 Radiation

The level of natural convection was estimated to be an order of magnitude higher than the rate of radiation heat transfer for large temperature differences between zones. For these reasons radiation was not modelled directly. As Section 5.3.7 will show its effect was considered in the calculation of heat transfer coefficients by adding a "pseudo-convection" allowance.

5.3.7 Heat Transfer Coefficients

The heat transfer coefficients (htc's) from apples to air and from the air to cardboard surfaces are a function of both the temperature difference between the two surfaces and air movement, i.e. both natural and forced convection. Initially a constant value for each heat transfer coefficient was used in the model. However this resulted in greater than measured heat transfer early in each simulation and less than measured heat transfer later. As a result it was decided to re-estimate heat transfer coefficients as the simulation proceeded. Eqn 5.57 was used to calculate the combined htc's using a weighting factor of 3. The following empirical correlations were used to determine the forced and natural htc's.

5.3.7.1 Apple To Air Heat Transfer Coefficients

The forced and natural convection heat transfer coefficients (htc's) from the apples were calculated using:

$$h_{conv} = \frac{Nu\ \lambda_a}{d} \tag{5.60}$$

where:

h_{conv} = convective heat transfer coefficient (W/m^2 K).

d = characteristic dimension (m).

Nu = Nusselt number.

For natural convection (Holman, 1990):

$$Nu = 2 + 0.43\ (Gr\ Pr)^{0.25} \tag{5.61}$$

For forced convection (Gaffney *et al.*, 1985a):

$$Nu = 2 + 0.522\ Re^{0.53}\ Pr^{0.33} \tag{5.62}$$

where:

Pr = Prandtl number

$$Re = \frac{\rho_a \, v \, d}{\mu} \tag{5.63}$$

$$v = \frac{m^j_{for,i,k}}{A_l} \tag{5.64}$$

The apple diameter was used as the characteristic dimension in Eqn's 5.60 and 5.63.

5.3.7.2 Cardboard To Air Heat Transfer Coefficients

Eqn 5.60 was used to calculate the cardboard to air htc's, both within the carton and from ambient air to the carton, using Nusselt numbers calculated from empirical correlations. For forced convection (Monteith & Unsworth, 1990):

$$Nu = 0.032 \, Re^{0.8} \tag{5.65}$$

For natural convection (Monteith & Unsworth, 1990):

$$Nu = 0.58 \, Gr^{0.25} \tag{5.66}$$

The length of the largest face was used as the *d* in Eqn's. 5.60 and 5.63.

Eqn 5.66 predicts very low heat transfer coefficients with very low temperature differences. Predictions using this approach underpredicted rates of heat transfer early in the simulations. It was decided that the radiation effects which had been ignored may have been important early in the simulations. The pseudo-convection radiation htc would remain relatively constant with temperature difference whereas the natural convection htc would increase with increasing temperature difference (Figure 5.7). As a result, a minimum htc value of 2.0 W/m^2 K was used in the model to account for radiation effects. This corresponds to a combined emissivity/view factor of about 0.5.

In modelling the cardboard it was assumed that the thermal mass of the cardboard was lumped midway through the cardboard. Hence the overall heat transfer coefficients

from the zone air to the cardboard, and from the cardboard to the bulk air both include the appropriate air boundary layer resistance and half the cardboard resistance as well as the resistance of any air gap trapped by the packaging:

$$\frac{1}{h_{a,i,j,k\rightarrow cd,n}} = \frac{1}{h_{conv}} + \frac{x_{card}}{\lambda_{card}} + \frac{x_{ag}}{\lambda_a} \tag{5.67}$$

where:

h_{conv} = convective heat transfer coefficient from the air to the cardboard surface (W/m^2 K).

x_{card} = cardboard half-thickness (m).

λ_{card} = cardboard thermal conductivity (W/m K).

x_{ag} = thickness of air gap (m).

λ_a = air thermal conductivity (W/m K).

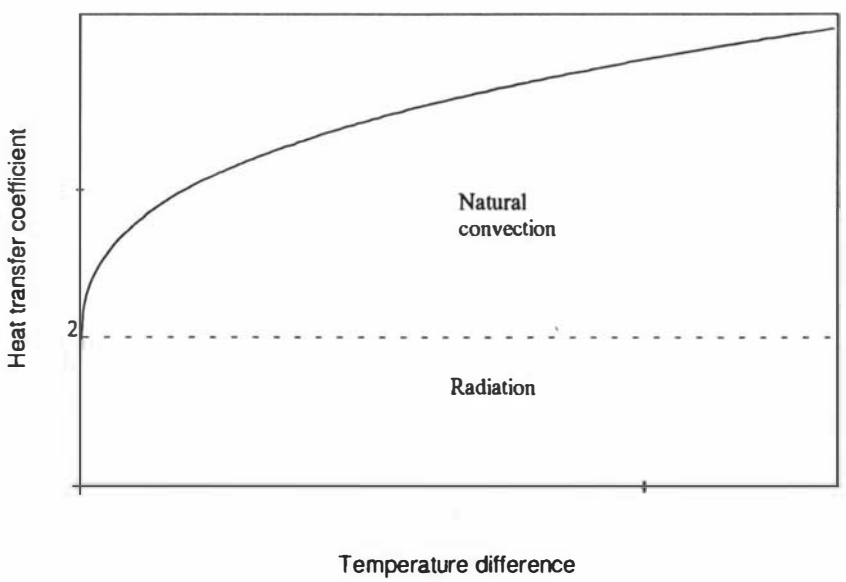

Figure 5.7 Effect of radiation and convection on effective heat transfer coefficient as a function of temperature difference.

5.3.7.3 Apple To Cardboard Heat Transfer Coefficients

Conduction from apples to cardboard was treated as pseudo-convection in the model, and the heat transfer coefficients used represent the contact resistance and half the cardboard resistance:

$$\frac{1}{h_{ap,i,j,k\rightarrow hor,i,j,k}} = \frac{1}{h_{cond}} + \frac{x_{card}}{\lambda_{card}} + \frac{x_{ag}}{\lambda_{ag}} \qquad (5.68)$$

where:

h_{cond} = conductive heat transfer from apple surface to cardboard (W/m^2 K).

For the top (k=K, Figure 5.2) and bottom layers (K=1) the friday trays and exterior cardboard were modelled together using one temperature, as they are in contact with one another and effectively form a continuous barrier to heat transfer from air within the carton to the air surrounding it.

5.3.8 Model Implementation

The model was programmed in Turbo Pascal v6.0 Professional and run on a 486DX 50 MHz personal computer. The source and executable codes for the model are provided on diskette 1 attached. The model was programmed with 150 zones (5 x 5 x 6) and consisted of 770 ordinary differential equations (ODE's) and more than 2000 algebraic equations. The Runge-Kutta-Fehlberg (RKF) numerical ODE solver with fourth order error estimation and local extrapolation to make it a fifth order method as described by Lovatt (1992) was used to solve the ODE's. The RKF method requires six model evaluations per time step and produces both fourth and fifth order solutions. The difference between the two solutions is an estimate of the error in the fourth order solution. This difference was used by a step size controller to control the integration error. The model took 4 hours to simulate a 24 hour cooling period.

Document files *carton.doc* (MS-Word for windows format) and *carton.wpd* (Word perfect 6.1 for windows format) are supplied on diskette 2. These files describe the main features of the carton model program.

CHAPTER 6: APPLE CARTON COOLING MODEL TESTING

6.1 INTRODUCTION

This chapter describes the validation of the apple carton cooling model formulated in Chapter 5. Validation consisted of two major steps: determination of appropriate model parameter values for the apple cartons used by the New Zealand Apple and Pear Marketing Board; and then comparison of predictions with measured data from apple carton cooling trials (Chapter 4).

6.2 DETERMINATION OF PARAMETER VALUES

Many parameter values were stated in Chapter 5. Remaining parameter values used in the model are given in Table 6.1. These values were either calculated based on empirical correlations, obtained from the literature, or measured data (Chapter 4).

The total apple surface area (A_{ap}) was calculated from measured radii by assuming that the apples approximated perfect spheres. Apple to cardboard contact surface areas ($A_{ap\text{-}hor,i,j,k}$ and $A_{ap\text{-}hor,i,j,k+1}$) were measured by placing apples onto friday trays covered in chalk dust. The percentage of apple surface covered by chalk was used to estimate contact surface area.

The carton and Friday trays were weighed to determine overall cardboard masses. Cardboard masses in each zone were calculated on a pro-rata basis based on surface areas and volumes.

The basis used to determine the various heat transfer coefficients (htc's) between the cardboard and apples or air is described in Section 5.3.7. In general terms, because the thermal mass of the cardboard was assumed to be lumped at the centre of the cardboard, the htc represents the combined heat transfer resistance of half the cardboard resistance, the boundary layer resistance (or contact resistance), plus any trapped air resistance. The inside boundary layer resistances were calculated at each time step in the simulation, whilst outside

boundary layer resistances were entered and assumed constant throughout the simulation. Cardboard thickness, thermal conductivity, and contact resistances used are given in Table 6.1.

Air flow proportioning coefficients used to determine air flow rates within the carton were set using the data of Table 4.8 as a guide. Values used are given in Table 6.1.

The model was run to simulate carton cooling without ventilation (v_{vent} set to 0); with suppressed surface heat transfer (outside htc's set to 0, v_{vent} set to 1.12 m/s); and for an unmodified carton (v_{vent} set to1.12 m/s), to allow comparison with measured data (Chapter 4).

Table 6.1

Parameter Values Used In Carton Model Testing

Parameter	Value Used
Number of zones	150
Zones down the carton length (J)	5
Zones across the carton (I)	5
Layers within the carton (K)	6
Measured Directly	
Bulk air RH	0.85
Bulk air temperature	0°C
Number of apples in carton	198
Apple radius (R)	0.027 m
Apple to top card surface area ($A_{ap\text{-}hor,i,j,k+1}$)	20% of A_{ap}
Apple to bottom card surface area ($A_{ap\text{-}hor,i,j,k}$)	20% of A_{ap}
Apple to air contact surface area ($A_{ap\text{-}a}$)	60 % of A_{ap}
Hand hole area (A_{vent})	0.00388 m^2
Net inlet velocity through vent (v_{vent})	0 or 1.12 m/s
Carton height	0.29 m
Carton width	0.32 m

Table 6.1 Continued

Carton length	0.515 m
Cardboard half thickness (x_{card})	0.0038 m
Total mass of carton exterior cardboard	1.03 kg
Mass of each friday tray	0.08 kg
Estimated From Other Measured Data	
Total apple surface area in carton	1.8 m^2
Apple surface area per zone (A_{ap})	0.012 m^2
Carton air volume (total)	0.026 m^3
Carton air volume (per zone)	0.000173 m^3
Apple volume in carton	0.021 m^3
Apple volume per zone (V_{ap})	0.00014 m^3
Surface areas between zones (A_l):	
Boundaries 2 & 4	0.00157 m^2
Boundaries 1 & 3	0.00249 m^2
Zone air to cardboard surface areas ($A_{a,i,j,k-front,i,j,k}$ etc):	
Front & back	0.00315 m^2
Right & left sides	0.00249 m^2
Horizontal cardboard surface areas ($A_{a,i,j,k-hor,i,j,k}$ & $A_{a,i,j,k-1-hor,i,j,k}$)	0.0048 m^2
Obtained From Literature	
Air total pressure (P_t)	101300 Pa
Apple Heat Capacity[1] (C_{ap})	3650 J/kg K
Apple density[1] (ρ_{ap})	830 kg/m^3
Apple thermal conductivity[1] (λ_{ap})	0.42 W/m K
Apple mass transfer coefficient[2] (k_g)	0.514×10^{-9} kg/m^2 s kPa
Latent heat of vaporisation (h_{fg})	2502 kJ/kg
Dry air heat capacity (c_a)	1010 J/kg K
Water vapour heat capacity (c_v)	1870 J/kg K
Water heat capacity (c_w)	4180 J/kg K
Kinematic viscosity of air (ν)	13×10^{-6} m^2/s
Thermal diffusivity of air (α)	18×10^{-6} m^2/s

Table 6.1 Continued

Air density	1.2 kg/m^3
air viscosity	120×10^{-7} N/s m^2
Cardboard thermal conductivity (λ_{card})	0.048 W/m K
Cardboard heat capacity[3] (c_{card})	1700 J/kg K
Cardboard Permeance[3] (Pe)	2×10^{-9} s/m
Calculated From Empirical Correlations:	
Outside cardboard surface heat transfer coefficients ($h_{front,i,j,k-a,b}$ etc):	
Right,left,front,back	7.0 W/m^2 K
Top,Bottom ($h_{hor,i,j,k-a,b}$)	5.3 W/m^2 K
Inside cardboard surface heat transfercoefficients ($h_{a,i,j,k-front,i,j,k}$ etc):	
Right,left,front,back	12.6 W/m^2 K
Top, bottom ($h_{a,i,j,k-hor,i,j,k}$, For k=1 and k=K+1)	3.5 W/m^2 K
Friday tray top & bottom ($h_{a,i,j,k-hor,i,j,k}$, For $1 < k \leq K$)	35 W/m^2 K
Apple to Friday trays ($h_{a,i,j,k-hor,i,j,k}$, For $1 < k \leq K$)	25 W/m^2 K
Apple to top and bottom cardboard surfaces ($h_{ap,i,j,k-hor,i,j,k}$, For k=1 and k=K+1)	15 W/m^2 K
Assumed Values:	
Apple water activity (a_w)	1.0
Air gaps in cardboard:	
Side faces (front, right, back,left)	0 mm
Top and Bottom faces	5 mm
Air Flow Proportioning Coefficients:	
$rv_{lay,1}$	0.1
$rv_{lay,2}$	0.075
$rv_{lay,3}$	0.075
$rv_{lay,4}$	0.25
$rv_{lay,5}$	0.275
$rv_{lay,6}$	0.225
$rv_{in,2,4}$	0.25

Table 6.1 Continued

$rv_{in,3,4}$	0.5
$rv_{in,4,4}$	0.25
$rv_{vert,1,k}$	0.275
$rv_{vert,2,k}$	0.15
$rv_{vert,3,k}$	0.15
$rv_{vert,4,k}$	0.15
$rv_{vert,5,k}$	0.275
$rv_{chan,1}$	0.375
$rv_{chan,2}$	0.1
$rv_{chan,3}$	0.05
$rv_{chan,4}$	0.1
$rv_{chan,5}$	0.375

[1] = Mellor (1976); [2] = Gaffney et al. (1985); [3] = CIBS guide, (1975).

6.3 COOLING WITHOUT VENTILATION

Figures 6.1 and 6.2 present model predictions and measured data for carton cooling without ventilation into the carton. There was only a small spread of measured data between the four cooling trials, indicating good repeatabilty and low experimental error (Figure 4.19). Greatest spread of data was evident for positions close to the exterior of the carton (e.g. position 1), with interior positions (e.g. position 4) showing smaller spread. A likely cause would be greater sensitivity of results to thermocouple positioning near the outer surfaces. Minor differences in thermocouple positioning between replicates would alter measured cooling rate more nearer the exterior cardboard surfaces where temperature gradients with position would be expected to be largest. Model predictions showed good fit with measured data for interior positions and progressively worse fit towards the exterior side zones within the carton (e.g. position 1 and 3). The observed lack of fit may be due to incorrect parameter values being used in the model, inadequacies in the model formulation or a combination of both. It was initially thought that the lack of fit for position 3 might be caused by an underestimation of the exterior heat transfer coefficients but sensitivity analysis showed that the predictions were not particularly sensitive to increased heat transfer coefficients. Another possible cause may be that, due to practical difficulties in

measurement, thermocouples were placed in the air close to the exterior cardboard surfaces, whereas the model predictions are for the exterior zone as a whole which includes a significant mass of apples. Of the exterior zones, position 1 which was close to the exterior front face of the carton, had thermocouples placed further from the cardboard surface than position 3. Model fit for position 1 was better than that shown for position 3. Use of a larger number of zones in the model so that the exterior zone more closely aligns with each measurement position may have reduced the lack of fit for position 3, but it would also have increased the computation time significantly.

The empirical correlation used for predicting natural convection flows within the carton ignores any natural convection arising between the two horizontal cardboard layers which are likely to be at different temperatures and there was doubt whether it was appropriate for the situation in an apple carton. The fit shown between measured and predicted data suggests that the simple approach taken is a reasonable compromise between accuracy and computational complexity, in spite of possible weaknesses in it.

A sensitivity analysis was performed to determine which parameter values were most influential on model predictions, and hence to determine the critical parameters which most limited accuracy.

It was found that the model predictions were not sensitive to the mass of air present within each zone. The actual volume of air present in the carton is 0.026 m^3. Computational speed was very slow when the model was run with this volume of air assumed to be present, because the buffering offered by such a small volume is very low and small time steps were required for stability and accuracy. The model was run with the air volume arbitrarily increased 10 and 100 fold. This increase in air volume had little effect on the predictions of apple and air temperatures, but allowed faster computational speed. The air volume was increased 10 fold in following simulations to give shortened computation times.

The model was run with the apple respiration rate halved and doubled to test sensitivity to internal heat generation. This was undertaken because the respiration rate is calculated

using a temperature correlation given by Gaffney *et al* (1985a) and there is a wide range of values published for apple respiration rate. The rate of apple cooling was not sensitive to internal heat generation rate.

The predictions were found to be sensitive to change in the contact area between apples and the cardboard surfaces, but less sensitive to change in heat transfer coefficients through the sides of the carton. This indicates that cooling of interior zones is probably dominated by conduction from the apples to the friday trays and then from the friday trays into zones that are nearer the carton top or bottom rather than by natural convection to the side faces of the carton.

Measured and predicted data in Figures 6.1 to 6.12 are for air temperatures unless stated otherwise. The initial temperature lag of about 30 minutes represents carton set-up before placement in the cooling tunnel. Predicted temperatures were offset by the same amount to allow direct comparison of data.

6.4 COOLING WITH SUPPRESSED SURFACE HEAT TRANSFER

Comparisons of model predictions with measured data for cartons with suppressed surface heat transfer are presented in Figures 6.3 to 6.6. The spread of experimental data between the four trials was greater than for the cooling without ventilation trials. This was probably due to differences in airflow within each of the cartons resulting from carton set-up variations. More often than not, model predictions fell within the range of measured data but some lack of fit between model predictions and measured data was evident. In general, the agreement was not as good as for the cooling without ventilation trials. This was probably due to both the difficulty of setting airflow proportioning coefficients within the carton and thermocouple positioning as discussed in Section 6.2.

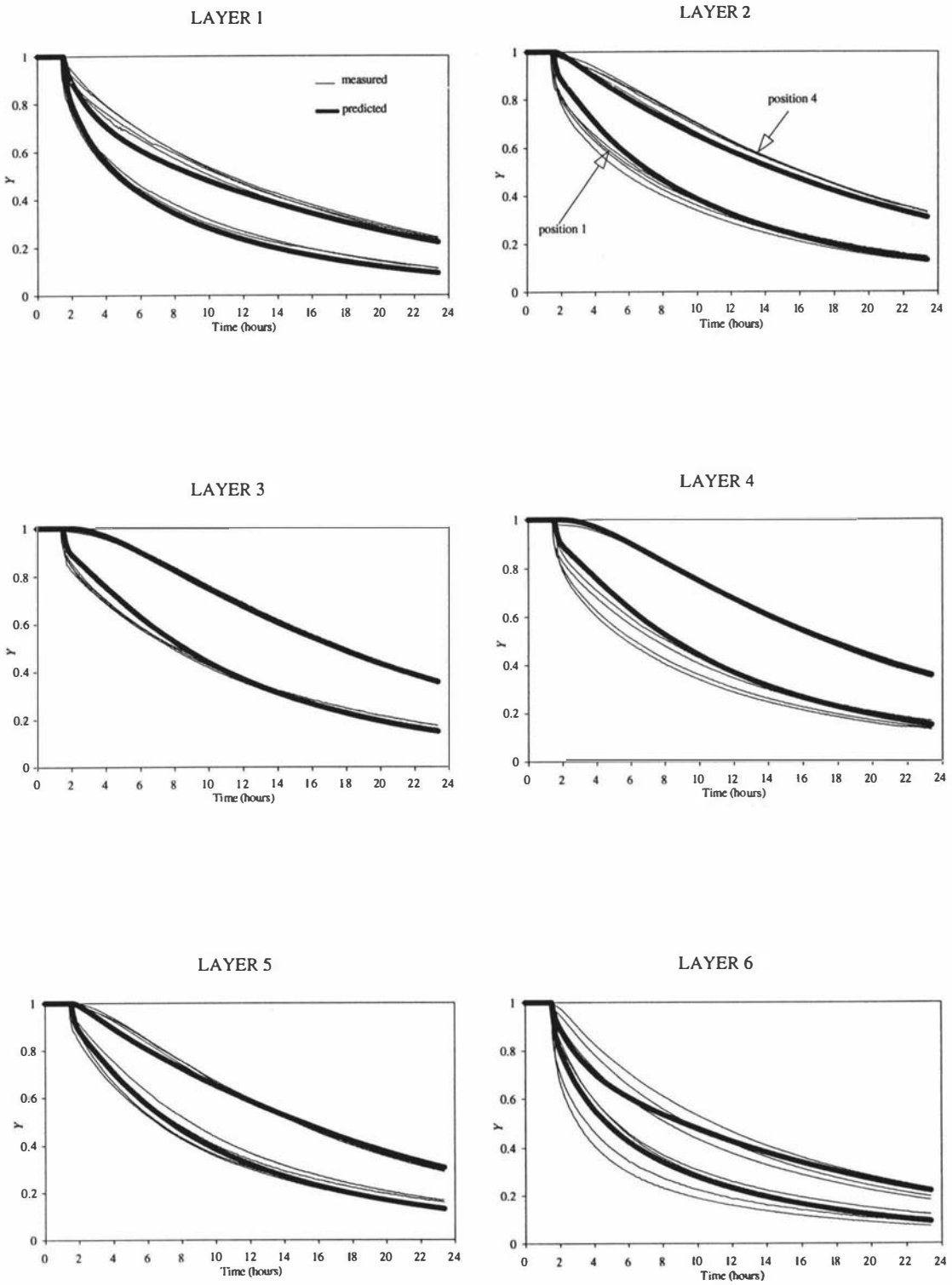

Figure 6.1: Comparison of model predictions and measured data for carton positions 1 and 4 during carton cooling trials without ventilation (labels shown for layers 1 and 2 apply for all layers).

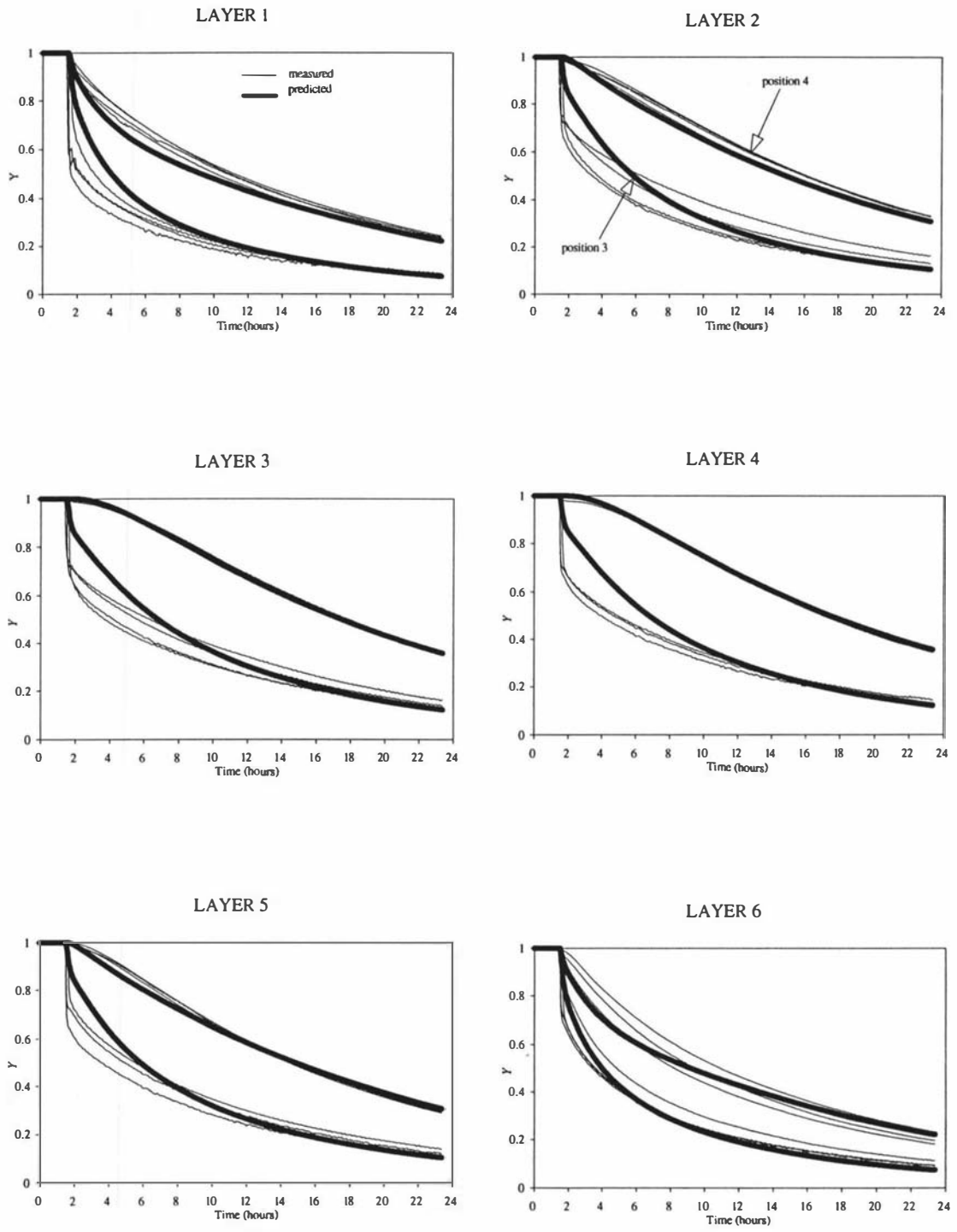

Figure 6.2: Comparison of model predictions and measured data for carton positions 3 and 4 during carton cooling trials without ventilation (labels shown for layers 1 and 2 apply for all layers).

Lack of fit was worst for positions close to both the front and back faces of the carton (e.g. positions 1 and 7). These two faces are where the largest airflows were assumed to occur within the carton and hence where sensitivity to uncertainty in air flow may have been greatest. Given the wide spread of experimental results, using a full hydrodynamic prediction of airflow within the carton may improve the model only slightly, but at considerable programming and computational cost.

Overall, it was difficult to decide whether the systematic offsets of predictions away from measurements were more due to model shortcomings, or to inaccurate data for parameter estimates, especially the air flow proportioning coefficients. However, as will be shown in Section 6.6, model predictions did match industrial practice, so it was concluded that the remaining lack of fit, whatever the cause, could be tolerated.

6.5 COOLING OF UNMODIFIED CARTONS

Results for model predictions and measured data for cooling trials with unmodified cartons are presented in Figures 6.7 to 6.12. The spread of experimental data was larger in these trials than it was for either the carton cooling trials without ventilation or with suppressed surface heat transfer. As was the case in the trials with suppressed surface heat transfer, most of the lack of fit was probably caused by uncertainty in the air flow proportioning coefficients being used, although the lack of fit shown by position 1, layer 4 (Figure 6.7) and position 7, layers 3, 4 , 5 and 6 (Figure 6.9) could also have been partly due to thermocouple positioning. Thermocouples were located at a distance from the cardboard surfaces at these locations, and hence they may not have been exposed to the airflow currents up the front and back faces of the carton to the same extent as other thermocouples nearer cardboard surfaces. Positions close to the side exterior cardboard (e.g. position 3) showed better fit than they did for the cooling without ventilation trials.

The measured air cooling rates at each of the positions were slightly lower than in the trials with suppressed surface heat transfer. This was probably due to lower airflow into the carton resulting from the slightly lower incident velocity onto the end of the carton in this

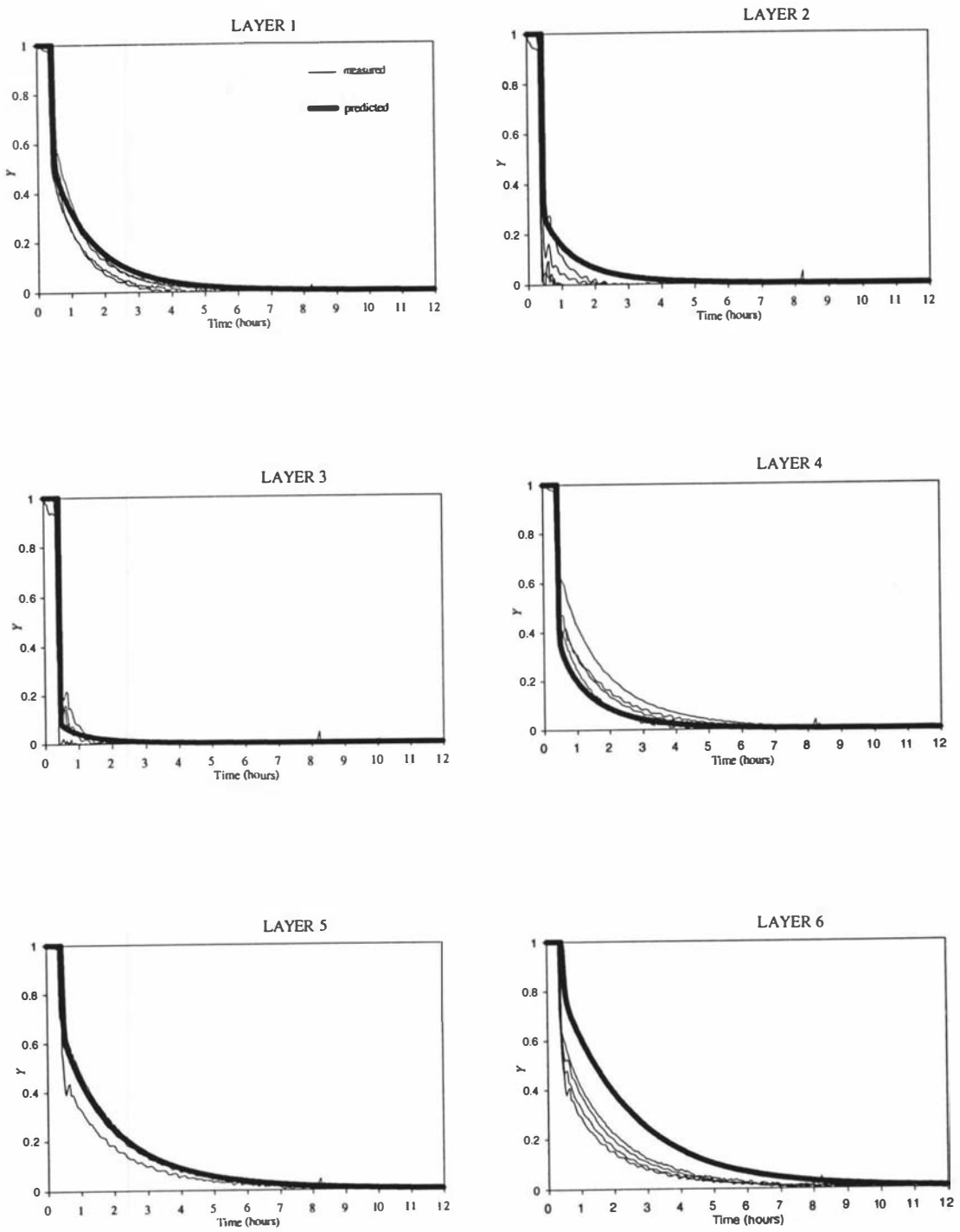

Figure 6.3: Comparison of model predictions and measured data for carton position 1 during the four carton cooling trials with suppressed surface heat transfer (labels shown for layer 1 apply for all layers).

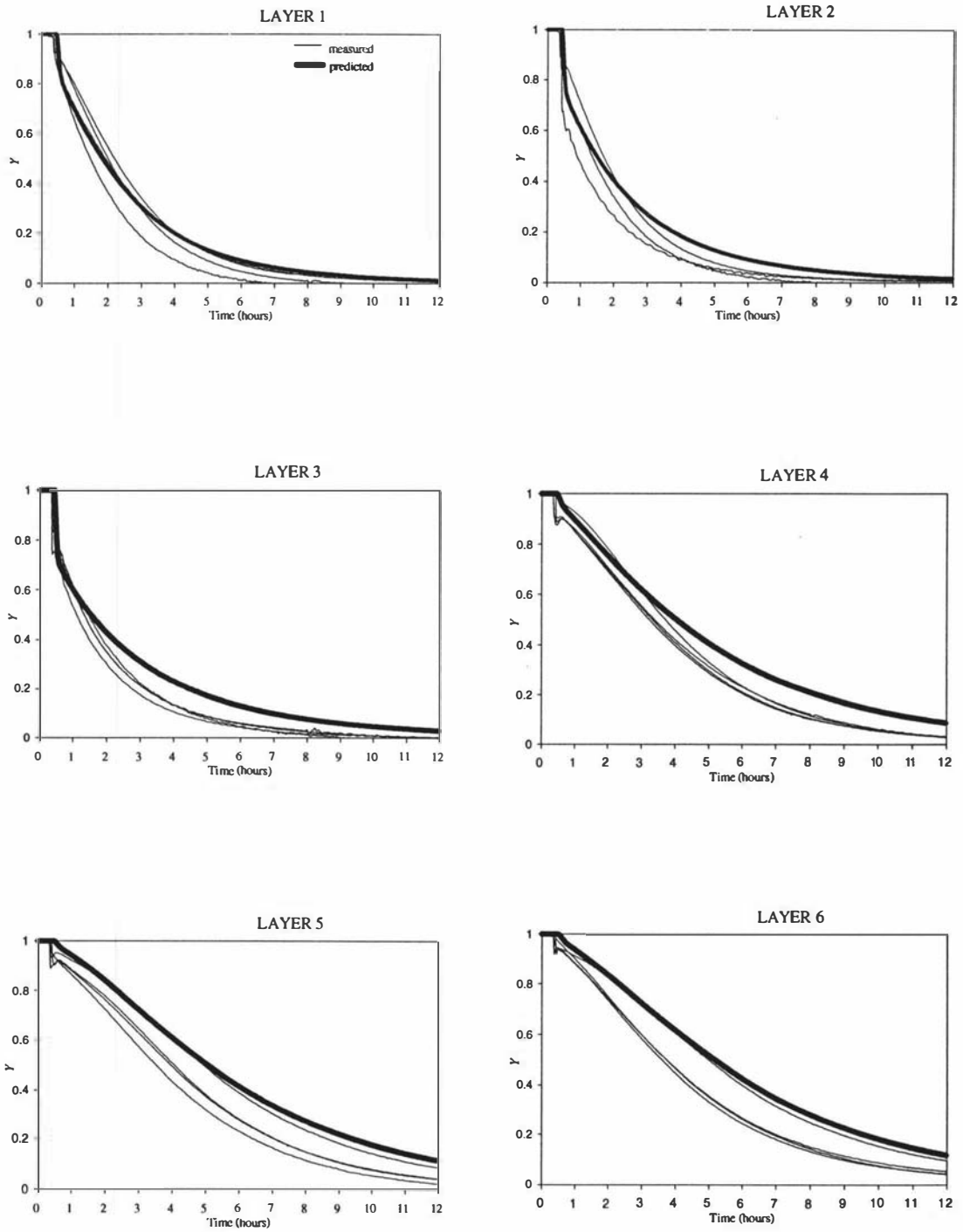

Figure 6.4: Comparison of model predictions and measured data for carton position 4 during the four carton cooling trials with suppressed surface heat transfer (labels shown for layer 1 apply for all layers).

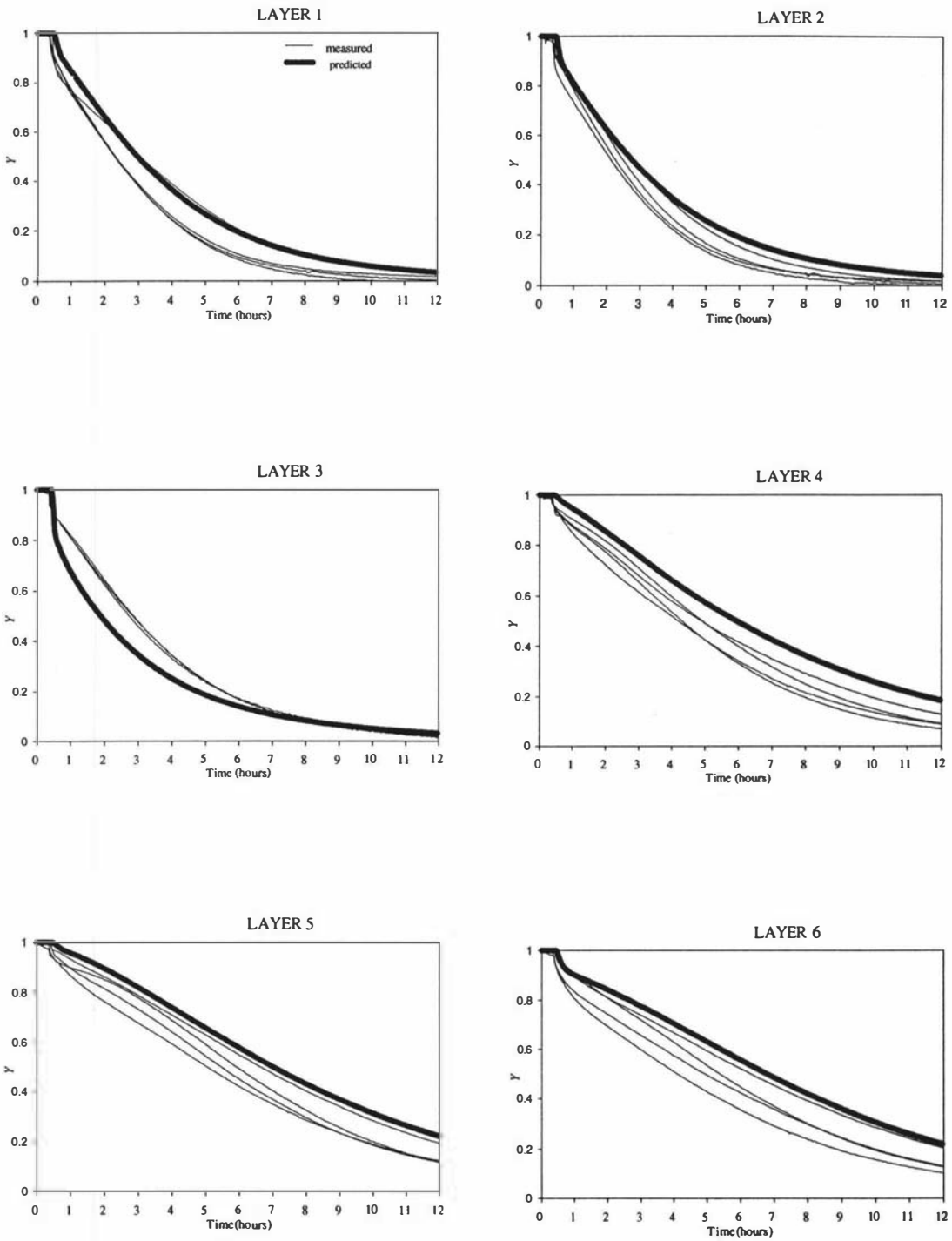

Figure 6.5: Comparison of model predictions and measured data for carton position 7 during the four carton cooling trials with suppressed surface heat transfer (labels shown for layer 1 apply for all layers).

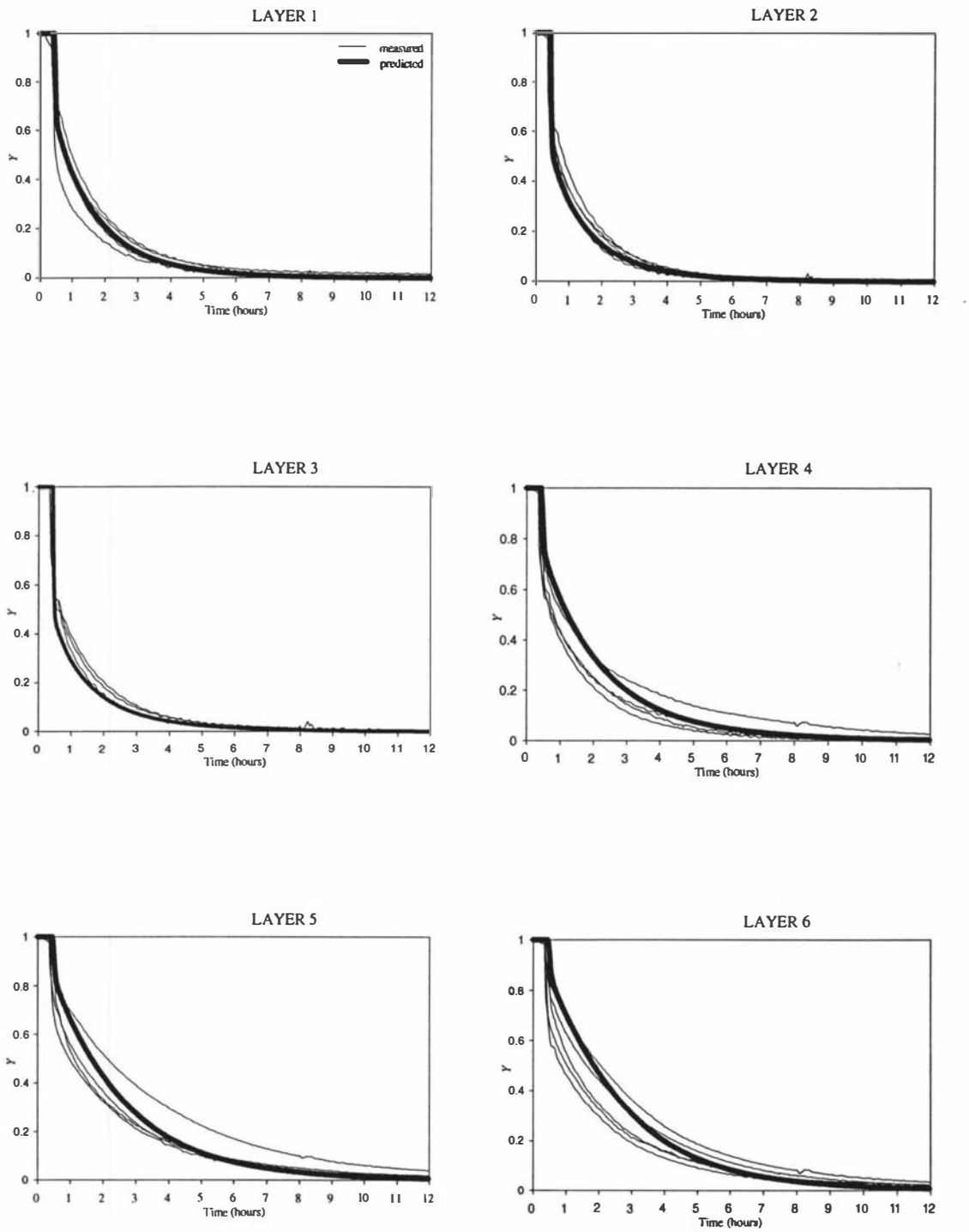

Figure 6.6: Comparison of model predictions and measured data for carton position 3 during the four carton cooling trials with suppressed surface heat transfer (labels shown for layer 1 apply for all layers).

series of trials (1.4 m/s compared with 1.7 m/s). A sensitivity analysis on incident air velocity was carried out, using vent air velocities into the carton of 0.8 m/s, 1.0 m/s and 1.2 m/s (Figure 6.12). It can be seen that a change in vent air velocity has a significant effect on cooling rates, particularly for centre zones. This means that in industrial practice a small difference in hand hole area or incident velocity could lead to a large change in air flow into the carton and hence a significant difference in apple cooling rates.

Figure 6.11 shows measured and predicted apple and air fractional unaccomplished temperature change values for several positions. Generally good agreement between measured and predicted data is shown, both for slow cooling positions (e.g. position 4,layer 6) where the apple cooling rate is close to the air cooling rate, and for fast cooling positions where there is a significant lag between apple and air cooling rates. These results suggest that the modified ordinary differential equation for modelling apple cooling rates (Eqn. 5.3) was adequate for the range of cooling conditions encountered.

6.6 COOLING OF CARTONS WITHIN THE INDUSTRIAL COOLSTORE

Figure 6.13 compares model predictions with data measured within the industrial pre-cooling trials (Chapter 4). The measured apple in Figure 6.13a was in carton position A2 on the pallet (Figure 4.3), meaning that the front and left hand side face of the carton were exposed, whilst all other faces were surrounded by other cartons. The model was run with a carton vent air velocity of 0.25 m/s and outside heat transfer coefficients of zero for unexposed faces. The apple for Figure 6.13b was within carton D6 on the pallet (Figure 4.3). Hence all the faces apart from the front of the carton were surrounded by other cartons. The measured carton had only 5 layers of fruit present so model predictions for a 6 layer carton are presented for both layers 2 and 3 to provide approximate spatial match with the measured data. A carton vent velocity of 0.25 m/s was used in this simulation. The apple on Figure 6.13c was in a carton at position D3. Hence the front and right hand side face were exposed, and all other faces were surrounded by cartons. A carton vent velocity of 0.25 m/s was again used. In all 3 cases the model predictions were considered reliable, given the uncertainties involved.

The model was run for a range of both carton positions on a pallet and carton vent air velocities consistent with observed industrial practice. Figure 6.14 compares the predicted cooling rate (expressed as half-cooling times) distribution for the industrial pre-coolers with measured data for the staggered stacking arrangement (Chapter 4). Taking into account both data uncertainties, and carton to carton, pallet to pallet, and stack to stack differences, generally good agreement is shown between the two distributions. Figure 6.15 shows the predicted cooling rate distribution for cooling within the bulk coolstore, which is also consistent with the few measured data available.

6.7 GENERAL DISCUSSION

From the testing reported in Sections 6.3 to 6.5, it was concluded that model shortcomings were certainly no more limiting than uncertainty in parameter data. Further, it was considered that adding even more model complexity would result in new data requirements, generating new uncertainties. Thus there was no guarantee of any improvement. Rather than seek refinements, based on further laboratory tests, it was decided to use the model to see if it gave results matching industrial practice.

The model is largely mechanistic allowing predictions for a wide range of carton positions on pallets. Both cooling within pre-coolers and within the bulk store can be simulated by the appropriate choice of inlet air velocity into the carton. Different carton positions within a pallet can be simulated by selecting appropriate heat transfer coefficient values for each carton face.

The model is too complex for direct incorporation into a full coolstore simulation model. However it allows a range of carton positions and incident velocities to be simulated to predict the distribution of cooling rates within the pre-coolers and coolstore. These could be used to form the basis of the product model for the coolstore simulation model.

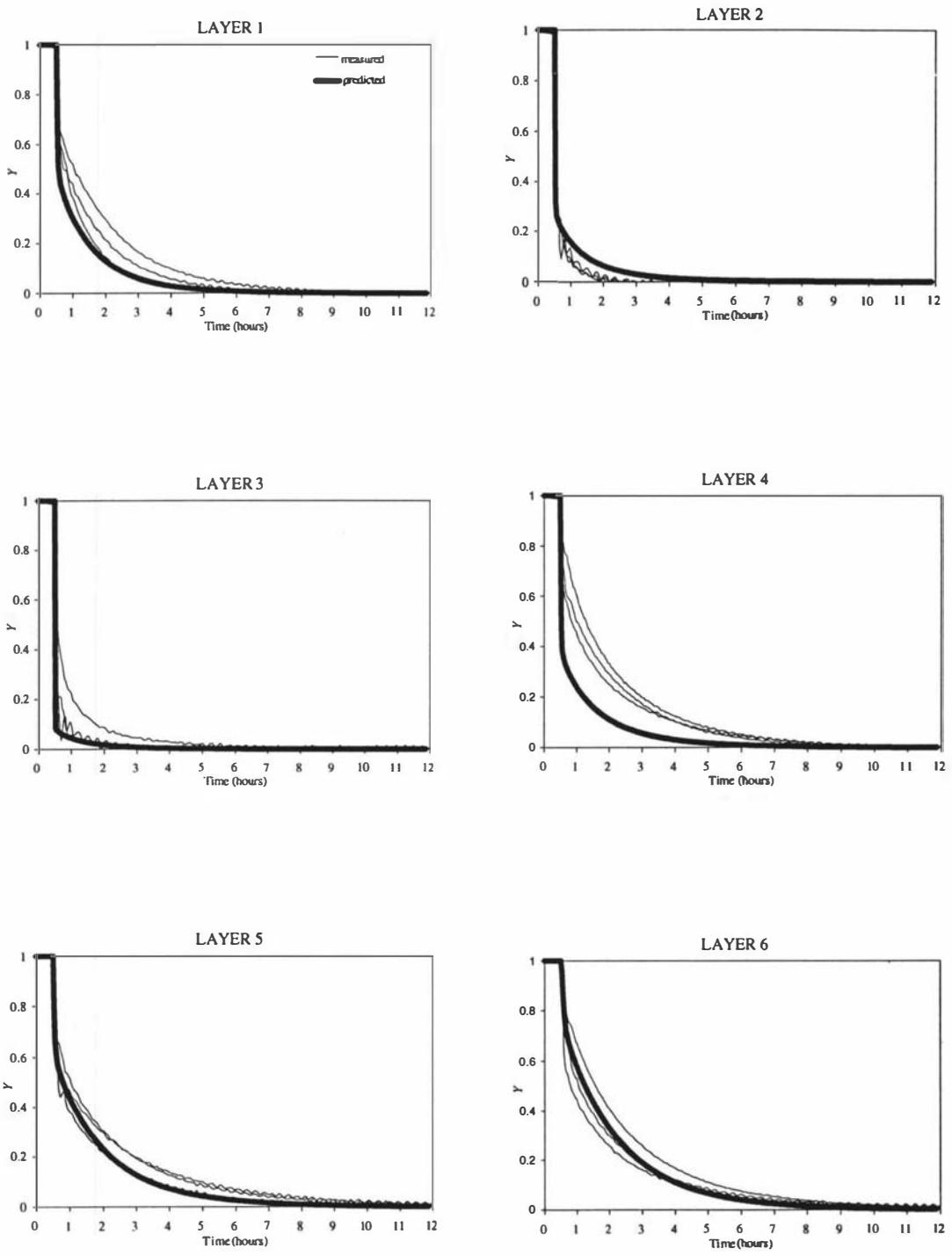

Figure 6.7: Comparison of model predictions and measured data for carton position 1 during unmodified carton cooling trials (labels shown for layer 1 apply for all layers).

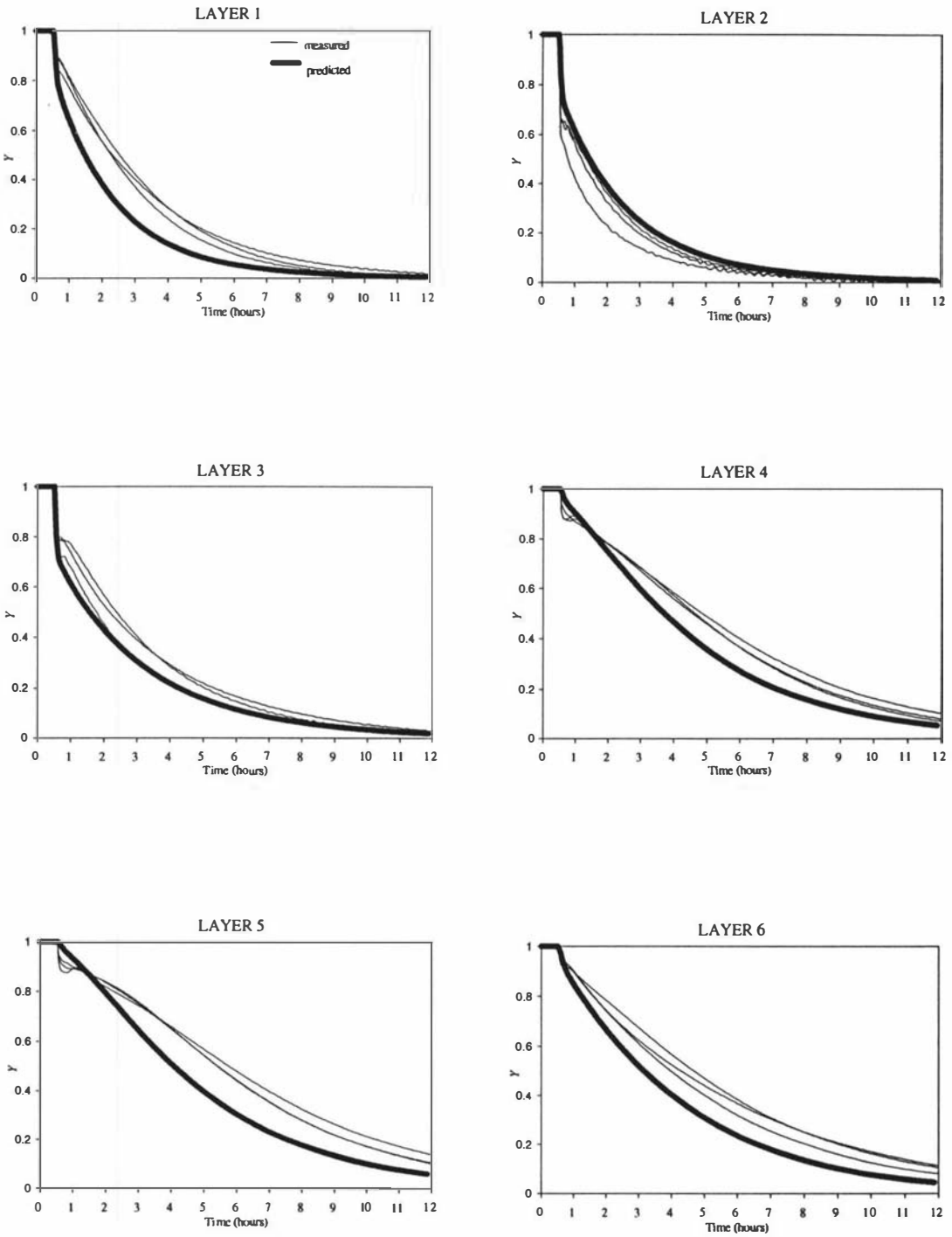

Figure 6.8: Comparison of model predictions and measured data for carton position 4 during unmodified carton cooling trials (labels shown for layer 1 apply for all layers).

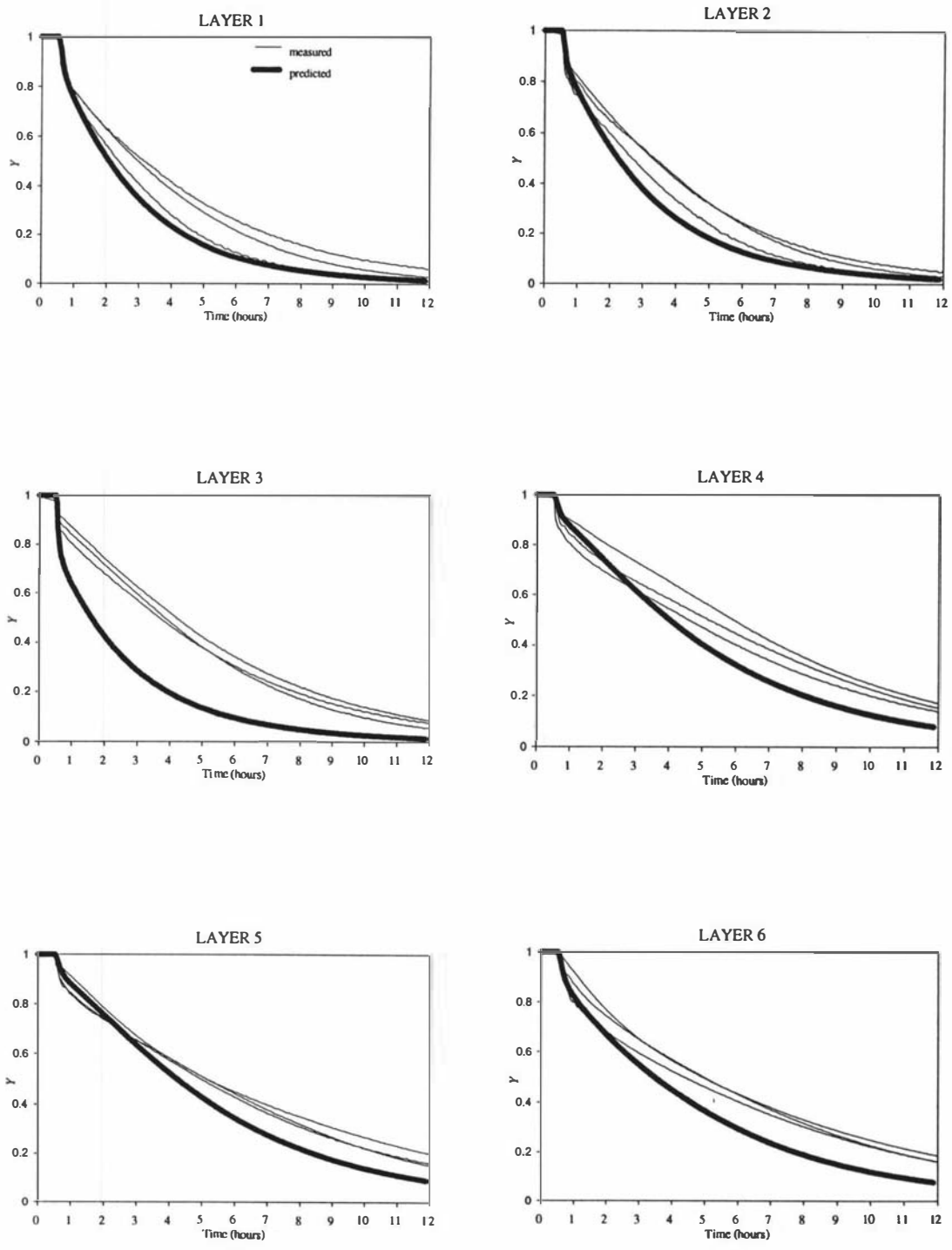

Figure 6.9: Comparison of model predictions and measured data for carton position 7 during unmodified carton cooling trials (labels shown for layer 1 apply for all layers).

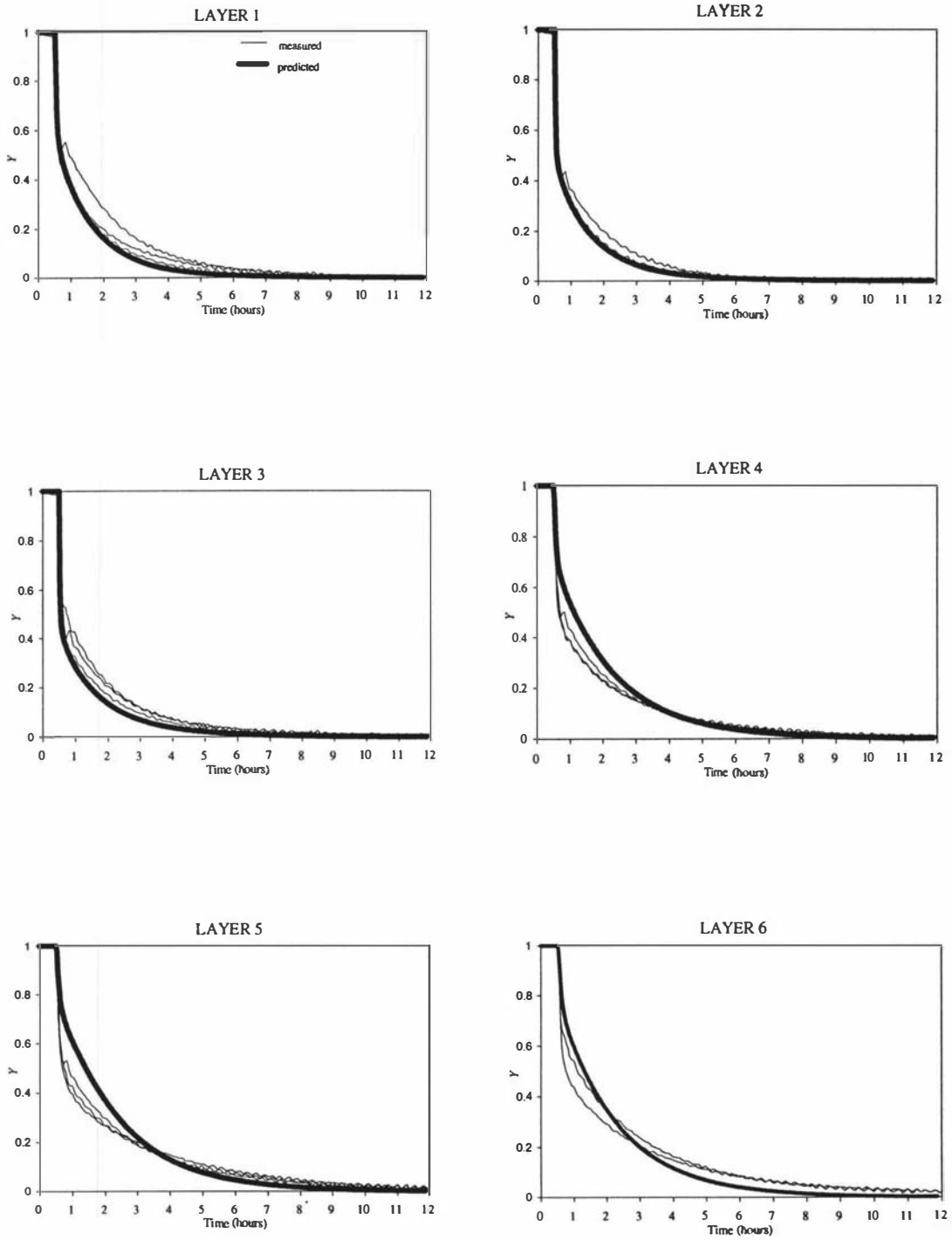

Figure 6.10: Comparison of model predictions and measured data for carton position 3 during unmodified carton cooling trials (labels shown for layer 1 apply for all layers).

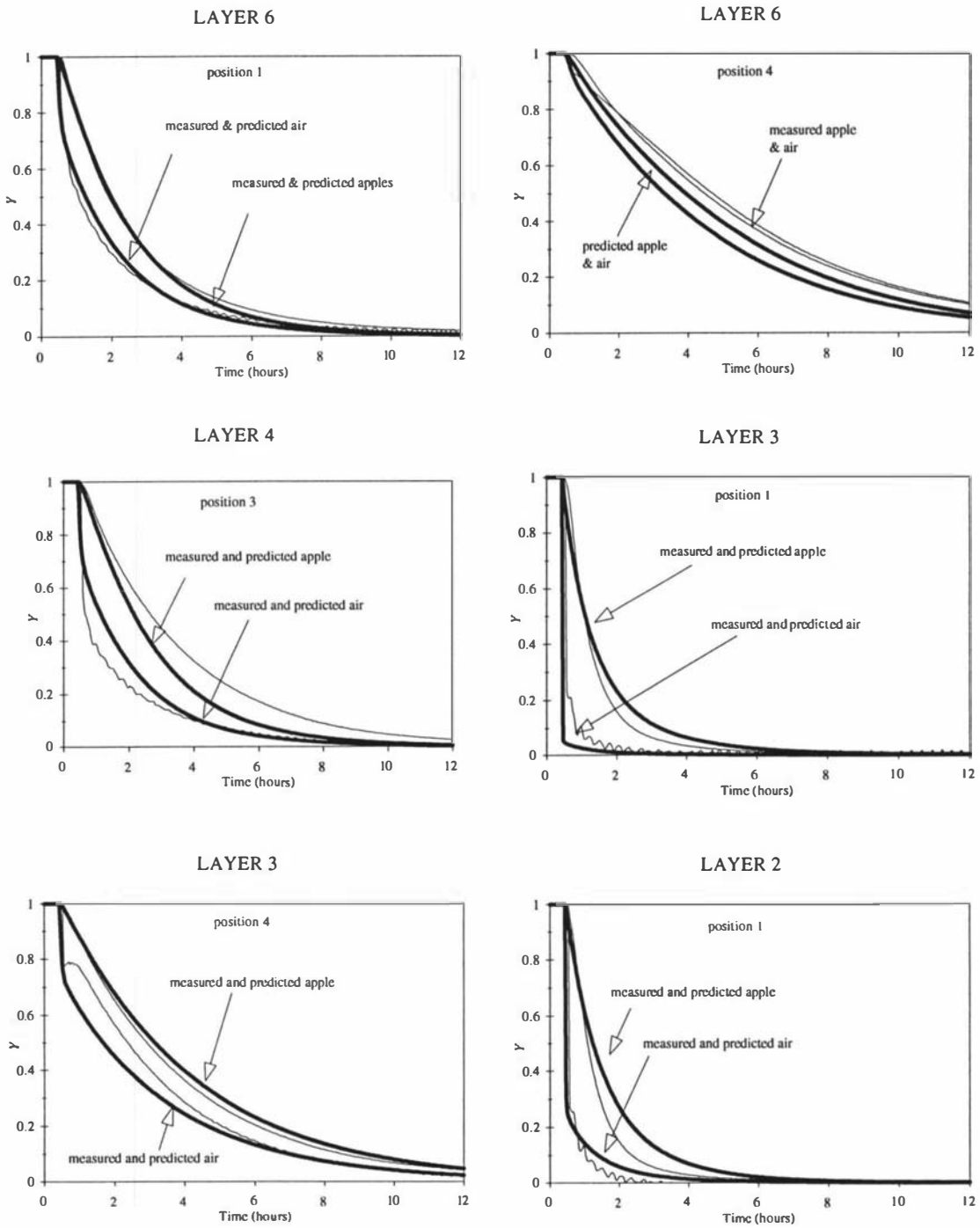

Figure 6.11: Comparison of model predictions and measured data for selected carton positions for both air and apples during an unmodified carton cooling trial.

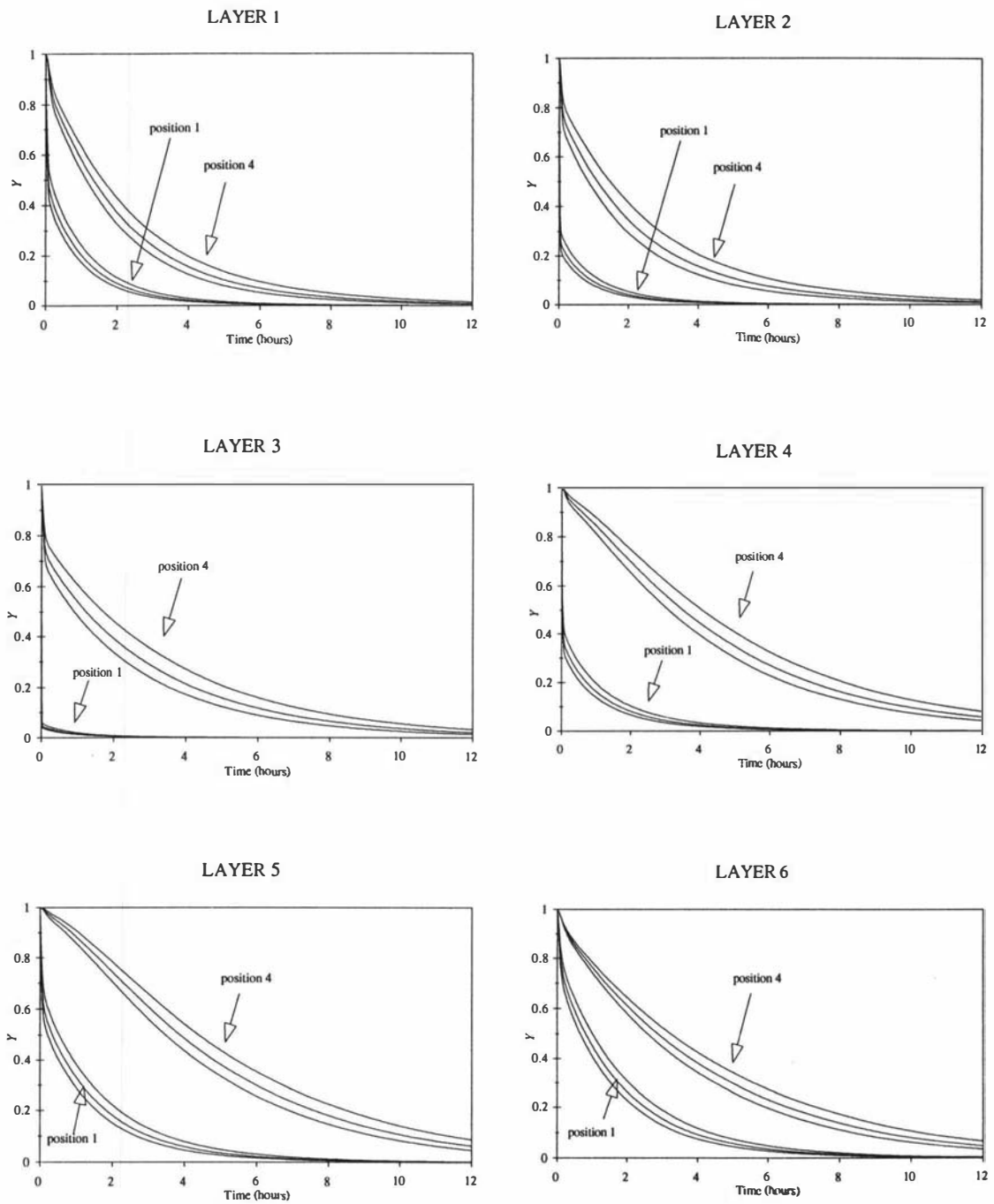

Figure 6.12: Model predictions for selected carton positions for incident air velocities of 0.8 (always the slowest), 1.0, and 1.2 m/s (always the fastest).

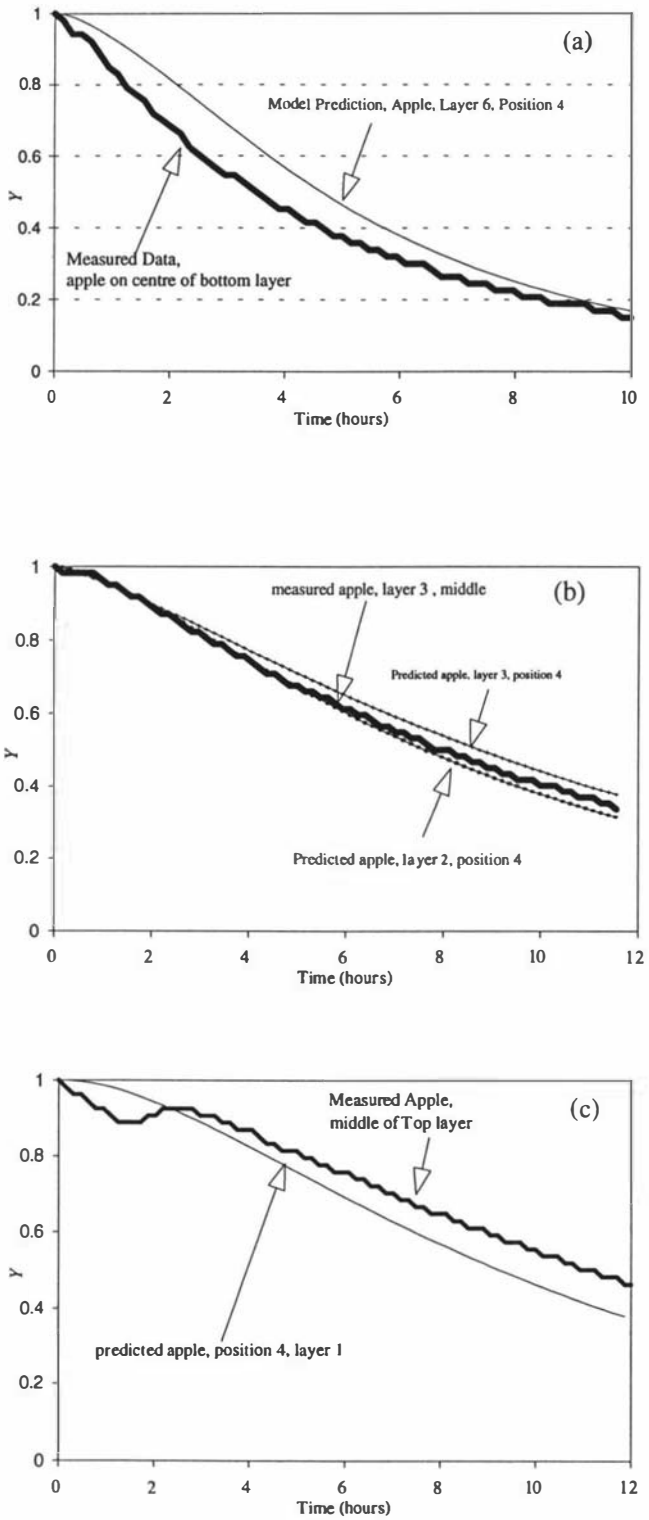

Figure 6.13: Comparison of model predictions versus measured data in the Whakatu pre-coolers: (a) carton at position D6 (Figure 4.3) on the pallet; (b) carton at position A2; (c) carton at position D3.

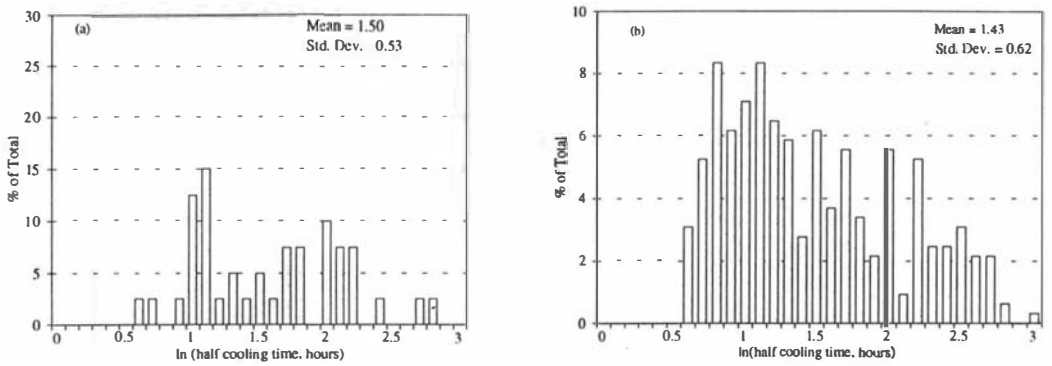

Figure 6.14: Distribution of apple half-cooling times for pre-cooling within industrial pre-coolers, (a) measured within staggered stacks (Chapter 4); (b) predicted using apple carton cooling model.

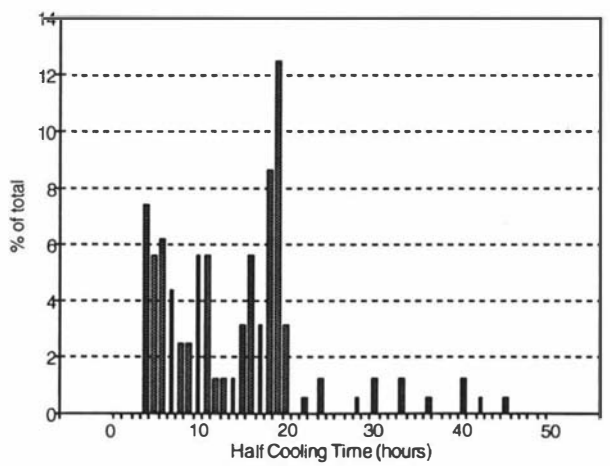

Figure 6.15: Distribution of apple half-cooling times for cooling within the bulk coolstore, predicted using apple carton cooling model.

The model predicts water loss from fruit and relative humidity of air within the carton. It was not possible to measure RH or weight loss within the carton accurately because of the methodology used to ensure that the carton was isothermal before it was placed in the test chamber. Fruit weights could only be taken before the carton was constructed and once the test was completed. It was therefore not possible to separate the weight loss occurring in the warm room from that occurring in the cooling trial, and so the RH and weight loss predictions remain untested.

6.8 CONCLUSION

In seeking to develop an accurate model, balance must be maintained to ensure that the benefits of more detailed and mechanistically correct equations on the one hand, are not countered by increasing uncertainty in data for the various parameters needed on the other. Judging the optimum balance between the two in an objective manner is very difficult and requires experience of the importance of the various contributing factors.

There are certainly shortcomings remaining in the carton model, but the work carried out suggests that the existing balance between model quality and data uncertainties may not be far from optimal. Major new benefits from further research seeking to improve model accuracy were difficult to forsee. Therefore, the model, as presented, was accepted as a working tool that could be used to make predictions for a variety of circumstances. Nevertheless, its application to very different carton configurations should be made with caution in case any of the remaining shortcomings are much more important in new situations than in the present apple carton.

CHAPTER 7: COOLSTORE SURVEYS

7.1 INTRODUCTION

Coolstore design and operational factors such as the layout of the coolstore, insulation levels, door protection devices, frequency of door use, air cooling coil and fan designs, associated control system design, air flow patterns, and product stacking arrangements can all influence the uniformity and time-variability of environmental conditions and therefore the rate of change of product quality within the coolstore.

Mathematical models are increasingly being used to assess the effect of the above factors on coolstore design and performance. Analysis of the system is then possible, and alternative systems can be easily studied with reduced need for expensive monitoring and/or experiments. Selection of model type and complexity is an important part of the modelling process. The model must take account of major sources of variation in a realistic manner if accurate prediction of product conditions is to be achieved. Two major decisions are required in selecting the type of model to use. These are firstly to select between a steady-state or unsteady-state modelling approach and secondly to decide on the type of space discretisation to be used. Several approaches used by other researchers for space discretisation were outlined in Chapter 2:

(i) a single perfectly mixed zone for the whole coolstore (e.g. Cleland, 1983, 1985);

(ii) flow of air in a well defined pathway (plug-flow) from the fan discharge to intake without backmixing (e.g. Marshall and James, 1975);

(iii) a number of interconnected perfectly mixed zones (e.g. Liao and Feddes, 1990);

(iv) full air hydrodynamic prediction of air movement linked to heat and mass transfer models using a complete finite difference, control volume, or finite element grid for the air space (e.g. Meffert and Van Beek, 1983 & 1988; Szczechowiak and Rainczak, 1987; Van Gerwen and Van Oort, 1990; Wang, 1991).

In any particular situation the most appropriate approach may not be obvious until the level of positional variability of conditions is either predicted or measured. For example, the first approach may be appropriate for determining overall heat loads on the refrigeration coils, or in small facilities where good air mixing and hence low variability in temperature and relative humidity (RH) are likely. For facilities such as freezers or chillers there can be a well defined air pathway and the second type may then be more appropriate. In many larger facilities there are definite air pathways but there is also a degree of backmixing and turbulence, which may in turn be influenced by location of the product. In such cases either of the third and fourth approaches may be appropriate. However the full hydrodynamic modelling approach is both data- and computationally-intensive, especially for large facilities, and where changes in product location are frequent.

A series of surveys measuring air temperature, RH and velocity; product temperature; and coolstore operating characteristics were undertaken in the industrial coolstore (described in Chapter 4) to quantify both time and positional variability, to postulate the most appropriate level of model complexity for such a system, and to provide test data for model validation.

7.2 DATALOGGING SYSTEMS

Data collection during coolstore surveys was made in a number of ways. Portable dataloggers were used for fruit temperatures and air temperature and RH (as outlined in Section 4.1). A handheld dewpoint meter and hot wire anemometer were used to measure air dry bulb and dew point temperature and air velocity respectively. In addition there were a number of fixed sensors located within the coolstore (Figure 4.1) including:

- coil air-on and air-off temperature using PT100 resistance probes (± 0.1°C) for coils 1 to 4;
- coil 1 air-on and air-off RH, using Vaisala HMP113Y capacitance probes (± 3% RH);
- fan mode (off, low speed, high speed) for all four fans;
- evaporator refrigerant pressure for all four evaporator sets (kPa);

- defrost mode (on or off);
- floor and underfloor temperature (Figure 7.1 shows locations), using PT100 resistance probes (± 0.1°C). Probes were located at the top, middle and bottom of the concrete floor slab for all 5 positions. In addition, for positions 1 and 2, probes were also placed 0.25 m and 0.5 m below the concrete slab in gravel aggregate used as a base course below the floor slab;
- building shell surface temperature (Figure 7.1 shows locations), using PT100 resistance probes (± 0.1°C);
- Door position (open or closed) on both main doors using microswitches.

All of the PT100 temperature probes were calibrated using ice points, RH probes were calibrated using saturated salt solutions as described in Section 4.1.1. All of the permanently mounted sensors listed above were linked into the coolstore management system and were continuously logged throughout the coolstore operating season.

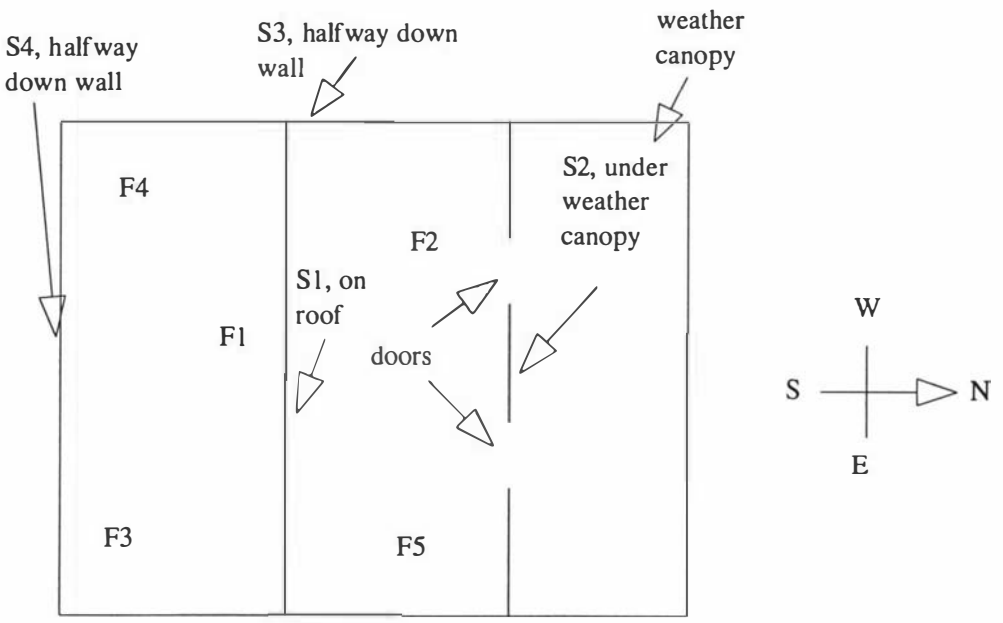

Figure 7.1: Location of under-floor (F1 to F5) and building surface (S1 to S4) temperature probes for the industrial coolstore.

7.3 MEASUREMENTS OF AIR TEMPERATURE, RELATIVE HUMIDITY AND VELOCITY

7.3.1 Methodology

To measure variation in air temperature, RH and velocity with respect to both position and time, a large number of dataloggers taking simultaneous readings would be required. In the absence of sufficient datalogger capacity, separate surveys were performed to assess the variation with respect to vertical position, then horizontal position and time.

7.3.1.1 Vertical Position Surveys

Surveys were undertaken on March 12, May 7 and May 23 1990. During these surveys the coolstore was about 70% full and pre-cooling of fruit was not occurring. Air velocities were measured with a Dantec 54N50 hot wire anemometer (2 minute average reading ±0.02 m/s), RH was calculated from dew point, and dry bulb temperature measured with a Michell Series 3000 cooled mirror dew point hygrometer accurate to ±0.3°C for dew point and 0.1°C for dry bulb temperature. Measurements were taken at 93 positions throughout the coolstore. Some were in aisles (Figure 7.2a), and others amongst bulk stacked pallets of fruit (Figure. 7.2b and 7.2c). At each position, readings were taken adjacent to each of the bottom pallet (about 0.5 m above the floor), the middle pallet (about 2 m above the floor) and the top pallet (about 4 m above the floor). This enabled paired comparisons of positional influence on air conditions within the three-pallet stack. The sampling order for the various positions was randomised to eliminate time effects as each survey took about 10 hours to perform.

7.3.1.2 Horizontal Position and Time Survey

In the 3 surveys just outlined horizontal positional differences were confounded with time-variability because data were measured at only one horizontal position at any time. In the fourth survey continuous measurements of both air and fruit temperature around the top

pallet for positions 1 to 8 shown on Figure 7.2d were made between April 7 and April 9 1992. This allowed both positional and time variability to be assessed. Air RH around both top and bottom pallets at positions 4 and 7, and air and fruit temperature at position 9 were also measured but for a shorter period. For each of the four air cooling coils measurements of air-on and air-off temperature, and fan speed were also taken. In addition, air-on and air-off RH for coil 1, door openings, floor, underfloor and building shell temperatures were also recorded during this period. The coolstore was both bulk storing and pre-cooling fruit during the fourth survey. Fruit transfers into and out of the coolstore were monitored daily.

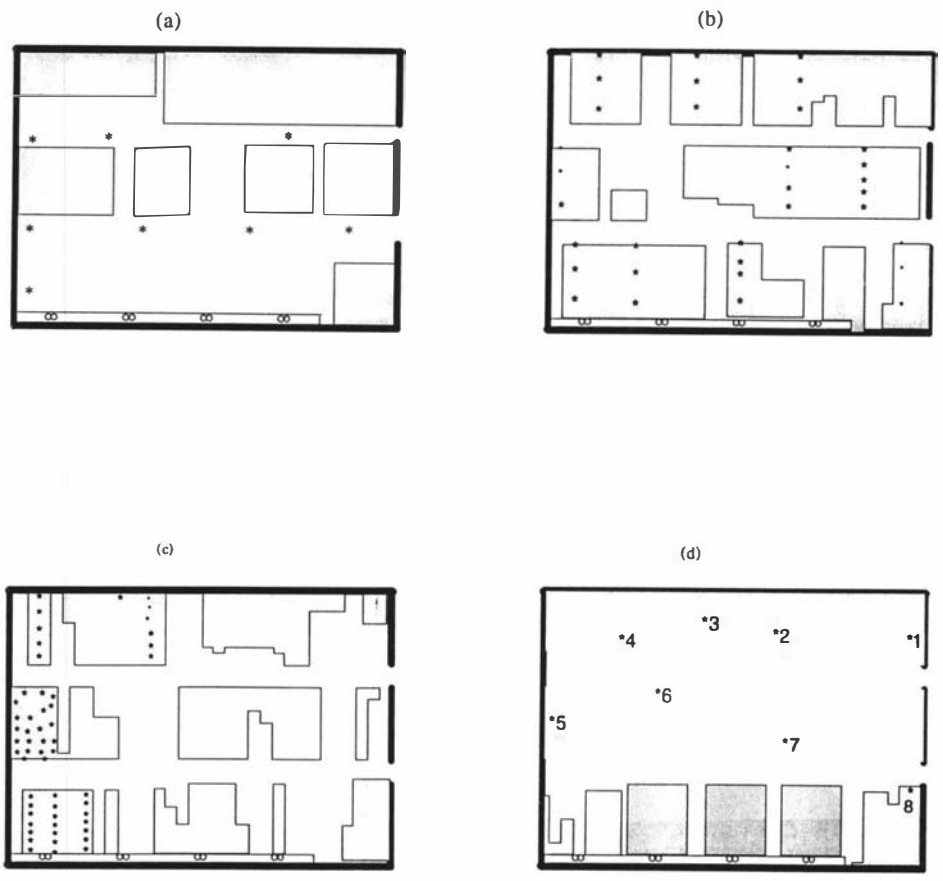

Figure 7.2: Store survey measurement positions (*) and stored product positions (shaded), (a) March 12 1990, (b) May 7 1990, (c) May 23 1990, and (d) April 7 to April 9 1992.

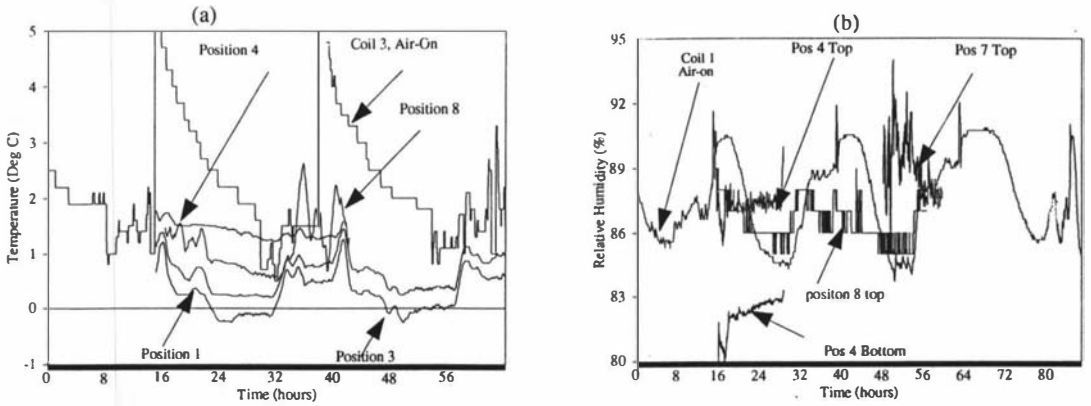

Figure 7.3: Typical measured data for the industrial coolstore from midnight April 7 1992: (a) air temperature, and (b) air RH, position codes shown in Figure 7.2.

7.3.1.3 Smoke Test

Air velocity measurements collected during the first 3 surveys indicated the magnitude of air velocities within the coolstore but not the direction, because a unidirectional hot wire anemometer was used. On March 13, 1991 a smoke test was carried out to ascertain air flow directions. The smoke test was carried out when the coolstore was empty, the doors were closed and all fans were operating on low speed. Smoke was released at a number of positions around the coolstore and the direction of smoke movement was observed.

7.3.2 Results and Discussion

The smoke test results (Figure 7.4) indicated well-defined air flow with some backmixing in three major air pathways (originating from the central duct, and each of the two ventilation slots). The central duct primarily discharged air towards the rear corners of the coolstore and this air was then drawn back towards the two central fans. Significant air short-circuiting occurred for air discharged out of the two slots. A small proportion of this

air was entrained into the return flow back to the central fans but the majority was drawn straight back into the end fans without mixing into the rest of the coolstore. Although the smoke test was performed in an empty coolstore, it was expected that the general pattern of air flow would be similar when pallets were present, although the air velocities may be different. It would be expected that more air would move along the top of pallets rather than along the floor compared to the smoke test. Hence pallets would be expected to affect the vertical distribution more than the horizontal distribution of air flow.

The air velocity distributions measured for all three vertical positions during the vertical position surveys were approximately log-normal. Table 7.1 summarises the measured air velocity distributions for each position and survey. Table 7.2 summarises paired comparisons of the measured air temperatures, RH's, and velocities for the 3 vertical positions. The first three surveys showed that the pallet stacks had considerable effect on variations in air velocity, temperature, and RH with vertical position. Measurements in aisles away from pallets showed no significant differences. By comparison velocities within pallet stacks were higher for the top position than the middle or bottom. This suggests that the pallet stacks were reducing movement of air down to the floor relative to the empty store, and a large proportion of the air returned to the fans along the top of the pallets and down aisles. This is consistent with the hypothesis advanced to explain the observations made in the smoke test.

Air temperature and RH variations were consistent with the air velocity measurements, being less variable in areas with high velocity, but also indicating that local heat sources were influential. Around the bottom pallets the temperature was on average 0.5°C higher and the RH 3.2% lower than around the middle or top pallet. Differences in absolute humidity were not significant (Table 7.2). The lower air velocities around the bottom pallets may have contributed to slower removal of heat from these pallets and hence the significantly higher temperatures on average. No difference in air temperature or RH between the middle and top pallets was found even though there was a significant difference in air velocity. This suggests that the heat entry through the uninsulated floor also had a significant influence on conditions around the bottom pallets, as well as the poorer air flow.

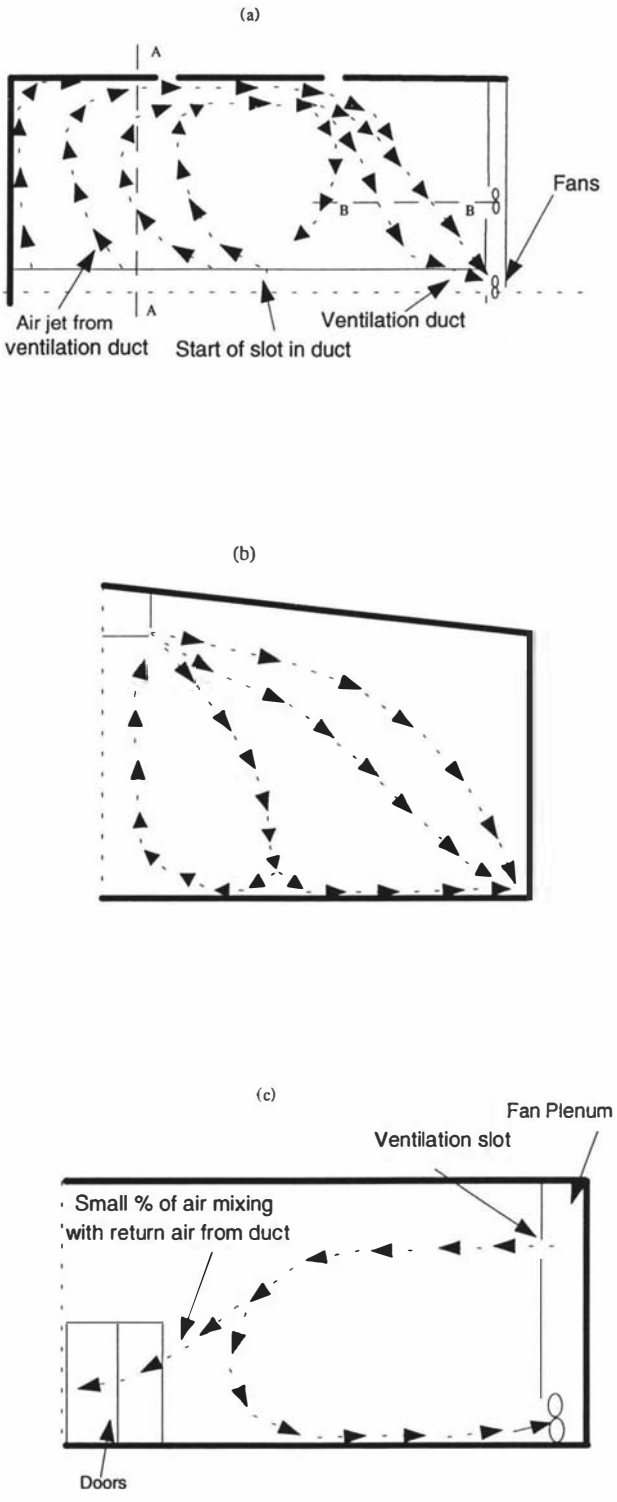

Figure 7.4 Air flow direction indicated by the smoke test in the empty coolstore, (a) plan view of distribution from the central duct, (b) cross-section at delivery end of coolstore (AA), (c) elevation at slot end of coolstore (BB).

Table 7.1

Summary of measured air velocity (m/s), for surveys on (A) March 12 1990 (in aisles), and (B) May 7 & May 23, 1990 (among bulk stacked pallets).

	Bottom		Middle		Top	
	A	B	A	B	A	B
Mean[a]	0.69	0.24	0.56	0.29	0.62	0.41
95 % minimum[a]	0.26	0.04	0.26	0.06	0.16	0.07
95 % maximum[a]	1.88	1.14	1.16	1.43	2.40	2.45

[a] Calculated using a log-normal statistical distribution

Table 7.2

Mean differences in air conditions between pairs of vertical position for surveys: (A) in aisles (March 12 1990), and (B) among bulk stacked pallets (May 7 and May 23,1990) (* indicates that mean difference is significantly different from 0 at 99% level)

Paired Comparison (Pallet Position)	Middle vs Bottom		Top vs Bottom		Top vs Middle	
	A	B	A	B	A	B
Air Velocity (m/s)	-0.20	0.08	-0.04	0.31*	0.17	0.23*
Temperature (°C)	0.08	-0.5*	0.05	-0.50*	0.05	-0.02
RH (%)	-0.8	3.2*	-0.9	3.3*	-0.1	0.1
Absolute Humidity (kg/kg)	1.4×10^{-5}	1.7×10^{-5}	-1.03×10^{-5}	1.2×10^{-5}	3.88×10^{-6}	-3.9×10^{-6}

Similarly, significant differences in air temperature with horizontal position occurred in the fourth survey (Table 7.3). The mean air temperature for each position was apparently related to both fruit temperature at that position and location within the store with respect to major heat sources such as doors. Areas with warmer fruit (positions 4, 5, 6 and 7) all had higher mean air temperatures than the other positions. Position 8 did not fit this pattern, but was close to one of the main doors.

The measured differences in temperature and RH between bottom and top pallets would have a significant effect on product quality. Using data given by Gaffney *et al.* (1985a) it was estimated that a 0.5°C increase in temperature and a 3% drop in RH would typically correspond to about an 8% increase in apple respiration rate and about 30% increase in the rate of moisture loss (due to increase in vapour pressure deficit), which are the two main processes contributing to the loss of quality during cool storage.

Figure 7.3 shows some typical measured data for the horizontal position and time survey. For coils associated with fruit pre-cooling there was a step change in air-on temperature, followed by a pulldown, corresponding to the pre-cooling cycle. Although pre-cooling of fruit is a significant heat source, use of air-off temperature control meant that the pre-cooling heat load had little or no effect on the temperature in the rest of the coolstore. However pre-cooling may have affected the RH in the bulk store to some extent because it changes the sensible heat ratio of the load that the refrigeration system must remove. Positions close to doors used for bulk stacking of pallets showed the largest fluctuations in temperature. The air temperature decreased at night, which corresponded to low door activity and reduced ambient temperatures. The overall increase in temperature during the day can be attributed to high door activity, increasing ambient temperatures and warm fruit being unloaded from pre-coolers and bulk stacked in the coolstore.

TABLE 7.3

Mean air and fruit temperatures for the horizontal position and time survey between April 7 and April 9 1992 (means with the same letter are not significantly different, 95% confidence level)

Position (Fig. 7.2d)	Air Temperatures (°C)		Fruit Temperatures (°C)	
	Mean	Grouping	Mean	Grouping
1	0.63	a	0.77	a
2	0.31	b	0.53	b
3	0.29	b	0.51	b
4	1.39	c	2.02	c
5	1.08	d	1.40	d
6	0.89	e	3.09	e
7	1.46	c	2.51	f
8	1.34	c	0.78	a

7.3.3 Selection Of Model Type For Room Air

The survey results suggest that any model of this coolstore would need to be dynamic due to cycles in activities causing heat load variation. Neither single zone or plug-flow models would allow the measured positional variability to be predicted. A full hydrodynamic model would be inappropriate as the arrangement of pallet stacking changed rapidly and often, causing the air flow distribution to change. The most appropriate model would thus appear to be a multi-zoned model in which each zone is assumed to be perfectly mixed. The measured variability shown in Table 7.2 suggests subdivision into at least 2 vertical levels

in the bulk-storage part of the store, separate zones for each pre-cooler, and separate zones near each door. In addition, separate zones for parts of the coolstore in which warm fruit were placed would be desirable (even though these regions changed from day to day), and a degree of subdivision along the 3 main airflow pathways may be necessary to model the gradual warming of the air as it passes through the coolstore.

7.4 MISCELLANEOUS COOLSTORE DATA

To identify the most appropriate models for other components within the coolstore, (such as doors, floor and surfaces), measurements were made of door usage, floor and underfloor temperatures, and building surface temperatures, throughout the 1990, 1991, and 1992 coolstore operating seasons.

7.4.1 Door Usage

Door usage was monitored using microswitches logged into the coolstore management system. These switches monitored when doors were open or closed. Figure 7.5 summarises door usage for the three coolstore operating seasons. The data is for open and closed time for both doors during the operating period of the coolstore for each day. Both sets of data were found to closely fit exponential distributions.

7.4.2 Floor and Underfloor Temperatures

Floor and underfloor temperatures were monitored using temperatures probes as outlined in Section 7.1. Figure 7.6 shows the data for position 1 (Figure 7.1) for the 1990 operating season. Similar trends were observed for the other positions measured, and for each of the two successive operating seasons, indicating a gradual pulldown in the underfloor temperature over an apple season, but complete reheating in the off-season when the coolstores were not operating. Subterranian water flow through the high water table of the site studied would provide much of the underfloor reheating effect. Other sites may display a more gradual pulldown of the subsoil over a number of seasons.

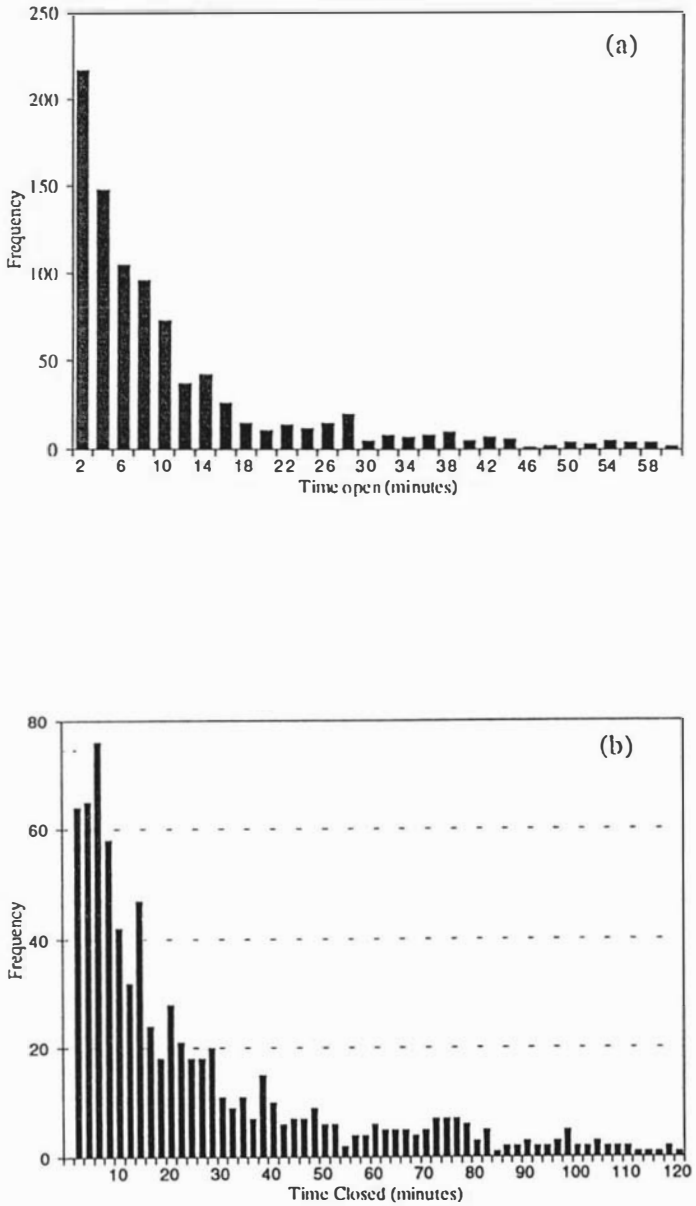

Figure 7.5: Measured door usage during the 1990, 1991, and 1992 coolstore operating seasons, (a) door open time, (b) door closed time.

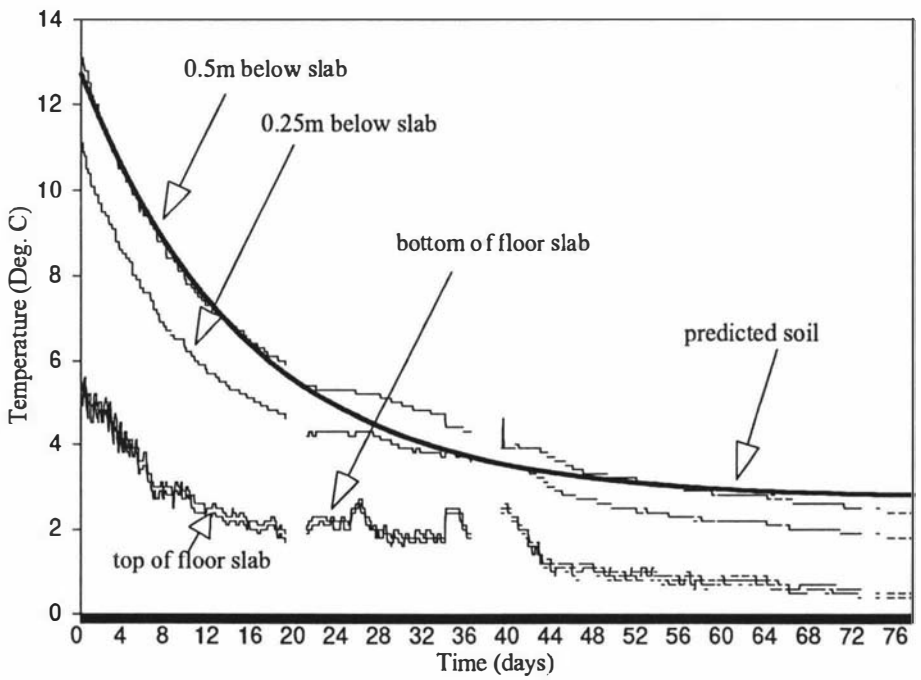

Figure 7.6: Measured and predicted floor and underfloor temperatures at position 1 (Figure 7.1) in the industrial coolstore during the 1990 operating season.

7.4.3 Building Shell Surface Temperatures

Surface temperatures were measured using PT100 temperature probes as outlined in Section 7.1. Figure 7.7 shows measurements for positions 1, 2 and 3 (Figure 7.1) over 3 days during the 1992 operating season. Position 1 which was on the roof of the coolstore and exposed to solar radiation, showed the greatest diurnal fluctuation, followed by position 3 which was on a west facing wall and would have been exposed to solar radiation for short periods in the afternoons. Position 2 which was on a north facing wall under a weather canopy showed the least fluctuation. Table 7.4 gives the maximum and minimum daily air temperatures recorded during the 3 day measurement period by the NZ Meterological Service.

7.4.4 Model Selection For Doors And Surfaces

Selection of appropriate models for doors, floors and surfaces are discussed in Sections 8.4.6, 8.4.2 and 8.4.1 respectively.

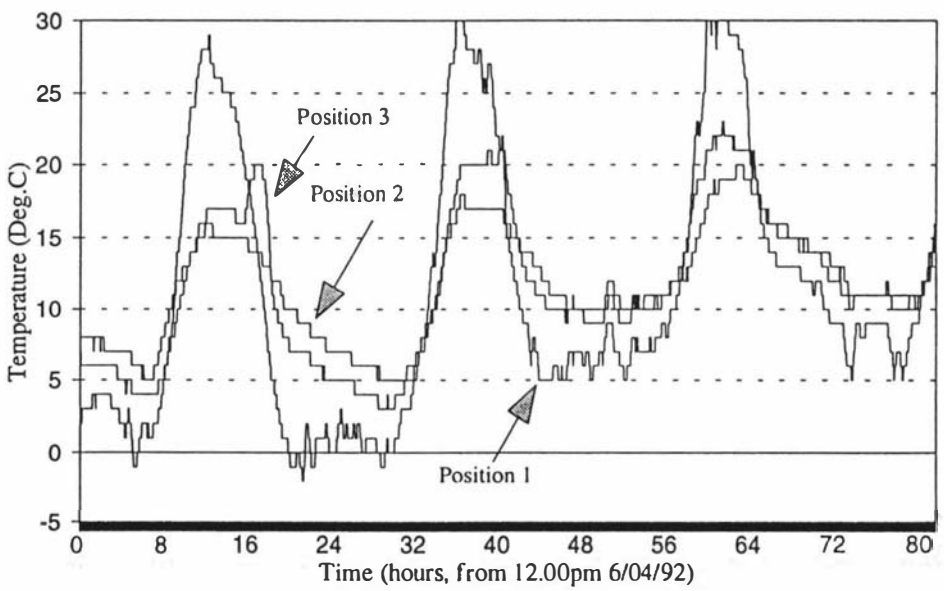

Figure 7.7: Measured building shell surface temperatures for positions 1,2 & 3 (Figure 7.1) on the industrial coolstore during the 1992 operating season.

Table 7.4

Measured Daily Outside Ambient Conditions.

(Measured at Lawn Road, Hastings, NZ Meterological Service)

Day	T_{min} (°C)	T_{max} (°C)	T_{dry}[1] (°C)	T_{wet}[1] (°C)	Solar Radiation (MJ/m^2 day)
1	9.4	15.3	10.5	9.7	8.8
2	4.2	15.9	7.5	7.2	15.8
3	3.4	19.7	6.0	6.0	13.4

[1] = measured at 9.00 am.

CHAPTER 8: COOLSTORE MODEL DEVELOPMENT

8.1 INTRODUCTION

The basis of many effective design and management processes is the use of predictive models. Appropriate mathematical models of a coolstorage system would allow quantitative prediction of important variables, study of alternative designs and management systems, and testing of "what-if" scenarios. Refrigerated storage room models developed by other researchers (Chapter 2), largely concentrated on heat transfer with less emphasis on water vapour transfer aspects, and did not consider time-variability of the coolstorage system or variation in environmental conditions throughout the coolstore.

The fifth objective of the present research was to develop mathematical models of heat transfer and water vapour (mass) transport in a large apple coolstore and to incorporate them into a computer simulation model. To achieve this objective appropriate component models were selected and incorporated into an overall simulation model. It was desirable that the model should be as general as possible so that it could be applied more generally than to just apple coolstores (i.e. different applications could be modelled by change to data, rather than changes in model formulation).

Both steady-state and unsteady-state modelling approaches were considered for modelling the apple coolstore. Steady-state models are easier and less costly to implement, have lower data requirements, yet can provide useful information on average conditions and likely long term trends, by successive application over periods for which average operating conditions are significantly different (Pham *et al.*, 1993). A steady-state model, (Amos *et al.*, 1993; Appendix 1), was used to assess seasonal trends in average air temperature and relative humidity (RH) within a coolstore by predicting 24 hour average conditions for four typical days over the season. The model was implemented via the RADS package (Cornelius, 1991), but included allowances for changes in weight loss with RH and adsorption of water vapour by

cardboard packaging. The predicted daily average air temperature and RH agreed with measured data from the surveys (Chapter 7), but the model did not allow continuous prediction of conditions for assessment of short term time transients within the system. The rest of this Chapter describes the development of a dynamic unsteady-state model, which is not limited in this manner.

The method used to model coolstore air conditions provides a cornerstone of any coolstore model because all other components interact with the air. In Chapter 7 it was concluded that the most appropriate model for the industrial coolstore surveyed would be a multi-zoned dynamic model. Given this decision, the major requirements for an overall model are to develop methods to describe how air moves between zones within the coolstore, to develop appropriate models for predicting the heat and mass transfer occuring within and between zones, and to develop models for predicting heat and mass transfer for non-zone components such as evaporators.

8.2 ZONE AIR FORMULATION

For a multizone model the coolstore air volume was assumed to be divided into a number of zones of arbitrary size. The same inherent model was applied to each zone. Heat and mass transfer pathways that can occur within each zone include those associated with wall, ceiling or floor surfaces, product batches (including packaging), inert materials such as structural components with large thermal capacity, doors, heat generators (such as fans) and evaporators. Evaporators and fans were linked to particular zones via appropriate airflow pathways, whilst models of outside ambient conditions were required in order to model heat and mass flow through doors, wall and ceiling surfaces, and the floor. These pathways are shown in Figure 8.1.

The air in each zone was assumed perfectly mixed, and in the manner of the carton model of Chapter 5, the density and hence mass of dry air in the coolstore was assumed constant to reduce model complexity. Energy and water vapour balances were performed on each zone to determine air enthalpy and absolute humidity and temperature was calculated algebraically from enthalpy and humidity.

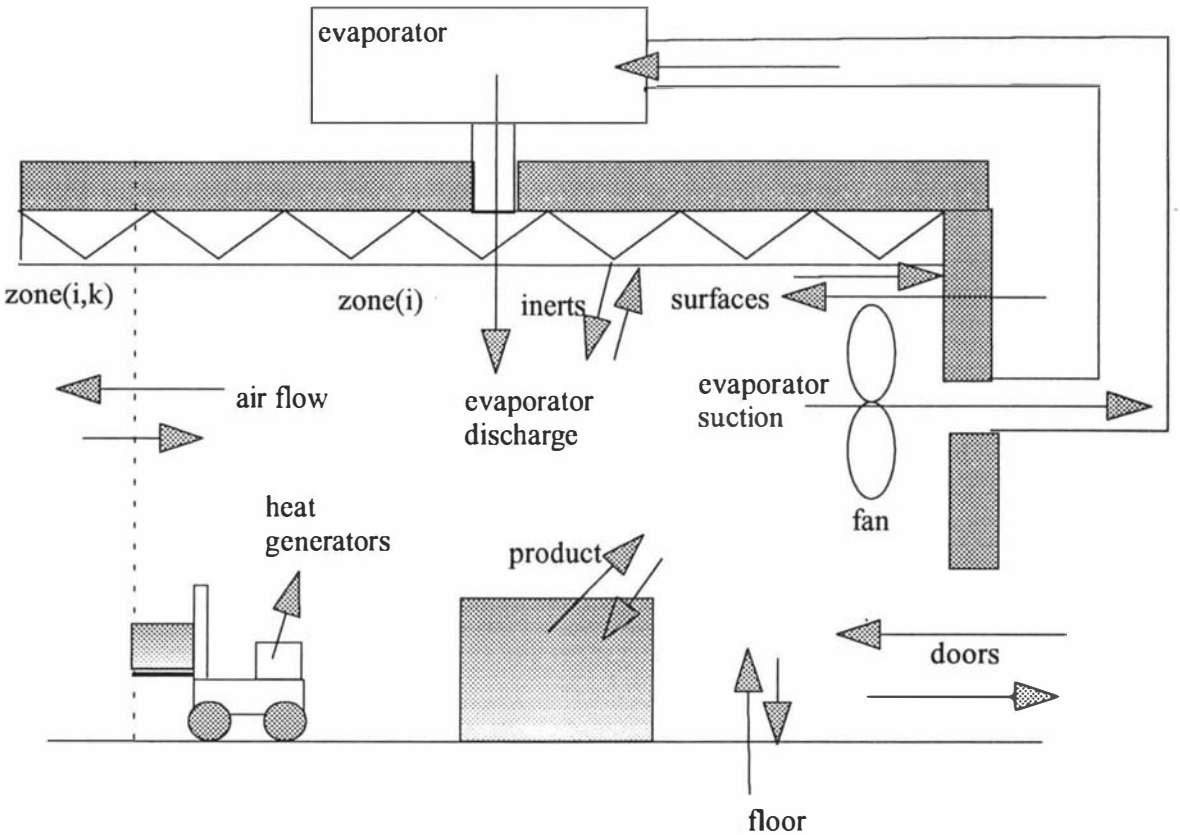

Figure 8.1: Possible heat transfer and water vapour transport pathways modelled for a generalised zone within the coolstore.

With the above assumptions, an energy balance for the air in the i[th] generalised zone can be stated as:

$$M_i \frac{d\ hh_i}{dt} = \phi_{door,i} + \phi_{floor,i} + \phi_{inert,i} + \phi_{surface,i} + \phi_{product,i} + \phi_{heatgen,i} + \phi_{air,i} \qquad (8.1)$$

where:

M_i	=	mass of dry air in the i[th] zone (kg).
hh_i	=	enthalpy of air in the i[th] zone (J/kg).
$\phi_{door,i}$	=	energy flow into the i[th] zone through doors (W).
$\phi_{floor,i}$	=	energy flow into the i[th] zone through the floor (W).
$\phi_{inert,i}$	=	energy flow into the i[th] zone from inerts (W).
$\phi_{surface,i}$	=	energy flow into the i[th] zone through surfaces (W).
$\phi_{product,i}$	=	energy flow into the i[th] zone from product batches (W).

$\phi_{air,i}$ = energy flow into the i[th] zone due to airflow from other zones or fans/evaporators (W).

$\phi_{heatgen,i}$ = energy flow into the i[th] zone from heat generators (W).

The water vapour balance for the air in a generalised zone is:

$$M_i \frac{dH_i}{dt} = m_{door,i} + m_{floor,i} + m_{inert,i} + m_{surface,i} + m_{product,i} + m_{heatgen,i} + m_{air,i} \quad (8.2)$$

where:

H_i = absolute humidity of the i[th] zone air (kg/kg).

$m_{door,i}$ = water vapour entering the i[th] zone through doors (kg/s).

$m_{floor,i}$ = water vapour entering the i[th] zone from the floor (kg/s).

$m_{inert,i}$ = water vapour entering the i[th] zone from inerts (kg/s).

$m_{surface,i}$ = water vapour entering the i[th] zone from surfaces (kg/s).

$m_{product,i}$ = water vapour entering the i[th] zone from product batches (kg/s).

$m_{air,i}$ = water vapour entering the i[th] zone due to airflow from other zones or fans/evaporators (kg/s).

$m_{heatgen,i}$ = water vapour entering the i[th] zone from heat generators (kg/s).

Once the enthalpy and humidity of the zone air have been determined using Eqn's. 8.1 and 8.2, the temperature of the zone air can be estimated algebraically using the equivalent of Eqn. 5.23 (Stoecker and Jones, 1982):

$$T_i \approx \frac{hh_i - H_i h_{fg}}{c_a + H_i c_v} \quad (8.3)$$

where:

T_i = temperature of the air in the i[th] zone (°C).

h_{fg} = latent heat of vapourisation of water (J/kg).

c_a = specific heat capacity of dry air (J/kg K).

c_v = specific heat capacity of water vapour (J/kg K).

8.3 INTERACTION BETWEEN ZONES

8.3.1 Air Flow

Air flow in the coolstore is primarily due to two mechanisms, natural convection due to localised density differences, and forced convection due to fans. Both mechanisms must be included in a multi-zoned model of a refrigerated facility. The approach taken needs to be flexible, in order to accommodate a variety of zone sizes and configurations, and a number of fans and fan speed combinations.

Two general approaches could be used to describe air flow for a multizone model: firstly, using numerical approximation to the fundamental equation for fluid flow (Navier-Stokes equations); or secondly, by defining forced convection pathways throughout the store, with natural convection mixing to adjacent zones. Using the second approach the forced convection pathways could be defined either in general terms or on a fan by fan basis.

The first approach was rejected because it is both data- and computationally-intensive, especially when the product loading pattern and fan operation can change frequently. The second approach, implemented on a fan by fan basis, would require multiple data input and would also be computationally intensive. Therefore the second approach was adopted implemented via a generalised forced convection pathway throughout the store plus natural convection mixing occurring between zones.

The air flow options between any two zones were then:

(1) no flow (zone has no common boundary).
(2) forced convection only (1-way);
(3) natural convection interchange only (2-way);
(4) both forced and natural convection.

The fourth and most general situation of combined one-way forced convection and

two-way natural convection interchange was implemented. The other options are achieved by appropriate choice of data.

8.3.1.1 Combined Natural and Forced Convection

Any particular zone can be modelled as having interaction with up to N other zones. Both forced and natural convection may occur between any two zones. The same approach as used in the carton model for combining forced and natural convection air flow between zones (Section 5.3.5.3) was used in the coolstore model:

$$m_{net,i\leftarrow n} = \left(m^3_{for,i\leftarrow n} + m^3_{nat,i\leftrightarrow n}\right)^{0.33} \tag{8.4}$$

where:

$m_{net,i\leftarrow n}$ = net flow rate of dry air into the i^{th} zone from the n^{th} associated zone due to forced and natural convection (kg/s).

$m_{for,i\leftarrow n}$ = forced convection of air into the i^{th} zone across the interface with the n^{th} associated zone (kg/s).

$m_{nat,i\leftrightarrow n}$ = natural convection of air into the i^{th} zone across the interface with the n^{th} associated zone (kg/s).

To maintain a mass balance for each zone, some back mixing returning to the n^{th} associated zone occurs:

$$m_{out,i\rightarrow n} = m_{net,i\leftarrow n} - m_{for,i\leftarrow n} \tag{8.5}$$

where:

$m_{out,i\rightarrow n}$ = air flow out of the i^{th} zone to the n^{th} associated zone (kg/s).

Each of $m_{net,i\leftarrow n}$ and $m_{out,i\rightarrow n}$ can be negative or positive, depending on the direction of $m_{for,i\leftarrow n}$.

8.3.1.2 Natural Convection

Natural convection mixing between adjacent zones could be modelled by a constant rate of interchange of air or by calculating the mass flow interchanged in some manner. A constant rate of air flow would be the simplest method to implement, but determining appropriate values would be difficult. Further, the rate is almost certainly not constant throughout the coolstore, depending on density gradients and orientations of zones. Tamm's equation as used for doors (Tamm, 1965) is one possibility for calculating mass flow at zone boundaries (as a function of density difference). However, this method was developed for unobstructed boundaries with a definite interface between air at different conditions. Zone boundaries have an arbitrary nature with little physical meaning, so the validity of using Tamm's equation in this situation is questionable.

Another possibility considered was to model the natural convection mixing in a similar fashion to the method used to calculate natural convection between zones in the apple cooling carton model (Section 5.3.5.1). This approach was based on an empirical correlation for natural convection in small enclosures. When applied to the coolstore zones it gave unrealistically high mass flow rates between the zones.

In the apparent absence of any better methodology, an arbitrary empirical relationship between zone temperature difference and natural convection velocity was postulated:

$$v_{i\leftarrow n} = 0.134\ (T_i - T_{i,n})^{0.5} \qquad (8.6)$$

where:

$v_{i\leftarrow n}$ = air velocity between the i^{th} zone and the n^{th} associated zone (m/s).

$T_{i,n}$ = air temperature of n^{th} zone associated with to the i^{th} zone (°C).

Over small temperature ranges, density difference is proportional to temperature difference, and Tamm's equation suggests a square root relationship to density difference (driving force) may be appropriate. The factor of 0.134 was chosen to match measured data for the industrial coolstore (Table 7.1). Without experimental

verification, it is unlikely that Eqn. 8.6 could be widely applied to different store configurations. However, it appears to give results consistent with those measured by Falconer (1993).

The natural convection flow is assumed to occur in each direction across half of the area of the boundary. Hence the mass interchange between two zones is:

$$m_{nat,i\leftarrow n} = v_{i\leftarrow n}\ \rho_a\ \frac{A_{i,n}}{2} \tag{8.7}$$

where:

ρ_a = density of air in the coolstore (kg/m^3).

$A_{i,n}$ = area of interface between the ith zone and the nth associated zone (m^2).

This approach was used for all vertical interzone boundaries and for horizontal interzone boundaries for which the temperature of the top zone was lower than the temperature of the bottom zone, i.e. the higher density air is above the lower density air. In situations with a horizontal interzone boundary where the top zone is warmer than the bottom zone, natural convection is unlikely to occur so $v_{i\leftarrow n}$ was set to zero.

8.3.1.3 Forced Convection

The forced convection pathways must be defined in a manner that ensures that the predicted air movement is responsive to changes in operation of the fans, and that an air mass balance is maintained. The method chosen was to define a hierarchy of zones along the air path, starting with those zones from which fans draw air and finishing with zones into which fans discharge air. The basic rule for solving the hierarchy is that all air flows out of a zone must be defined before the air flows into the zone are defined.

Given this hierarchy, for a generalised zone there can be up to J flows out to other zones that have been previously evaluated, and N-J flows in from other zones still to be evaluated, plus discharges and/or suctions to up to M fans/evaporators. As has

been shown, natural convection was assumed to always give balanced mass flow rate interchange, so the forced convective components must independently maintain the mass balance. For example, Figure 8.2 shows a typical zone with 4 adjacent zones. There are 2 air inflows, one fan/evaporator discharge, 2 air outflows and one fan/evaporator suction (not necessarily at the same flow rate as the fan/evaporator discharge).

The net flow of dry air into the ith zone from zones still to be evaluated (associated zones J+1 to N) is given by:

$$I_{net,i} = \sum_{m=1}^{M} E_{s,i\rightarrow m} - \sum_{m=1}^{M} E_{d,i\leftarrow m} - \sum_{n=1}^{J} m_{for,i\leftarrow n} \qquad (8.8)$$

where:

$I_{net,i}$ = net airflow into the ith zone (kg/s).

$E_{s,i\rightarrow m}$ = air flow from the ith zone to the mth fan/evaporator (kg/s).

$E_{d,i\leftarrow m}$ = air discharge into the ith zone from the mth fan/evaporator (kg/s).

Because of the hierarchial evaluation procedure, for n = 1 to J, the values of $m_{for,i\leftarrow n}$ will have been estimated as part of calculations for zones earlier in the hierarchy.

The airflows into the ith zone from associated zones that are still to be evaluated (n = J+1 to N) are calculated based on defined fractions of the net flow into the ith zone:

$$m_{for,i\leftarrow n} = F_{i,n}\ I_{net,i} \qquad (8.9)$$

where:

$F_{i,n}$ = fraction of the net airflow into the ith zone that is drawn from the nth associated zone.

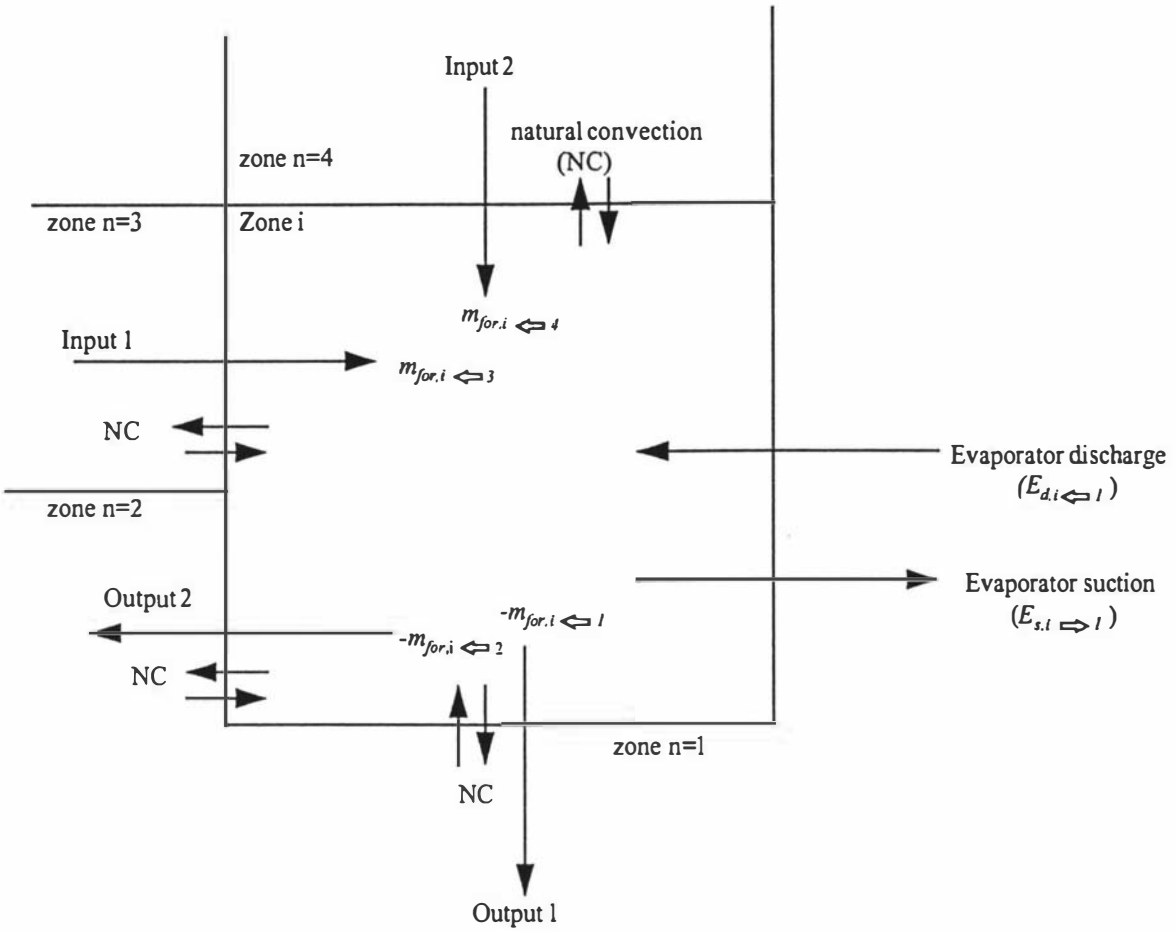

Figure 8.2: Forced convective air flow into and out of a typical zone within a coolstore with 2 inflows and 2 outflows and both an evaporator suction and discharge.

To ensure a mass balance on the i[th] zone, necessary conditions are that:

$$\sum_{n=J+1}^{N} F_{i,n} = 1.0 \qquad (8.10)$$

$F_{i,n} \geq 0$, $E_{s,i \rightarrow m} \geq 0$, and that $E_{d,i \leftarrow m} \geq 0$.

Values of $m_{for,i \leftarrow n}$ can be negative if $I_{net,i}$ or I_{net} for the n[th] associated zone are negative. It is possible to have zones with only evaporator suction and no other forced convection outputs, or zones with only evaporator discharge and no other forced convection inputs, or combinations of each. In practice, for each zone the $F_{i,n}$ values were selected to model the actual air flow distribution in the store.

8.3.2 Energy and Water Vapour Flows

Given the above rates of air flow between zones the associated energy and water vapour flows are:

$$\phi_{air,i} = \sum_{n=1}^{N} m_{net,i\leftarrow n}\ hh_n - \sum_{n=1}^{N} m_{out,i\rightarrow n}\ hh_i + \sum_{m=1}^{M} E_{d,i\leftarrow m}\ hh_{m,off} - \sum_{m=1}^{M} E_{s,i\rightarrow m}\ hh_i \tag{8.11}$$

$$m_{air,i} = \sum_{n=1}^{N} m_{net,i\leftarrow n}\ H_n - \sum_{n=1}^{N} m_{out,i\rightarrow n}\ H_i + \sum_{m=1}^{M} E_{d,i\leftarrow m}\ H_{m,off} - \sum_{m=1}^{M} E_{s,i\rightarrow m}\ H_i \tag{8.12}$$

where:

hh_n = air enthalpy of the nth zone associated with the ith zone (J/kg).

$hh_{m,off}$ = air enthalpy off the mth evaporator associated with the ith zone (J/kg).

H_n = air humidity of the nth zone associated with the ith zone (kg/kg).

$H_{m,off}$ = air humidity off the mth evaporator associated with the ith zone (kg/kg).

8.4 ZONE COMPONENT MODELS

8.4.1 Surface Model

A surface is defined as any planar solid structure which separates the ith zone air from other zones or from ambient air outside the coolstore. Insulated walls and the roof are examples of typical surfaces within an industrial coolstore. Important mechanisms for a surface are heat transfer by convection and radiation to the outside surface, conduction through the surface, heat accumulation in the materials of the surface, and possible moisture deposition on the inside surface (Figure 8.3). The surface model should be capable of predicting heat flow through the surface and the rate of water condensation or evaporation on the inside surface. The surface temperature on the zone side is required to perform water vapour transfer

calculations. Models of varying complexity could be used:

(1) Ignoring the thermal capacity of the surface and determining heat flow through the surface based solely on resistance to heat transfer and the temperature difference across the surface. The inside surface temperature would be determined by a steady-state heat balance.

(2) Lumping the thermal capacity of the surface at one position and modelling the change in temperature of the wall at this position. This leads to one ordinary differential equation (ODE) for temperature at the selected position.

(3) Distributing the thermal capacity of the surface either at a number of lumped positions, or continuously. Such a distributed model leads to a partial differential equation (PDE) or a number of ODE's for temperature as a function of time and position through the surface (Wang, 1991).

(4) Dissociate the wall resistance and thermal capacity, by allowing heat flow through the surface directly into the zone air, and having the zone air linked to the surface thermal capacity separately (Lovatt, 1992).

The first method does not model any thermal buffering effect offered by the surface and may lead to incorrect heat loadings on the zone air, but is simple to use. The third method would add considerable complexity to the overall model, particularly if the full finite difference approach was adopted. As a compromise between accuracy and complexity the second method was adopted as a slight enhancement on the fourth. It allows the buffering effect of the surface mass to be approximated, but may not lead to accurate prediction of surface temperature. A decision was made to locate the total mass and thermal capacity of the surface at the inside face of the surface as shown in Figure 8.3 so that all the resistance was outside. This was considered appropriate for the industrial coolstore studied, because a large fraction of the thermal mass (timber rafters, purlins and steel portal frame) was located near the inside surface of the walls. It also allows the inside surface temperature to be predicted directly from the ODE integration.

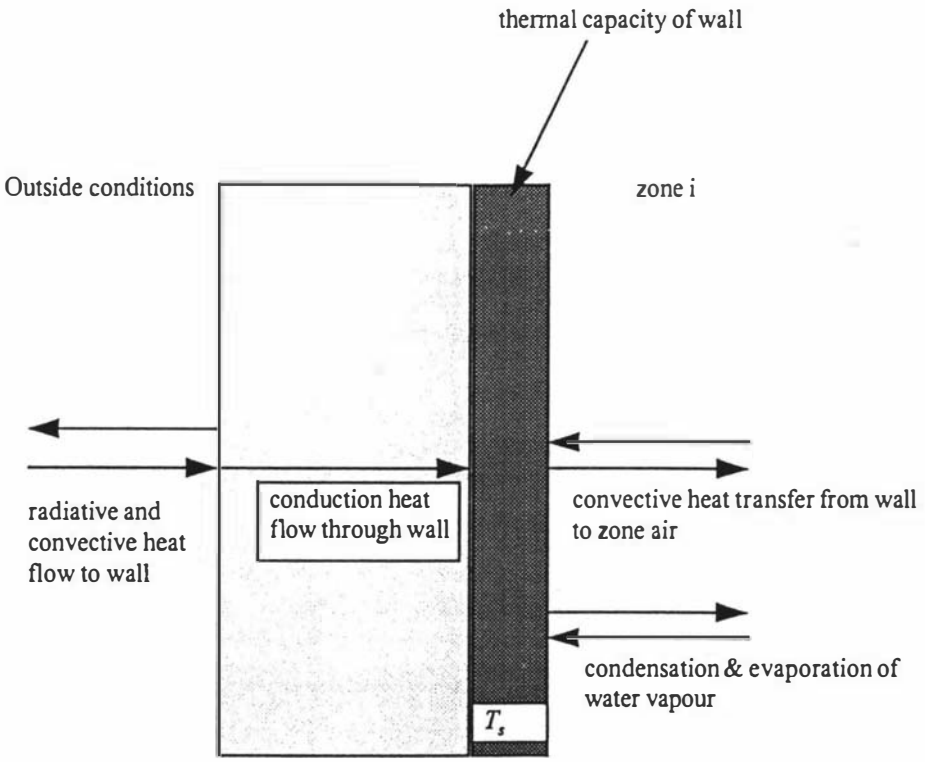

Figure 8.3: Heat transfer and water vapour transport pathways modelled for surfaces

Assuming condensed water does not ever freeze, an energy balance on a surface associated with the i[th] zone yields an equation for the inside surface temperature:

$$\frac{d(M_s c_s + M_{w,s} c_w) T_s}{dt} = \phi_{s,out} + \phi_{s,in} + \phi_{w,s} \qquad (8.13)$$

where:

$\phi_{s,out}$ = energy flow to surface from air outside the surface (W).

$\phi_{s,in}$ = energy flow to surface from zone air (W).

$\phi_{w,s}$ = energy flow to surface due to water transfer from zone air (W).

M_s = surface mass (kg).

$M_{w,s}$ = condensed water mass on the inside face of the surface (kg).

T_s = surface inside temperature (°C).

c_s = specific heat capacity of the surface (J/kg K).

c_w = specific heat capacity of water (J/kg K).

This equation can be decoupled using the chain rule giving:

$$(M_s c_s + M_{w,s} c_w) \frac{dT_s}{dt} = \phi_{s,out} + \phi_{s,in} + \phi_{s,w} - c_w T_s \frac{dM_{w,s}}{dt} \quad (8.14)$$

For the outside face of the surface both convection and radiation were modelled as solar radiation may be important for some surfaces. Water vapour condensation/evaporation was considered unlikely. A sol-air temperature was defined to take account of both these mechanisms in terms of a convection-style equation:

$$\phi_{s,out} = U_s A_s (T_{sol} - T_s) \quad (8.15)$$

where:

U_s = heat transfer coefficient from outside air to the position where the thermal mass is located (W/m^2 K).

A_s = surface area of the surface (m^2).

T_{sol} = sol-air temperature for the outside face of the surface (°C).

The overall heat transfer coefficient for the outside face of the surface (U_s) was calculated from:

$$U_s = \frac{1}{\frac{1}{h_{o,s}} + \sum_{l=1}^{L} \frac{x_{s,l}}{k_{s,l}}} \quad (8.16)$$

where:

$h_{o,s}$ = convective heat transfer coefficient for the outside face (W/m^2 K).

$x_{s,l}$ = thickness of the lth layer of the surface (m).

$k_{s,l}$ = thermal conductivity of the lth layer of the surface (W/m K).

The sol-air temperature (T_{sol}) was calculated using:

$$T_{sol} = T_a + \frac{SolRad\ \varepsilon}{h_{o,s}} \quad (8.17)$$

where:

T_a = ambient temperature on the outside of the surface (°C).

SolRad = solar radiation incident on the outside surface (W/m^2).

ε = emissivity of the outside face of the surface.

The ambient air temperature (T_a) and the solar radiation (*SolRad*) were either determined using an ambient model (Section 8.5.1), or if the surface was between two zones, were equal to the temperature of the zone outside the surface and zero respectively.

Convection and water vapour condensation/evaporation were modelled from the inside of the surfaces to the zone air. Any radiation was approximated as pseudo-convection. The energy flow to the surface due to convection with the zone air is given by:

$$\phi_{s,in} = h_{in,s} A_s (T_i - T_s) \qquad (8.18)$$

where:

$h_{in,s}$ = convective heat transfer coefficient for the inside face of the surface (W/m^2 K).

The energy flow to the surface due to water deposition was estimated by:

$$\dot{\Psi}_{s,w} = \frac{dM_{w,s}}{dt} (h_{fg} + c_v T_i) \qquad (8.19)$$

To allow Eqn. 8.19 to be used for both evaporation and condensation of water, it was assumed that the sensible heat component of the enthalpy of the water vapour deposited is always equal to that of the water vapour in the zone air. If it is assumed that water only condenses to, or evaporates from the surface and is not absorbed, the rate of water deposition can be modelled by:

$$\frac{dM_{w,s}}{dt} = mtc_s \, A_s \, Ef \, (\, H_i - H_{s,s} \,) \qquad (8.20)$$

When $M_{w,s} > 0$

where:

mtc_s = mass transfer coefficient for water vapour to the surface from the zone air (kg/m^2 s).

$H_{s,s}$ = saturation humidity of water at T_s (kg/kg).

Ef = evaporation correction factor.

However, if conditions are such that evaporation should occur yet there is no water on the surface then the transfer must be nil. Therefore:

$$\frac{dM_{w,s}}{dt} = 0 \qquad (8.21)$$

When $M_{w,s} = 0$

The mass transfer coefficient can be determined from the heat transfer coefficient if the Lewis relationship is assumed to hold (Stoecker and Jones, 1982):

$$mtc_s = \frac{h_{in,s}}{c_a + H_i \, c_v} \qquad (8.22)$$

Ef is an empirical factor to take into account the fact that the area, for evaporation in particular, may be different from the surface area, due to the formation of droplets rather than a uniform film of water. It can have different values for condensation ($H_i > H_{s,s}$) and evaporation ($H_i < H_{s,s}$). Eqn. 8.20 assumes that the distribution of water on the surface does not affect the temperature distribution and that *Ef* is independent of the amount of condensed water. In practice, on vertical faces in particular, drainage may occur, but no attempt was made to model this.

By substituting Eqn's. 8.15, 8.18 and 8.19 into Eqn. 8.14 it can be shown that:

$$(M_s c_s + M_{w,s} c_w)\frac{dT_s}{dt} = U_s A_s (T_{sol} - T_s) + h_{in,s} A_s (T_i - T_s) + \frac{dM_{w,s}}{dt}(h_{fg} + c_v T_i - c_w T_s) \quad (8.23)$$

The final surface model consists of Eqn's. 8.16, 8.17, 8.20, 8.21, 8.22 and 8.23, plus the ambient models for surfaces exposed to ambient conditions (Section 8.5.1).

Separate sets of equations are required for every zone/surface combination. The net heat and water vapour flows from the S surfaces associated with any particular zone are given by:

$$\phi_{surface,i} = -\sum_{s=1}^{S} \phi_{s,in} \quad (8.24)$$

$$m_{surface,i} = -\sum_{s=1}^{S} \frac{dM_{w,s}}{dt} \quad (8.25)$$

8.4.2 Floor Model

The floor was modelled in a similar fashion to surfaces, except that the ambient air temperature on the outside face was replaced by the underfloor soil temperature, and the solar radiation term was eliminated. Also conduction through both the soil and the concrete floor slab as well as insulation if it was present was considered. The thermal mass of a floor is considerably greater than most other surfaces and both the resistance and capacitance are distributed more evenly than in ceiling and wall surfaces. Although use of the single lumped parameter model may be less accurate than for other surfaces it was decided to use the single lumped approach because of its simplicity. Locating the floor thermal mass at the surface of the floor slab, and by equivalent procedures to those used to derive Eqn. 8.23:

$$(M_f c_f + M_{wf} c_w) \frac{dT_f}{dt} = U_f A_f (T_{soil} - T_f) + h_{in,f} A_f (T_i - T_f) + \frac{dM_{wf}}{dt}(h_{fg} + c_v T_i - c_w T_f) \quad (8.26)$$

where:

T_f = floor surface temperature (°C).

M_f = floor mass (kg).

c_f = effective specific heat capacity of the floor (J/kg K).

T_{soil} = temperature of the soil beneath the floor (°C).

U_f = overall heat transfer coefficient through the soil and floor slab (W/m^2 K).

A_f = surface area of floor exposed to the ith zone air (m^2).

$h_{in,f}$ = convective heat transfer coefficient from zone air to floor (W/m^2 K).

M_{wf} = mass of water condensed on the floor (kg).

The overall heat transfer coefficient (U_f) takes into account the heat transfer resistance through the soil from the position where T_{soil} was measured, through any insulation under the floor, and through the floor slab to the inside surface:

$$U_f = \frac{1}{\frac{x_{concrete}}{k_{concrete}} + \frac{x_{insul}}{k_{insul}} + \frac{x_{soil}}{k_{soil}}} \quad (8.27)$$

where:

$x_{concrete}$ = thickness of concrete slab (m).

$k_{concrete}$ = thermal conductivity of concrete (W/m K).

x_{insul} = thickness of insulation (m).

k_{insul} = thermal conductivity of insulation (W/m K).

x_{soil} = thickness of soil below concrete slab to temperature measurement position (m).

k_{soil} = thermal conductivity of soil (W/m K).

The rate of water condensation onto the floor or evaporation from the floor was determined by equivalent versions of Eqn's. 8.20, 8.21 and 8.22.

The net heat and water vapour flows into any zone from the associated F floor sections was given by:

$$\phi_{floor,i} = - \sum_{f=1}^{F} h_{in,f} A_f (T_i - T_f) \tag{8.28}$$

$$m_{floor,i} = - \sum_{f=1}^{F} \frac{dM_{w,f}}{dt} \tag{8.29}$$

8.4.3 Inert Materials Model

Inert materials were classified as being any material present within the coolstore, other than surfaces, floors and product (which are considered separately), which have significant thermal mass and heat capacity. Inert materials will provide some degree of thermal buffering within the coolstore, may require cooling, and may have water condensing on or evaporating from them. Inert materials were treated in a similar fashion to surfaces except that they only interact with zone air, as shown in Figure 8.4. As most inert materials within the store are either metallic with high thermal conductivity or have large surface area to volume ratios, it was assumed that inert materials can be modelled as a single zone by a uniform temperature, i.e. no attempt was made to model temperature profiles through an inert material. It was also assumed that water is not absorbed into an inert material, (it can only be present on its surface).

Each air zone was modelled as interacting with R batches of inert materials. By equivalent procedures to those used to derive Eqn 8.23, the equation for the temperature of each batch of inert materials in the i^{th} zone is:

$$(M_{irt}\, c_{irt} + M_{w,irt}\, c_w)\, \frac{dT_{irt}}{dt} = h_{irt}\, A_{irt}\, (T_i - T_{irt}) + \frac{dM_{w,irt}}{dt}(h_{fg} + c_v\, T_i - c_w\, T_{irt}) \tag{8.30}$$

where:

T_{irt} = inert material temperature (°C).

M_{irt} = inert material mass (kg).

$M_{w,irt}$ = mass of water condensed on the inert material surface (kg).

c_{irt} = inert material effective specific heat capacity (J/kg K).

h_{irt} = convective heat transfer coefficient from the zone air to the inert material surface (W/m^2 K).

A_{irt} = surface area of inert material exposed to zone air (m^2).

The rate of water condensation onto or evaporation off an inert material was determined by equivalent versions of Eqn's. 8.20, 8.21 and 8.22.

The net heat and water vapour flows into any zone from inert materials were given by:

$$\phi_{inert,i} = -\sum_{r=1}^{R} h_{irt}\, A_{irt}\, (T_i - T_{irt}) \tag{8.31}$$

$$m_{inert,i} = -\sum_{r=1}^{R} \frac{dM_{w,irt}}{dt} \tag{8.32}$$

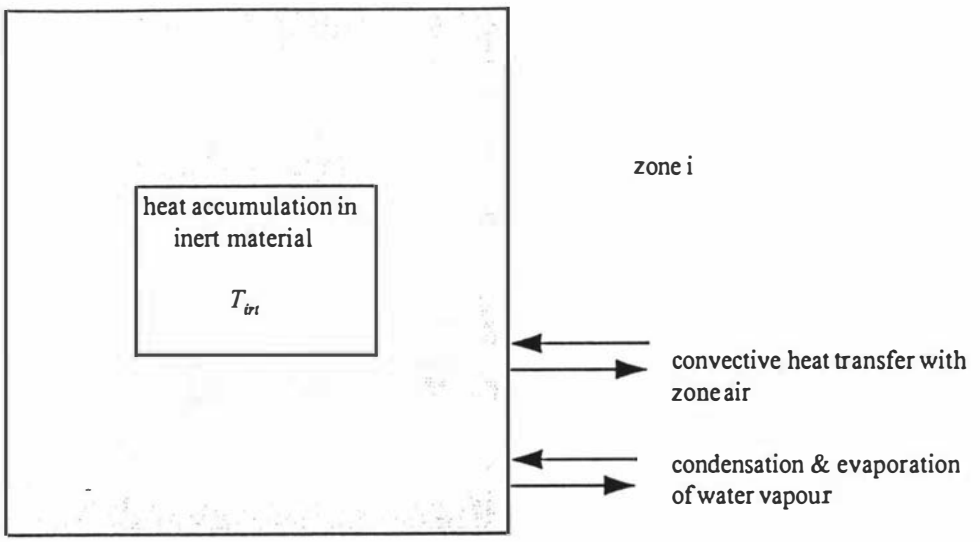

Figure 8.4: Heat and water vapour pathways modelled from inert materials present within the coolstore.

8.4.4 Product Model

The product model contains appropriate algorithms for both product which is pre-cooled and for bulk stacked product within the coolstore. In both cases, mechanisms that must be modelled include: conduction within the product; convection, radiation and evaporation from the air to the product; heat generation within the product; and heat and mass transfer for packaging associated with the product, particularly the adsorption of water by paper-based materials.

8.4.4.1 Product Pre-cooling Model

The problems of modelling product heat transfer were discussed in detail in Chapters 4 to 6. Results from pre-cooling trials at the Whakatu coolstores, showed that the cooling process could be closely described by a constant half-life conduction model but that there was large variation in half cooling times ($t_{1/2}$) within the forced-draught pre-cooling stacks (Chapter 4). This variation could not be attributed to any positional criteria and hence the carton model as presented in Chapters 5 and 6 was developed.

Use of the full carton model for each carton present in the pre-cooler was impractical due to the large data and computational requirements. Modelling each pallet of product separately was also considered both impractical, due to the large number of pallets, and inappropriate, as there was variation in cooling rates within a pallet.

The compromise chosen was to consider each pre-cooler batch of product and packaging being pre-cooled as 6 equal sized sub-batches, each with a different cooling rate. The subdivision does not represent specific pallets or cartons, rather a fraction of the batch mass with similar cooling rate. A necessary condition is that each pre-cooler batch is contained within a single air zone. Six sub-batches was considered a realistic compromise between accuracy and complexity.

Subdivison of the packaging associated with product into 6 sub-batches was not considered necessary because most of the packaging was on the outside of the product and therefore in more direct contact with zone air than the product. The adsorption of water from the air by the packaging could also be described independently of the heat transfer. The packaging was therefore modelled as a single batch and the model focussed on its moisture content and not its thermal response.

In this manner, the product pre-cooling model consists of 13 ordinary differential equations (ODE's) for each pre-cooling stack (6 ODE's for product temperature, 6 ODE's for product mass, and 1 ODE for mean packaging moisture content). For heat transfer modelling, the small thermal mass of the packaging was included with the product thermal mass, in each sub-batch, rather than introduce separate ODE's for packaging temperature. This implies a simplification of the real process but the errors were expected to be small in their effect on the overall model.

For each sub-batch the constant half-life convection/conduction model (Lovatt *et al.*, 1993a) was used. It reduces the combined mechanisms of conduction within product plus heat transfer at the surface to a single differential equation for mass-average temperature. This allows the product heat load to be determined but supplementary

techniques are required to predict product centre or surface conditions.

For each product sub-batch in the i[th] zone an energy balance yields:

$$\frac{d(M_p c_p + M_{dp} c_{dp} + M_{w,p} c_w) T_p}{dt} = \phi_{prodair} + \phi_{resp} + \phi_{evap} + \phi_{pack} \qquad (8.33)$$

where:

T_p	=	product sub-batch mass-average temperature (°C).
M_p	=	mass of product in sub-batch (kg).
c_p	=	specific heat capacity of product (J/kg K).
M_{dp}	=	mass of dry packaging in each sub-batch (kg).
c_{dp}	=	specific heat capacity of dry packaging (J/kg K).
$M_{w,p}$	=	mass of water in packaging in each sub-batch (kg).
$\phi_{prodair}$	=	sensible heat transfer from air to product (W).
ϕ_{resp}	=	product heat of respiration (W).
ϕ_{evap}	=	heat transfer due to water gain by product from the air (W).
ϕ_{pack}	=	heat transfer due to water movement between air and packaging (W).

Eqn. 8.33 can be decoupled to give:

$$(M_p c_p + M_{w,p} c_w + M_{dp} c_{dp}) \frac{dT_p}{dt} = \phi_{prodair} + \phi_{resp} + \phi_{evap} + \phi_{pack} - c_p T_p \frac{dM_p}{dt} - c_w T_p \frac{dM_{w,p}}{dt} \qquad (8.34)$$

as the mass of dry packaging (M_{dp}) will not change.

ϕ_{resp} was defined as:

$$\phi_{resp} = rr\, M_p \qquad (8.35)$$

where:

rr	=	respiration rate (W/kg).

rr was determined by an appropriate function of temperature (e.g. Gaffney *et al.*, 1985a) for the product of interest.

Heat transfer due to evaporative cooling (condensation heating) from the product to the zone air was calculated from the rate of water transfer between the product and the air and the change in enthalpy of the water from the product surface to the air:

$$\phi_{evap} = \frac{dM_p}{dt} (h_{fg} + c_v T_p) \tag{8.36}$$

The rate of water transfer between the product in each sub-batch and the air can be found from:

$$\frac{dM_p}{dt} = mtc_p A_p (p_i - p_p) \tag{8.37}$$

where:

mtc_p = product water vapour transfer coefficient (kg/m^2 s Pa).

A_p = product exposed surface area in each sub-batch (m^2).

p_p = water vapour partial pressure at the product surface (Pa).

p_i = partial pressure of water vapour in the ith zone air (Pa).

Eqn's. 5.12, 5.31, and 5.32 were used to calculate the product surface temperature from T_i and T_p. Product and air water vapour pressures were then calculated as functions of temperature, air humidity, and water activity using standard psychrometric relationships.

The heat transfer due to water movement between packaging in each sub-batch and zone air is:

$$\phi_{pack} = \frac{dM_{wp}}{dt} (h_{fg} + c_v T_i) \tag{8.38}$$

Eqn. 8.38 uses T_i to calculate the vapour enthalpy rather than the more correct T_p because only one ODE was used for cardboard moisture content, whereas six product sub-batches were modelled. The effect of using T_i rather than selecting a mean T_p value was likely to be small.

The mass of water within the packaging in each sub-batch was found from:

$$M_{wp} = \left(\frac{mc}{100 - mc} \right) M_{dp} \tag{8.39}$$

where:

mc = packaging moisture content (%).

Eqn. 8.39 can be differentiated to yield the rate of change of packaging water mass:

$$\frac{dM_{wp}}{dt} = \left(\frac{100 \frac{dmc}{dt}}{(100 - mc)^2} \right) M_{dp} \tag{8.40}$$

Unwaxed cardboard packaging continuously absorbs or desorbs water to reach a equilibrium moisture content (*emc*), depending on the surrounding air relative humidity (RH). A first order model was assumed:

$$\frac{dmc}{dt} = k_{mc} (emc - mc) \tag{8.41}$$

where:

emc = equilibrium package moisture content (%).

k_{mc} = rate constant for water absorption or desorption (s^{-1}).

The rate constants of absorption and desorption were assumed to be the same. It was also assumed that *emc* does not vary over small temperature ranges (Steadman, 1993) and that any hysteresis effect on *emc* was ignored. The *emc* was determined from the Guggenheim-Anderson-De Boor (G.A.B.) moisture isotherm equation (Bizot, 1983):

$$emc = \frac{\frac{RH}{100}}{\beta_1 (\frac{RH}{100})^2 + \beta_2 \frac{RH}{100} + \beta_3} \tag{8.42}$$

where:

RH = air relative humidity (%)

$\beta_1, \beta_2, \beta_3$ = absorption constants for the packaging.

The sensible heat transfer between the air and the product sub-batch was given by:

$$\phi_{prodair} = UA_{sens} (T_i - T_p) \quad (8.43)$$

where:

UA_{sens} = effective sensible UA from product to zone air (W/K).

Values of UA_{sens} must be determined from known half cooling time ($t_{1/2}$) values for the product being considered. However $t_{1/2}$ values include the effect of all the possible heat transfer mechanisms, so the sensible cooling effect needs to be separated from the other mechanisms. Cleland (1990) stated that an overall UA value for all mechanisms is given by:

$$UA_{tot} = \frac{-\ln(0.5)}{t_{1/2}} M_p c_p \quad (8.44)$$

where:

UA_{tot} = overall UA from product to the zone air (W/K)

$t_{1/2}$ = half cooling time of product batch (s).

M_p = mass of product batch (kg).

c_p = specific heat capacity of product batch (J/kg K).

The effective UA value contributed by evaporative cooling was assumed to be:

$$UA_{evap} = \frac{k_p A_p (p_p - p_i) h_{fg}}{T_p - T_i} \quad (8.45)$$

where:

UA_{evap} = effective UA value due to evaporative cooling effect (W/K).

Assuming the effect of respiration and water adsorption by packaging on the overall rate of apple cooling is small and that the UA_{evap} value is both constant with time,

and equal to its initial value at the start of the cooling process, the effective sensible *UA* value (UA_{sens}) was estimated using:

$$UA_{sens} = UA_{tot} - UA_{evap} \tag{8.46}$$

The above calculation method is adequate if UA_{evap} is small compared to UA_{tot}. In some cases it may be necessary to calculate UA_{sens} for each time step in the simulation for greatest accuracy.

8.4.4.2 Bulk-Stacked Product Model

For product bulk-stacked within the coolstore heat and mass transfer are important in two situations. Firstly, product may enter the store significantly above the air temperature (e.g. product which is not pre-cooled or product which leaves the pre-cooling units at temperatures above the bulk store temperature). Secondly, once at storage temperature, the product exerts a thermal buffering effect if there are air temperature fluctuations and there will be ongoing respiration and transpiration. It is desirable to use just one model to cover both these situations.

There are several possible approaches which could be used to model bulk-stacked product in the bulk store including: using a finite difference grid through the packaged product; using a single lumped parameter; or splitting the product mass up into several lumped parameters as for the pre-cooler. The first option would give the most positional detail about the product in terms of temperature and weight loss, but would be the most complex and computationally intensive, and it would be difficult to determine appropriate input data for such a system. Using a single lumped parameter model would not allow differences in cooling rates within the bulk-stack to be modelled, but it would be the simplest system to implement and would be the least computationally intensive of the three approaches.

It was decided that the lumped parameter model used for pre-cooling would also be used for bulk-stacked product. To limit overall model size each bulk-stacked product batch was split into three rather than six sub-batches. The three blocks were chosen

to represent product on the outside of the bulk stack, product on the inside of each stack, and product at intermediary positions.

There are two possible approaches to defining cooling rates. Firstly, the 3 sub-batches could each be referenced to the zone air and $t_{1/2}$ values chosen to reflect the likely faster response of product on the outside of a stack and slower for the inside sub-batch. Alternatively, similar $t_{1/2}$ values could be applied for each sub-batch, but the cooling could be referenced to "surrounding" conditions to approximate transfer through the carton stack (rather than to the outside air). For example, the outer sub-batch would reference to zone air, the intermediate sub-batch to the outer sub-batch, and the centre sub-batch to the intermediate sub-batch. In this way the insulating effect of the stack might be more realistically modelled. For simplicity, it was decided to use the first approach because the carton model predicted distributions of cooling rates referenced to the zone air, meaning that the insulating effect of the block stack has already been taken into account indirectly.

A restriction on selection of batch size, is that each batch must reside wholly within a single air zone. It is desirable that all product in each batch has similar initial temperature and other characteristics.

Given this subdivision of bulk-stacked batches, the equations used for each sub-batch are Eqn. 8.34 for determining the product temperature, and Eqn. 8.37 for product mass. Carton moisture content is modelled separately for each of the three blocks using Eqn's. 8.40 and 8.41.

8.4.4.3 Net Product Load On Zone Air

The net product heat and water vapour flows for P pre-cooling batches and B bulk-stacked batches associated with the i^{th} air zone are given by:

$$\phi_{product,i} = -\sum_{p=1}^{P}\sum_{1}^{6}(\phi_{prodair} + \phi_{evap} + \phi_{pack}) - \sum_{b=1}^{B}\sum_{1}^{3}(\phi_{prodair} + \phi_{evap} + \phi_{pack}) \quad (8.47)$$

$$m_{product,i} = -\sum_{p=1}^{P}\sum_{b=1}^{B}\left(\frac{dM_p}{dt} + \frac{dM_{w,p}}{dt}\right) \quad (8.48)$$

8.4.5 Heat Generator Model

Heat generators were defined as any devices which place a heat load on the zone air, such as forklifts, lights, fans and people. The heat load from heat generators is the sum of the sensible and latent heat loads imposed by the heat generator:

$$\phi_{HGtot} = \phi_{HGsens} + \phi_{HGlat} \quad (8.49)$$

where:

ϕ_{HGtot} = heat generator total heat load (W).

ϕ_{HGsens} = heat generator sensible heat load (W).

ϕ_{HGlat} = heat generator latent heat load (W).

The rate of water vapour addition to the i^{th} zone air was determined by the latent heat load:

$$m_{HG} = \frac{\phi_{HGLat}}{h_{fg}} \quad (8.50)$$

where:

m_{HG} = rate of water vapour addition to coolstore air (kg/s).

Both the sensible heat load and the rate of water vapour addition to the zone air were assumed to be constant for the operating period of the heat generator. As well as the sensible and latent heat loads, the time period that the heat generator is present within each zone must be specified.

Fans are the most significant heat generators. In reality, some of the fan heat is released throughout the coolstore. A major part is due to motor and fan efficiency. This part enters the air as heat as it passes through the fan itself, but the rest is converted from kinetic energy to heat by frictional pressure drop as the air circulates through the coolstore. For simplicity in modelling, but at the loss of some accuracy it was assumed that all fan heat is released as heat in the zone from which the fan draws air. Each fan was restricted to draw air from only one zone.

Forklifts and lights are other heat generators which were modelled. All their heat was released into the zone in which they were present.

The net heat and water vapour flows due to the Hg heat generators associated with the i^{th} air zone were given by:

$$\phi_{heatgen,i} = \sum_{hg=1}^{Hg} \phi_{HGtot} \tag{8.51}$$

$$m_{heatgen,i} = \sum_{hg=1}^{Hg} m_{HG} \tag{8.52}$$

8.4.6 Door Model

The instantaneous heat and water vapour transfer through open doors was modelled using:

$$\phi_{doortot} = v_d \frac{A_d}{2} \rho_{in} (hh_{out} - hh_i) \tag{8.53}$$

$$m_{door} = v_d \frac{A_d}{2} \rho_{in} (H_{out} - H_i) \tag{8.54}$$

where:

$\phi_{doortot}$ = total heat load through door (W).

m_{door} = water vapour flow through door (kg/s).

hh_{out} = enthalpy of air outside the door (J/kg).

H_{out} = humidity of air outside door (kg/kg).

v_d = velocity of air moving through the door (m/s).

A_d = Cross-sectional area of the door (m^2).

ρ_{in} = density of inside air (kg/m^3).

These equations assume half the door area is used for inward flow and half for outward flow. To ensure a mass balance of air within the coolstore it was assumed that the masses of air entering and leaving through the door are constant. Although warm outside air entering the coolstore has lower density and displaces less mass of cold inside air, eventually it will cool and contract. This will cause more outside air to be drawn in through seals etc., so the overall effect is equal mass exchanged.

A modified Tamm's equation (Pham and Oliver, 1983) was used to calculate mean air velocities through doors:

$$v_d = 5.91\ CF \left[\frac{h_d \left(1 - \frac{\rho_{out}}{\rho_{in}} \right)}{\left\{ 1 + \left(\frac{\rho_{out}}{\rho_{in}} \right)^{0.333} \right\}^3} \right]^{0.5} \qquad (8.55)$$

where:

ρ_{out} = outside air density (kg/m^3).

h_d = height of the door (m).

CF = correction factor depending on door type and protection.

Standard psychrometric relationships were used to determine ρ_{in}, ρ_{out}, H_i, H_{out}, hh_i, and hh_{out} from air temperature and relative humidity. As the overall model assumed a constant mass of air and hence ρ_a in the store, the door model recalculated the localised density ρ_{in} for use in Eqn. 8.55.

The length of time that the door was open and closed was required to determine total heat loadings on the zones associated with doors. Possibilities for determining door

open and closed times include: using fixed open and closed times occurring for some user supplied percentage of the operating period, using actual values read in from a data file, calculating values from a statistical distribution generated from measured data, or calculating open time based on the number of product batches entering and leaving through the door over a time period and the average time of opening per product batch. Two door submodels previously used in dynamic models of refrigerated facilities are those of Cleland (1985a) and Lovatt (1992). Cleland (1985a) modelled randomly distributed openings of each door, but fixed open times to give the correct average overall frequency. Lovatt (1992) used a door model which assumed that door openings occur at irregular intervals and that the times from closing to the next door opening followed an exponential distribution, whilst door open durations were assumed to follow a normal distribution.

The approach using constant values for door open and closed times is not consistent with measured data in the industrial coolstore (Figure 7.6) so it was rejected. Using actual door opening data from a data file relies on the data file having a representative range of heavy and light usage days and these need to be matched closely to other operational parameters such as product loadings or unloadings. This was possible but it was considered that the efforts would not be justified because the resulting data are likely to be site specific and hence expensive to determine.

It was decided to use a similar approach to that of Lovatt (1992). Both door opening times and closing times were calculated as the simulation proceeded based on appropriate distributions. This kept data requirements to a minimum yet allowed different situations to be simulated. Measured data for door opening and closing times (Figure 7.6) were both approximated by exponential distributions:

$$f(x) = \frac{1}{\lambda} e^{-\frac{t_{door}}{\lambda}} \tag{8.56}$$

where:

$f(x)$ = probability of a particular door open or closed duration.

t_{door} = duration of the door open or closed period (s).

λ = mean door open or closed time (s).

The position within the distribution was determined by a random number so for any door the duration of the next open or closed period was defined from:

$$t_{door} = \lambda \ln (1 - rand) \quad (8.57)$$

where:

rand = random number between 0 and 1.0.

The net heat and mass flows into the i^{th} air zone through the D associated doors are given by:

$$\phi_{door,i} = \sum_{d=1}^{D} \phi_{doortot} \quad (8.58)$$

$$m_{door,i} = \sum_{d=1}^{D} m_{door} \quad (8.59)$$

8.5 NON-ZONE COMPONENT MODELS

Non-zone components include evaporators which are linked to zones by forced convection airflow through the interzone model (Section 8.2), and models of ambient air conditions for predicting heat and mass flow through surfaces and doors. Details of the ambient model are given first, followed by details of the evaporator model.

8.5.1 Ambient Model

An ambient model is required to determine air temperature, relative humidity and solar radiation of the air surrounding the coolstore.

8.5.1.1 Air Temperature

Possibilities for modelling outside air temperature include: assuming a constant

outside temperature, fitting a sinusoidal wave through values for maximum and minimum temperatures for the simulation period, using daily measured maximum and minimum temperatures for the location and an appropriate curve fit for temperatures at intermediate times, or use of actual measured data for air temperature versus time for the location in question. The first option does not allow for any daily or seasonal temperature variation which occurs in practice. The second option removes the difficulty surrounding diurnal temperature fluctuations, although it does not easily allow for seasonal variation in minimum and maximum temperatures. Also diurnal fluctuation in temperature does not follow a perfect sine wave. The third option allows for diurnal variation, daily differences in minimum and maximum temperatures and seasonal variation to be modelled. It is however more data intensive, with minimum and maximum temperature values required on a day by day basis. The last option would require extensive data files which would be difficult to obtain. The third option was chosen for this simulation model as daily maximum and minimum temperature data are available for a large number of sites within New Zealand at reasonable cost. The procedure developed by Kimball and Bellamy (1986) for calculating diurnal temperature patterns based on minimum and maximum temperature values was used:

If $\tau_{min} < \tau \leq (12 + D_a/2)$ then:

$$T_{amb} = T_{min} + (T_{max} - T_{min}) \cos \left[\frac{\pi (\tau - 12 + \frac{D_a}{4})}{24 + \frac{D_a}{2} - \tau_{min}} \right] \qquad (8.60)$$

Else, if $0 < \tau \leq \tau_{min}$ or $(12 + D_a/2) < \tau \leq 24$ then:

$$T_{amb} = T_{sky} + (T_{set} - T_{sky}) e^{-k_s \left[\tau - (12 + \frac{D_s}{2} - 0.06 D_s) \right]} \qquad (8.61)$$

A necessary condition for the use of Eqn. 8.61 is:

$$\text{If } 0 < \tau \leq \tau_{min} \text{ then } \tau = 24 + \tau.$$

where:

τ = time on a 24 hour clock (h).

T_{amb} = air temperature (°C).

T_{max} = daily maximum temperature (°C).

T_{min} = daily minimum temperature (°C).

τ_{min} = time of the minimum temperature (h).

T_{set} = temperature at the start of the night time decay (°C).

T_{sky} = temperature of the sky (°C).

D_a = astronomical daylength (h).

k_d = decay constant.

Other equations required are:

$$\tau_{min} = 12 - \frac{D_a}{2} + 0.06\ D_a \tag{8.62}$$

$$T_{set} = T_{min} + 0.91\ (\ T_{max} - T_{min}\ ) \tag{8.63}$$

$$T_{sky} = \left[\frac{T_{set} + 273 + T_{min} + 273}{2}\right] \varepsilon^{\frac{1}{4}} - 273 \tag{8.64}$$

$$\varepsilon_{sky} = 1 - 0.261\ e^{\left[-7.77 \times 10^{-4} \left(\frac{T_{set} + T_{min}}{2}\right)^2\right]} \tag{8.65}$$

$$k_d = \frac{\ln\left[\frac{T_{set} - T_{sky}}{T_{min} - T_{sky}}\right]}{24 - D_a + 0.12\ D_a} \tag{8.66}$$

$$D_a = 7.64 \arccos\ [-\tan(\ l\ )\ \tan(\ \delta\ )] \tag{8.67}$$

$$\delta = 0.41 \cos\left[\frac{2\pi\ (\ jd - 172\ )}{365}\right] \tag{8.68}$$

where:

jd = julian day.

ϵ_{sky} = sky emittance.

δ = declination.

l = latitude (°).

8.5.1.2 Relative Humidity

Kimball and Bellamy (1986) have shown that in New Zealand the water vapour pressure fluctuations over a day are relatively small and hence water vapour pressure can be treated as being constant throughout the day with small error resulting. The relative humidity was determined using standard psychrometric relationships from dry bulb temperature as presented in Section 8.5.1.1 and daily water vapour pressure obtained from wet and dry bulb temperature measured daily at 9.00 am (New Zealand Meterological Service).

8.5.1.3 Solar Radiation

Solar radiation on a surface was calculated from daily measured total solar radiation by assuming that the distribution could be approximated by a half sinusoid as presented by Dayan *et al.* (1989):

If $(\tau < 12 - D_a/2)$ or $(12 + D_a/2 < \tau)$ then $SolRad = 0$ Otherwise:

$$SolRad = \frac{139\ Cf\ \pi}{D_a} Rad_{daily} \sin\left[\frac{\pi\ (\tau - 12 - \frac{D_a}{2})}{D_a}\right] \tag{8.69}$$

Where:

Rad_{daily} = daily total solar radiation (MJ/m^2 day).

Cf = correction factor for wall orientation.

The total daily radiation (Rad_{daily}) was obtained from the New Zealand Meterological service, whilst the correction factor was a user input value.

8.5.2 Evaporator Model

8.5.2.1 Heat Flow Model

Evaporators were modelled by a quasi-steady-state model that assumed that the capacity of the refrigeration system was not limiting in determining evaporator performance. Thus the refrigeration system and pipelines have not been modelled. The evaporation temperature for each evaporator was calculated solely as a function of the control strategy used. It was also assumed that there was no variation of the evaporation temperature within the evaporator. This assumption is satisfactory for many large commercial coolstores in New Zealand where a number of rooms are connected to one central refrigeration plant. Evaporators were modelled as being linked to a fan drawing air from a zone, rather than having them positioned within an individual zone. This allowed the evaporator to discharge air into any number of zones, but restricted to being able to draw air from only one zone.

The mass flow rate of air through the evaporator ($m_{a,e}$) is equal to the flow rate through the associated fan. The temperature (T_{on}) and humidity (H_{on}) onto the evaporator were equal to the temperature and humidity of the zone air from which the fan draws air.

For evaporators operating under frosting conditions it is difficult to predict the effect of the frost build up on the air mass flow rate through the coil and the overall heat transfer performance in a simple manner (O'Hagan *et al.*, 1993a). In the absence of a comprehensive yet simple evaporator model, the model outlined by Cornelius (1991) was used. This model assumed that the air flow rate and heat transfer performance are independent of the extent of frosting, and that the humidity of air leaving the evaporator (H_{off}) can be estimated by assuming a straight line approach of the air to the saturation condition at the mean evaporator surface temperature:

$$H_{off} = H_{on} + \left[\frac{T_{off} - T_{on}}{T_{on} - T_{e,s}}\right] (H_{on} - H_{s}) \qquad (8.70)$$

$$T_{e,s} = T_{on} - X\,(T_{on} - T_e) \tag{8.71}$$

$$T_{off} = T_{on}\, e^{-\left[\frac{U_e A_e}{m_{a,e}\,(c_a + H_{on} c_v)}\right]} + T_e \left(1 - e^{-\left[\frac{U_e A_e}{m_{a,e}\,(c_a + H_{on} c_v)}\right]}\right) \tag{8.72}$$

$$hh_{off} = T_{off}\,(C_a + H_{off}\, c_v) + H_{off}\, hfg \tag{8.73}$$

where:

U_e	=	overall heat transfer coefficient from air to the refrigerant for the evaporator (W/m^2 K).
A_e	=	evaporator surface area (m^2).
$m_{a,e}$	=	mass flow rate of air through the evaporator (kg/s).
T_{on}	=	temperature of air on to the evaporator coil (°C).
T_{off}	=	temperature of air off the evaporator coil (°C).
T_e	=	refrigerant evaporation temperature in the evaporator coil (°C).
H_{on}	=	humidity of air on to the evaporator coil (kg/kg).
H_{off}	=	humidity of air leaving the evaporator (kg/kg).
$T_{e,s}$	=	evaporator coil average surface temperature (°C).
H_s	=	saturation air humidity at the evaporator coil surface temperature (kg/kg).
X	=	approach factor for air-on to the evaporator temperature.
hh_{off}	=	enthalpy of air leaving the evaporator (J/kg).

The value of X is dependent on the type of evaporator used. Typical values for different evaporator types were given by Cornelius (1991). H_s was calculated using standard psychrometric equations.

Use of this model for an average coolstore heat load analysis gave good prediction of mean measured RH, indicating that both the dehumidification and sensible components of the model were sufficiently accurate (Amos *et al.*, 1993; Appendix 1).

When an evaporator defrost cycle occurs, the fans delivering air are turned off ($m_{a,e}$ = 0). It was assumed that none of the heat supplied for defrost entered the coolstore air.

Many coolstores in New Zealand use evaporation pressure control for temperature control, so this was assumed. The evaporators could be controlled based on air-on temperature or air-off temperature. A Proportional Integral (PI) control system with a specified minimum evaporation temperature was modelled:

$$T_e = Prf\,(T_{a,e} - SP) + \frac{\int (T_{a,e} - SP)\,dt}{Irf} \qquad (8.74)$$

where:

SP = air temperature set point (°C).

Prf = proportional response factor.

Irf = integral response factor.

$T_{a,e}$ = evaporator air-on or air-off temperature (°C).

Limit control was simulated:

$$\text{if } T_e < T_{e,min} \text{ then } T_e = T_{e,min} \text{ and } \int (T_{a,e} - SP)\ dt = 0.$$

where:

$T_{e,min}$ = minimum evaporation temperature (°C).

8.5.2.2 Net Air Flowrates Through Evaporator Coils

The air flow between zones and evaporator coils can be determined from:

$$E_{s,i\rightarrow m} = m_{a,e}\, FS_{i,m} \qquad (8.75)$$

$$E_{d,i\leftarrow m} = m_{a,e}\, FD_{i,m} \qquad (8.76)$$

where:

$FS_{i,m}$ = proportion of the total air flow through the mth fan/evaporator from the ith associated zone.

$FD_{i,m}$ = proportion of the total air flow through the m^{th} fan/evaporator discharged into the i^{th} associated zone.

Necessary conditions are that:

$$\sum_{m=1}^{M} FS_{i,m} = 1.0 \qquad (8.77)$$

$$\sum_{m=1}^{M} FD_{i,m} = 1.0 \qquad (8.78)$$

Because the model was implemented with the evaporator drawing air from only one zone, Eqn. 8.75 was not strictly required.

8.6 MODEL IMPLEMENTATION

The model was programmed in Borland Pascal v7.0 Professional. The source and executable code for the model are provided on diskette 2.

Data can be input via the keyboard or read in from previously prepared data files. Data requirements for each of the components are discussed in Chapter 9. Within the contraints of computer memory and knowledge of system data, the program models a coolstore split into a number of zones, each of which can have a number of surfaces, doors, floors, heat generators, inert materials, and product batches. Fans/evaporators can be linked to any zone, and any zone can have a number of airflow inputs or outputs to other zones or fans/evaporators. Product batches can be moved within the coolstore during the simulation and can also be split into sub-batches and sent to different zones if required, but each sub-batch must be placed in one air zone.

An event handler is used which allows discrete events to occur at appropriate times during the simulation, i.e. entry or exit of product batches, defrost cycles, heat generator entry and exit times, fan speed changes. Each of these times are user specified in initial data input procedures, and passed to the event handler at the start

of the simulation. Numerical integration of the differential equations occurs from one event to the next at which stage the number of equations and data is adjusted according to the nature of the event.

The Runge-Kutta-Felhberg (RKF) method as described in Section 5.3.8 was used for the numerical integration. The model was programmed using object orientated code to allow a flexible simulation platform, for modelling coolstores using models with a range of complexity (Lovatt, 1992). It was also programmed in a modular fashion which allowed testing in isolation of each of the component models against analytical solutions or known results for extreme data values. For example, the surface and floor models were tested against the standard conduction equation by setting the outside and inside conditions to constant values; the door model was tested against steady-state predictions using Tamm's equation by setting conditions inside and outside the doors to constant values; water condensation onto surfaces, floors and inerts were tested by setting the humidity of the zone air to a constant value in excess of the saturation humidity; and evaporation was tested by arbitrarily initialising the surfaces, floors or inert materials with water present on their surfaces. Good agreement with the test solution was found in all cases. Detailed testing of the overall model was difficult because of its complexity and the interaction between component models.

To help reduce initial value problems, such as incorrect initial values for temperatures or water vapour, for a three day simulation, the model was run for six days with the results of the last three days used in model testing. The model took 12 hours to simulate six days for the 5-zone model. Chapter 9 describes the detailed validation of the model.

Document files *coolsim.doc* (MS-Word for windows format) and *coolsim.wpd* (Word Perfect 6.1 for windows format) are supplied on diskette 2. These files outline the structure of the program, describe each of the units used, give examples of the data used in each of the text files, and outlines runtime options.

CHAPTER 9: COOLSTORE MODEL VALIDATION

9.1 INTRODUCTION

This Chapter describes the validation of the coolstore model described in Chapter 8. Validation consisted of two major steps: firstly, determination of appropriate model parameter values for the industrial coolstore in which measurements were made (described in Chapter 4); and secondly comparison of predictions with measured data (Chapter 7). The period used for validation was a 72 hour period from midnight April 6th 1992. A description of the coolstore and the activities during this period is given in Chapter 4.

9.2 ZONE SUBDIVISION

One aspect of particular interest was the sensitivity of predictions to the number and location of air zones used to describe the industrial coolstore. In order to assess the effect of the number of coolstore zones, predictions were made for 1, 5, 8, and 34 zone models (Figure 9.1). These combinations were selected based on the design and operational characteristics of the industrial coolstore. In particular, the measured variability discussed in Chapter 7 suggested subdivision into at least 2 vertical levels in the bulk-storage part of the store, separate zones for each pre-cooler, and separate zones near each door. Additionally, separate zones for parts of the coolstore in which warm fruit have been placed was considered desirable (even though these regions change from day to day), and a degree of subdivision along the 3 main airflow pathways may be necessary to model the gradual warming of the air as it passes through the coolstore.

The simplest approach was to use a single zone for the whole coolstore (Figure 9.1 a). The 5-zone model allowed differentiation of the bulk storage and pre-cooling areas within the coolstore by using 1 zone for the bulk storage areas and 1 zone for each of the pre-coolers (Figure 9.1 b). The next level of complexity chosen was the 8 zone model (Figure 9.1 c), in which the bulk-storage zone was further divided into two zones (one for the bottom half, one for the top half), plus separate zones for each of the two doors. Compared with the 5-zone model this configuration allowed predictions of

differences in conditions with vertical position within the bulk coolstore and would consider the localised effect of door loads on the coolstore. The 34-zone model represented an attempt to predict a greater degree of positional variation in the bulk store, by more closely matching zones with "warm" fruit batches (Figure 9.1 d).

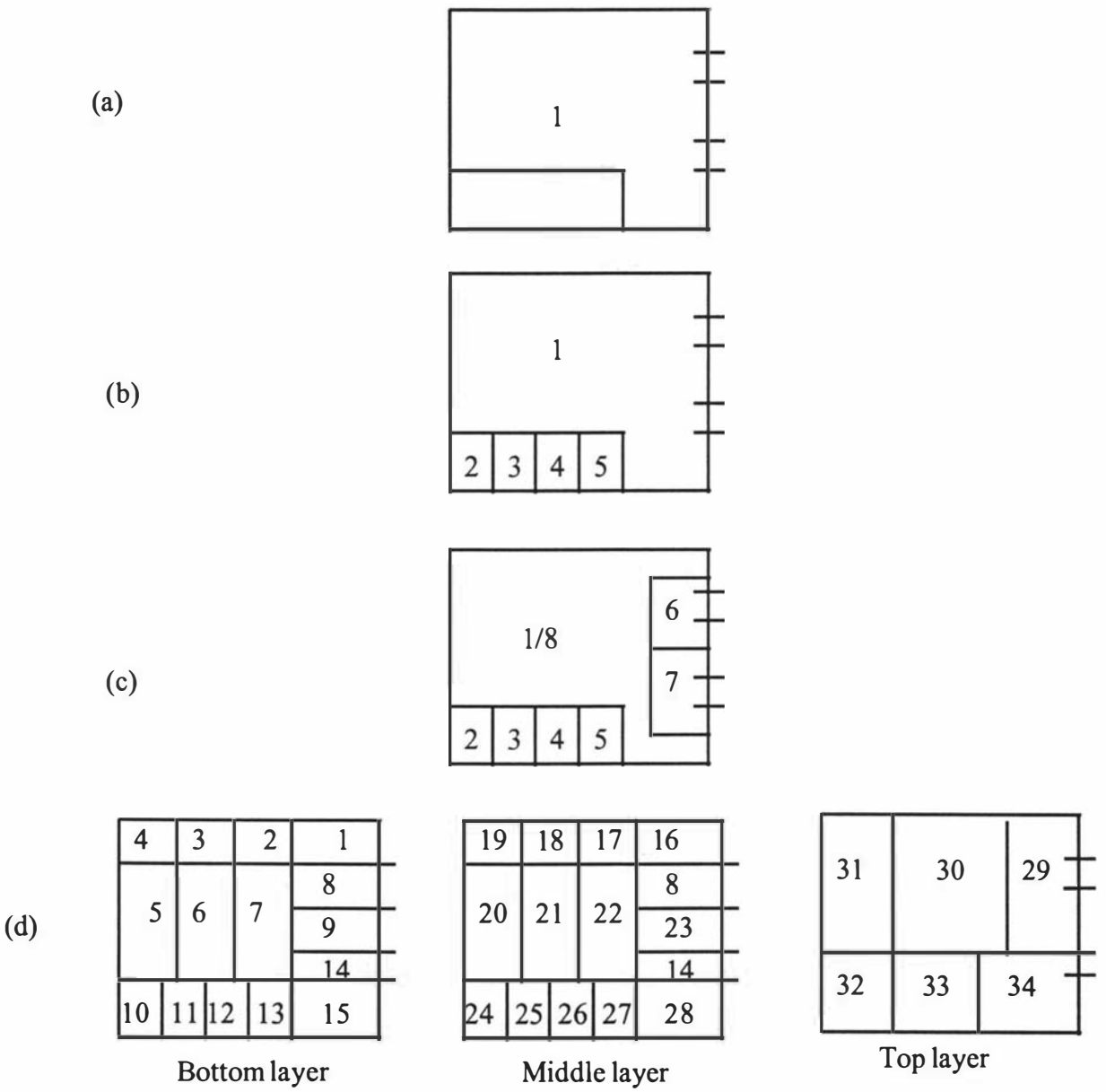

Figure 9.1: Plan views of the zones used in the four coolstore models tested: (a) 1-zone model; (b) 5-zone model; (c) 8-zone model; and (d) 34-zone model (x/y: x = bottom zone, y = top zone).

9.3 DETERMINATION OF PARAMETER VALUES

9.3.1 Zone Data

Table 9.1 lists the dimensions and initial conditions for each of the zones used in each of the four models tested. For simplicity zones were defined as being rectangular. For those that were not rectangular in practice, average dimensions were used. Initial air temperature and RH values were set to be consistent with the measured data for the appropriate position within the coolstore. To improve computational speed the air density was arbitrarily increased by a factor of 10, in a similar fashion to that discussed in the carton model (Chapter 6). Other general zone data used in all four model types is given in Table 9.13.

9.3.2 Air Flow Data

The parameters describing the air flow paths within the coolstore ($F_{i,n}$, $E_{s,i\rightarrow m}$, $E_{d,i\leftarrow m}$) were set for each of the four models to approximate the flow paths identified by the smoke test in the coolstore (Chapter 7). Table 9.2 lists these data and also gives the air zone calculation hierarchy for each of the four models. Figure 9.2 illustrates the air flow distribution used for the 8-zone model as listed in Table 9.2. The small air flows between the pre-cooling zones (zones 2,3,4 and 5) shown on Figure 9.2 were set to approximate observed flow from the smoke test (Chapter 7).

Table 9.1

Zone Dimensions and Initial Conditions Used In Each Of The Four Models

Model Type	Zone Number	Length (m)	Width (m)	Height (m)	Temperature (°C)	Relative Humidity (%)
1-Zone	1	57	60	10.6	1.0	88
5-Zone	1	57	47	10.6	1.0	88
	2	10.75	13.75	10.6	1.0	85
	3	10.75	13.75	10.6	1.0	85
	4	10.75	13.75	10.6	1.0	85
	5	10.75	13.75	10.6	1.0	85

Table 9.1 Continued

8-Zone	1	57	47	5.3	1.0	85
	2	10.75	13.75	10.6	1.0	85
	3	10.75	13.75	10.6	1.0	85
	4	10.75	13.75	10.6	1.0	85
	5	10.75	13.75	10.6	1.0	85
	6	10	5	5.3	1.0	85
	7	10	5	5.3	1.0	85
	8	57	47	5.3	1.0	85
34-Zone	1	15	14.5	1.55	0.25	85
	2	15	14.25	1.55	0.0	85
	3	15	14.25	1.55	0.0	85
	4	15	14.5	1.55	1.5	80
	5	22.5	14.5	1.55	2.5	80
	6	22.5	14.25	1.55	1.0	84
	7	22.5	14.25	1.55	2.0	83
	8	3.5	14.5	4.65	0.0	85
	9	14.5	22.5	1.55	1.0	87
	10	19.25	13.75	1.55	0.5	85
	11	10.75	19.25	1.55	1.0	88
	12	10.75	19.25	1.55	2.0	88
	13	10.75	19.25	1.55	0.0	85
	14	3.5	14.5	4.65	0.5	88
	15	14.5	22	1.55	0.25	88
	16	14.5	15	3.1	0.0	87
	17	14.25	15	3.1	0.0	85
	18	14.25	15	3.1	1.5	82
	19	14.5	15	3.1	1.5	83
	20	14.5	22.5	3.1	1.0	85
	21	14.25	22.5	3.1	2.0	85
	22	14.25	22.5	3.1	0.75	86
	23	14.5	19	3.1	0.5	87
	24	13.75	19.25	3.1	1.0	88
	25	10.75	19.25	3.1	2.0	88
	26	10.75	19.25	3.1	3.0	88
	27	10.75	19.25	3.1	0.5	88
	28	14.5	19	3.1	0.5	88
	29	14.5	37.5	4.6	0.0	88
	30	28.5	37.5	4.6	0.0	88
	31	14.5	37.5	4.6	0.0	88
	32	14.5	19.25	4.6	0.0	88
	33	20	19.25	4.6	0.0	88
	34	23	22	4.6	0.0	88

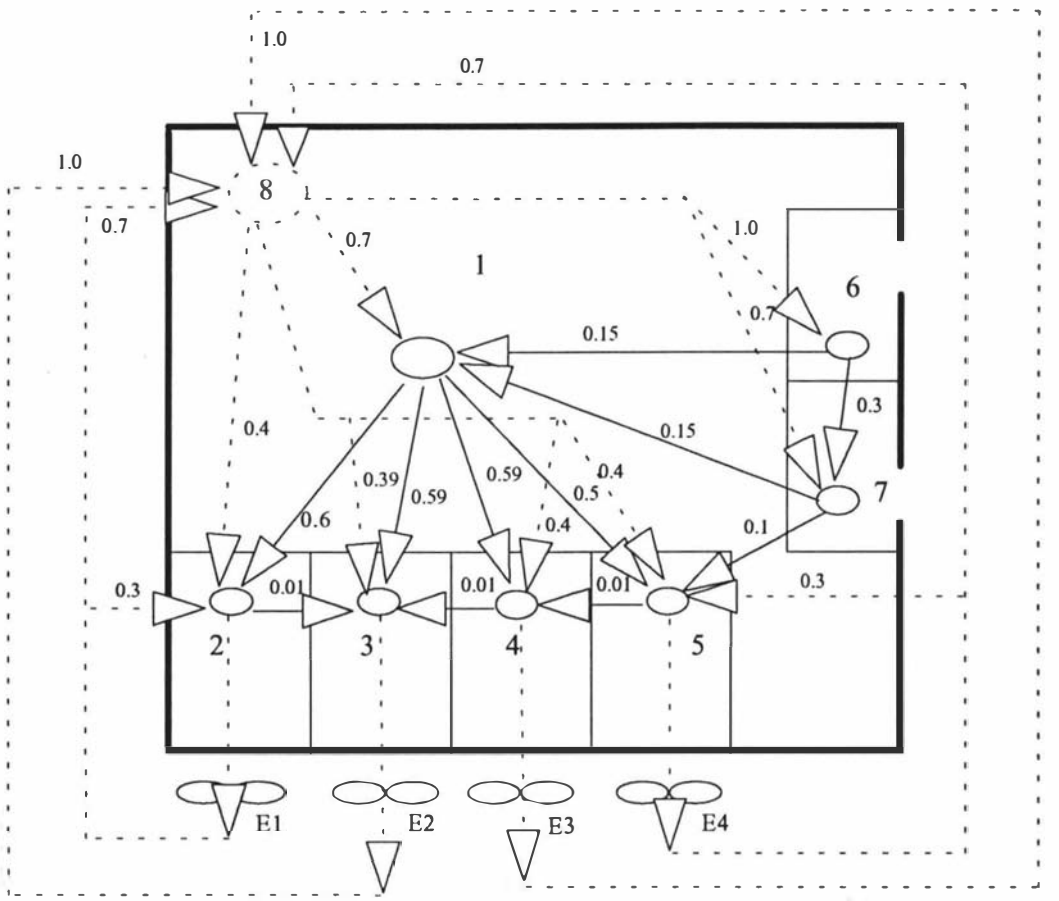

Figure 9.2: Net air flow fractions ($F_{i,n}$) and fan/evaporator discharge fraction ($F_{d,i\leftarrow n}$) and fan/evaporator suction fractions ($F_{s,i\rightarrow m}$) used to describe air flow pathways between zones for the 8-zone model.

Table 9.2

Air Flows Between Zones For Each Of The Four Model Types

Model Type	Zone Number (*i*)	Outputs[1]	Inputs[2]	Zone Hierarchy Order (*n*)
1-Zone	1	E1; E2; E3; E4	E1/1.0; E2/1.0; E3/1.0; E4/1.0;	1
5-Zone	1	2; 3; 4; 5	E1/0.5; E2/0.75; E3/0.75; E4/0.5;	5
	2	E1; 3	E1/0.5; 1/1.0	3
	3	E2	E2/0.25; 1/0.99; 2/0.01;	1
	4	E3	E3/0.25; 1/0.99; 5/0.01;	2
	5	E4; 4	E4/0.5; 1/1.0	4
8-Zone	1	3; 4; 2; 5	8/0.7,T; 6/0.15; 7/0.15	5
	2	E1; 3	E1/0.3; 1/0.6; 8/0.4;	3
	3	E2	2/0.01; 4/0.01; 1/0.59; 8/0.39	1
	4	E3	5/0.01; 1/0.59; 8/0.4	2
	5	E4; 4	E4/0.3; 1/0.5; 8/0.4; 7/0.1	4
	6	1; 7	8/1.0,T	7
	7	5; 1	8/0.7,T; 6/0.3	6
	8	3; 4; 2; 5; 1,B, 6,B; 7,B	E1/0.7; E2/1.0; E3/1.0; E4/0.7	8
34-Zone	1	8	16/0.5,T; 2/0.5	23
	2	7; 1	17/1.0,T	24
	3	6; 4	18/1.0,T	22
	4	5	19/0.5,T; 3/0.5	21
	5	11; 10; 6	20/0.25,T; 4/0.75	7
	6	12	21/0.2,T; 3/0.7,S; 5/0.1	6
	7	11; 12	22/0.3,T; 2/0.4; 8/0.2; 9/0.1,S	14
	8	7; 9; 22; 23	1/0.2; 16/0.8	20
	9	14; 7	1/0.5,T; 8/0.5	15
	10	E1	24/0.5,T; 5/0.5	4
	11	E2	22/0.5,T; 5/0.075; 21/0.35; 7/0.075	1
	12	E3	26/0.5,T; 6/0.075; 7/0.35; 14/0.075	2
	13	E4	27/0.5,T; 15/0.3; 14/0.2	3
	14	12; 13; 15; 26; 27; 28	9/0.5; 23/0.5	13
	15	13	28/0.75,T; 14/0.25	5
	16	8; 1,B	29/0.8,T; 17/0.2	27
	17	22; 2,B; 16	30/1.0,T	28
	18	21; 3,B; 19	30/1.0,T	26
	19	20; 4,B	31/0.8,T; 18/0.2	25
	20	5,B; 25; 24; 21	31/0.75,T; 19,0.25	17

Table 9.2 Continued

21	11; 6,B; 25; 26	30/0.75,T; 20/0.05; 18/0.2	16
22	25; 26; 7,B	30/0.7,T; 17/0.2; 8/0.05; 23/0.05	18
23	14; 9,B; 22	29/0.75,T; 8/0.25	19
24	10,B; 25	32/0.7,T; 20/0.3	10
25	11,B	24/0.1; 20/0.2; 21/0.6; 22/0.1,S	8
26	12,B	21/0.1; 22/0.6; 14/0.2; 27/0.1,S	9
27	13,B; 26	34/0.3,T; 14/0.3; 28/0.4	11
28	15,B; 27	34,0.75,T; 14/0.25	12
29	23,B; 16,B	30/0.5; 34/0.5	29
30	21,B; 22,B; 31; 18,B; 17,B; 29	E2/1.0; E3/1.0; 32/0.5; 34/0.5	31
31	20,B; 19,B	30/0.75; 32/0.25	30
32	24,B; 31; 30	34/1.0; E1/1.0; 33/0	32
33	-	32/0; 34/0	34
34	27,B; 28,B; 30; 29; 32	E4/1.0; 33/0	33

[1] Format is: (zone number, n or evaporator number, m), (orientation of associated zone). E = evaporator; side by side orientation unless stated otherwise, T = top; B = bottom;.

[2] Format is: (evaporator number, m or zone number, n) / (discharge, suction or net flow fraction), (orientation of associated zone as in [1]), e.g. E1/0.75 means 75 % of the total discharge from evaporator number 1 enters that zone (FD_{i-1}= 0.75). 30/0.5,T means input from zone 30, equal to 50% of the net inflow to the zone ($F_{i,30}$ = 0.5), and that zone 30 is above the zone of interest.

9.3.3 Surfaces Data

The only surfaces modelled were the outside walls and ceiling. These consisted of a sheet steel exterior, timber rafters and purlins, steel portal frames and sprayed in-situ polyurethane foam. Table 9.3 gives surface characteristics for each surface used in each of the four models. These characteristics were determined from coolstore plans and material properties on a mass-averaged basis. All surfaces were modelled as consisting of one layer in terms of the heat transfer resistance (L=1). General surface data is given in Table 9.13.

9.3.4 Floor Data

The coolstore floor, which was uninsulated, was split into fifteen sections to allow each floor level zone of the 34-zone model to interact with a single floor section. Tables 9.4 and 9.13 provide detailed data for each section, determined from coolstore plans and material properties on a mass-averaged basis. The inside heat transfer coefficient from the floor to the zone air ($h_{in,f}$) was estimated to be 2 W/m^2 K using mixed convection heat transfer correlations (Holman, 1990), based on an air velocity of 0.25 m/s over the floor. This value was derated by assuming that 75% of the floor was covered by pallets with an assumed effective heat transfer coefficient of 1 W/m^2 K.

Measured data for soil temperatures beneath the industrial coolstore at a depth of 0.5 m (Figure 7.7) were used as the basis for determining soil temperatures. Regression analysis gave the following best-fit model, which Figure 7.6 shows adequately predicts measured data:

$$T_{soil} = 2.72 + 15.33\ e^{-0.0642\ (\ jd\ -\ 56.34\ )} \qquad (9.2)$$

where:

jd = time (Julian day).

9.3.5 Inert Material Data

The only inert material in the coolstore with significant thermal mass not taken into account as part of the product, surface, or floor models was the central air distribution duct. Sections of the duct were placed in the air zone in which they were present. Tables 9.5 and 9.13 give data for each of the inerts modelled in each of the four models. Mass and surface area was calculated from material data and reference to plans of the industrial coolstore. Effective thermal properties were calculated from component values on a mass-average basis, whilst heat transfer coefficients were calculated based on an air velocity of 0.5 m/s over the inerts. The initial temperature of the inert was assumed to be the same as zone air.

Table 9.3

Characteristics Of Each Surface Used In Each Of The Four Models

Model Type	Surface Number	Exposed to Solar Radiation[1]	Inside Zone (i)	Surface Area, A_s (m^2)	Mass, M_s (kg)	c_s (J/kg K)
1-Zone	1	Y	1	3220	32000	1400
	2	N	1	1740	20000	1200
5-Zone	1	N	1	1580	17426	1197
	2	N	2	146	1861	1085
	3	Y	1	2622	22428	1567
	4	Y	2	146	2382	1469
	5	Y	3	146	2382	1469
	6	Y	4	146	2382	1469
	7	Y	5	146	2382	1469
8-Zone	1	N	1	790	8713	1197
	2	N	2	146	1861	1085
	3	N	8	790	8713	1197
	4	Y	8	2622	22428	1567
	5	Y	2	146	2382	1469
	6	Y	3	146	2382	1469
	7	Y	4	146	2382	1469
	8	Y	5	146	2382	1469
34-Zone	1	N	1	46	702	1109
	2	N	2	22	417	1317
	3	N	3	22	417	1317
	4	N	4	46	702	1109
	5	N	5	35	426	1160
	6	N	9	35	426	1160
	7	N	10	30	350	1198
	8	N	15	34	419	1164
	9	N	16	92	1404	2218
	10	N	17	44	834	1317
	11	N	18	44	834	1317
	12	N	19	92	1404	2128
	13	N	20	70	852	1160
	14	N	23	70	852	1160
	15	N	24	60	700	1198
	16	N	28	68	838	1164
	17	N	29	239	3004	939
	18	N	30	131	2148	1148
	19	N	31	239	3004	939
	20	N	32	88	811	860
	21	N	34	101	983	839
	22	Y	29	544	5457	1565
	23	Y	30	1069	11514	1573
	24	Y	31	544	5457	1565
	25	Y	32	265	2382	1469
	26	Y	33	385	3254	1334
	27	Y	34	506	4182	1425

Table 9.4

Characteristics Of Floor Sections Used For Each Of The Four Models

Floor Number	Mass, M_f (kg)	Surface Area, A_f (m^2)	Zone Linked To For Each of the four Models			
			1-Zone	5-Zone	8-Zone	34-Zone
1	75038	218	1	1	1	1
2	73744	214	1	1	1	2
3	73744	214	1	1	1	3
4	75038	218	1	1	1	4
5	112556	326	1	1	1	5
6	110616	320	1	1	1	6
7	110616	320	1	1	1	7
8	17509	51	1	1	1	8
9	95047	275	1	1	1	9
10	96298	279	1	2	2	10
11	71393	207	1	3	3	11
12	71393	207	1	4	4	12
13	71393	207	1	5	5	13
14	17509	51	1	1	1	14
15	60677	227	1	1	1	15

Table 9.5

Characteristics Of Inerts Used In Each Of The Four Models

Inert Number	Mass, M_{int} (kg)	Surface Area, A_{int} (m^2)	Zone of Residence			
			1-Zone	5-Zone	8-Zone	34-Zone
1	8024	339	1	1	8	29
2	23458	1058	1	1	8	30
3	8024	342	1	1	8	31
4	2751	116	1	2	2	32
5	9234	432	1	3,4 & 5[1]	3,4 & 5[1]	33
6	5502	232	1	1	8	34

[1] Split on an equal mass and surface area basis to each zone.

9.3.6 Product Data

Product batches were defined which approximated the actual movement of product within the industrial coolstore over the measurement period. Table 9.6 provides details of product batches moved into and out of the coolstore, while Table 9.7 gives details for product batches moved within the coolstore during the simulation. For batches moved within the coolstore the initial temperatures of the sub-batches shifted was taken as the mass-average temperature of the same sub-batches in the previous zone. This was done because sub-batches represented mass fractions of the overall batch not specific locations and it was likely that the shift would change the relative location of the individual pallets. General product parameter data are given in Table 9.13.

To determine half cooling time ($t_{1/2}$) values for the various product sub-batches the carton model (Chapters 5 and 6) was used to simulate a variety of carton positions on a pallet, for a range of airflow rates consistent with those measured in the Whakatu coolstore, for both product being pre-cooled and for product in the bulk coolstore. The distribution of half cooling times obtained from this analysis was consistent with that measured in the Whakatu coolstores (Figures 6.14 and 6.15). The resulting data used in simulations are given in Table 9.8.

Coefficients for the G.A.B. model (Eqn. 8.43; Bizot, 1983) used to describe the moisture isotherm for cardboard packaging were determined by curve-fitting the mean of absorption and desorption curves for cardboard (Figure 9.3; Wink, 1961). The mass transfer coefficient to describe the rate of absorption/desorption was estimated from measured data (Steadman, 1993)

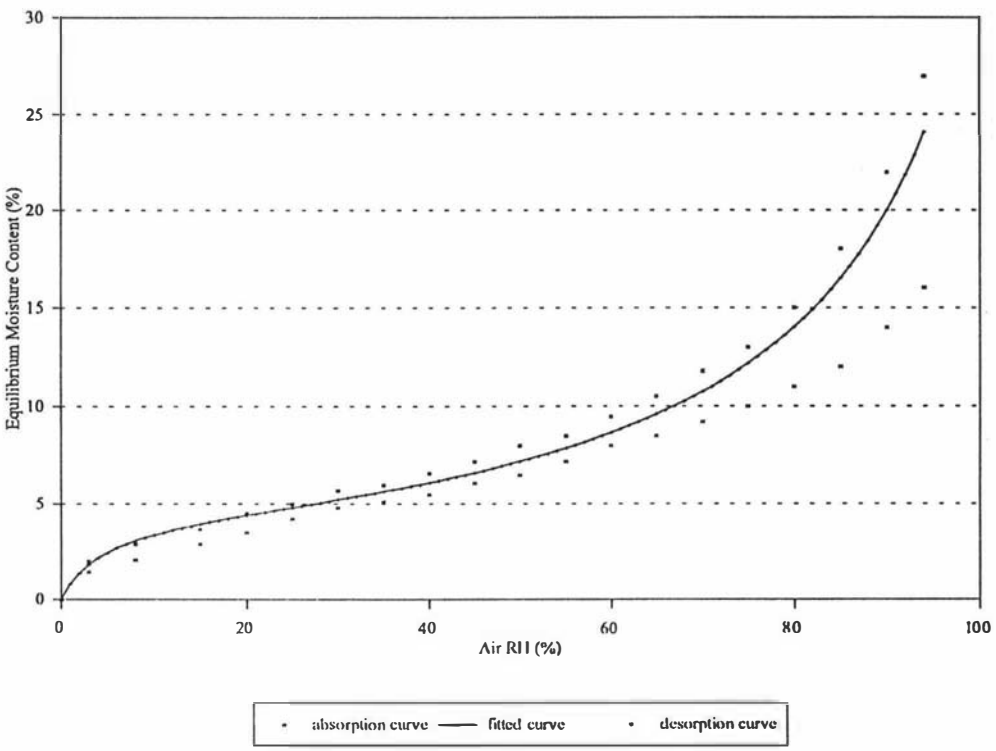

Figure 9.3: Typical moisture sorption isotherms for cardboard and fitted G.A.B isotherm for *emc* used in the product model.

Table 9.6

Characteristics of Product Batches

Batch Number	Number of Pallets	Initial Temperature T_p (°C)	Cooling Mode[1]	Entry Time (hrs)	Exit Time (hrs)[2]	Destination[3]	Initial Packaging Moisture, *mc* (%)	Zone of Residence			
								1-Zone Model	5-Zone Model	8-Zone Model	34-Zone Model
1	58	1.00	B	0	Z	Z	15.0	1	1	1	1
2	75	0.75	B	0	Z	Z	15.0	1	1	1	2
3	65	0.50	B	0	Z	Z	15.0	1	1	1	3
4	72	2.50	B	0	48	72,O	12.5	1	1	1	4
5	96	2.50	B	0	48	8,O; 88,C	12.5	1	1	1	5
6	36	4.50	B	0	Z	Z	12.5	1	1	1	6
7	96	2.50	B	0	48	9,O; 87,C	12.5	1	1	1	7
8	115	1.08	B	0	48	8,O; 107,C	15.0	1	1	6	9
9	48	0.80	B	0	Z	Z	15.0	1	2	2	10
10	48	12.00	P	18	31	48,C	10.0	1	3	3	11
11	48	12.00	P	42	54.5	48,O	10.0	1	3	3	11
12	48	12.00	P	66	79	48,O	10.0	1	3	3	11
13	48	6.00	P	0	8	48,O	12.5	1	4	4	12

Table 9.6 Continued

14	48	12.00	P	14	30	48,C	10.0	1	4	4	12
15	48	12.00	P	38	54.5	29,O; 19,C	10.0	1	4	4	12
16	48	12.00	P	68	78.5	48,O	10.0	1	4	4	12
17	48	6.00	P	0	8	48,O	10.0	1	5	5	13
18	36	12.00	P	20	31	36,C	10.0	1	5	5	13
19	48	12.00	P	41	54	48,C	10.0	1	5	5	13
20	48	12.00	P	65	78.5	48,O	10.0	1	5	5	13
21	77	0.50	B	0	24	13,O; 64,C	15.0	1	1	1	15
22	116	1.00	B	0	Z	Z	15.0	1	1	8	16
23	150	0.50	B	0	Z	Z	15.0	1	1	8	17
24	126	0.25	B	0	Z	Z	15.0	1	1	8	18
25	138	2.25	B	0	48	138,O	12.5	1	1	8	19
26	175	2.25	B	0	Z	Z	12.5	1	1	8	20
27	12	2.25	B	0	48	12,O	12.5	1	1	8	20
28	67	4.00	B	0	Z	Z	12.5	1	1	8	21
29	168	2.50	B	0	Z	Z	12.5	1	1	8	22
30	21	2.50	B	0	48	21,O	12.5	1	1	8	22
31	214	1.80	B	0	Z	Z	12.5	1	1	7	23

Table 9.6 Continued

32	16	1.80	B	0	48	16,O	12.5	1	1	8	23
33	93	0.80	B	0	Z	Z	15.0	1	2	2	24
34	48	12.00	P	18	31	48,C	10.0	1	3	3	25
35	48	12.00	P	42	54.5	48,O	10.0	1	3	3	25
36	48	12.00	P	66	79	48,O	10.0	1	3	3	25
37	48	6.00	P	0	8	48,O	12.5	1	4	4	26
38	48	12.00	P	14	30	48,C	10.0	1	4	4	26
39	48	12.00	P	38	54.5	48,O	10.0	1	4	4	26
40	48	12.00	P	68	78.5	48,O	10.0	1	4	4	26
41	48	6.00	P	0	8	48,O	12.5	1	5	5	27
42	36	12.00	P	20	31	48,C	10.0	1	5	5	27
43	48	12.00	P	41	54	48,C	10.0	1	5	5	27
44	48	12.00	P	65	78.5	48,O	10.0	1	5	5	27
45	125	0.50	B	0	Z	Z	12.5	1	1	8	28
46	13	0.50	B	0	48	13,O	12.5	1	1	8	28
47	14	0.50	B	0	24	14,O	12.5	1	1	8	28

[1] B = within the bulk coolstore; P = within pre-cooling units
[2] Z = remains within the zone throughout the simulation
[3] Format is: number of pallets , destination, O = outside; C = moved within coolstore; - = remains within the zone, Refer to Table 9.7 for destination zones.

Table 9.7

Destinations For Product Batches Moved Within The Coolstore

Batch Number	Destination Zones[1]			
	1-Zone Model	5-Zone Model	8-Zone Model	34-Zone Model
5	88/1	88/1	88/1	88/5
7	87/1	87/1	87/1	87/7
8	107/1	107/1	107/6	107/9
10	48/1(48)	48/1(48)	18/1(48); 30/8(48)	3/7(48); 4/22(48); 15/6(48); 26/21(48)
14	48/1(48)	48/1(48)	11/1(48); 32/8(48); 6/6(48)	24/19(48); 2/5(48); 8/20(48); 8/4(48); 6/9(48)
15	19/1	19/1	19/8	19/21
18	36/1	36/1	17/1; 19/8	12/1; 18/16; 5/2; 1/17
19	48/1	48/1	18/1; 30/8	7/1; 13/16; 4/2; 8/17; 7/3; 9/18
21	64/1	64/1	64/1	64/15
34	48/1	25/2; 23/1	16/8; 25/2; 7/1	2/21; 7/5; 14/20; 18/10; 7/24
38	48/1	48/1	2/6; 11/1; 35/8	11/6; 35/21; 1/9; 1/23
42	36/1	36/1	10/1; 26/8	9/17; 10/3; 17/18
43	48/1	48/1	5/1; 43/8	5/18; 5/6; 38/21

[1] Format used is: number of pallets / zone (exit time, hrs); e.g. 6/9(48) = 6 pallets enter zone 9 and leave the coolstore after 48 hours from the start of the simulation. Batches without an exit time remain within the zone to the end of the simulation.

Table 9.8

Product Half Cooling Times Used For Pre-Cooling And Bulk-Storage Sub-Batches

	$t_{1/2}$ (hours)					
Sub-Batch	1	2	3	4	5	6
Pre-cooler	2.1	3.0	4.5	6.4	9.0	12.8
Bulk-Storage	7.0	18.0	30.0	-	-	-

9.3.7 Heat Generator Data

Other than fans, which are discussed below, heat generators which were modelled were electric forklifts and lights. People load was assumed to be insignificant and was not modelled. An average load over the operating period (6:30 to 20:00 hr each day) was used for each heat generator assuming they were continuously operating. Table 9.9 lists the heat generators modelled and the zones they were resident in.

9.3.8 Door Data

Access to the coolstore was exclusively through two identical doors. Data describing the physical and operating characteristics of the doors are given in Table 9.13.

The door open and closed duration distribution data were determined from the data shown in Figure 7.6. Each door was permanently closed every night between 20:00 hrs and 6:30 hrs. Table 9.10 gives the zone each door opened into for each of the four models.

9.3.9 Evaporator And Fan Data

The industrial coolstore had four identical evaporator and fan units. Each was controlled independently using evaporator back pressure values (EBPV) based on either air-on (coolstore mode) or air-off temperature (pre-cool mode). Evaporators and fans were linked together in the model, with fans assumed to be located within the zone that air was drawn from from a heat load point of view.

Table 9.9

Characteristics Of Heat Generators Modelled

Heat Generator Number	Heat Generator Type	Sensible Heat Load (ϕHG_{sens}) (kW)	Latent Heat Load (ϕHG_{lat}) (kW)	Zone of Residence For Each Model Type			
				1-Zone	5-Zone	8-Zone	34-Zone
1	light	0.9	0	1	1	8	33
2	light	5.4	0	1	1	8	30
3	forklift	1.0	0	1	1	1	1
4	forklift	1.0	0	1	1	1	2
5	forklift	1.0	0	1	1	1	3
6	forklift	1.0	0	1	1	1	4
7	forklift	1.0	0	1	1	1	5
8	forklift	1.0	0	1	1	1	6
9	forklift	1.0	0	1	1	1	7
10	forklift	1.0	0	1	1	1	8
11	forklift	1.0	0	1	1	1	9
12	forklift	1.0	0	1	2	2	10
13	forklift	1.0	0	1	3	3	11
14	forklift	1.0	0	1	4	4	12
15	forklift	1.0	0	1	5	5	13
16	forklift	1.0	0	1	1	1	14
17	forklift	1.0	0	1	1	1	15

Table 9.10

Zones Linked To Each Door For Each Of The Four Models

Door Number	Zone Through Door			
	1-Zone Model	5-Zone Model	8-Zone Model	34-Zone Model
1	1	1	6	8
2	1	1	7	14

Air could only be drawn from the zone in which the fan was located, but could be discharged into any zone within the coolstore. Table 9.2 lists the zones air was drawn from and discharged into for each of the four models. Other data used for each evaporator are given in Table 9.13.

The fans used in the industrial coolstore were modelled with three speed settings (off, during defrosts; low speed in coolstore mode; high speed in pre-cool mode). Table 9.11 lists the air flow rate and sensible heat load for each mode. These were based on measurements of airflow through the evaporators when partly frosted and current drawn by the fan motors. The latent heat load (ϕ_{HGlat}) was zero for all fan speeds.

Fan speed changes were made during the simulations (Table 9.12) to match measured data including co-ordination with movement of pre-cooler product batches and defrosts. Defrosts occurred once per day for each evaporator for 30 minutes and the defrost time varied slightly from day to day. For programming simplicity the model only allowed defrosts to occur at the same time each day. Thus exact match of modelled defrost times was not achieved.

9.3.10 Ambient Data

Ambient data used in the model testing is given in Table 7.4.

Table 9.11

Fan Sensible Heat Load And Air Flow Rates For The 3 Speed Settings

Fan Speed	ϕ_{HGsens} (kW)	Air Flow, $m_{a,e}$ (kg/s)
1 (off)	0	0
2 (low speed)	13.2	27
3 (high speed)	30	45

Table 9.12

Fan Speed Changes Modelled During Each Simulation

Time (hrs)	Fan Number	Fan Speed	Time (hrs)	Fan Number	Fan Speed
0.0	1	2	38.0	4	0
0.0	2	2	38.5	1	2
0.0	3	3	38.5	3	3
0.0	4	3	38.5	4	2
8.0	4	2	39.0	2	0
8.0	3	2	39.5	2	2
14.0	1	0	41.0	4	3
14.0	3	0	42.0	2	3
14.0	4	0	54.0	3	2
14.5	1	2	54.5	4	2
14.5	3	3	54.5	2	2
14.5	4	2	62.0	1	0
15.0	2	0	62.0	3	0
15.5	2	2	62.0	4	0
18.0	2	3	62.5	1	2
20.0	4	3	62.5	3	2
30.0	3	2	62.5	4	2
31.0	2	2	63.0	2	0
31.0	4	2	63.5	2	2
38.0	1	0	66.0	4	3
38.0	3	0	68.0	3	3

Table 9.13

General Parameter Data

Zone Air Data		Product Data (apples)	
Air density (ρ_a)[1]	12.9 kg/m^3	Heat capacity (c_p)	3650 J/kg K
Total air pressure (P_t)	101300 Pa	Mass (M_p)	925 kg (per pallet)
Dry air heat capacity (c_a)	1010 J/kg K	Packaging mass (M_{dp})	50 kg (per pallet)
Latent heat of vapourisation (h_{fg})	2502 kJ/kg	Dry packaging heat capacity (c_{dp}) (Incropera & De Witt, 1985)	1200 J/kg K
Water heat capacity (c_w)	4180 J/kg K	Surface area (A_p)	90 m^2 (per pallet)
Water vapour heat capacity (c_v)	1870 J/kg K	Mass transfer coefficient (k_p) (Gaffney *et al.*, 1985a)	0.514×10^{-9} kg/m^2 s kPa
Surface Data		Cardboard moisture uptake coefficients:	
Thermal conductivity (k_s)	0.03 W/m K	β_1	-0.1999
Wall thickness (x_s)	50 mm	β_2	0.219
Ceiling Thickness (x_s)	65 mm	β_3	0.00979
Inside heat transfer coefficient ($h_{in,s}$)	10 W/m^2 K	Rate of moisture absorption/desorption (k_{mc}):	
Outside heat transfer coefficient ($h_{o,s}$)	10 W/m^2 K	Pre-cooling	7.83×10^{-5} 1/s
Evaporation factor (Ef)	1.0	Bulk-stacked 1	7.83×10^{-5} 1/s
Emmissivity (ε)	0.1	Bulk-Stacked 2	9.36×10^{-5} 1/s
Initial condensed water mass ($M_{w,s}$)	0	Bulk-stacked 3	1.3×10^{-4} 1/s
Floor Data		Respiration rate (rr) (Gaffney *et al.*, 1985a)	$4.59\times10^{6}(T_p+17.8)^{2.66}$ W/kg
Floor slab heat capacity (c_f)	880 J/kg K	Door Data	
Concrete thermal conductivity ($k_{concrete}$),(Incropera & De Witt 1985)	1.6 W/m K	Height (h_d)	3.6 m
Concrete slab thickness ($x_{concrete}$)	150 mm	Surface area (A_d)	10 m^2
Insulation thickness ($x_{insulation}$)	0 mm	Tamm's equation correction factor (CF)	1.0
Soil (gravel) thermal conductivity (k_{soil}) (Incropera & De Witt 1985)	3 W/m K	Mean door open time (λ_{open})	1054 s
Soil thickness (x_{soil})	0.5 m	Mean door closed time (λ_{closed})	2500 s
Initial temperature (T_f)	1.8 °C	Evaporator/Fan Data	
Inside heat transfer coefficient ($h_{in,f}$)	2 W/m^2 K	Evaporator surface area (A_e)	2220 m^2
Initial condensed water mass ($M_{w,f}$)	0	Overall Heat transfer coefficient (U_e)	17 W/m K
Inert Materials Data		Set point (Sp)	0°C Coolstore mode -1°C Pre-cool mode
Heat capacity (c_{irt}) (Incropera & De Witt, 1985)	465 J/kg K	Proportional response factor (Prf)	1.5
Initial condensed water mass ($M_{w,irt}$)	0	Integral response factor (Irf)	500
Heat transfer coefficient (h_{irt})	10 W/m^2 K		
Evaporation factor (Ef)	1.0		

[1]Air density arbitrarily increased by a factor of 10 as discussed in Section 9.3.1

9.4 COMPARISON OF PREDICTED AND MEASURED DATA

9.4.1 Air Conditions

9.4.1.1 1-Zone Model

Figures 9.4, 9.5 and 9.6 show predicted and measured air temperature, RH and absolute humidity respectively for a number of positions (Figure 7.2) within the bulk-storage area of the coolstore for the single zone model. The predicted air temperature was consistently lower than the measured values within pre-coolers and higher on average than values measured amongst bulk-stacked product. The predicted RH was lower than measured around the top pallets in the bulk store and higher than that measured around the bottom pallets. No measurements of RH within the pre-coolers were possible during the test data collection period. However, Figure 4.6b shows pre-cooler RH measured in earlier trials. The predicted air RH for the simulation period was higher than these measurements. Predicted absolute humidity was close to the measured values indicating that the overall model water vapour mass balance for the coolstore air was accurate even though the temperature and RH prediction displayed greater differences. Sensitivity analysis using the model showed that RH was significantly influenced by cardboard moisture absorption. Predicted RH followed a diurnal pattern with an amplitude of about 10% RH if moisture absorption was ignored (Figure 9.5). The cardboard acted as a moisture buffer preventing large fluctuations in RH.

Using a single zone model was not accurate for showing more than the broadest trends as the pre-coolers and doors which represent large heat and/or water vapour loads must be in the same zone as the bulk-storage areas. Therefore the average predictions were inaccurate for each of pre-cooling, bulk-storage, areas close to doors, and areas with warm fruit present. Also, the variation in conditions with height in the store could be predicted. It is worthwhile to note that the single zone model, without moisture absorption can be regarded as state of the art amongst published simulation models (apart from full hydrodynamic models) that preceded this study.

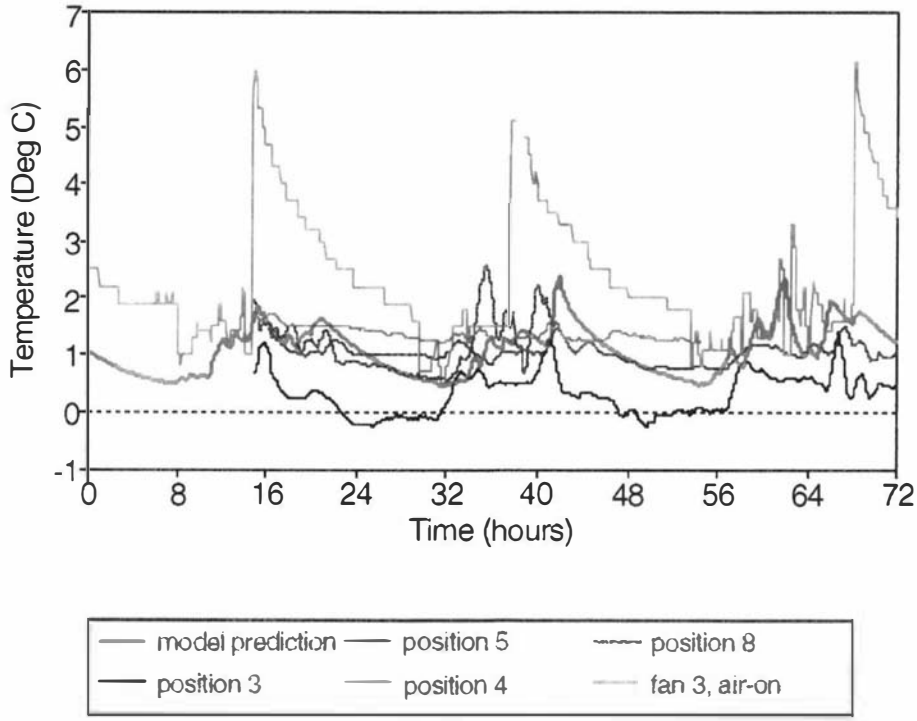

Figure 9.4: Comparison of predicted and measured air temperatures within the industrial coolstore for the 1-zone model (positions within the coolstore are given in Figure 7.2).

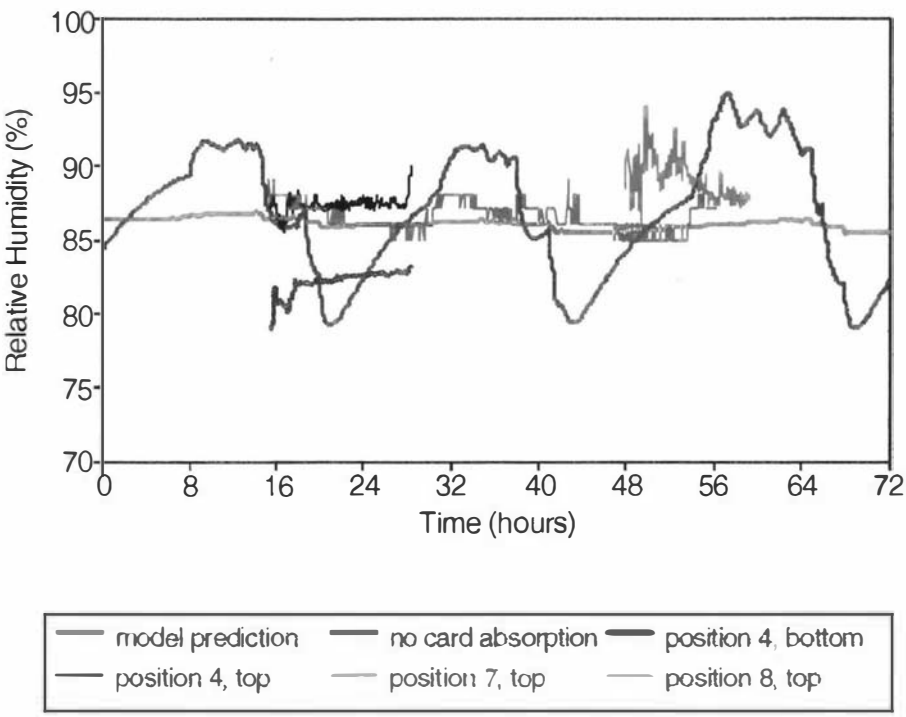

Figure 9.5: Comparison of predicted and measured air RH within the industrial coolstore for the 1-zone model (positions within the coolstore are given in Figure 7.2).

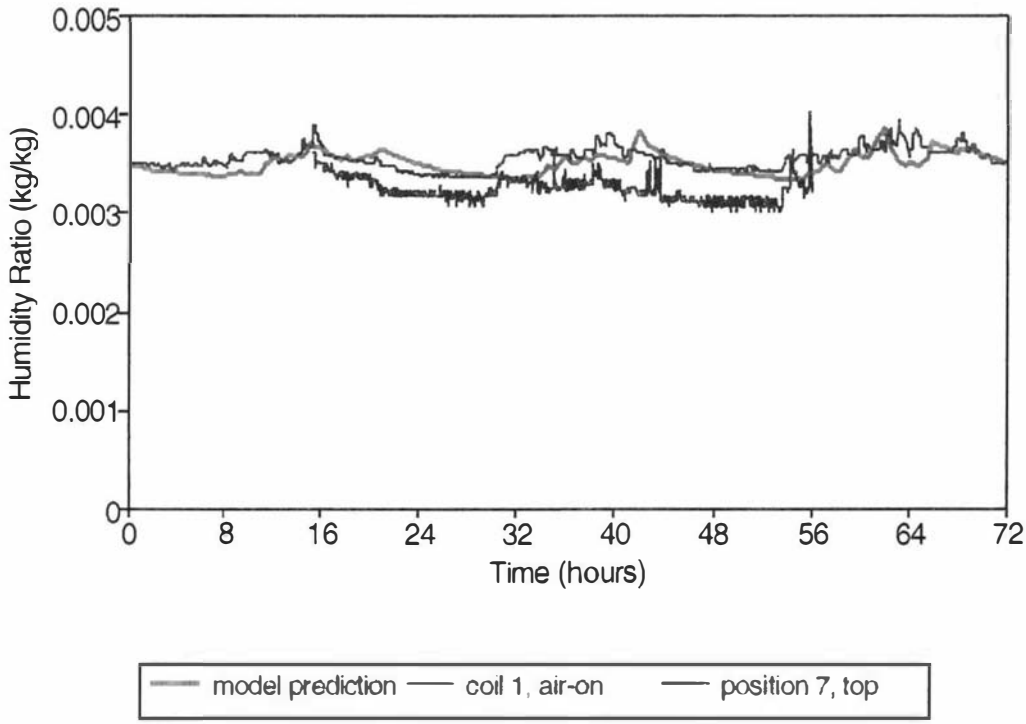

Figure 9.6: Comparison of predicted and measured air absolute humidity within the industrial coolstore for the 1-zone model (positions within the coolstore are given in Figure 7.2).

9.4.1.2 5-Zone Model

Figures 9.7, 9.8 and 9.9 show predicted and measured air temperature, RH and absolute humidity respectively for a number of positions (Figure 7.2) within the bulk-storage area of the coolstore for the 5-zone model. There is good agreement between measured and predicted temperature for positions within the coolstore where the fruit was already down to storage temperature (e.g. positions 1 and 2), but for positions where the fruit temperature was above the storage temperature (e.g. position 4) the predicted air temperatures were consistently lower than measured. The predicted rise in air temperature to about 2.0°C at 40 and 64 hours (Figure 9.7) was higher than measured. These periods coincide with peak door activity in the coolstore. With the single bulk-storage zone any door heat load is effectively transferred throughout the coolstore immediately. This suggests that using separate zones around doors (8-zone model) may improve predictions as air in the bulk-storage area would be buffered from the door load. As for the 1-zone model use of a single bulk coolstore zone did not allow predictions of vertical differences, which were found to be significant (Chapter 7).

Better agreement between predicted and measured absolute humidity in the bulk- storage areas than the 1-zone model was achieved (Figure 9.8). Predicted RH was slightly higher than the measured values and higher than the 1-zone model prediction (Figure 9.9). The higher RH prediction mainly reflects the lower predicted air temperature with the 5-zone model due to the sensible load of the pre-coolers not directly entering the bulk-storage zone, rather than changes in predicted absolute humidity.

Figure 9.10 gives predicted and measured air-on and air-off temperature as well as the fan mode (mode 3 = high speed, mode 2 = low speed) for the evaporator coil in zone 4, a pre-cooling zone (Figure 9.1 b). The other pre-cooling zones gave similar results. There is good agreement between measured and predicted data. Predicted air-off temperature does not fluctuate to the same extent as the measured, perhaps indicating the evaporator control used in the model performed better than the actual controller.

It can therefore be concluded that separation of the pre-cooling and bulk-storage areas of the coolstore in the 5-zone model led to significant improvement in the predictions of the air conditions compared with the 1-zone model.

9.4.1.3 8-Zone Model

Figures 9.11 and 9.12 show comparison of measured and predicted air temperature and RH within the bulk-storage area for the 8-zone model. Figure 9.13 shows the comparison of measured and predicted air temperature for a zone close to the two doors for the 34-zone model (zone 23, Figure 9.1 d). Predictions for door zones for the 8-zone model were similar to those for the 34-zone model, so only the latter have been presented.

Predictions for the pre-cooler zones for the 8-zone model were similar to those for the 5-zone model, so they are not presented.

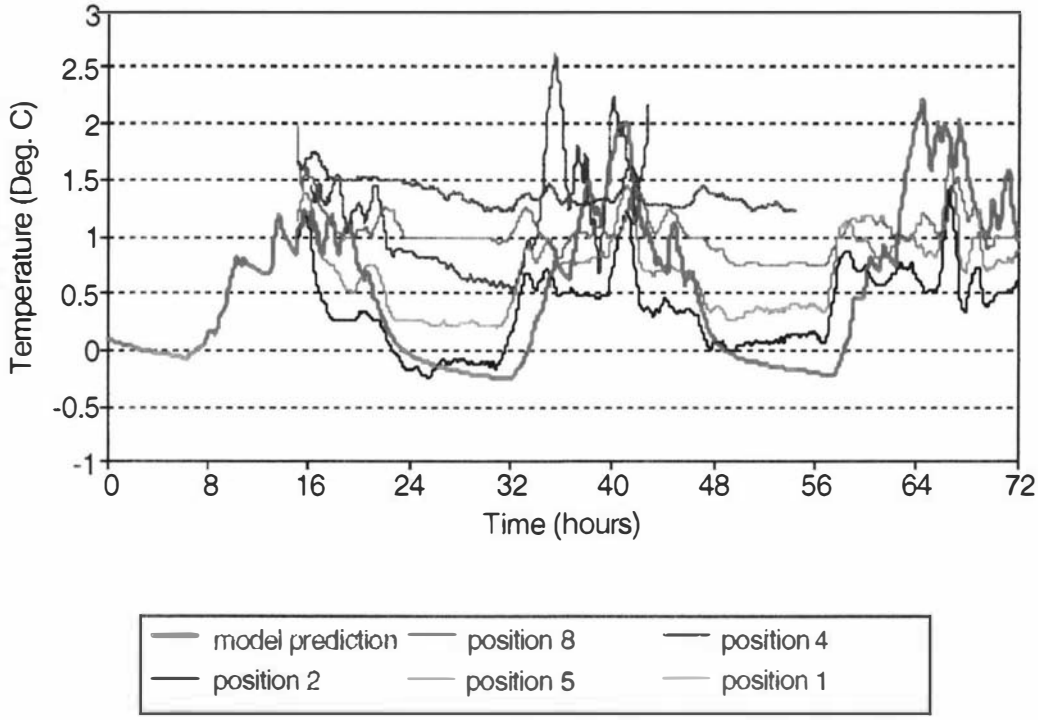

Figure 9.7: Comparison of predicted (zone 1) and measured air temperature within the bulk-storage area of the industrial coolstore for the 5-zone model (positions within the coolstore are given in Figure 7.2).

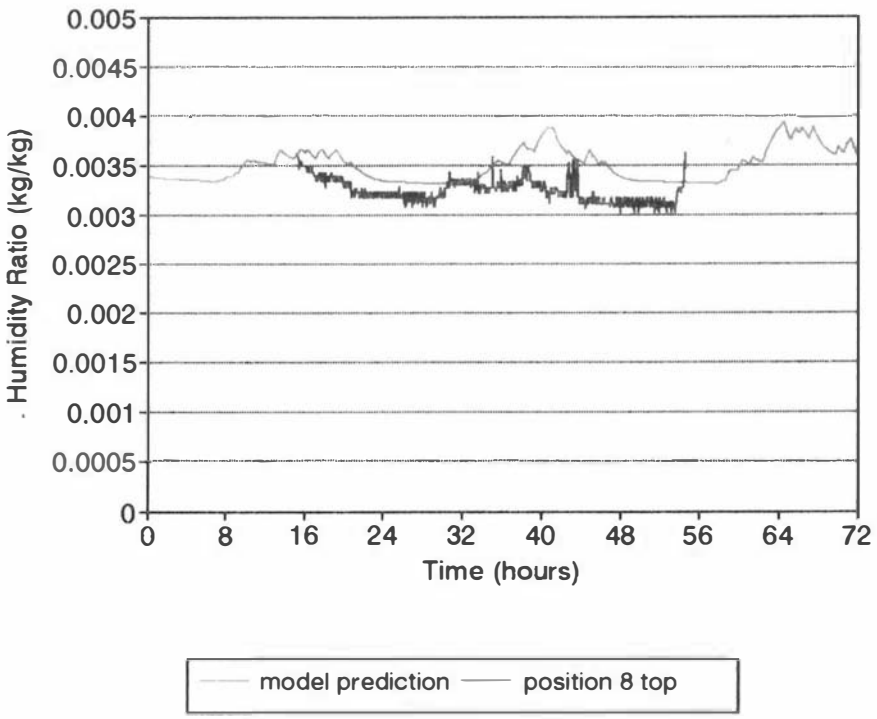

Figure 9.8: Comparison of predicted (zone 1) and measured air absolute humidity within the bulk-storage area of the industrial coolstore for the 5-zone model (positions within the coolstore are given in Figure 7.2).

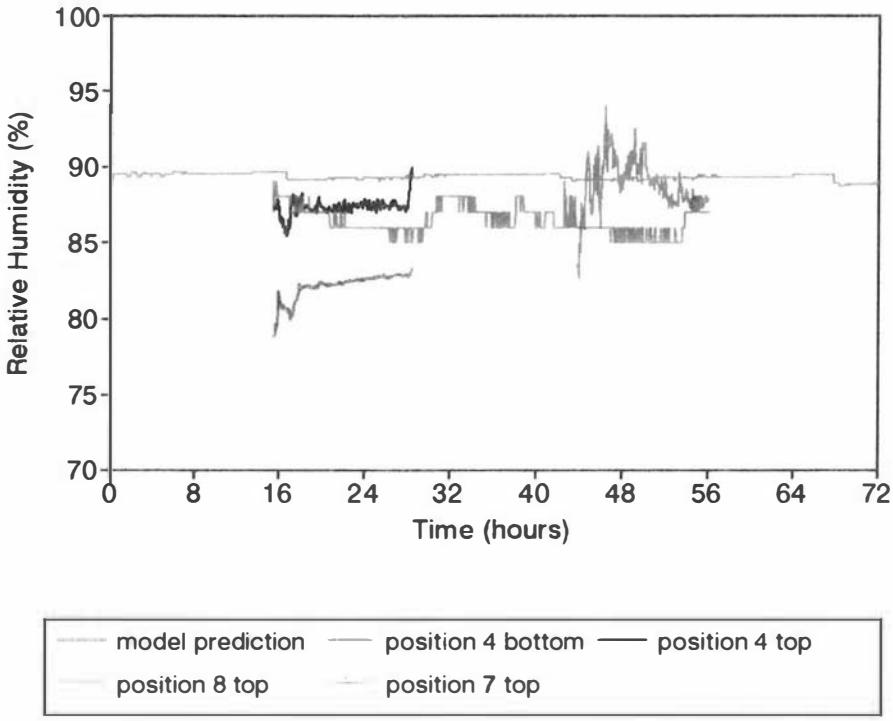

Figure 9.9: Comparison of predicted (zone 1) and measured air RH within the bulk-storage area of the industrial coolstore for the 5-zone model (positions within the coolstore are given in Figure 7.2).

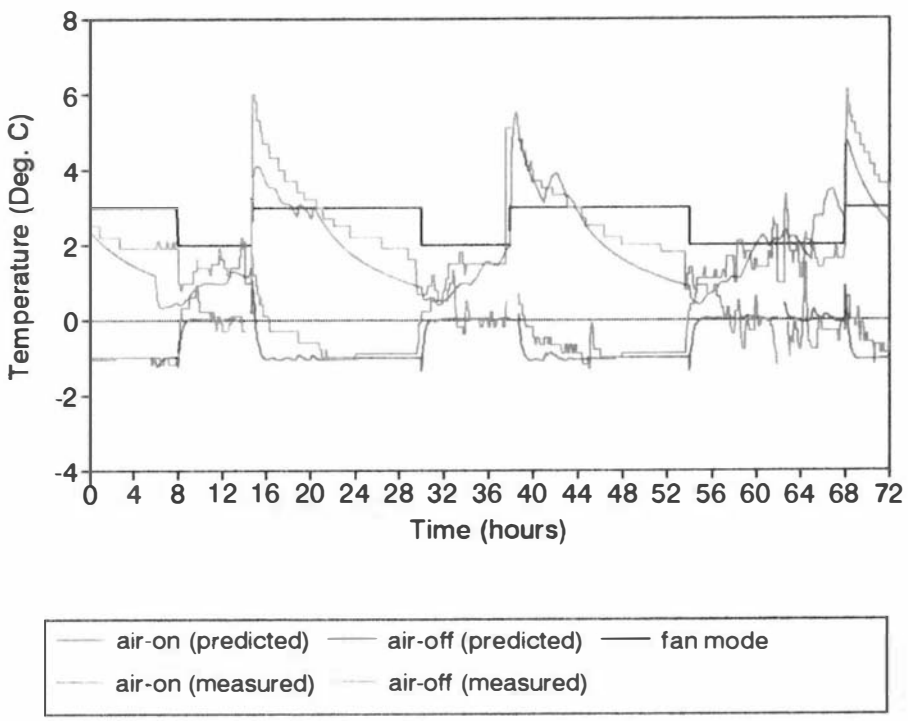

Figure 9.10: Comparison of predicted and measured air-on and air-off temperature for the evaporator located in zone 4 (a pre-cooler) of the industrial coolstore (Figure 9.1 b) for the 5-zone model.

The predicted bulk-storage area air temperatures followed similar trends to the measured data and have a consistent 0.5°C to 1.0°C difference between the top and bottom zone. This compares favourably to the mean measured difference of 0.5°C between the top and bottom pallets obtained from the coolstore surveys (Chapter 7). However, the predicted temperatures were both consistently lower than the measured and lower than the 5-zone model. Other than model shortcomings, which would be shared with the 5-zone model in any case, the most likely explaination is that the extra data required in moving from 5 to 8 zones were not sufficiently accurate. Possibilities include the airflow rates between zones used by the model, particularly between door zones and the bulk-storage zones, being lower, or less well defined than in the actual coolstore. Greater mixing between the door zones and the bulk-storage zone would reduce the bulk-storage temperature offset, but may make door zone prediction worse. Nevertheless, Figure 9.13 shows that predicted door zone air temperatures showed good agreement with measured data. Some of the measured temperature peaks were not matched exactly, because the model calculates door open and closed duration using a random approximation to the measured distribution. This means that on average the total door open duration should be equalled, but over any time period exact matches in opening and closing times would not occur. Door zone predictions would be affected if the flowrates between door zones and surrounding zones were wrong. From the limited data available it was not possible to establish whether the offset was due to difficiencies in the models of air flow, or just use of inappropriate air flow pathway data, or a mixture of both causes.

Predicted RH for the bulk-storage area agreed well with measured RH. A 3 to 5% difference between the top and bottom zones was predicted, which is consistent with that measured in the coolstore surveys (Chapter 7).

In summary, the 8-zone model allowed the vertical gradients in air conditions in the bulk-storage area and the localised effect of doors to be predicted, but introduced considerably greater data requirements and uncertainty related to the modelling of air flow within the coolstore.

9.4.1.4 34-Zone Model

Similar predictions to those obtained with the 8-zone model were obtained with the 34-zone model. Figure 9.14 compares the measured and predicted air temperature at position 1 (Figure 7.2 d) in the bulk coolstore. As for the 8-zone model, the correct daily trend was predicted but the model predictions were consistently lower than the measured values. The move from the 8-zone to the 34-zone more than trebled the data requirements especially with respect to defining the air flow pathways between zones. It was difficult to judge whether the data used matched actual air flows as the only evidence was indirect (e.g. comparison of product and zone air temperatures and humidity).

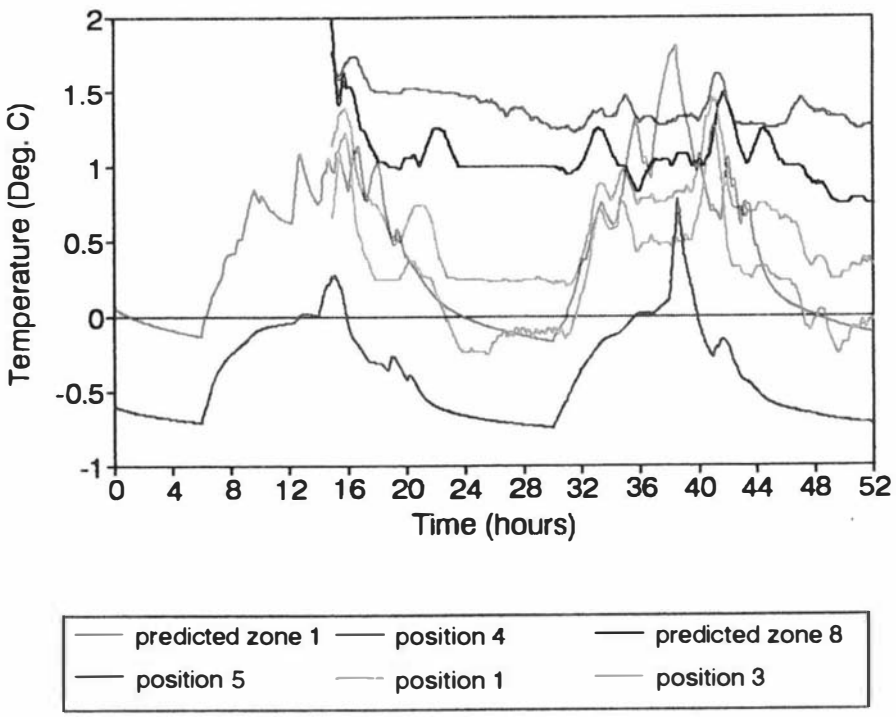

Figure 9.11: Comparison of predicted and measured air temperature for the bulk-storage area (zone 1 & 8, Figure 9.1 c) for the 8-zone model (positions within the coolstore are given in Figure 7.2).

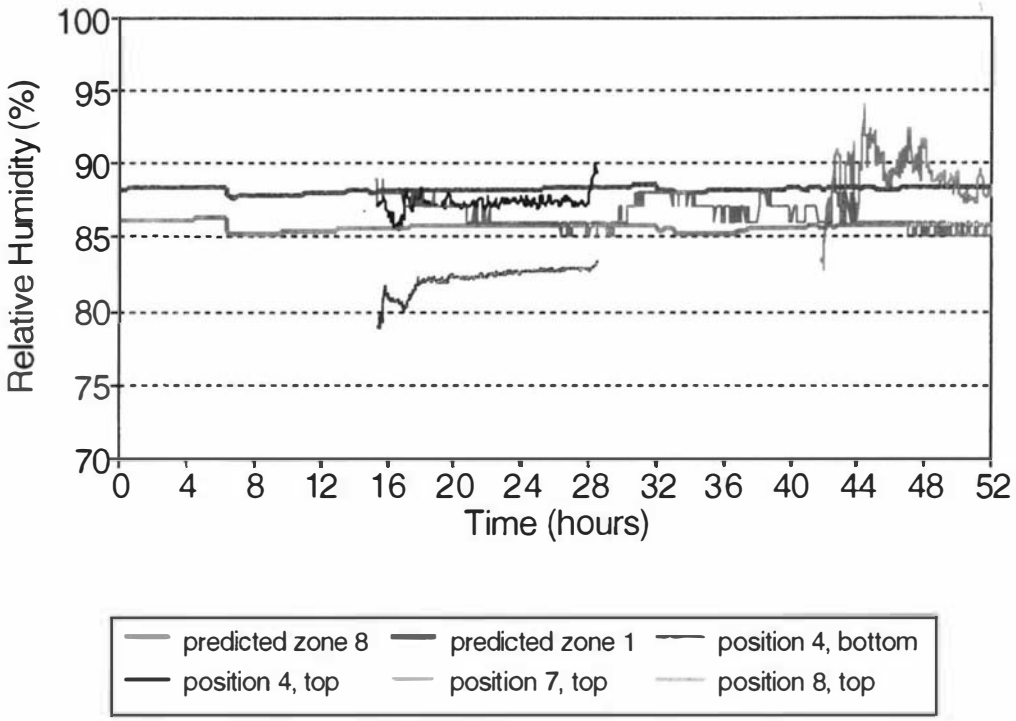

Figure 9.12: Comparison of predicted and measured air RH for the bulk-storage area (zone 1 & 8, Figure 9.1 c) for the 8-zone model (positions within the coolstore are given in Figure 7.2).

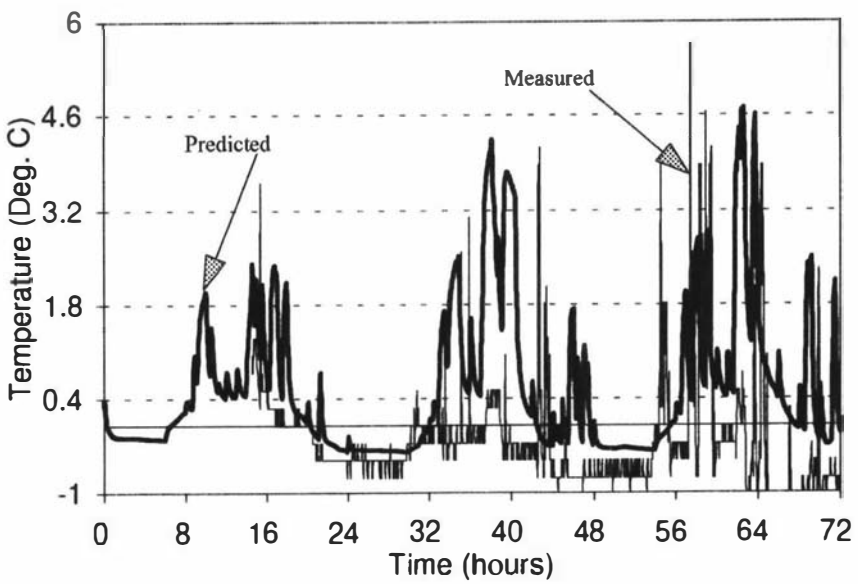

Figure 9.13: Comparison of predicted and measured air temperature for a door zone (zone 23, Figure 9.1 d) for the 34-zone model.

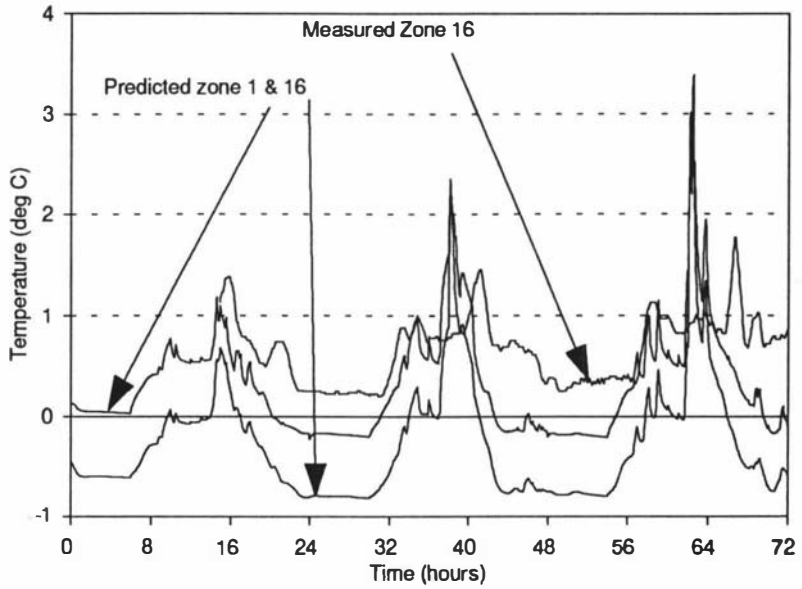

Figure 9.14: Comparison of predicted and measured air temperature for position 1 (Figure 7.2) for the 34-zone model.

9.4.2 Apple Temperature and Water Loss

Figure 9.15 shows predicted and measured apple temperatures for apples cooling within the bulk-storage area using the 5-zone model. The predictions for the 3 sub-batches gave similar cooling rates to that measured and the predicted product temperatures are similar, or slightly lower than measured (as was predicted air temperature). Figure 9.16 shows predicted and measured apple temperatures for apples in the bulk-storage area already at storage temperature using the 5-zone model. The predicted apple temperatures fluctuate more than the measured, but as the resolution of the dataloggers used was ±0.25°C a definite conclusion about model accuracy was difficult to reach. Figure 9.17 shows predicted fruit temperatures for each of the six sub-batches within a pre-cooler. No fruit temperatures were measured during the test period, so the predicted values cannot be directly compared with measured data. However, these predictions were similar to pre-cooling rates measured at other times (Chapter 4). Apple temperature predictions for other models showed similar trends. Differences in apple temperature with vertical position were predicted with the 8- and 34-zone models, associated with the difference in air temperature. For each of these, apple temperatures followed the air temperature in a similar fashion to that shown in Figure 9.15.

Table 9.14 gives results for predicted weight loss for apples being pre-cooled. Measured weight loss within the pre-coolers during 1990 averaged 0.114% with a range of 0.027% to 0.201%. Predicted values were in good agreement with these values, especially given the difficulty in measuring weight loss during pre-coolers, as outlined in Chapter 4.

Table 9.15 shows weight loss data both for apples which were cooled in the bulk storage area and for apples stored within the bulk storage area already at storage temperature. Measured rates of weight loss for fruit at storage temperature in the bulk storage area of the industrial cool store ranged from 0.015 %/day to 0.026 %/day, whilst those for fruit cooling in the bulk storage area averaged 0.03 %/day. All models predicted differences in weight loss for the three sub-batches for each product batch. The 8- and 34-zone models predicted significant differences in weight loss for different positions within the coolstore, (close to the floor, the doors, or the ceiling). The model predicted that the weight loss close to the floor was 18% higher than in ceiling zones. The predicted weight loss for apples cooling or stored within the bulk-storage area were higher than those measured by about 30%. The over prediction may be due to incorrect parameter values being used in the model, shortcomings in the model formulation, or a combination of both. The mass transfer coefficient used in the model may have been too high, as it was based on data for a range of apple cultivars which may not have been appropriate for the varieties in the coolstore during the simulation period. The product model describes mass transfer by relating the fruit in the cartons to the bulk air temperature and RH in the zone. This is likely to be lower than the localised temperature and RH in the carton due to the incomplete air mixing. This weakness in the product model cannot be overcome without making the model significantly more complex. Improvement of the product weight loss model could not be justified until data allowing a more detailed investigation of the reasons for lack of fit are available. Any uncertainty arising from the weight loss model does not appear to have significantly influenced overall heat and mass transfer balances for the coolstore.

Overall, the main advances in the product model used over previous models was separate consideration of heat and mass transfer and the use of sub-batches to simulate variation in cooling rates within the product stack. These allow prediction of relative

weight loss and differentiation of the prediction of product response. However, the measured data were sparse, so that the accuracy of the more sophisicated prediction and hence its value relative to the increase in model complexity could not be fully assessed.

Table 9.14

Predicted Apple Weight Loss Within A Pre-Cooler Using The 8-Zone Model

Cooling Rate ($t_{1/2}$, hrs)	2.1	3.0	4.5	6.4	9.0	12.8
Weight Loss (% over 10 hrs)	0.067	0.072	0.080	0.091	0.107	0.132

Table 9.15

Predicted Apple Weight Loss Within The Bulk-Storage Area Of The Industrial Coolstore Using The 8-Zone Model

Cooling Rate ($t_{1/2}$, hrs)	7	18	30
Weight loss for apples cooled within the bulk-storage area (%/day)	0.0410	0.0491	0.0543
Weight loss for apples stored near the floor (%/day)	0.0360	0.0364	0.0371
Weight loss for apples stored near the ceiling (%/day)	0.0291	0.0298	0.0309
Weight loss for apples stored near the doors (%/day)	0.0308	0.0313	0.0321

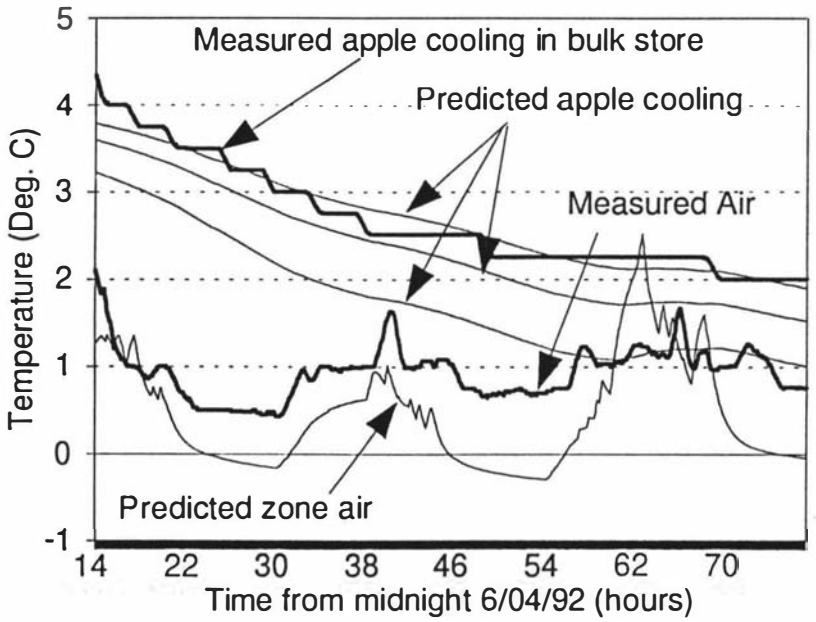

Figure 9.15: Comparison of predicted and measured apple temperature for apples cooling in the bulk coolstore using the 5-zone model.

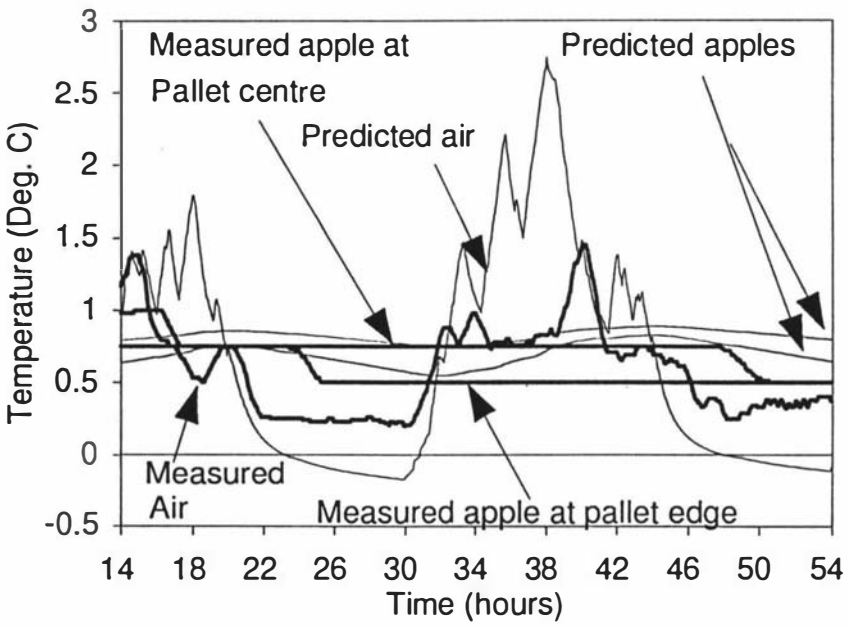

Figure 9.16: Comparison of predicted and measured apple temperature for apples at storage temperature in the bulk coolstore using the 5-zone model.

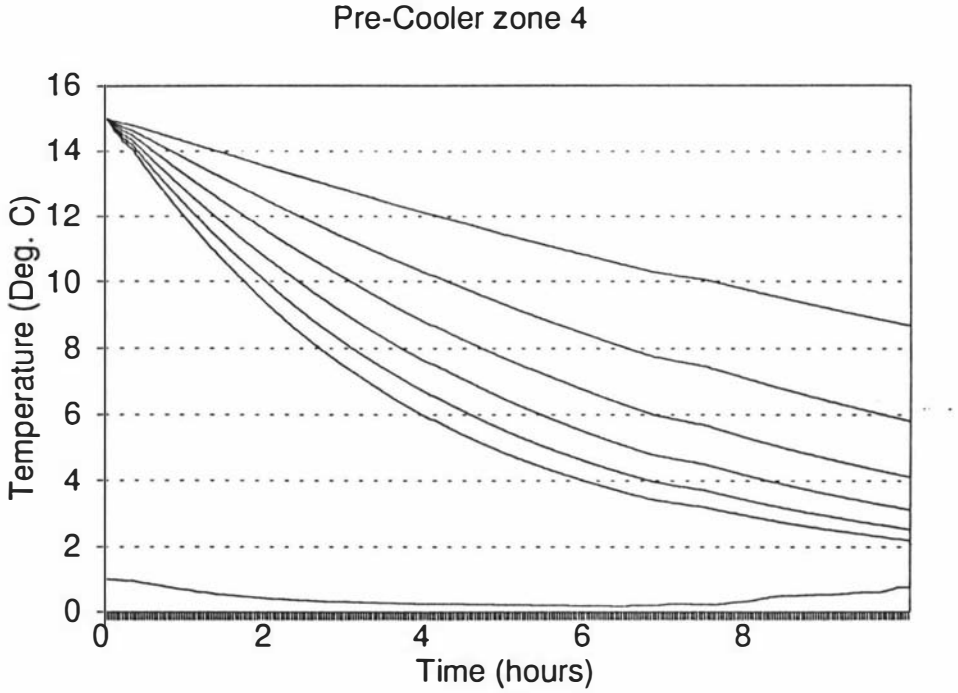

Figure 9.17: Predicted apple temperature for apples pre-cooled using the 5-zone model.

9.4.3 Other Predictions

9.4.3.1 Wall Temperatures

Figure 9.18 shows both measured and predicted outside surface temperatures for positions 1 and 3 (Figure 7.1) for the 5-zone model (other models gave nearly identical results). Good agreement is shown between measured and predicted temperature for position 3 which is a side wall. Predictions for position 1 (on the roof) do not agree as well with the measured data. This is possibly due to radiation effects not being modelled exactly. The model ignored radiation at night, which may explain the lack of fit during the night period. The deviation during the day suggests that the amount of solar radiation absorbed by the roof has been under estimated, possibly due to an underestimation of the roof emissivity. This deviation is not expected to have a significant effect on overall heat load as the heat load through surfaces is one of the smaller loads on the store. The results suggests that the current model does represent a significant improvement on previous models which totally ignored radiation.

No data were available for inside wall temperatures, so detailed assessment of the validity of lumping the thermal mass at the inside of the surfaces could not be performed.

9.4.3.2 Floor Temperatures

Figure 9.19 shows measured and predicted floor temperature for the bulk-storage zone of the 5-zone model. The predicted floor surface temperature was higher on average and fluctuated less than the measured data. This could be caused by inappropriate parameter data (e.g. heat transfer coefficient or soil and concrete thermal conductivity data), or by deficiences in the floor model, such as lumping of all the thermal mass at the surface. Also, the measured data had significant uncertainty. Soil thermal conductivity is highly dependent on the soil composition and moisture content, both of which could not be measured. The inside heat transfer coefficient ($h_{in,f}$) is dependent on air velocity over the surface, and would be affected by the presence of pallets in some areas. The results do suggest that the total heat load through the floor was probably accurately predicted, even if the floor temperature itself was slightly offset.

9.4.3.3 Packaging Moisture Absorption

Figure's 9.20 and 9.21 show predicted cardboard moisture content and air RH for a pallet within a pre-cooling zone and cooling within the bulk-storage area of the coolstore respectively, using the 5-zone model. No packaging moisture data were measured during the measurement period. At different times cardboard moisture contents in excess of 18% have been measured in the same coolstore (McLeod, 1992).

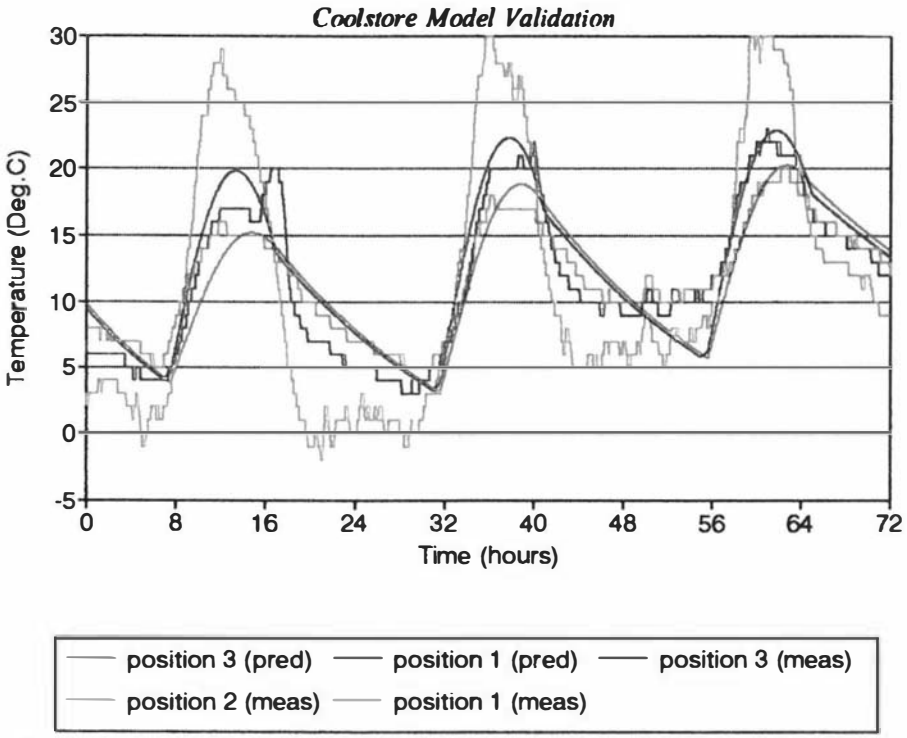

Figure 9.18: Comparison of predicted and measured outside wall temperatures for positions 1 & 3 (Figure 7.1) using the 5-zone model.

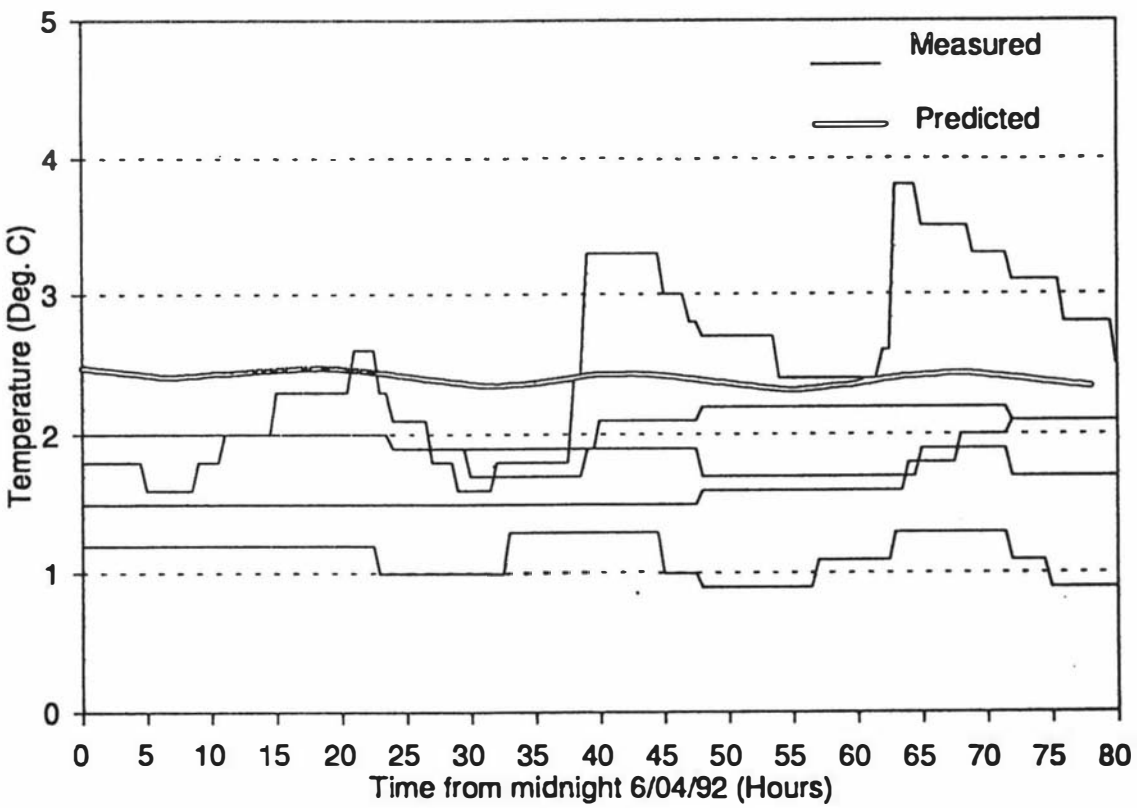

Figure 9.19: Comparison of predicted and measured floor surface temperatures using the 5-zone model.

Cardboard moisture absorption was shown to be highly influential on the coolstore water balance, by buffering the air against rapid fluctuations in moisture content. In terms of the overall coolstore water balance, the cardboard contains more than 100 times more water than is held in the air. For example, for the coolstore with an average air absolute humidity of 0.0035 kg/kg, and a air mass of 47,500 kg, the air would contain 166 l of water. If the store was full of pallets (3770 pallets) each with a cardboard moisture content of 20% then the cardboard would contain 41,422 l of water. Hence small changes in cardboard moisture content has a large effect on the overall moisture content of the air.

The predicted overall absolute humidity and RH levels were close to that measured (Section 9.3.1), which suggests that the model used for cardboard moisture absorption was accurate. However estimation of some of the input data was difficult, and this may require further study in the future. Linking the cardboard to bulk-air RH and ignoring the potential for localised RH within cartons does not appear to have introduced any significant errors.

Overall, inclusion of moisture absorption in packaging was considered an important advance on previous models.

9.4.3.4 Condensation

The data available did not allow assessment of the surface, floor or inert condensation submodels. There was no evidence of condensation observed during the data collection period, and none of the models predicted that condensation would occur. This suggests that for the coolstore modelled condensation could have been ignored without affecting accuracy. However, condensation may occur, in coolstore applications using waxed packaging, where packaging moisture absorption is not possible, and in some cold store applications where more extreme localised RH conditions can exist near doors. Therefore retention of this model feature is recommended until such systems can be studied.

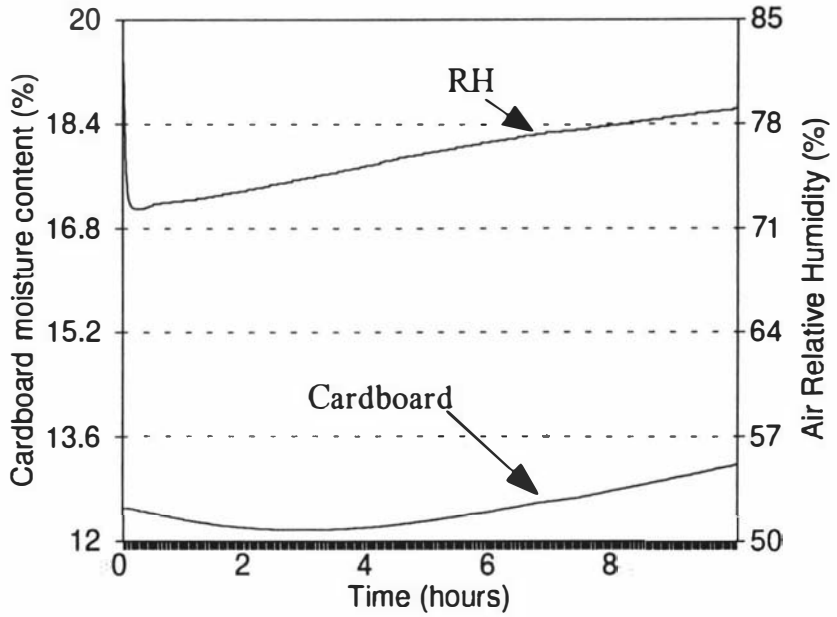

Figure 9.20: Predicted cardboard moisture content in a pre-cooler using the 5-zone model.

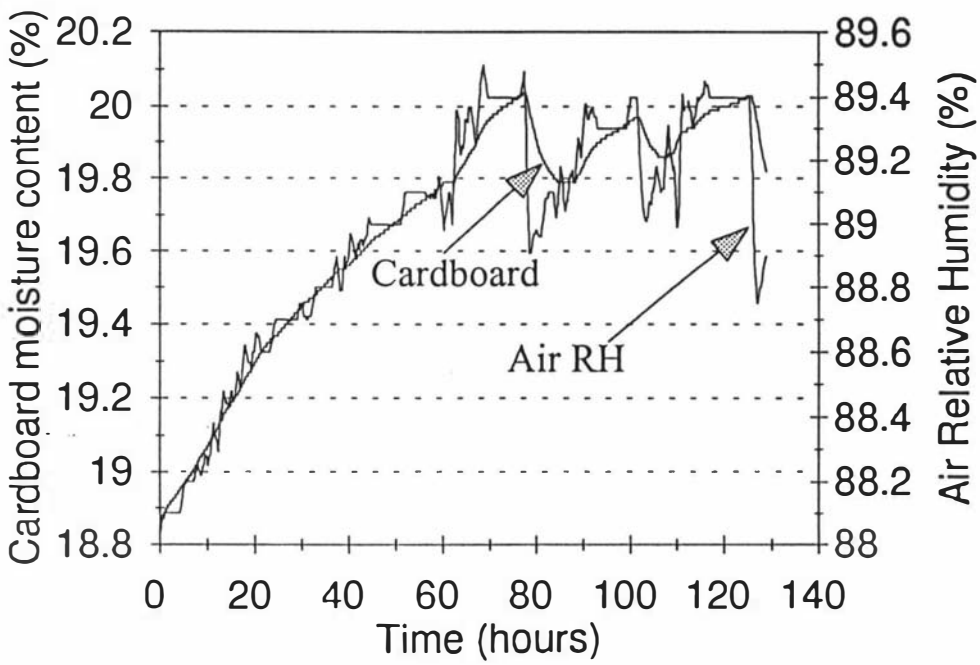

Figure 9.21: Predicted cardboard moisture content for a pallet cooling in the bulk-storage area of the industrial coolstore using the 5-zone model.

9.4.4 Comparison of Models

Figures 9.22 and 9.23 compare predicted air temperature data from all four models for one position, with measured data. It is clear that the 1-zone model provides an average value for coolstore activities, but does not provide any ability to model positional variability within the coolstore. Separate pre-cooling and bulk-storage zones were critical to accurately predict conditions when both processes are occurring. Predictions for the 5-zone model tended to fluctuate more than the measured data, which suggested that the bulk-storage area was not sufficiently buffered from the door heat load. The 8-zone and 34-zone models overcame this problem using separate door zones and allowed the vertical temperature gradient to be accurately approximated, but the bulk-storage zones showed a systematic offset from the measured data. The systematic offset could be due to data uncertainty (such as interzone air flow pathways), model inadequacies, or both. It was considered likely that the data uncertainty, particularly due to air flow (e.g. data used meant that some of the door load by-passed the bulk-storage areas entirely), was a major contibutor to the offset. It was possible that the bulk-storage zones were too isolated from the door zones in both the 8 and 34-zone models, due to the choice of air flow pathway data made.

Increasing the number of zones from 8 to 34 had little beneficial effect on the ability to predict variation in conditions with respect to position, yet greatly increased the data requirements particularly with respect to interzone air flow rates. The 8-zone model allowed most of the major sources of variation to be modelled. It was noted that during data definition for the 8-zone model the uncertainty associated with defining air flowrate data was significant, and this difficulty worsened for the 34-zone model. Therefore it would be difficult to justify a model with greater positional subdivision than 8-zones for the coolstore studied until the air flow pattern can be more closely defined.

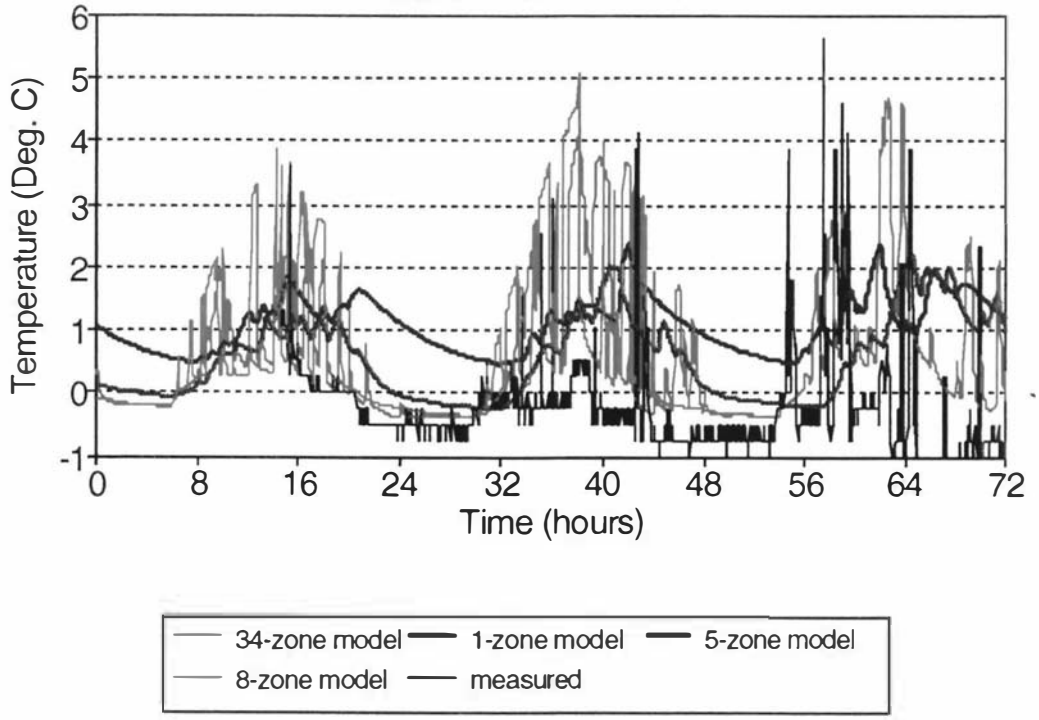

Figure 9.22 Comparison of measured data for a door zone and predicted data from each of the 1-zone, 5-zone, 8-zone, and 34-zone models.

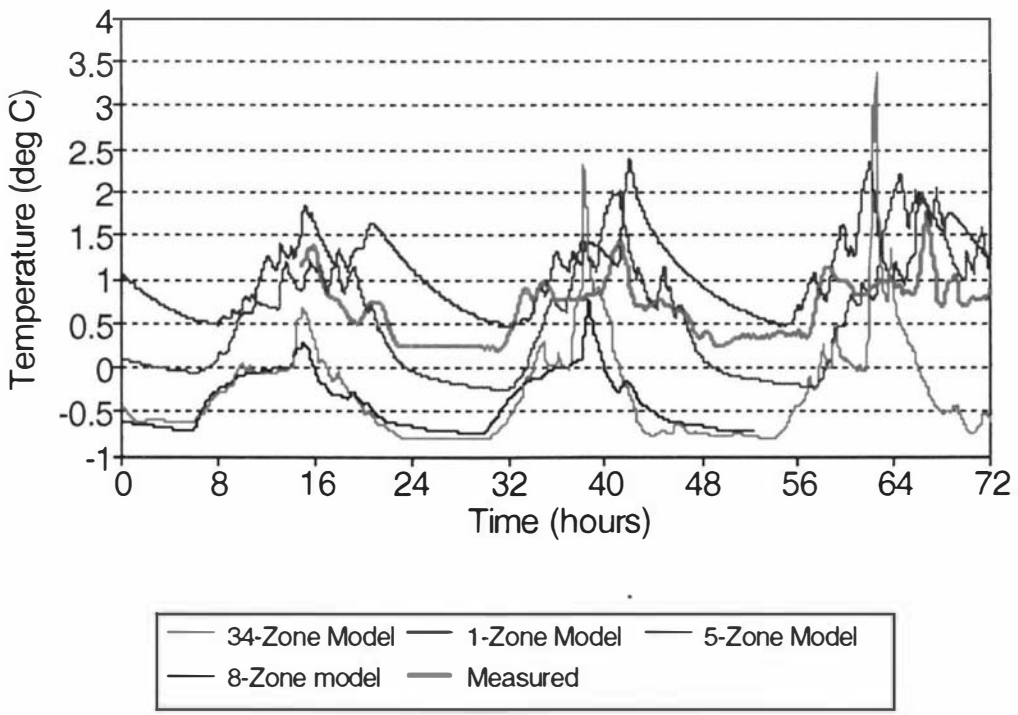

Figure 9.23 Comparison of measured data for a bulk-storage zone (position 1, figure 7.2) and predicted data from each of the 1-zone, 5-zone, 8-zone, and 34-zone models.

9.5 DISCUSSION AND CONCLUSION

Determining the appropriate complexity of component models for refrigerated facilities is difficult, given the major interactions between the various components of the system. The temperature and humidity within the industrial coolstore were accurately predicted on average by all models, suggesting no major deficiencies in heat and mass transfer component models. Detailed testing of all the individual component models, or individual features of each component was not possible, because of lack of detailed data.

A major benefit of the present model over previously published models is the ability to predict positional variability using multi-zoning. Using multiple zones, the model allowed prediction for separate pre-cooling zones, door zones, and prediction of positional variation in conditions which were identified as being important in Chapter 7. However, the level of multi-zoning used became limited by data uncertainty, particularly related to air flow pathway data. For the system studied, the 5-zone or 8-zone models represent the best compromise between accuracy and complexity.

Modelling air flow within the store based on a user defined air pathway allowed air flow to be split between zones, and allowed new air flows to be calculated when fan speeds are changed in relation to pre-cooling or bulk-storage modes. Modelling air flow in this manner is less complex than using full hydrodynamic analysis. Nevertheless, it must be noted that determining appropriate air flow pathway data, particularly for large numbers of zones, is difficult. It is still unclear whether the perceived problems with interzone air flow are due to data uncertainty or shortcomings in the models used.

Another benefit of the model was that it allowed more accurate prediction of air humidity and product weight loss, than previous models. However, direct interaction of product subbatches and the zone air may not be the most appropriate, as potentially important localised effects of temperature and humidity within product stacks cannot be predicted. Until a more detailed analysis of this effect can be performed increasing the complexity of the model could not be justified.

Modelling moisture absorption by packaging was shown to be important for this application. The packaging was shown to hold more than 100 times as much water as was present in the vapour in the coolstore air. Hence the packaging buffered the air from large fluctuations in RH. This feature also allows the effect of other coolstore design and operational features on air RH, package moisture change and hence packaging strength to be predicted.

The ability to move product batches within the store, and to split product batches into several sub-batches, each going to different zones enabled operational practice to be more closely matched. For example, product entering the store to be pre-cooled and then being moved to the bulk-storage area could be modelled.

Condensation was not predicted to occur on any surface, floor, or inert material. This suggests that simplier component models could have been used in this application. However other refrigerated applications may have condensation occurring on surfaces, so retention of the proposed models is recommended until their appropriateness can be more fully assessed.

The surface model underestimated radiation on the outside surface of surfaces, but otherwise good fit between measured and predicted outside surface temperatures was achieved. Predicted floor surface temperatures were high, attributed to uncertainty in input data, in particular, thermal property data. Assessment of the appropriateness of lumping the thermal mass of the floor and surfaces at the inside of each was difficult because of the lack of detailed data.

Overall, it was considered that the model predictions were much better than could have been achieved with any previous model. Adding even more complexity to the component models was probably not justified, particularly as data uncertainty would not allow adequate assessment of enhanced models.

The model would allow the effect of changes in design and operation conditions of similar coolstores to be assessed with some confidence. However, its application to very

different applications should be undertaken with care, in case deficiencies in some of the features that were not significant and hence not apparant for the apple coolstore are significant in other applications.

CHAPTER 10: CONCLUSIONS

Most previously published refrigeration models considered heat transfer only, did not consider positional variation of air and product conditions within the refrigerated application, did not attempt to model water vapour transport in any detail and were situation specific. No application of full hydro-dynamic models to facilities where product stacking and operational characteristics are time-variable has been reported.

Measurements in apple carton pre-coolers showed that the cooling rates in staggered stacks of cartons on pallets were 30% faster on average than for in-line stacks. For both stacking arrangements the large observed variation in cooling rates could not be correlated with carton or pallet positional factors. It was attributed to different carton ventilation rates arising from limited vent size into the cartons and imprecision in both pallet positioning within the stacks and carton placement into the pallets.

For pallets within the bulk store there were significant differences in cooling rate between different positions within cartons and between pallets, but small variations in cooling rate between cartons on a pallet. The rates of cooling were significantly slower then in the pre-cooler due to the reduced level of ventilation.

Heat conduction based models of cooling were inappropriate for apple cartons due to ventilation through the cartons. A multi-zone model including both natural and forced convection airflow effects fitted measured temperature data satisfactorily, but the accuracy of water loss and internal air relative humidity (RH) predictions could not be assessed due to insufficient data. Difficulties in developing methodology to accurately define the patterns of airflow within cartons were not adequately overcome so measurements to determine airflow patterns would be required before predictions could be made for alternative packaging systems.

Significant variations in air temperature and RH were found with respect to both position within the coolstore and time. Variability was partly attributed to localised or time-variable

heat sources such as doors, pre-coolers, bulk-stored warm fruit, the uninsulated floor, but positional variations in air movement were also important. To predict the variations observed a model of heat transfer and water vapour movement within horticultural coolstores needs to be both dynamic (time-variable) and multi-zoned (position-variable).

A 1-zone model predicted mean air conditions within the store adequately, but not positional variations. Both a 5-zone model incorporating separate pre-cooling zones and an 8-zone model which also subdivided the bulk-storage area, predicted positional variations consistent with measured data. Little improvement in accuracy was achieved by further subdivision (up to 34 zones), probably because of imprecision in defining and predicting interzone air flowrates. Irrespective of the number of zones, inclusion of water absorption by packaging, in addition to product water loss, moisture ingress via door infiltration and deposition of moisture on evaporators was required to accurately model air RH.

Further studies on coolstore airflow to improve the knowledge base surrounding air pathways in relation to duct positioning, pallet locations and door openings are warranted. Full hydrodynamic modelling of airflow might assist, but such models are too complex to be incorporated into dynamic simulations of a large facility such as that studied, in which fan speed changes and pallet positioning changes were frequent.

Further studies on the product packaging model are warranted, particularly seeking to improve understanding of the effects of localised conditions on heat and mass transfer, and to quantify airflow around and through different package designs.

The major remaining weaknesses of the overall model are in the description of air flow between zones, and the manner in which effects of localised conditions on product sub-batches were modelled. Although not fully tested due to data limitations, the model represents a significant advance on previous models for refrigerated applications.

NOMENCLATURE

The nomenclature has been split into three sections: general notation specific to all Chapters, notation specfic to the carton model (Chapters 5 and 6) and notation specific to the coolstore model (Chapters 8 and 9)

General

Bi	Biot number
c	Specific heat capacity (J/kg K)
c_a	Specific heat capacity of dry air at constant pressure (J/kg K)
c_v	Specific heat capacity of water vapour (J/kg K)
c_w	Specific heat capacity of water (J/kg K)
Gr	Grashof number
h_{fg}	Latent heat of vaporisation of water vapour at 0.01°C (J/kg)
hh	Air enthalpy (J/kg)
H	Air Humidity (kg/kg)
M	Mass (kg)
Nu	Nusselt number
Pr	Prandtl number
Re	Reynolds number
t	Time (s)
$t_{1/2}$	Half cooling time (s)
$T_{ap,t}$	Apple temperature at time t (°C)
T_a	Air temperature (°C)
$T_{ap,init}$	Initial apple temperature (°C)
$T_{ap,\infty}$	Equilibrium apple temperature (°C)
Y	Fractional unaccomplished temperature change
α	Thermal diffusivity of air (m^2/s)
β	Volume coefficient of expansion of air (K^{-1})
λ	Thermal conductivity (W/m K)
λ_a	Air thermal conductivity (W/m K)
λ_e	Effective thermal conductivity of air including the effect of natural convection (W/m K)

ρ_a	Air density (kg/m^3)
ν	Kinematic viscosity of air (m^2/s)

Carton Model

a_w	Water activity at apple surface
A_n	Exposed area of the n^{th} cardboard surface associated with zone (i,j,k) (m^2)
$A_{a,i,j,k \to hor,i,j,k}$	Cardboard area exposed to the air in zone (i,j,k) (m^2)
$A_{a,i,j,k-1 \to hor,i,j,k}$	Cardboard area exposed to the air in zone (i,j,k-1) (m^2)
A_{ap}	Total apple surface area (m$^{2)}$
$A_{ap \to a}$	Apple surface area exposed to air (m^2)
$A_{ap,i,j,k \to hor,i,j,k}$	Apple to cardboard contact area in zone (i,j,k) (m^2)
$A_{ap,i,j,k-1 \to hor,i,j,k}$	Apple to cardboard contact area in zone (i,j,k-1) (m^2)
$A_{ap \to hor,i,j,k}$	Contact area between apple and bottom friday tray (m^2)
$A_{ap \to hor,i,j,k+1}$	Contact area between apple and top friday tray (m^2)
$A_{back,i,j,k}$	Exposed surface area between zone (i,j,k) air and the bulk air surrounding the carton and the back cardboard surface (m^2)
$A_{front,i,j,k}$	Exposed surface area between zone (i,j,k) air and the bulk air surrounding the carton and the front cardboard surface (m^2)
$A_{hor,i,j,k \to ab}$	Cardboard area exposed to bulk air (m^2)
A_l	Cross-sectional area of the l^{th} zone boundary (m^2)
$A_{left,i,j,k}$	Exposed surface area between zone (i,j,k) air and the bulk air surrounding the carton and the left cardboard surface (m^2)
$A_{right,i,j,k}$	Exposed surface area between zone (i,j,k) air and the bulk air surrounding the carton and the right cardboard surface (m^2)
A_{vent}	Area of the vents (m^2)
c_{ap}	Specific heat capacity of apple (J/kg K).
$c_{back,i,j,k}$	Specific heat capacity of the cardboard on the back of the carton with respect to zone (i,j,k) (J/kg K)
$c_{front,i,j,k}$	Specific heat capacity of the cardboard on the front of the carton with respect to zone (i,j,k) (J/kg K)

$c_{hor,i,j,k}$ Specific heat capacity of the cardboard below the apples in zone (i,j,k) (J/kg K)

$c_{left,i,j,k}$ Specific heat capacity of the cardboard on the left of the carton with respect to zone (i,j,k) (J/kg K)

$c_{right,i,j,k}$ Specific heat capacity of the cardboard on the right of the carton with respect to zone (i,j,k) (J/kg K)

d Characteristic dimension (m)

d_{ap} Distance between apples (m)

$h_{a,i,j,k \to hor,i,j,k}$ Convective heat transfer coefficient from the air in zone (i,j,k) to the bottom cardboard surface (W/m^2 K)

$h_{a,i,j,k-1 \to hor,i,j,k}$ Convective heat transfer coefficient from the air in zone (i,j,k-1) to the top cardboard surface (W/m^2 K)

$h_{ap \to a}$ Apple to air convective heat transfer coefficient (W/m^2 K)

$h_{ap \to hor,i,j,k}$ Heat transfer coefficient from apple to bottom friday tray (W/m^2 K)

$h_{ap \to hor,i,j,k+1}$ Heat transfer coefficient from apple to top friday tray (W/m^2 K)

$h_{ap,i,j,k \to hor,i,j,k}$ Convective heat transfer coefficient from the apples in zone (i,j,k) to the bottom cardboard surface (W/m^2 K)

$h_{ap,i,j,k-1 \to hor,i,j,k}$ Convective heat transfer coefficient from the apples in zone (i,j,k-1) to the top cardboard surface (W/m^2 K)

$h_{a \to cd,n}$ Convective heat transfer coefficient from zone (i,j,k) air to the n^{th} cardboard surface (W/m^2 K)

$h_{combined}$ Combined heat transfer coefficient (W/m^2 K)

h_{cond} Conductive heat transfer from apple surface to cardboard (W/m^2 K)

h_{conv} Convective heat transfer coefficient (W/m^2 K)

h_{forced} Forced convection heat transfer coefficient (W/m^2 K)

$h_{hor,i,j,k \to ab}$ Heat transfer coefficient between the cardboard surface and the bulk air surrounding the carton (W/m^2 K)

$h_{natural}$ Natural convection heat transfer coefficient (W/m^2 K)

$hh_{i,j,k}$ Enthalpy of air in zone (i,j,k) (J/kg)

hh_l Enthalpy of the l^{th} surrounding zone (J/kg)

$H_{i,j,k}$ Humidity of air in zone (i,j,k) (kg/kg)

H_l	Humidity of the l^{th} associated zone (kg/kg)
i,j,k	Zone co-ordinates, ranging from 1 to I, 1 to J, and 1 to K
I	Number of zones across carton
J	Number of zones along carton
K	Number of zones up carton
k_{ap}	Mass transfer coefficient from apple to air (s/m)
l	l^{th} associated zone
m	Weighting factor
$m^j_{for,i,k}$	Flowrate of dry air from zone (i,j-1,k) to zone (i,j,k) (kg/s)
$m^k_{for,i,j}$	Flowrate from the $(K-1)^{th}$ to the k^{th} layer in the i^{th} channel across the carton (kg/s)
$m^i_{for,j,k}$	Flowrate from zone (i-1,j,k) to zone (i,j,k)
$m_{l,for}$	Forced convective air flow across the boundary between zone (i,j,k) and the l^{th} associated zone (kg/s)
$m_{l,in}$	Mass flowrate of dry air from the l^{th} zone to zone (i,j,k) (kg/s)
$m_{l,out}$	Mass flowrate of dry air from the zone (i,j,k) to the l^{th} zone (kg/s)
$m_{l,nat}$	Natural ventilation air flowrate across the boundary with the l^{th} zone (kg/s)
m_{tot}	Total air flow into and out of the carton through the vents (kg/s)
$M_{ap,i,j,k}$	Mass of apple in zone (i,j,k) (kg)
$M_{a-cd,n}$	Rate of water vapour diffusion through the n^{th} cardboard surface associated with zone (i,j,k) (kg/s)
$M_{back,i,j,k}$	Mass of the cardboard surface on the back of the carton with respect to zone (i,j,k) (kg)
$M_{front,i,j,k}$	Mass of the cardboard surface on the front of the carton with respect to zone (i,j,k) (kg)
$M_{hor,i,j,k}$	Mass of cardboard below the apples in zone (i,j,k) (kg)
$M_{i,j,k}$	Mass of dry air within zone (i,j,k) (kg)
$M_{left,i,j,k}$	Mass of the cardboard surface on the left of the carton with respect to zone (i,j,k) (kg)
$M_{right,i,j,k}$	Mass of the cardboard surface on the right of the carton with respect to zone (i,j,k) (kg)

$M_{v,l}$	Water vapour gain by ventilation from the l^{th} zone associated with zone (i,j,k) (kg/s)
n	n^{th} cardboard surface associated with zone (i,j,k)
Nu	Nusselt number
p_{ab}	Partial pressure of water in the bulk air surrounding the carton (Pa)
$p_{ap,i,j,k}$	Partial pressure of water vapour at the apple surface (Pa)
$p_{i,j,k}$	Partial pressure of water vapour within zone (i,j,k) (Pa)
p_n	Partial pressure of water outside the n^{th} cardboard surface associated with zone (i,j,k) (Pa)
$p_{s,ap,i,j,k}$	Water vapour pressure at apple surface temperature in zone (i,j,k) (Pa)
p_t	Total air pressure (Pa)
Pe	Permeance of cardboard to water vapour (s/m)
Pr	Prandtl number
$Q_{i,j,k}$	Heat generation rate due to apple respiration (W)
$rv_{chan,i}$	Proportion of the total flow down the k^{th} layer which flows in the i^{th} channel across the carton
$rv_{in,i.k}$	Proportion of total flow into the carton which enters the i,1,k^{th} or leaves the i,J,k^{th} zone
$rv_{lay,k}$	Proportion of total air flow into the carton which flows into the k^{th} layer
$rv_{vert,i}$	Proportion of the total air flow which moves up the i^{th} vertical channel across the carton
R	Apple radius (m)
t	Time (s)
T_{ab}	Temperature of air surrounding the carton (°C)
$T_{aps,i,j,k}$	Apple surface temperature in zone (i,j,k) (°C)
T_{av}	Average air temperature (^{O}K)
$T_{hor,i,j,k}$	Temperature of the friday tray below apple (°C)
$T_{hor,i,j,k+1}$	Temperature of the friday tray above apple (°C)
$T_{i,j,k}$	Air temperature in zone (i,j,k) (°C)
T_l	Temperature of the l^{th} zone (°C)
$T_{ma,i,j,k}$	Mass average apple temperature in zone (i,j,k) (°C)

T_n	Temperature of the n^{th} cardboard surface associated with zone (i,j,k) (°C)
T_{z1}	Temperature of apples in zone 1 (°C)
T_{z2}	Temperature of apples in zone 2 (°C)
v_{vent}	Air velocity through vent (m/s)
V_{ap}	Apple volume (m^3)
$V_{i,j,k}$	Volume of zone (i,j,k) (m^3)
$W_{ap,i,j,k}$	Cumulative water loss from apples in zone (i,j,k) (kg)
x_{ag}	Thickness of air gap (m)
x_{card}	Cardboard half-thickness (m)
$Y_{aps,i,j,k}$	Fractional unaccomplished surface temperature change for apples in zone (i,j,k)
$Y_{ma,i,j,k}$	Fractional unaccomplished mass average temperature change for the apples in zone (i,j,k)
λ_{ap}	Apple thermal conductivity (W/m K)
λ_{card}	Cardboard thermal conductivity (W/m K)
δ	Distance between friday trays (m)
$\phi_{a,i,j,k \to hor,i,j,k}$	Convective heat transfer between zone (i,j,k) air and the cardboard surface at the bottom of the zone (W)
$\phi_{a,i,j,k-1 \to hor,i,j,k}$	Convective heat transfer between zone (i,j,k-1) air and the cardboard surface at the top of the zone (W)
$\phi_{a \to cd,n}$	Convection from air to n^{th} surrounding cardboard surface (W)
$\phi_{ap \to a}$	Convection from apple surface to zone air (W)
$\phi_{ap \to hor,i,j,k}$	Heat transfer from apple to bottom friday tray (W)
$\phi_{ap \to hor,i,j,k+1}$	Heat transfer from apple to top friday tray (W)
$\phi_{ap,i,j,k \to hor,i,j,k}$	Conductive heat transfer between apple in zone (i,j,k) and the cardboard surface below the apples (W)
$\phi_{ap,i,j,k-1 \to hor,i,j,k+1}$	Conductive heat transfer between apple in zone (i,j,k-1) and the cardboard surface above the apples (W)
ϕ_{evap}	Energy flow by evaporation from apple surface (W)
$\phi_{hor,i,j,k \to ab}$	Convective heat transfer between the cardboard and the bulk air surrounding

	the carton (W)
$\phi_{v,l}$	Ventilation from the l^{th} surrounding zone (W)
$\rho_{i,j,k}$	Air density in zone (i,j,k) (kg/m^3)

Coolstore Model

A_d	Cross-sectional area of the door (m^2)
A_e	Evaporator surface area (m^2)
A_f	Surface area of floor exposed to the ith zone air (m^2).
$A_{i,n}$	Area of interface between the ith zone and the nth associated zone (m^2)
A_{irt}	Surface area of inert material exposed to zone air (m^2)
A_p	Product exposed surface area in each sub-batch (m^2)
A_s	Surface area of the surface (m^2)
b	b^{th} bulk-stored product batch associated with the ith zone
B	Number of bulk-stored product batches associated with the ith zone
c_{dp}	Specific heat capacity of dry packaging (J/kg K)
c_f	Effective specific heat capacity of the floor (J/kg K)
c_{irt}	Inert material effective specific heat capacity (J/kg K)
c_p	Specific heat capacity of product batch (J/kg K)
c_s	Specific heat capacity of the surface (J/kg K)
Cf	Correction factor
d	d^{th} door associated with the ith zone
D	Number of doors associated with the ith zone
D_a	Astronomical daylength (h)
emc	Equilibrium package moisture content (%)
$E_{d,i\leftarrow m}$	Air discharge into the ith zone from the mth fan/evaporator (kg/s)
Ef	Evaporation correction factor
$E_{s,i\rightarrow m}$	Air flow from the ith zone to the mth fan/evaporator (kg/s)
f	f^{th} floor section associated with the ith zone
F	Number of floor sections associated with the ith zone
$F_{i,n}$	Fraction of the net airflow into the ith zone that is drawn from the nth associated zone

$Fd_{i,m}$	Proportion of the total air flow through the mth fan/evaporator discharged into the ith associated zone
$Fs_{i,m}$	Proportion of the total air flow through the mth fan/evaporator from the ith associated zone
$f(x)$	Probability of a particular door open or closed duration
h_d	Height of the door (m)
hg	hg^{th} heat generator associated with the ith zone
$h_{in,f}$	Convective heat transfer coefficient from zone air to floor (W/m^2 K)
$h_{in,s}$	Convective heat transfer coefficient for the inside face of the surface (W/m^2 K)
h_{irt}	Convective heat transfer coefficient from the zone air to the inert material surface (W/m^2 K)
$h_{o,s}$	Convective heat transfer coefficient for the outside face of a surface (W/m^2 K)
hh_i	Enthalpy of air in the ith zone (J/kg)
$hh_{m,off}$	Air enthalpy off the mth evaporator associated with the ith zone (J/kg)
hh_n	Air enthalpy of the nth zone associated with the ith zone (J/kg)
hh_{off}	Enthalpy of air leaving an evaporator (J/kg)
hh_{out}	Enthalpy of air outside a door (J/kg)
Hg	Number of heat generators associated with the ith zone
H_i	Humidity of the ith zone air (kg/kg)
H_n	Air humidity of the nth zone associated with the ith zone (kg/kg)
$H_{m,off}$	Air humidity off the mth evaporator associated with the ith zone (kg/kg)
H_{off}	Humidity of air leaving an evaporator (kg/kg)
H_{on}	Humidity of air on to an evaporator coil (kg/kg)
H_{out}	Humidity of air outside doors (kg/kg)
$H_{s,e}$	Saturation air humidity at the evaporator coil surface temperature (kg/kg)
$H_{s,s}$	Saturation humidity of water at T_s (kg/kg)
i	i^{th} zone in the coolstore
I	Number of zones in the coolstore
$I_{net,i}$	Net airflow into the ith zone (kg/s)

Irf	Integral response factor
j	j^{th} air flow out of the i^{th} zone to associated zones
jd	Julian day
J	Number of air flows out of the i^{th} zone to associated zones
$k_{concrete}$	Thermal conductivity of concrete (W/m K)
k_d	Decay constant
k_{insul}	Thermal conductivity of insulation (W/m K)
k_{mc}	Rate constant for water absorption or desorption (s^{-1}).
$k_{s,l}$	Thermal conductivity of the l^{th} layer of a surface (W/m K)
k_{soil}	Thermal conductivity of soil (W/m K)
l	Latitude (°)
m	m^{th} evaporator associated with the i^{th} zone
$m_{a,e}$	Mass flow rate of air through an evaporator (kg/s)
$m_{air,i}$	Water vapour entering the i^{th} zone due to airflow from other zones or fans/evaporators (kg/s)
mc	Packaging moisture content (%)
m_{door}	Water vapour flow through door (kg/s)
$m_{door,i}$	Water vapour entering the i^{th} zone through doors (kg/s)
$m_{floor,i}$	Water vapour entering the i^{th} zone from the floor (kg/s)
$m_{for,i\leftarrow n}$	Forced convection of air into the i^{th} zone across the interface with the n^{th} associated zone (kg/s)
$m_{heatgen,i}$	Water vapour entering the i^{th} zone from heat generators (kg/s)
m_{HG}	Rate of water vapour addition to coolstore air from a heat generator (kg/s)
$m_{inert,i}$	Water vapour entering the i^{th} zone from inerts (kg/s)
$m_{nat,i\leftarrow n}$	Natural convection of air into the i^{th} zone across the interface with the n^{th} associated zone (kg/s)
$m_{net,i\leftarrow n}$	Net flow rate of dry air into the i^{th} zone from the n^{th} associated zone due to forced and natural convection (kg/s)
$m_{out,i\rightarrow n}$	Air flow out of the i^{th} zone to the n^{th} associated zone (kg/s)
$m_{product,i}$	Water vapour entering the i^{th} zone from product batches (kg/s)
mtc_p	Product water vapour transfer coefficient (kg/m^2 s Pa)
mtc_s	Mass transfer coefficient for water vapour to a surface from the zone air

	(kg/m^2 s)
$m_{surface,i}$	Water vapour entering the i^{th} zone from surfaces (kg/s)
M	Number of evaporators associated with the i^{th} zone
M_{dp}	Mass of dry packaging in each sub-batch (kg)
M_f	Floor mass (kg)
M_i	Mass of dry air in the i^{th} zone (kg)
M_{irt}	Inert material mass (kg)
M_p	Mass of product in sub-batch (kg)
M_s	Surface mass (kg)
$M_{w,f}$	Mass of water condensed on the floor (kg)
$M_{w,irt}$	Mass of water condensed on an inert material surface (kg)
$M_{w,p}$	Mass of water in packaging in each product sub-batch (kg)
$M_{w,s}$	Condensed water mass on the inside face of a surface (kg)
n	n^{th} zone associated with the i^{th} zone
N	Number of zones associated with the i^{th} zone
p	p^{th} pre-cooling batch in the i^{th}zone
p_i	Partial pressure of water vapour in the i^{th} zone air (Pa)
p_p	Water vapour partial pressure at the product surface (Pa)
P	Number of pre-cooling batches in the i^{th} zone
Prf	Proportional response factor
r	r^{th} inert material associated with the i^{th} zone
$rand$	Random number between 0 and 1.0
rr	Respiration rate (W/kg)
R	Number of inert materials associated with the i^{th} zone
Rad_{daily}	Daily total solar radiation (MJ/m^2 day)
RH	Air relative humidity (%)
s	s^{th} surface associated with the i^{th} zone
S	Number of surfaces associated with the i^{th} zone
$SolRad$	Solar radiation incident on the outside of a surface (W/m^2)
SP	Air temperature set point (°C)
t	Time (s)

t_{door}	Duration of a door open or closed period (s)
$t_{1/2}$	Half cooling time of product batch (s)
T_a	Ambient air temperature (°C)
$T_{a,e}$	Evaporator air-on or air-off temperature (°C)
T_{amb}	Ambient temperature on the outside of a surface (°C)
T_e	Refrigerant evaporation temperature in the evaporator coil (°C)
$T_{e,min}$	Minimum evaporation temperature (°C)
$T_{e,s}$	Evaporator coil average surface temperature (°C)
T_f	Floor surface temperature (°C)
T_i	Temperature of the air in the i^{th} zone (°C)
$T_{i,n}$	Air temperature of n^{th} zone associated with to the i^{th} zone (°C)
T_{irt}	Inert material temperature (°C)
T_{max}	Daily maximum temperature (°C)
T_{min}	Daily minimum temperature (°C)
T_{off}	Temperature of air off the evaporator coil (°C)
T_{on}	Temperature of air on to the evaporator coil (°C)
T_p	Product sub-batch mass-average temperature (°C)
T_s	Surface inside temperature (°C)
T_{soil}	Temperature of the soil beneath the floor (°C)
T_{sol}	Sol-air temperature for the outside face of a surface (°C)
T_{set}	Temperature at the start of the night time decay (°C)
T_{sky}	Temperature of the sky (°C)
U_e	Overall heat transfer coefficient from air to the refrigerant for the evaporator (W/m^2 K)
U_f	Overall heat transfer coefficient through the soil and floor slab (W/m^2 K)
U_s	Heat transfer coefficient from outside air to the position in a surface where the thermal mass is located (W/m^2 K)
UA_{evap}	Effective product *UA* value due to evaporative cooling effect (W/K)
UA_{sens}	Effective sensible *UA* from product to zone air (W/K)
UA_{tot}	Overall *UA* from product to the zone air (W/K)
v_d	Velocity of air moving through a door (m/s)
v_{i-n}	Air velocity between the i^{th} zone and the n^{th} associated zone (m/s)
$x_{concrete}$	Thickness of concrete slab (m)

x_{insul}	Thickness of insulation (m)
$x_{s,l}$	Thickness of the l^{th} layer of a surface (m)
x_{soil}	Thickness of soil below the floor slab to temperature measurement position (m)
X	Approach factor for air-on to the evaporator temperature
λ	Mean door open or closed time (s)
$\beta_1, \beta_2, \beta_3$	Absorption constants for the packaging
δ	Declination
ϵ	Emissivity of the outside face of the surface
ϵ_{sky}	Sky emittance
ρ_a	Density of air in coolstore (kg/m^3)
ρ_{in}	Density of inside air adjacent to doors (kg/m^3)
ρ_{out}	Outside air density (kg/m^3)
$\phi_{air,i}$	Energy flow into the i^{th} zone due to airflow from other zones or fans/evaporators (W)
$\phi_{door,i}$	Energy flow into the i^{th} zone through doors (W)
$\phi_{doortot}$	Total heat load through door (W)
ϕ_{evap}	Heat transfer due to water gain by product from the air (W)
$\phi_{floor,i}$	Energy flow into the i^{th} zone through the floor (W)
$\phi_{heatgen,i}$	Energy flow into the i^{th} zone from heat generators (W)
ϕ_{HGlat}	Heat generator latent heat load (W)
ϕ_{HGsens}	Heat generator sensible heat load (W)
ϕ_{HGtot}	Heat generator total heat load (W)
$\phi_{inert,i}$	Energy flow into thc i^{th} zone from inerts (W)
ϕ_{pack}	Heat transfer due to water movement between air and packaging (W)
$\phi_{prodair}$	Scnsible heat transfer from air to product (W)
$\phi_{product,i}$	Energy flow into the i^{th} zone from product batches (W)
ϕ_{resp}	Product heat of respiration (W)
$\phi_{s,in}$	Energy flow to surface from zone air (W)
$\phi_{s,out}$	Energy flow to surface from air outside the surface (W)
$\phi_{surface,i}$	Energy flow into the i^{th} zone through surfaces (W)
$\phi_{w,s}$	Energy flow to surface due to water transfer from zone air (W)
τ	Time on a 24 hour clock (h)
τ_{min}	Time of the minimum temperature (h)

REFERENCES

Abdul Majeed, P.M., Srinivasa Murthy, S. & Krishna Murthy, M.V. (1980). Prediction of aircooling characteristics of moist food products, *Trans. ASAE,* **23**: 788-792.

Amato, W.S. & Tien, C. (1972). Free convection heat transfer from isothermal spheres in water, *Int. J. Heat Mass Transfer,* **15**: 327-338.

Amodio, U. (1982). Problems related to air circulation through the load of perishable foodstuffs, *Refrig. Sci. & Technol.,* **1982-1**: 241-245.

Amos, N.D., Cleland, D.J. & Banks N.H. (1993). Effect of pallet stacking arrangement on fruit cooling rates within forced-air pre-coolers, *Refrig. Sci. & Technol.,* **1993-3**: 232-241.

Anon. (1991). *Precooling Performance of Kiwifruit Packs.* DSIR Industrial Development Report No. EAHEC0834, Auckland, New Zealand.

Ansari, F. A., Charan, V., Varma, H. K. (1984). Heat and mass transfer analysis in air-cooling of spherical food products, *Int. J. Refrig.*, **7**: 194-197.

Arce, J. & Sweat, V.E. (1980). Survey of published heat transfer coefficients encountered in food refrigeration processes, *ASHRAE Trans.*, **86** (2): 235-260.

Arfin, B.B. & Chau, K.V. (1988). Cooling of strawberries in cartons with new vent hole designs, *ASHRAE Trans.*, **94** (1): 1415-1425.

ASHRAE (1990). *ASHRAE Handbook - Refrigeration Systems and Applications.* American Society of Refrigeration and Air Conditioning Engineers Publishers, Atlanta Ga.

Azzouz, A., Gosse, J. & Duminil, M. (1993). Experimental determination of cold loss caused by opening industrial cold-room doors, *Int. J. Refrig.* **16**: 57-66.

Badari Narayana, K. & Krishna Murthy, M.V. (1981). Heat and mass transfer characteristics and the evaluation of thermal properties of moist food materials, *Trans ASAE,* **24**:789-793.

Baehr, H.D. (1953). Die berechnung der kuhldauer bei ein- und mehr-dimensionalen warmefluss, *Kaltetechnik.* **5**: 255-259.

Baird, C.D., & Gaffney, J.J. (1976). A numerical procedure for calculating heat transfer in bulk loads of fruits and vegetables, *ASHRAE Trans.,* **82** (2): 525-540.

Baird, C.D., Gaffney, J.J., Talbot, M.T. (1988). Design criteria for efficient and cost effective forced air cooling systems for fruits and vegetables, *ASHRAE Trans.*, **94**: 1434-1454.

Bakker-Arkema, F.W. & Bickert, W.G. (1966). A deep-bed computational cooling procedure for biological products, *Trans. ASAE,* **9**: 834-845.

Bakker-Arkema, F.W., Bickert, W.G. & Patterson, R.J. (1967). Simultaneous heat and mass transfer during the cooling of a deep bed of biological products under varying inlet air conditions, *J. Agric. Engng. Res.* **12** (4): 297-307.

Balbach, G.C. & Schmitz, K.R. (1991). Door selection for cold storage warehouses, *Proc. 18th Int. Congr. of Refrig.*, **4**: 1983-1987.

Ball, C.O. (1923). Thermal process time for canned food, *National Research Council Bull.*, **37**.

Ball, C.O. & Olson, C.W. (1957). *Sterilization in Food Technology.* McGraw-Hill Book Co., New York.

Bazan, T., Chau, K.V. & Baird, C.D. (1989). Heat transfer simulation of the bulk cooling of fruits, ASAE Paper No. 896559.

Beukema, K.J. & Bruin, S. (1983). Three-Dimensional natural convection in a confined porous medium with internal heat generation, *Int. J. Heat Mass Transfer*, **26** : 451-458.

Bizot, H. (1983). Using the GAB model to construct moisture isotherms, In: *Physical properties of foods* (R. Jowitt, F. Escher, B. Hallstrom, *et al.* Eds.), Applied science, Essex, Chapt 4.

Bonacina, C. & Comini, G. (1971). On a numerical method for the solution of the unsteady state heat conduction equation with temperature dependent parameters, *Proc. 13th Int. Congr. Refrig.*, **2**: 329-336.

Bonte, A. & Veldhoven, B.V. (1983). Dynamic behaviour of a refrigeration plant, *Proc. 16th Int. Congr. Refrig.*, **2**: 845-851.

Broersen, P.M.T. & van der Jagt, M.F.G. (1980). Hunting of evaporators controlled by a thermostatic expansion valve, *Trans.* ASME, **102**:130-135.

Buchberg, H., Catton, I. & Edwards, D.K. (1976). Natural convection in enclosed spaces - a review of application to solar energy collection, *Trans. ASME,* **98**: 182-188.

Carslaw, H.S. & Jaeger, J.C. (1959). *Conduction of Heat in Solids* (2nd edn). Claredon Press, Oxford.

Chau, K.V. & Gaffney J.J. (1990). A finite-difference model for heat and mass transfer in products with internal heat generation and transpiration, *J. Food Sci.*, **55**: 484-487.

Chau, K.V., Gaffney, J.J. & Bellagha, S. (1984). Simulation of heat and mass transfer in products with internal heat generation and transpiration, ASAE Paper No. 84-6513.

Chau, K.V., Gaffney, J.J., Romero, R.A. (1988a). A mathematical model for the transpiration from fruits and vegetables, *ASHRAE Trans*, **94** (1): 1541-1552.

Chau, K.V., Romero, R.A., Baird, C.D., Gaffney, J.J. (1988b). Transpiration coefficients for certain fruits and vegetables, *ASHRAE Trans*, **94** (1): 1553-1562.

Chi, J. & Didion, D. (1982). A simulation model of the transient performance of a heat pump, *Int. J. Refrig.*, **5**(3): 176-184

Choi, Y. & Okos, M.R. (1986). Effects of temperature and composition on the thermal properties of foods. In *Food Engineering and Process Applications*. ed. Le Mageur, M. & Jelen, P., Elsevier, London.

Chuntranuluck, S., Serrallach, G.F. & Cleland, A.C. (1989). Shape factors for prediction of chilling times of irregular shapes, *Proc. Int. Conf. On Technical Inovation in Freezing and Refrigeration of Fruit and Vegetables*, University of California, Davis, July 1989: 215-222.

CIBS Guide, (1975). Condensation and moisture problems. Vol. **A**: Section A10.

Clary, B.L., Nelson, G.L. & Smith, R.E. (1971). The application of the geometry analysis technique in determining the heat transfer rates from biological materials, *Trans. ASAE,* **14**: 586-589.

Cleland, A.C. (1983). Simulation of industrial refrigeration plants under variable load conditions, *Int. J. Refrig.*, **6**: 11-19.

Cleland, A.C. (1985a). Experimental verification of a mathematical model for simulation of industrial refrigeration plants, *Int. J. Refrig.*, **8**: 275-282

Cleland, A.C. (1985b). RADS-a computer package for refrigeration analysis, design and simulation, *Int. J. Refrig.*, **8**: 372-374

Cleland, A.C. (1990). *Food Refrigeration Processes - Analysis, Design and Simulation*, Elsevier Science Publishers, London.

Cleland, A.C. & Earle, R.L. (1982). A simple method for prediction of heating and cooling rates in solids of various shapes, *Int. J. Refrig.*, **5**: 98-106.

Cleland, A.C. & Cleland, D.J. (1992). *Cost-Effective Refrigeration*, Dept. of Biotechnology, Massey University, Palmerston North.

Cleland, D.J., Boyd, N.S. & Cleland, A.C. (1982). A model for fish freezing and storage on board small New Zealand fishing vessels, *Refrig. Sci. & Technol.*, **1982-1**: 81-88.

Cleland, D.J. & Cleland A.C. (1989). Appropriate level of model complexity in dynamic simulation of refrigeration systems, *Refrig. Sci. & Technol.*, **1989-1**: 261-268.

Cornelius, M. (1991). *Refrigeration Analysis, Design and Simulation Package: "RADS" - Notes for Users (revised),* Release 3.1, Food Technology Research Centre, Massey University, Palmerston North, New Zealand.

Dayan, E., Jones, J.W., van Keulen, H. & Challa, H. (1989). Technical documentation of the tomato crop growth model TOMGRO V1.1, In: *On-Line Computer Control System for Greenhouses Under High Radiation and Temperature Zones.* Final Research Report Bard Project **US-871-84**, Agricultural Engineering Dept., University of Florida, Gainesville. ed. Jones, J.W., Dayan, E., Jones, P.,Seginer, I., Allan L.H. & Zipori I.

Dhar, M. & Soedel, W. (1979). Transient analysis of a vapour compression refrigeration system, *Proc. 15th Int. Congr. Refrig.*, **2**:1035-1068.

De Baerdemaeker, J., Singh, R.P. & Segerlind, L.J. (1977). Modelling heat transfer in foods using the finite-element method, *J. Food Proc. Engng.*, **1**: 37-50.

De Bruijn, M., van de Jagt, M.F.G. & Machielsen, C.H.M. (1979). Simulation experiments on a compression-refrigerator system, *Proc. IMACS, Congr. on Simulation Systems*, Sorrento,645-665.

Devres, Y.O. (1988). Energy saving in cold stores, *Proc. Chamber of Mech. Engrs.*, 9th-11th March, Istanbul, Turkey.

Devres, Y.O. (1989). Temperature and weight loss analyses of some fruit and vegetables in cold storage, Institute Environmental Engineering Research Memo. No. 113, South Bank Polytechnic, London.

Devres, Y.O. & Bishop, C.F.H. (1992). A computer model for weight loss and energy conservation in a fresh produce refrigerated store, Institute Environmental Engineering Research Memo. No. 134, South Bank Polytechnic, London.

Dominguez, M., Pinillos, J.M., Sanz, P.D. & Mascheroni, R.H. (1991). Use of electrical analogy by computer in the modelling of beef cooling tunnels, *Proc 18th Int. Congr. Refrig.*, **4**: 1898-1901.

Dossat, R.J. (1981). *Principles of Refrigeration* (2nd edn, SI), J. Wiley & Sons, New York.

Draper, N.R. & Smith, H. (1981). *Applied Regression Analysis*, 2nd edn. J. Willey & Sons, New York.

Earle, R.L. & Fleming, A.K. (1967). Cooling and freezing of lamb and mutton carcasses -1. Cooling and freezing rates in legs, *Food Technol.*,**21**(1):79-84.

Falconer, R.M. (1993). Cooling air distribution in a cheese store, *Refrig. Sci. & Technol.*, **1993-3**: 406-413.

Fikiin, A.G. (1983). Investigating the factors for intensifying fruit and vegetable cooling, *Int. J. Refrig.* **6**: 176-181.

Fikiin, A.G. & Fikiina, I. (1971). Calculation de la duree de refrigeration des produitis alimentaires et des corps solides, *Proc. 13th Int. Congr. Refrig.*, **2**: 411-414.

Flack Jr, R.D. & Witt, C.L. (1979). Velocity measurements in two natural convection air flows using a laser velocimeter, *Trans. ASME,* **101**: 256-260.

Fockens, F.H. & Meffert, H.F.Th. (1972). Biophysical properties of horticultural products as related to loss of moisture during cooling down, *J. Sci. Fd. Agric.*, **23**: 285-298.

Fritzsche C. & Lilienblum, W. (1968). Neue Messungen zur Bestimmung der Kalteverluste an Kuhlraumturen, *Kaltetechnik Klimatisierung*, **20**: 9-15

Gaffney, J.J., Baird, C.C., Chau, K.V. (1985a). Methods for calculating heat and mass transfer in fruits and vegetables individually and in bulk, *ASHRAE Trans*, **91** (2B): 333-352.

Gaffney, J.J., Baird, C.D., Chau, K.V. (1985b). Influence of airflow rate, respiration, evaporative cooling, and other factors affecting weight loss calculations for fruits and vegetables, *ASHRAE Trans.*, **91** (1B): 690-707.

Gan, G. & Woods, J.L. (1989). A deep bed simulation of vegetable cooling, *Proc. 11th Int. Congr. Agric. Engng.*, 2301-2308.

Gatchilov, T.S., Ivanova, V.S., Kaltchev, K.I. (1979). Some aspects of construction and exploitation of extended surface air coolers, operating under frosting conditions, *Proc. 15th Int. Congr. Refrig.*, **2**: 991-995

Gentry, J.P. (1970). *A Procedure for Rapidly Determining Transpiration Rates and Epidermal Permeabilities of Fruits.* Ph.D. Thesis, Michigan State University.

Gloeckner, G., Findeisen, F. (1984). The computing program LF74: A software solution for typical simulation problems of air and refrigeration engineering, *Refrig. Sci. & Technol.*, **1984-2**: 231-236.

Gloeckner, G., Hofer, B., Kluge, C.H., Schroth, H.H. & Wobst, E. (1990). Simulation of refrigerating plants for cold stores, *Refrig. Sci. & Tecnol.*, **1990-4**: 487-493.

Gosney, W.B. & Olama, H.A.L. (1975). Heat and enthalpy gains through cold room doorways, Institute of Refrigeration Paper, The Polytechnic of the South Bank, London, 4th December.

Haas, E. & Felsenstein, G. (1985). Factors affecting the cooling rate of avocados packed in corrugated cartons, *Refrig. Sci. & Technol.* **1985-5**: 291-300.

Haghighi, K. & Sergerlind, L.J. (1988). Modelling simultaneous heat and mass transfer in an isotropic sphere - a finite element approach, *Trans. ASAE* **31**(2): 629-637.

Hayakawa, K. (1971). Estimating food temperatures during various processing or handling treatments, *J. Food Sci.*, **36**: 378-385.

Hayakawa, K. (1978). Computer simulation for heat transfer and moisture loss from an idealized fresh produce, *Trans. ASAE*, **21**: 1015-1024.

Hayakawa, K. & Succar, J. (1982). Heat transfer and moisture loss of spherical fresh produce, *J. Food Sci.*, **47**: 596-605.

Hargraves, M.R.O. & James, R.W. (1979). A model for a marine chilled water plant for microprocessor control development, *Proc. Inst. Refrig. (GB),* **76**: 28-38.

Heisler, M.P. (1947). Temperature charts for induction and constant temperature heating, *Trans ASME,* **69**: 227-236.

Henderson, S.M. & Perry, R.L. (1955). *Agricultural Process Engineering*, Wiley, New York.

Holdredge, R.M. & Wyse, R.E. (1982). Computer simulation of the forced convection cooling of sugarbeets, *Trans. ASAE,* **25**: 1425-1430.

Holman, J.P. (1990). *Heat Transfer* (7th edn) McGraw Hill, New York

Hunter, J.H. (1985). Heat of respiration and weight loss from potatoes in storage, ASAE Paper No. 85-4035

Incropera, F.P. & De Witt, D.P. (1985). *Fundamentals of Heat and Mass Transfer*, J. Wiley & Sons, New York.

Irving A.R & Sharp, A.K. (1976) Measurement of air circulation in a refrigerated ISO container, *Refrig. Sci. & Technol.*, **1976-1**: 485-492

Jamieson, D.J., Cleland, D.J. & Falconer, R.M. (1993). Modelling of bulk-stacked cheese cooling in coolstores, *Refrig. Sci. & Technol.*, **1993-3**: 268-278.

James, K.A., James, R.W. & Dunn, A. (1986). A critical survey of dynamic mathematical models of refrigeration systems and heat pumps and their components, Institute Environmental Engineering Technical Memo. No. 97, South Bank Polytechnic, London.

Kimball, B.A. & Bellamy, L.A. (1986). Generation of diurnal solar radiation, temperature, and relative humidity patterns, *Energy Agric.*, **5**: 185-197.

Kondepudi, S.N. & O'Neal, D.L. (1987). The effects of frost growth on extended surface heat exchanger performance: a review, *ASHRAE Trans.*, **93** (2): 258-274.

Kondepudi, S.N. & O'Neal, D.L. (1991). Modelling tube-fin heat exchangers under frosting conditions, *Proc. 18th Int. Congr. Refrig.*, **3**: 1289-1293.

Kondepudi, S.N. & O'Neal, D.L. (1993a). Performance of finned-tube heat exchangers under frosting conditions: I. Simulation model, *Int. J. Refrig.* **16**: 175-180.

Kondepudi, S.N. & O'Neal, D.L. (1993b). Performance of finned-tube heat exchangers under frosting conditions: II. Comparison of experimental data with model, *Int. J. Refrig.* **16**: 181-184.

Kopelman, I.J. & Pflug, I.J. (1968). The relationship of the surface, mass average and geometric center temperatures in transient conduction heat flow, *Food Technol.*, **22**: 141-146.

Lentz, C.P. & Rooke, E.A. (1964). Rates of moisture loss of apples under refrigerated storage conditions, *Food Technol.*, **18**(8): 119-121.

Levy, F.L. (1981). A modified Maxwell-Eucken equation for calculating the thermal conductivity of two-component solutions or mixtures, *Int. J. Refrig.*, **4**: 223-225.

Liao, C.M. & Feddes, J.J. (1990). Mathematical analysis of a lumped-parameter model for describing the behaviour of airborne dust in animal housing, *Applied Mathematical Modelling*, **14**: 248-257.

Liao, C.M. & Feddes, J.J. (1992). A lumped-parameter model for predicting airborne dust concentration in a ventilated airspace, *Trans. ASAE,* **35**: 1973-1978.

Liebenspacher, F. & Weisser, H. (1989). Sorption of water vapour and its kinetics in cellulosic packaging material for food, *Proc. 5th Int. Cong. Engng. & Food,* 28 - 3 June, Cologne, Germany, pp 610-623.

Lin, Z., Cleland, A.C., Serrallach, G.F. & Cleland, D.J. (1993). Prediction of chilling times for objects of regular multi-dimensional shapes using a general geometric factor, *Refrig. Sci. & Technol.*, **1993-3**: 259-267.

Lovatt, S.J. (1992). *A Dynamic Modelling Methodology for the Simulation of Industrial Refrigeration Systems*, PhD Thesis, Massey University, Palmerston North, New Zealand.

Lovatt, S.J., Pham, Q.T., Cleland, A.C. & Loeffen, M.P.F. (1993a). A new method of predicting the time-variability of product heat load during food cooling - Part 1: Theoretical considerations, *J. Food Engng.*, **18**: 13-36.

Lovatt, S.J., Pham, Q.T., Loeffen, M.P.F. & Cleland, A.C. (1993b). A new method of predicting the time-variability of product heat load during food cooling - Part 2: Experimental testing, *J. Food Engng.*, **18** : 37-62.

MacArthur, J.W. (1984). Transient heat pump behaviour: a theoretical investigation. *Int. J. Refrig.*, **7**:173-132.

Marshall, S.A. & James, R.W. (1975). Dynamic analysis of an industrial refrigeration system to investigate capacity control, *Proc. Inst. Mech. Engrs.*, **189**: 437-445.

McDonald, B. (1990). Cooling of Apples, DSIR report No.9022(2), Auckland, New Zealand.

McDonald, B., Billing, D.P. & Wilks, B.G. (1993). Coolstore performance and specifications, *Refrig. Sci. & Technol.*, **1993-3**: 390-398.

McLeod S. (1992) Formerly, Research Manager, NZAPMB, Hastings, Personal communication.

Meffert, H.F.Th. & Van Beek, G. (1983) Basic elements of a physical model for refrigerated vehicles I - Air circulation and distribution, *Proc. 16th Int.Congr. Refrig.*, **4**: 465-476.

Meffert, H.F.Th. & Van Beek, G. (1988) Basic elements of a physical model for refrigerated vehicles II - Temperature distribution, *Refrig. Sci. & Technol.*, **1988-1**: 221-231.

Mellor, J.D. (1976). Thermophysical properties of foodstuffs. 1. Introductory review. *Bull. I.I.R.*, **56**: 551-563.

Mellor, J.D. (1978). Thermophysical properties of foodstuffs. 2. Theorectical aspects. *Bull. I.I.R.*, **58**: 569-584.

Metais, B. & Eckert, E.R.G. (1964). Forced, mixed, and free convection regimes, *Trans. ASME*: 295-296.

Miles, C.A., Van Beek, G. & Veerkamp, C.H. (1983). Calculation of thermophysical properties of foods, In *Physical Properties of Foods,* ed R. Jowitt. Applied Science Publishers, London, pp 269-313.

Misra, R.N. & Young, J.H. (1979). The finite element approach for solution of transient heat transfer in a sphere, *Trans. ASAE,* **22**: 944-949.

Monteith, J.L. & Unsworth, M.H. (1990). *Principles of Environmental Physics,* 2nd edn., Edward Arnold Pub.,London.

Moreno, J. (1987). Air interchange rate through a cold store open door, *Proc. 17th Int. Congr. Refrig.*, **4**: 138-143.

Najork, H. (1975). Investigation on the dynamic behaviour of evaporators with thermostatic expansion valve, *Proc. 14th Int. Congr. Refrig.*, **1**: 1021-1028.

Neves, L.C., Vanrg, L., Rooke, E.A. (1983). Effect of airflow on weightloss and temperature gradients in bulk stored produce, *Proc. 16th Int. Congr. Refrig.*, **4**: 249-252.

Newell, M.E. & Schmidt, F.W. (1970) Heat transfer by laminar natural convection within rectangular enclosures, *Trans. ASME, 92*: 159-168.

Newman, A.B. (1936). Heating and cooling rectangular and cylindrical solids, *Ind. Engng Chem.,* **28**(5): 545-548.

Nicholas, R.C. & Pflug, I.J. (1961). Heat processing characteristics of fresh cucumber pickle products, 1. Heating rates of whole pickles. *Quart. Bull. of the Michigan Agric. Expt. Stat.,* **43** (3) : 522-531.

O'Hagan, A.N., Cleland, D.J., & Cleland, D.J. (1993a). Air cooling coil performance under frosting conditions. Part 1: performance measurement and results, *Refrig. Sci. & Technol.*, **1993-3**: 345-354.

O'Hagan, A.N., Cleland, D.J., & Cleland, D.J. (1993b). Air cooling coil performance under frosting conditions. Part 2: Modelling, *Refrig. Sci. & Technol.*, **1993-3**: 355-362.

O'Neal, D.L. & Tree, D.R. (1985). A review of frost formation in simple geometries, *ASHRAE Trans.*, **91** (2A): 267-281.

Ofoli, R.Y. & Burgess, G.J. (1986). A thermodynamic approach to heat and mass transport in stored agricultural products, *J. Food Eng.,* **5**: 195-216.

Pala, M. & Devres, Y.O. (1988). Computer simulated model for power consumption and weight loss in a cold store, *Refrig. Sci. & Technol.*, **1988-1**: 233-241.

Parsons, R.A., Mitchell, F.G. & Mayer, G. (1972). Forced-air cooling of palletized fresh fruit, *Trans. ASAE,* **15**: 729-731.

Patankar, S.V. (1980). *Numerical Heat Transfer and Fluid Flow*, McGraw Hill, New York.

Patel, P.N. & Sastry, S.K. (1988a). Effects of temperature, relative humidity and storage time on the transpiration coefficients of selected perishables, *ASHRAE Trans.*, **94** (1): 1563-1587.

Patel, P.N. & Sastry, S.K. (1988b). Effect of temperature fluctuation on transpiration of selected perishables: mathematical models and experimental studies, *ASHRAE Trans.*, **94** (1): 1588-1601.

Pflug, I.J. & Nicholas, R.C. (1960). Heat processing characteristics of fresh cucumber pickle products, 1. Heating rates of spears, *Quart. Bull. of the Michigan Agric. Expt. Stat.,* **43** (2): 407-414.

Pflug, I.J. & Blaisdell, J.L. (1963). Methods of analysis of precooling data, *ASHRAE Journal.*

Pflug, I.J., Blaisdell, J.L. & Kopelman, I.J. (1965). Developing temperature-time curves for objects that can be approximated by a sphere, infinite plate or infinite cylinder, *ASHRAE Trans.,* **71**(1): 238-248.

Pham, Q.T. (1990). Prediction of thermal conductivity of meats and other animal products from composition data, In *Energy & Food, Volume 1 - Physical Properties and Process Control,* W.E.L. Spiess & H. Schubert eds., Elsevier Applied Science, London: pp 408-423.

Pham, Q.T. & Oliver, D.W. (1983). Infiltration of air into cold stores, *Proc. 16th Int. Congr. Refrig.*, **4**: 67-72.

Pham, Q.T. & Willix, J. (1989). Thermal conductivity of fresh lamb meat, offals and fat in the range -40 to +30°C : Measurements and correlations, *J. Food Sci.,* **54** (3): 508-515.

Pham, Q.T., Wee, H.K., Lovatt, S.J., Lindsay, D. & Kemp, R.M. (1993). A quasi-steady state approach to the design of meat plant refrigeration systems, *Refrig. Sci. & Technol.* **1993-3**: 215-223.

Reynoso, R.O. & de Michelis, A. (1988). Simulation of batch cryogenic freezers, *Int. J. Refrig.,* **11**: 6-10.

Romero, R.A. & Chau, K.V. (1987). A mathematical simulation for transpiration from fruits and vegetables in bulk storage, ASAE Paper No. 87-6007.

Romero, R.A., Chau, K.V. & Gaffney, J.J. (1986). Transpiration coefficients of selected fruits and vegetables, ASAE Paper No. 86-6014.

Rutov, D.J. (1958). Calculation of the time of cooling of food products, *Refrig. Sci. & Technol.,* **1958-1**:415-421.

Sastry, S.K., Sudhir, K., Baird, C.D. & Buffington, D.E. (1978). Transpiration rates of certain fruits and vegetables, *ASHRAE Trans.*, **84**: 237-255.

Sastry, S.K., Zuritz, C.A., Anantheswaran, R.C. (1985). Interaction between heat and mass transfer in foods, *ASHRAE Trans.*, **91** (2B): 353-370.

Sastry, S.K. & Buffington, D.E. (1983). Transpiration rates of stored perishable commodities: a mathematical model and experiments on tomatoes, *Int. J. Refrig.*, **6**: 84-96.

Schwartzberg, H.G. (1976). Effective heat capacities for the freezing and thawing of food, *J. Food Science,* **41**: 152-156.

Schwartzberg, H.G. (1977). Effective heat capacities for the freezing and thawing of food, *Refrig. Sci. & Technol.,* **1977-1**: 303-310.

Sekulic, D.P. (1983). Heat and mass transfer in cryogenically cooled surface under frosting conditions - A survey of research efforts and analysis - frosting of air coolers Part II, *Proc. 16th Int.Congr. Refrig.*, **2**: 541-550.

Smith, G.R. (1989). Theoretical cooling coil calculations at freezer temperatures to avoid unfavourable frost, *AHSRAE Trans.*, **95**(2): 1138-1148.

Smith, R.E., Nelson, G.L. & Henrickson, R.L. (1967). Analyses on transient heat transfer from anomalous shapes, *Trans. ASAE,* **10**: 236-245.

Srinivasa Murthy, S. Krishna Murthy, M.V. & Ramachandran, A. (1974). Heat transfer during the air cooling and storing of moist food products, *Trans. ASAE*, **17**: 769-773.

Srinivasa Murthy, S. Krishna Murthy, M.V. & Ramachandran, A. (1976). Heat transfer during the air cooling and storing of moist food products, II. Spherical and cylindrical shapes, *Trans. ASAE*, **19**: 577-583.

Steadman, R. (1993). Research and Development Manager, NZ Forest Products Ltd. Kinleith, Personal communication

Stoecker, W.F. (1966). Stability of an evaporator-expansion valve control loop, *ASHRAE Annual Meeting,* Toronto, **No. 2007** ASHRAE, Atlanta, GA.

Stoecker, W.F. & Jones, J.W. (1982). *Refrigeration and Air Conditioning.* (2nd edn) McGraw-Hill Book Comp., New York.

Szczechowiak, E. & Rainczak,J .(1987). The cooling chamber and the air-cooler operation in unsteady states, *Proc. 17th Int. Congr. Refrig.*, **2**: 864-869.

Talbot, M.T. (1973). *Transpiration Rates of Snap Green Beans.* M.S. Thesis, University of Florida.

Tamm, W. (1965). Air flow within air curtains to protect cold rooms, *Proc. 11th Int. Congr. Refrig.,* **2**:1025-1033.

Touber, S. (1984). Principles and methods for mathematical modelling the steady-state and dynamic behaviour of refrigeration components and installations, *Refrig. Sci. & Technol.,* **1984-2**: 163-175.

Upadhyaya, S.K. & Rumsey, T. (1989). A finite element model for coupled equations, ASAE Paper No. 89-6578.

Van Beek, G. (1983). Weight loss of hard fruit during storage as influenced by cold room climate and transpiration coefficient, *Proc. 16th Int. Congr. Refrig.*, **4**: 225-230.

Van Beek, G. & Ficek, L. (1979). Prediction of relative humidity in a transport container, *Proc. 15th Int. Congr. Refrig.,* **4**: 367-377.

Van Der Meer, J.S. (1987). *Simulation of a Refrigerator Evaporator*, PhD Thesis, Delft University of Technology, Delft.

Van Der Ree, H., Basting, W.J. & Nievergeld, P.G.M. (1974). Temperature distributions in cargoes with the method of finite elements, *Refrig. Sci. & Technol.* **1974-2**: 195-220.

Van Gerwen, R.J.M. & Van Oort, H. (1989). The use of fluid dynamics simulation models in cold store design, *Refrig. Sci. & Technol.,* **1989-1**: 233-240.

Van Gerwen, R.J.M. & Van Oort, H. (1990). Optimization of cold store design using fluid dynamics models, *Refrig. Sci. & Technol.,* **1990-4**: 473-478.

Van Gerwen, R.J.M., Van der Sluis, S.M. & Van Oort, H. (1991). Computer modelling of carcass chilling processes, *Proc. 18th Int. Congr. Refrig.,* **4**: 1893-1897.

Villa, L.G. (1973). *Single Particle Convective Moisture Loss from Horticultural Products in Storage*, Ph.D. Thesis, Michigan State University.

Wade, N.L. (1984). Estimation of the refrigeration capacity required to cool horticultural produce, *Int. J. Refrig.*, **7**: 358-366.

Wadsworth, J.I. & Spadaro, J.J. (1969). Transient temperature distribution in whole sweetpotato roots during imersion heating, 1. Thermal diffusivity of sweetpotatoes, *Food Technol.*, **23**: 85-89.

Wadsworth, J.I. & Spadaro, J.J. (1970). Transient temperature distribution in whole sweetpotato roots during imersion heating, 2. Computer simulation, *Food Technol.*, **24**: 77-84.

Wang, H.W. (1991). *Modelling of a Refrigerating System Coupled with a Refrigerated Room*, PhD Thesis, Delft University of Technology, The Netherlands.

Wang, I.H. & Touber, S. (1987). Prediction of air flow patterns in cold stores based on temperature measurements, *Proc. 17th Int. Congr. Refrig.*, **4**: 52-60.

Wang, H.W. & Touber, S. (1988). Simple non-steady state modelling of a refrigerated room accounting for air flow and temperature distributions, *Refrig. Sci. & Technol.*, **1988-1**: 211-219.

Wang, H.W. & Touber, S. (1990). Distributed dynamic modelling of a refrigerated room, *Int. J. Refrig.*, **13** : 214-222.

Wang, H.W. & Touber, S. (1991). Distributed and non-steady-state modelling of an air cooler, *Int. J. Refrig.*, **14** : 98-111.

Warrington, R.O. JR. & Powe, R.E. (1985). The transfer of heat by natural convection between bodies and their enclosures, *Int. J. Heat Mass Transfer*, **28**: 319-330.

Watkins, J.B. (1990). *Forced-Air Cooling.* Queensland Department of Primary Industries Information Series Q188027.

Wink, W.A. (1961). The effect of relative humidity and temperature on paper properties, *TAPPI*, **44** (6):172-180.

Wedekind, G.L. & Stoecker, W.F. (1966). Transient repsonse of the mixture -vapour transition point in horizontal evaporating flow, *ASHRAE J.*, November: 74-77.

Yasuda, H., Touber, S. & Machielsen, C.H.M. (1983). Simulation model of a vapour compression refrigeration system, *ASHRAE Trans.*, **88** (2A): 408-425.

Yavuzkurt, S., Gogus, A.Y. & Ceylan, T. (1976). Heat and mass transfer during precooling, *Refrig. Sci. & Technol.*, **1976-2**: 87-96.

Yuge, T. (1960). Experiments of heat and mass transfer from spheres including combined natural and forced convection, *J. Heat Transfer*, **82**: 214-220.